

Aus dem Physiologischen Institut

Direktor: Prof. Dr. Hans-Rudolf Lüscher

Arbeit unter der Leitung von PD Dr. Thomas Berger und Prof. Dr. Hans-Rudolf Lüscher

Network activity in the mammalian brain in vitro

Inaugural-Dissertation zur Erlangung der
Doktorwürde der Philosophie im Fach Neurowissenschaften
der Medizinischen Fakultät der Universität Bern

vorgelegt von

Florian Bernd Neubauer

aus Deutschland

Von der Medizinischen Fakultät der Universität Bern auf Antrag der
Dissertationskommission als Dissertation genehmigt.

Promotionsdatum:

Der Dekan der Medizinischen Fakultät:

Contents

Summary	vii
I Introduction.....	1
1 The pivotal role of network activity in a unified model of brain and mind.....	1
1.1 The goal of brain research	1
1.2 The explanatory gap.....	6
1.3 The middle level gap	10
1.4 Necessity of invasive research on network activity.....	11
1.5 What is the desirable vocabulary for a unified theory of brain and mind?.....	13
2 Technical and theoretical background of research on network activity	14
2.1 Technical constraints	14
2.2 Constraints within the theoretical background of network activity.....	16
2.3 Towards a less biased view of network activity.....	23
3 Chapter summary and aim of my PhD work.....	35
II Guide to publications	37
• Publication 1	
“Somatodendritic Integration under Increased Network Activity in Layer 5 Pyramidal Cells of the Somatosensory Cortex”	37
• Publication 2	
“Reassembling a System from the Sensor to Cerebral Representation: The Olfactory System In Vitro”	57
• Publication 3	
“Combined Voltage and Calcium Epifluorescence Imaging In Vitro and In Vivo Reveals Subthreshold and Suprathreshold Dynamics of Mouse Barrel Cortex”	77
• Publication 4	
“Modulation of Network Activity through GABA _b receptor-mediated Tonic Inhibition in the Rat Medial Prefrontal Cortex <i>In Vitro</i> ”	93
Bibliography.....	151
Abbreviations	157
Curriculum Vitae.....	159
Acknowledgements.....	161

Summary

To exercise its functions the brain exploits mechanisms which emerge from the hierarchical organization of its components. Due to different methods of exploration, the vocabulary used for the description of the highest level of brain function, i.e. the mind, differs completely from the vocabularies used for lower levels in the hierarchy, which employ physical, chemical, and biological terms. This is one, but not the only reason for the identification of an “explanatory gap” between high- and low-level models of brain function. Another reason is that the scientific description of an unknown number of intermediary levels of emergence, associated with the network activity of interconnected brain cells, is still missing. It is very likely that filling in this “middle level gap” will reduce the difficulty of finding bridge laws that allow for the explanation of mental functions in terms of neurophysiological activity, which is the basis for a unified model of brain and mind. For the identification and description of the missing middle levels of emergence, experimental research on network activity is of crucial importance. Neither theoretical extrapolation from lower levels nor philosophical inference has been able to predict how network activity actually implements the mind. Rather it seems that established theoretical paradigms have restricted the search space within which experimental neuroscientists expect to detect relevant activity. Therefore I argue that not only further development of technical methods is needed to make experimental research on network activity more successful, but also more openness about which kinds of emergent mechanisms are possible in the brain. An important prediction, which can be made about network activity based on the axiom of physical monism, is that each mental activity must have a correlate on lower levels of the system. I suggest using this as a more liberal guideline for the design of explorative studies on network activity. Every type of low-level activity can be considered as possible correlate for mental functions and therefore should be taken into account. At the same time, all kinds of simultaneous mental activity should be included in the interpretation of a given signal related to low-level activity. Taken together, in the first and theoretical part of this thesis I point out the pivotal role of experimental research on network activity for a unified theory of brain and mind, and suggest a broader conceptual framework for experiments to reach this goal of neuroscience. In the second part I give an introduction to the experimental studies to which I contributed during my PhD work. These studies add to the knowledge about network activity and improve methods for research on network activity (Berger et al., 2007; Markopoulos et al., 2008; Neubauer and Berger, 2008; Wang et al., submitted 02/2009).

I Introduction

1 The pivotal role of network activity in a unified model of brain and mind

Brain research is far away from providing a comprehensive theory of the performances of the human brain. The task to complete such a theory seems tremendous. Important products of the brain like perception, recollection, feeling, thinking, motivation, decision-making, volition, speech, and action still await their scientific explanation. Gaps remain at many locations inside the patchwork of the current picture of the brain, but especially those higher, or mental functions would be interesting to understand for experts and non-experts as they shape our personal and social experiences day by day. So what do we commonly want to know when we ask for an explanation of brain functions? We want to know what the cells and areas in the brain are doing when we talk or think or feel.

1.1 The goal of brain research

Scientific explanations. In the context of natural science, an explanation is the effort to compile a model of the studied phenomenon which assigns multiple observations to unifying principles, describes causal relations, and provides intelligibility (cf. Niiniluoto, 2008; Woodward, 2008). Intelligibility needs simplification which is achieved by generalization. The idea behind this concept is that if one example is understood and the principles are clear, the details for other specific cases can be omitted. A good scientific model of the functioning of the brain therefore should group crucial anatomical elements into common functional structures and abstract their recurrent interactions. Its information content should be reduced in comparison to the actual multiplicity of the brain's ongoing neurophysiology. And in the end, the model must explain the human mind.¹

The mind: Information processing and consciousness. One immediately feels the dichotomy in terminology; "cells" and the "brain" as an anatomical organ on one hand, and "personal experiences" and the "mind" on the other hand. Before I deal with this dichotomy later, I want to start with a definition of the explanandum, a definition of the mind.

¹ In this thesis I confine myself to fundamental research and put applied medical questions aside. The knowledge of the intact functions of the brain can of course help to understand and treat neurological and psychiatric diseases.

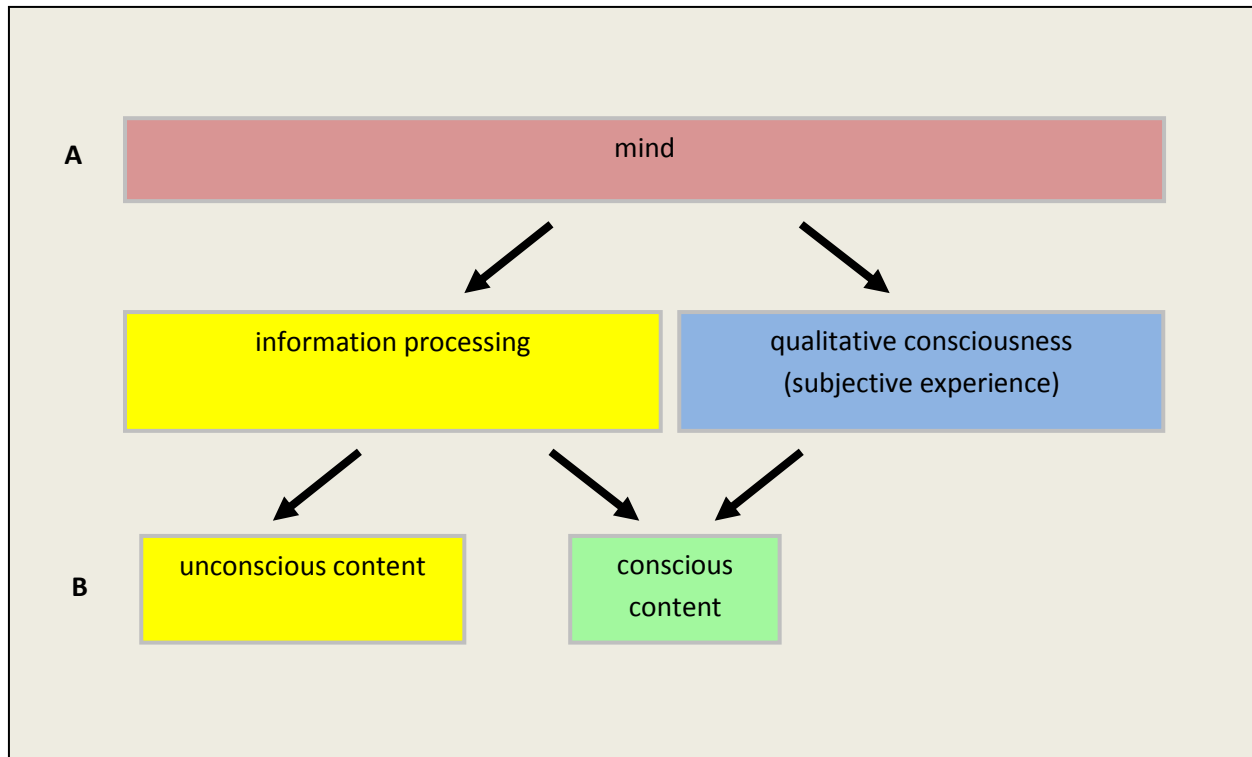


Fig. 1. Definition of the term “mind”.

A) The level of the mind comprises two basic functions, information processing in the widest sense and qualitative consciousness.

B) Whereas information processing happens without involving consciousness in many cases, consciousness always has a specific content and thus in general depends on information processing.

Although there is no canonical concept, philosophy of mind and cognitive science commonly consider two aspects which are present in the variety of mental functions as basic and as distinct: the aspect of information processing and the involvement of qualitative consciousness (Fig. 1A). Both terms are simplifications in the abovementioned sense, intended to increase intelligibility by generalization.

Information processing. Information processing is involved in all mental tasks like perception, language, and decision making, because these tasks always have specific content and in this regard “are about something specific”. This “specific aboutness” is a subject-matter of information theory.

According to Shannon (Shannon, 1948), information is a pattern carried by a message which is correlated to one specific state of the message’s source. Based on this, information processing in the widest sense comprises the discrimination between received input patterns, the combination and transformation into new patterns, and finally making some use of them. In the context of the brain, the ultimate purpose is to add the processed patterns to memory as a

future source of experience or to select an appropriate behavior for the present moment. Understanding how informational patterns are processed in the brain is a major part of understanding the mechanism underlying mental tasks.

Qualitative consciousness. The second important general aspect of mental functions is that they imply qualitative consciousness. Definitions of consciousness comprise several dimensions (see Van Gulick, 2004). Here I want to focus on the qualitative aspect and I will use consciousness in the following in this restricted sense. Using a term coined by Nagel, qualitative consciousness is the “subjective character of experience” (Nagel, 1974) also called the “first-person perspective” of experience.

Consciousness is closely related to information processing as consciousness necessarily has a specific content (putting aside some kinds of meditation). This content is the result of information processing in the brain. Watching visual scene A, for example, is specific and subjectively different from watching visual scene B. This is the representational aspect of qualitative consciousness. However, information processing is not identical to qualitative consciousness. Whereas consciousness always implies a processed content, information processing in the brain does not necessarily imply consciousness (Fig. 1B). Precise calculations needed for the adequate recruitment of muscles during complex motor tasks are conducted without the involvement of consciousness. Other examples are the unconscious use of grammatical rules during the generation of speech and the unconscious hypothalamic contribution to the regulation of vegetative homeostasis.

Taken together, a scientific model of the mind would comprise an explanation of information processing and an explanation of qualitative consciousness.

Physical monism. Most neuroscientists nowadays (including me) are confident that it is in principle possible to construct an explanatory model of brain functions on the basis of natural science which eventually also includes the mind as the “highest” function of the brain. This is based on an axiomatic view of the world called “physical monism” which states: “Necessarily, all things with mental properties are also things with physical properties” (Crane, 2000). In other words, physical monism holds that the mind is generated by the brain and that, like all other properties of the physical brain, the mind can be subjected to the explorative methods of natural science.² The concept of physical monism has gained strength with the expansion of neurophysiological research which revealed countless correlations (not yet explanations) between mental events and processes in the brain. Simple examples, which may support the view of physical monism, are the obvious and reproducible causality which psychoactive

² The opposite view, dualism, claims that the mind is non-physical, belonging to a separate ontological category.

substances like drugs or anesthetics have on the mind, or the functional magnetic resonance imaging which confirms a physical correlate for all kinds of mental activity. Taking for granted the unity of nature, a problem remains for physical monism: Does a shared ontological basis also guarantee that there is a way to describe both, the mind and the brain in a unifying model? In addition, if so, can and should this model use the terms and equations of physics? The basis for these questions, which physical monism has to solve for a coherent model of brain functions, is emergence.

Emergence is a property of complex systems and denotes the fact that a system as a whole has additional properties which none of its constituting parts have (Bedau, 2003). Emergent properties can, in turn, influence in a top-down manner the parts of the system. A biological example is a bee colony which builds a hive with rooms for nurseries and food storage. A single bee is not able to do so but profits itself, in terms of survival, from the community. As complex systems can be a composition of subsystems, there can be successive levels of emergent properties which are based on top of each other. "The behavior of large and complex aggregates of elementary particles, it turns out, is not to be understood in terms of a simple extrapolation of the properties of a few particles. Instead, at each level of complexity entirely new properties appear (...)" (Anderson, 1972). Emergence is a consequence of the organization of the parts of a system, the kind and the degree of their specific interactions, reaching beyond structural aspects of the parts (for organization in biological systems see [Rosen, 1985]). Emergence is not a matter of the size of a system. It is observed in systems from the scale of elementary particles, where emergence can be related to the physical concept of symmetry breaking (Anderson, 1972), over the scale of living organisms where emergence seems to be abundant, to the scale of the universe which as a system is believed to have a fate different from the fate of its parts.

Special sciences and the brain. The layered structure of naturally occurring biological systems is reflected in the layered structure of the sciences describing them. The existence of hierarchical emergent phenomena within a biological system causes discrete levels of description, at least in the initial stages of scientific exploration when the interrelations of levels are not yet understood. This principle holds true for neuroscience, too. The brain is a composed system whose components, networks of cells, themselves are complex systems. In addition, it is an open system in terms of energy transfer and information flow, a regulator circuit system with non-linear feedback loop effects, an anticipatory system in its interaction with the environment, and a self-organizing system with respect to its plastic encoding of events. Hence, the scientific explanation of the brain has to deal with several levels of emergence.

Starting with the level of particle physics, an imaginary ladder of "special sciences" (Fodor, 1974) dealing with the brain continues in the bottom-up direction with the disciplines of many body physics, chemistry, organic chemistry, biochemistry, molecular biology, and cellular

biology including single cell electrophysiology. A neuron as a cell has emergent properties which biomolecules do not have. An example is the membrane potential including the possibility for the neuron of generating an action potential or staying subthreshold, providing this cell with the signaling capability of a binary state. On the next rung of the emergence ladder, interconnected assemblies of neurons, in turn, have functions which single cells do not have, like the reception of sensory input patterns or the plastic formation of simultaneously active populations of cells. From these examples it becomes clear that what we consider to be the “highest” brain functions at the top of the ladder, cognitive abilities, attention, consciousness, and behavior are only some of the brain’s emergent phenomena in a long row. Consciousness might be the most interesting emergent phenomenon, as it seems to constitute a distinct dimension not observed elsewhere in the physical world, but it is by no means the only one.

Independent vocabularies. The fragmentation of the description of the brain provided by neuroscience reflects the hierarchical nature of emergent phenomena in the brain as a system. Different levels of emergence have had distinct starting points for research and theorization in the past and have generated sub-models of the brain, or parts of the brain, of their own. Due to the diverse nature of emergent phenomena, each level of description has developed its own vocabulary for its respective paradigm, its own assumptions of how to reverse engineer the brain, and its own hierarchy of findings. Therefore the type of notations and terms differ to a large extent between the disciplines of neuroscience.

Bridge laws. Of course, the goal of neuroscientists remains to find a more integrative and complete explanation of higher brain functions. To be coherent, such an overall explanatory model should account for observations at all levels of emergence and exhaustively define their conditions. The way to reach this goal is to connect the existing levels of description by applying rules, commonly called “bridge laws” (Nagel, 1961), which tell how to express the model of one level in the vocabulary of another level’s model. This translation renders emergent phenomena better intelligible, as long as it is well understood how to use the deployed vocabulary (Crane, 2000).

Bridge law example. One important bridge law in neuroscience is the model of the action potential established by Hodgkin and Huxley (Hodgkin and Huxley, 1952). The story of its tremendous success is in no small amount based on the bridge between the level of electrophysiological properties of excitable cells (membrane potential) and the lower level of properties of molecular structures (activation and inactivation of voltage-gated ion conductances³). Translating cytological vocabulary into the precise and well-established

³ Interestingly, the biomolecules realizing the conductances predicted by the model as well as their conformational changes and related open probabilities were discovered only years later.

language of electrical circuits (in this case build by biomolecules) made the action potential much more understandable. On the one hand, the Hodgkin and Huxley model exemplifies how the organization of parts of a system (cell membrane, concentration gradients of ions, voltage-gated ion channels, ion pumps) generate an emergent property of the system (the action potential) and on the other hand, again, how this emergent phenomenon changes the behavior of the parts of the system (opening of voltage-gated conductances; “downward causation”). Differing structures of sub-models, which have been defined independently of each other, can make it difficult to find appropriate bridge laws. On the other hand, vocabularies might be harmonized once they are traced back to each other by bridge laws.

1.2 The explanatory gap

The most peculiar remaining difference in the vocabulary for brain functions can be found between sciences, which investigate the abilities of the mind in a non-invasive way manipulating the brain only with natural sensory stimuli and evaluating behavioral responses, and sciences, which use invasive methods including direct, physical manipulation of the brain as a constitutive part of the experimental setting.

The non-invasive approach. The empirical, but non-invasive approach of (cognitive) psychology and psychophysics uses what can be observed from outside the brain of tested subjects and what regularities can be derived from introspection. It builds models which describe the performances of the brain without including biological mechanisms. This approach is the only one up to now to collect and list the abilities of the mind. Models obtained by the non-invasive disciplines of neuroscience often use vocabularies close to natural language. They mainly define the interest of the public for brain research and tell the invasive neuroscientists what needs to be explained at all and what the borders of the scope are. They also can tell from measurements of response latencies what the brain in general must be able to compute within which time. However, they cannot explain how this is done in terms of biological implementation.

The invasive approach. The other and invasive approach of neurophysiological research, in contrast, tries to find the mechanisms by which the biological brain accomplishes these performances. For this, it has to study and to interfere physically with the internal parts of the brain. It is important to mention that, according to this classification, EEG/MEG and fMRI techniques, which are non-invasive in a surgical sense, belong to the “invasive” approach as they directly measure physical signals generated by the brain.

Definition of the explanatory gap. Due to radically differing methodologies, paradigms about the brain and vocabularies of models differ widely between non-invasive and invasive approaches. This is the reason why we still lack an explanation of the mental in terms of the physical (Levine, 1999). To date it is not clear at all how the vocabulary of mental functions including

consciousness could be translated into the highly differing vocabulary of neurophysiology. How can the mind be an emergent property of matter? This ongoing epistemological incommensurability constitutes the classical “explanatory gap” of neuroscience (Levine, 1983; Fig. 2A). It is the modern, monism-based form of the mind-body-problem that philosophy has been dealing with for millennia.

Upholding physical monism. Reading the literature one gets the impression that it is impossible to overcome the explanatory gap. The perplexity about it seems to be so overwhelming that philosophers of mind often raise it to a metaphysical problem and don't dare to ask for an experimental, evidence-based answer anymore. Also researchers tend to assign a status to the mind which is fundamentally different from the one of the brain, in this way openly falling back to dualism (e.g. Popper and Eccles, 1977), or avoid explaining the mind at all. Physical monism is defended in two ways against such fallacies. One way is by claiming that there is no explanatory gap. In this view, mental and neurophysiological vocabularies indicate the very same thing and the less precise of them (the mental vocabulary) could be discarded (Papineau, 2003). "Having feelings is just what it is to be in certain material states, when we are in those states. Once we fully accept this, and stop sliding back into dualism, then we can stop looking for any explanation of why those states are what they are." (Papineau, 1998). In my opinion, this “eliminative” approach has a weak point. It doesn't account for the fact that the current vocabulary of the mental (“having feelings”) refers to the highest level of emergence whereas the current vocabulary of neurophysiology belongs to the lower level of single cell physiology (“material states”). It is ignored that both vocabularies are non-overlapping in their subject-matter and in this sense are not just different sides of the same coin. At least for now, eliminating the psychological vocabulary doesn't make the emergence of cognition and consciousness more intelligible at all. Therefore there is a continuing interest in understanding the mind using terms of the underlying neurophysiological vocabulary. The explanatory gap remains.

The other way to uphold physical monism is simply to continue looking for new bridge laws, for new ways of bridging the explanatory gap. “The current absence of a compelling argument for a link between the brain and the conscious mind cannot be taken as evidence that such a link does not exist.” (Koch, 2004, p. 6) – “The explanatory gap argument doesn't demonstrate a gap in nature, but a gap in our understanding of nature. “ (Levine, 1999). In this context, Levine further suggests to look for a reason for the explanatory gap, to ask, why it is so difficult to unite the disciplines describing the biological brain with the disciplines describing the mind.

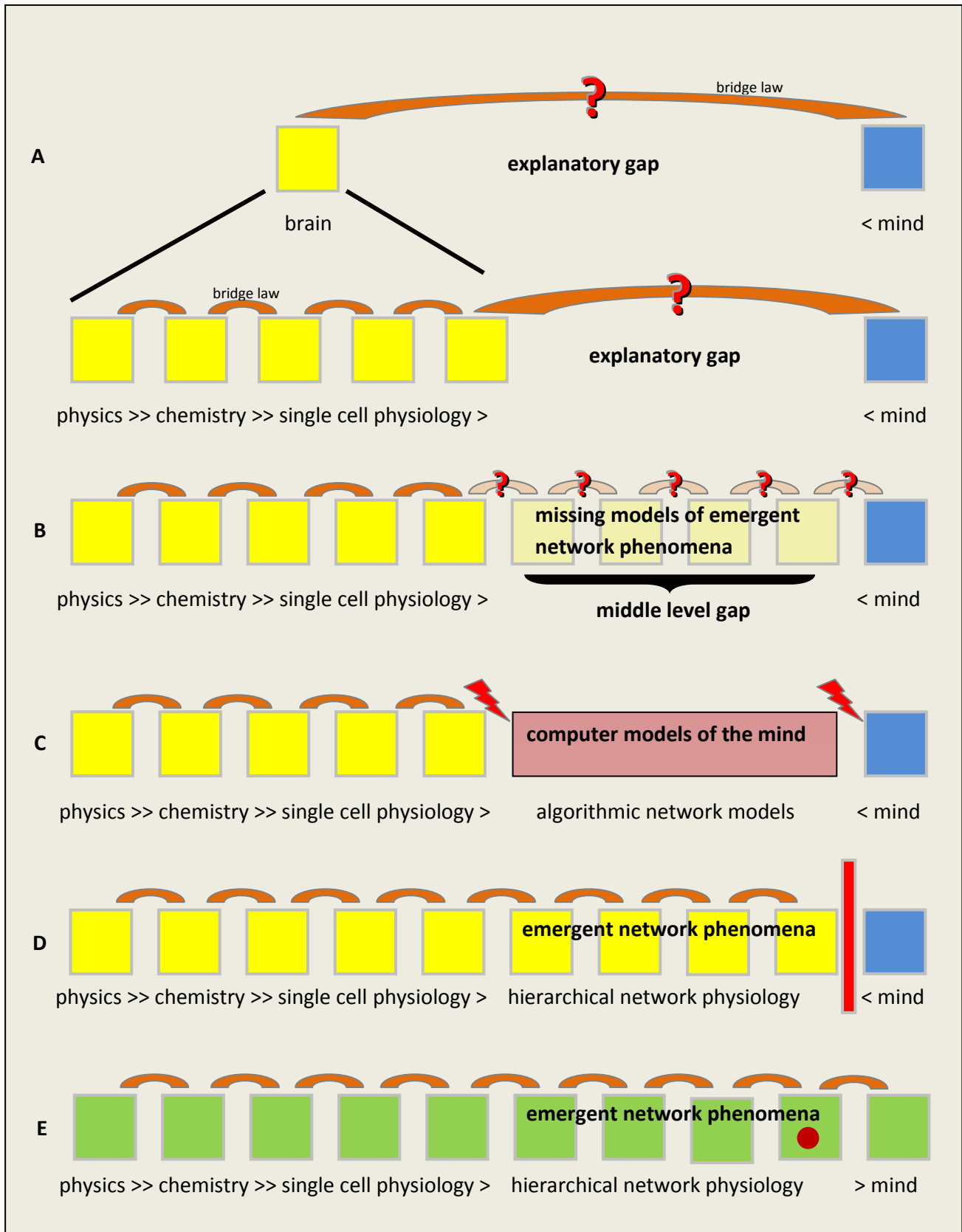


Fig. 2. Toward an unified model of brain and mind.

A) *Upper row:* The explanatory gap in the philosophy of mind denotes the lack of any useful vocabulary which explains the mental in terms of the physical (Levine, 1983; Levine, 1999).

Lower row: The ladder of special sciences used to describe the hierarchy of emergent properties in the brain. At present, on the left side of the explanatory gap the highest well-established paradigm is physiology of neurons as excitable cells, and on the right side observable mental phenomena including cognitive abilities and consciousness. I propose that the fact that it seems to be intractable is due to the “explanatory distance” between these domains.

B) The explanatory distance can be reduced by filling in the “middle level gap” of neurophysiological knowledge. The middle level gap comprises an unknown number of levels of emergence within the domain of network activity of brain cells. Only invasive brain research can identify these levels and describe them. The “explanatory distance” of the intermediary explanatory gaps, which remain afterwards between neighboring levels of emergence, will be minimized (small question marks). This way finding bridge laws between paradigms can be expected to become easier.

C) The computational theory of mind, which had a high impact in the philosophy of mind in the 20th century pretended to fill the middle level gap, but does not provide a theory of how mental functions are actually implemented in the brain. Although its successor, connectionism, offers a more plausible bridge to the single cell level (networks of artificial neurons), a notion about the emergence of mental functions is completely missing.

D) Once the phenomena on the so far missing levels of emergence are described by invasive neuroscience, initially bridge laws still could be hard to establish. Incommensurability (vertical red bar) might remain between vocabularies. It is an open debate whether in this case a scientific revolution (Kuhn, 1962) would be needed which could require a new kind of application of current physics or even a new extension of fundamental physical concepts.

E) Taking physical monism for granted, in the end a unifying theory of the brain should be achievable which explains both, biological activity as well as mental functions, linking formerly separate vocabularies by means of appropriate bridge laws. To use natural language as far as possible, the explanation of the mind in terms of network activity will probably be based on the vocabulary of the highest level of emergent phenomena in the neurophysiological domain (tagged with red dot).

1.3 The middle level gap

I propose here that the key is hidden in the notion that the explanatory gap is not a matter of missing bridge laws between an already entire model of mental brain functions on the one hand and a coherent neurobiological concept of brain functions on the other. Rather, the explanatory gap lies between an apparitional model of the mental and an incomplete sketch of neurophysiology. It is important to underline that already *within* the domain of invasive neuroscience the model of the brain is highly fragmented and that a large gap of missing knowledge is located solely within the neurophysiological domain. So far, in the chain of emergent transitions observed in the brain, the highest level for which neurophysiological research provides an established paradigm is the (electrical) activity of single cells. Already on the next highest level, the level of activity of cellular networks, the number of emergent steps and the kind of emergent mechanisms are unknown. It is obvious that a unifying explanation of brain functions has to fail when looking for a direct bridge between single cell behavior and mental functions. The scope of network activity matters. Most likely, there is more than one functional level of emergence contained within the domain of network activity, for which no neurophysiological model exists (Fig. 2B). The existence of several histological scales in cellular networks (microcircuits, layers, nuclei, long-range connections of gray matter) fortifies this assumption. In the following, I will refer to the whole range of lacking scientific concepts within the layered model of physiological brain functions as the “middle level gap” (Fig. 2B).

Proposed relation between explanatory gap and middle level gap. If emergent properties of a system are hierarchical in that an emergent property depends on subordinate emergent properties, it is likely that a model of the system requires a kind of multi-level explanation. One needs a vocabulary for the phenomena exactly one level down in the hierarchy of emergence in order to use it to explain the upper level of organization (“hierarchical reductionism” [Dawkins, 1986]). This view makes plausible why the explanatory gap in its present form seems to be so intractable. The particular level of emergence needed to explain mental functions, i.e. the highest level of activity directly below the mental level, is simply not yet known. The necessary chain of emergent phenomena is interrupted by the remaining middle level gap. The “explanatory distance” between current models of the mind and current models of the physical brain, defined as the number of intermediate missing levels of emergence, might be simply too large. This distance cannot be bridged directly by rules of translation in any meaningful way.

To sum up, I propose that the existence of the explanatory gap between mind and brain, which is an epistemological matter of explanation and missing bridge laws, mainly rests on the middle level gap, which is just a matter of lacking neurophysiological models for levels of emergence contained in the functionality of cerebral cellular networks⁴ (Fig. 2A-B).

1.4 Necessity of invasive research on network activity

Assuming this, bridging the explanatory gap and establishing a unified theory of neuroscience, is a two-step process.

Step one: Filling in the middle level gap reduces the explanatory distance. The first step is filling in the middle level gap with new paradigms for the missing layers of emergence, which all are situated within the scale of networks of brain cells and their activity. This step necessarily requires invasive neurophysiological research (invasive in the sense as defined in section 1.2). The reason is that there are no rules about how to derive emergent phenomena from lower levels of a system in a theoretical way, when the particular principle of system organization is unknown. As Anderson puts it, “The ability to reduce everything to simple fundamental laws does not imply the ability to start from those laws and reconstruct the universe” (Anderson, 1972; cf. Simon, 1962; cf. Koch, 2004, p. 11)]. In the case of brain functions, it is not possible to infer theoretically the missing emergent phenomena on the level of network activity in a bottom-up manner from single cell physiology, even if single cell physiology can be used to explain them once they have been found. Similarly, philosophical attempts without evidence from experimental research have to fail. In the words of Koch, “Philosophical arguments, based on logical analysis (...) are not powerful enough to deal with the real brain with all of its subtleties in a decisive manner. The philosophical method is at its best when formulating questions, but does not have much of a track record at answering them.” (Koch, 2004, p. 7). Thus, precise experimental characterization of the specific interactions of brain cells is indispensable for identification and mapping of the missing emergent phenomena on the level of network activity.

⁴ Here I avoid the term „neural networks“ as glial cells might crucially be involved.

Step two: Bridging adjacent levels in the completed hierarchy. As a result of the first step, the original explanatory gap would be replaced with intermediary gaps of minimum explanatory distance, situated between single cell phenomena and network phenomena, network phenomena and next higher network phenomena, and highest network phenomena and mental phenomena (Fig. 2B). In the following second step, adjoining bridge laws have to be found to connect the paradigms of the completed set of emergent levels (Fig. 2E).⁵

Whether a unified model will be possible is an empirical question. Step one has to be done before step two. The answer to the question “Will scholars in the end be able to conclusively explain mental functions in terms of brain physiology?” can only be given empirically after a full description of missing emergent network phenomena has been completed. This is not a matter of philosophy. With the current knowledge about the network level of brain activity, the discussion whether the explanatory gap really implicates a “hard problem of consciousness” (Chalmers, 1995) is pointless. First of all, further invasive research on the connectivity and activity of cerebral networks is needed to describe them thoroughly and to extract anchor points and hints for emergent functions. When this is achieved, there are two possibilities.

a) As soon as the mid-level gap is filled, the explanatory gap dissolves easily as bridging principles (of the Hodgkin and Huxley model type) immediately become obvious. The goal is reached (Fig. 2E).

b) Even with completed paradigms about the intermediary levels of emergence, bridge laws initially remain hard to establish. Even when then the explanatory distance is as low as possible, it still might be large for the intellectual power of humans. Then the vocabulary of the highest plane of network physiology initially could remain unlinked to the vocabulary used for mental experience (Fig. 2D). If this incompatibility of levels would persist (despite their apparent completeness), an improved redraft of paradigms would be necessary to finally achieve the successful translation between the vocabularies (Fig. 2E). It is a matter of debate whether such a scientific revolution (Kuhn, 1962) will be necessary and whether it will require further development of established physics. Koch and Hepp suggest that classical physics is enough to prepare the ground for the explanation of the mind (Koch and Hepp, 2006). Penrose and Hameroff postulate the requirement of a deeper utilization of quantum physics (Hameroff and Penrose, 1996), and Chalmers even calls for an extension of current physics adding subjective

⁵ This two-step process implies an interesting aspect for the publication policy of scientific journals. Research articles, which try to explain an emergent phenomenon by speculating about bridge laws to a lower or higher level of emergence, often seem to be ranked higher than comparable articles, which simply describe the phenomenon. However, if bridge laws only can be established when the model of an emergent phenomenon is coherent and mature to a certain degree, the precise description of a phenomenon is valuable per se in the first place and should have the same impact as “a good story”, especially in the case that the explanatory story uses crude bridge laws.

experience as a new fundamental entity of the universe like mass, charge, or space-time (Chalmers, 1995).

1.5 What is the desirable vocabulary for a unified theory of brain and mind?

When bridge laws eventually interconnect all level of emergence, the challenge for the all-comprising model of neuroscience will be to explain brain and mind consistently using a single vocabulary. Which of the established levels of description should be chosen then to represent cognitive functions and consciousness in the most intelligible way?

Reductionism. According to strong reductionism, the relations on a higher level of scientific description are special cases of the laws governing the lower level and can be “reduced” to them (Nagel, 1961). Because of this principle, by sequential application of hierarchical bridge laws all brain-related phenomena including the mind ultimately could be described using the terminology of particle physics. The existence of emergent properties in organized systems does not conflict with this concept of strong reductionism because emergent causal powers in a system can consistently be explained from the causal powers of lower level components (Anderson, 1972; Bedau, 2003).

The desirable vocabulary is context-dependent. Assuming it has become *possible* to adopt the formal language of physics in giving an account of the mind, the question arises whether it is also *desirable*. If the focus is to unify natural science, the answer would be positive. Reforming the fundamental theories of physics in a way that the functions of the brain, including the mind, can be represented in equations, would be an impressive unification of science. However, if the claim is comprehensibility or practicability, the answer is probably no. The lowest-level explanation of a natural phenomenon, even if it exists, is not the best way to understand it (this argument is used to criticize “greedy reductionism” [Dennett, 1996]). Physical equations tend to lack an intuitive interpretation. In addition, the equations which were needed to simulate the brain as a many-particle system could just not be solved. Not even the behavior of a protein can be fully modeled to date using the equations of quantum mechanics (Besley, 2007), not to mention cells. Taken together, a physical model of the mind probably would lack both, an intuitive way to understand it and practical applicability. Furthermore, from a philosophical point of view, physics has no explanatory priority per se over other vocabularies given the justifiable autonomous interest in emergent phenomena (Anderson, 1972; Crane, 2000).

Following hierarchical reductionism (Dawkins, 1986) I assume that whenever non-mental vocabulary will be called for to give an insight to the underlying mechanisms of cognition and consciousness, the vocabulary of the highest level of emergence within the domain of network activity of brain cells will be used (the one labeled with a red dot in Fig. 2E). Such an explanation can be expected to be the most understandable because it stays closest to everyday language. Nevertheless, it will be sufficient to translate mental vocabulary into neurophysiological

vocabulary. At present, the kind of scientific vocabulary for this level cannot be predicted because this level, as discussed earlier, is part of the middle level gap.

In other cases, the vocabulary in which cerebral activity is expressed probably will depend on the context. In the context of medical drug effects, for example, the reduction to molecular biology and receptor-mediated signal transduction might continue to be the most illustrative solution. In the context of pedagogics, the usage of classical psychological terminology about motivation might remain more appropriate than neurophysiology. In general, restricted concepts of today's neuroscience might stay in use despite a unified theory, as Newtonian mechanics easily survived quantum mechanics.

2 Technical and theoretical background of research on network activity

A unified explanation of brain and mind, as we have seen, needs a more complete description of the concerted activity of networked cells, which only invasive research can explore. However, evidence from experimental studies about the details of network activity is still sparse in comparison, for example, to the knowledge about single cell activity. One reason, for sure, is the limited availability of suitable methods. Another reason, as I will try to make plausible, is self-imposed restraints of the theoretical framework which is the basis for the design of experimental studies. Both, technical limitations and “paradigmatic preoccupations” have to be resolved to make experimental research on network activity more progressive.

2.1 Technical constraints

For the detection of emergent properties in the patterns of network activities both, the anatomical connectivity and the physiological interactions between classified cell types has to be known in detail. Despite large advancements of techniques, this important low-level map of the brain is not yet completed.

The anatomical requirements include the number and subcellular location of synaptic and junctional contacts as well as the spatial arrangement of defined cell types which is important for the understanding of their non-synaptic biochemical interactions via neuromodulators and cytokines. However, despite advanced genetic and immunohistochemical staining methods and the recent progress of electron microscopy techniques allowing for a reconstruction of millimeter-scale brain histology with subcellular resolution (Briggman and Denk, 2006), the puzzle of ultrastructural anatomy is not yet solved. To name a few problems, computerized image processing and 3D reconstructions from spaced slices, exact localization of subcellular structures like synapses, and automated classification of cell types due to their morphology remain a challenge.

On the physiological side, a genuine model of network level activity depends on methods which provide population dynamics with single cell resolution. At the same time, the involved cell types and their connectivity should be known. Multi-cell patch-clamp recordings have expanded the field of single cell electrophysiology, which provides high temporal resolution, to the scale of microcircuits, revealing local connectivity and circuitry activation rules. State-of-the-art examples are the study by Lefort on the cerebral cortex of mice (Lefort et al., 2009) and the study by Molnár on human tissue (Molnar et al., 2008). Optical imaging techniques provide network activity patterns with cellular resolution for larger populations in the range of hundreds of cells (Cossart et al., 2005; Maclean et al., 2005). Genetical staining methods allow for the identification of at least one cell type during experiments. So pieces are constantly added to the puzzle. The available methods complement each other. However, even in combination, their power is still limited. The largest constraint is that the synaptic connectivity of more than a few cells cannot be determined at the same time in order to relate it to the measurements of network activity. The insufficient temporal resolution of large-scale imaging methods, which are able to show many cells at the same time, is another obstacle. Finally, the full power of many methods is not available in vivo, where natural stimuli can be applied to the brain (discussed in [Neubauer and Berger, 2008]). Other methods like EEG, MEG, PET, and fMRI approach brain activity on a global level. To date, they are the only ones yielding biophysical signals caused by network activity, which can directly be correlated with the time course of mental activity in humans. The most important contribution to the knowledge about network activity is that they report the (coarse) topographic localization of network activation. The spatio-temporal sequential changes can be analyzed concerning their temporal relation to mental tasks and their spatial relation to specialized brain areas. These remain pure correlations between different levels of emergence, but these correlations afforded by EEG and fMRI are very likely to be important for the framing of bridge laws between mental functions and network activity in the future. However, because these methods do not yield cellular resolution, they do not add directly to the knowledge about the mechanism of emergence in cellular networks.

Taken together, experimental methods have to be developed further in order to reveal the spatio-temporal sequence of cellular activation in defined networks with sufficient precision to reveal anchor points for emergent properties. In addition, as we will discuss later, methods might need to be optimized for the detection also of other types of activity than electrophysiological.

2.2 Constraints within the theoretical background of network activity

Experimental research also builds on theoretical assumptions to make a choice about the questions to focus on, the methods to use, and the way of how to deal with findings. Observation is always “theory-laden”(Hanson, 1958) and in that scientific success depends also on theoretical considerations of what should be looked for and what could be expected to be found. To quote from a lecture by Louis Pasteur: “In the fields of observation, change favors only the prepared mind.” The attention of researchers who evaluate their measurements is primed towards what they are ready to expect. In the best case, research advances in a circular improvement of experiments and results: experimental data are used to infer a preliminary model; this model is used to improve the methods and to design the next round of experiments and so on. This principle holds true, of course, for research on network activity. However, because experimental evidence from the network level has been very sparse in the past due to limited methods, same-level models of network activity could not be established. As a replacement, so to speak, less evidence-based and more hypothetical theories were developed, which tried to explain properties of the mind without knowledge about the particular mechanisms of emergence on the level of network activity. In the following part, I want to introduce two such theories, the “computational theory of mind” and the more recent “connectionism”. The computational theory of mind tries to stay within the level of the mind to explain its rules, avoiding the question of how it emerges from network activity, and denies the importance of this question by pointing out the “multiple realizability” of the mind (making its actual “implementation” less important). Connectionism, in contrast, builds on observations from single cell anatomy and physiology and tries to extrapolate from this lower level of emergence to the level of network activity. Both theories were very powerful in coining basic paradigms about the information processing aspect of the mind in the past. Having outlined these theories, I will argue that paradigms related to them are still predominant in neuroscience in the sense that they strongly influence experimental research on network activity and the development of methods in the laboratories. I think that these paradigms restrict the view of which kinds of emergent properties can be expected in network activity and thereby are likely to slow down experimental advancements in the field. Therefore I will propose to use a less restrictive framework as a theoretical background for experimental research on network activity.

2.2.1 Established models of the mind

Computational theory of mind.

Following the "cognitive revolution" in the 1950s in response to behaviorism which tried to completely avoid descriptions of mental processes, an intellectual movement later coined "cognitive science" developed a "computational theory of mind". This theory directly implicates a computer model of the brain and emphasizes the aspect that mental activity is information-processing (Horst, 2008; Thagard, 2008; Fig. 1). One primary aim of the founders was to be able to talk about independent rules and structures of mental processes without being forced to directly relate them to behavior in a reflex-like manner. Based on work of Hilary Putnam (Putnam, 1980) and Jerry Fodor (Fodor, 1975, 1994) cognitive tasks like perception and thought are regarded as rule-based manipulations of formal symbols, i.e. as syntax-based information processing. The symbols represent properties of the environment or of memories. Accordingly, the human brain is seen as a computer, whereby a computer is defined as an universal information processing system or an universal Turing machine (Turing, 1937). The concept of universal Turing machines implies the concept of "multiple realizability" (Putnam, 1967; Fodor, 1974) because a universal Turing machine can be technically implemented in any way. Its implementation in hardware is irrelevant for its function on the level of symbol manipulation. Consequently, the brain is seen as just one possible implementation of a universal Turing machine as it is any (serial) computer. In an interplay with the field of artificial intelligence and computer science, it is assumed that mind and brain are related to each other like software and hardware. Due to this reduction of the mind to rule-based information processing, mental functions are described on an abstract level without knowing their implementation in the biological brain at all. The internal "meaning " of a current state of the mind is defined only functionally, insofar as it deterministically causes the transition from this state to a defined next state, like in a Turing machine. Fodor suggests which algorithms the brain actually uses in his draft of a "Language of Thought" by deriving from non-invasive observations of mental tasks (Fodor, 1975). Furthermore, in the computational theory of mind "strong" artificial intelligence is claimed to be possible: As rational processes of the human mind are completely algorithmic, it is technologically feasible to copy the software of the mind into suitably powerful hardware, and such a simulation will lead to truly intelligent computers (Minsky, 1982). The computational theory of mind also has an implicit strong link to linguistics, as grammars can be treated as a collection of syntactical rules for building sentences from words which are symbols. Like Putnam, the linguist Chomsky advocates for a rule-based level of cognitive mechanisms below the surface of behavior (Chomsky, 1966). A similar interdisciplinary link exists between the computational theory of mind and the field of mathematical logic.

Taken together, it was attractive to adopt the vocabulary used for computers and other rule-based systems, which can be well understood by humans, for the mind. As a consequence, the computational theory of mind became a very strong paradigm in 20th century.

A significant aspect in Shannon's model of information is that the actual message is one selected from a set of possible messages, which correlate to a finite set of alternative states of the source (Shannon, 1948). An important weakness of the computational theory of mind is that it is based on this definition and therefore a symbol which carries a piece of information has to be one out of a predefined set. However, real sensory experience in an open environment is never a selection from a set of predefined experiences. The computational theory of mind drives the analogy between computers and the brain too far. Categorization of patterns due to similarities as well as the concept of generalization are not within its scope.

Connectionism.

This problem was solved with the advent of connectionism (McCulloch and Pitts, 1943; Garson, 2008). In contrast to the computational theory of mind, connectionism does not distinguish between hardware and software anymore. Information is represented sub-symbolically in the weight, or strengths of (synaptic) connections between neurons in an (artificial) network. In addition, the definition of information is less restricted as now the requirement of a limited set of predefined patterns is abandoned and input patterns can be continuous and of infinite number. In the connectionist model of the mind, a specific state of information processing can be implemented as the activity of a specific assembly of neurons within the network. This population coding releases connectionist model from requiring mechanisms to copy information from one location (analogy: static memory) to another location (analogy: processing unit or working memory). Information is now transformed from one into the following state by recruiting previously inactive neurons into the active assembly or releasing active neurons from the assembly. All kinds of information processing can be realized in connectionist models, including such ones which are not associated with symbolic or language-related representation at all, e.g. sensory-motor skills. Approximations, generalizations, and reaction to previously unknown input are possible, a potential which the computer model cannot provide. The objection of proponents of the computer model and of linguistics that explicit knowledge needs language, and language needs symbolic representations, is rebutted by connectionism in the following way. Neuronal networks can be shown to have at least the computational power of universal Turing machines (Siegelmann and Sontag, 1995). In addition, neuronal networks can learn categories from input patterns (Kim et al., 2008), and distinct categories in fact play the same functional role as symbolic abstractions. Thus neuronal networks actually have the power to realize abstract forms of information representation including processing of symbolic items according to explicit logical and syntactical rules. But they do so only when this is needed, for example in the case of language requiring a defined encoding system for the exchange of messages between subjects, or in the cases of logical thinking and mental calculation. Even then, the symbolic meta-level is realized on the very same basis of synaptic plasticity and distributed weights in neural network as the processing of non-symbolic, implicit information is. Taken together, connectionism can claim to comprise and implement the computer model of

the mind (cf. Fodor and Pylyshyn, 1988; Garson, 2008) but at the same time to provide more degrees of freedom for information processing.

What have both theories, the computational theory of mind and connectionism to say about the emergence of a) information processing and b) qualitative consciousness from network activity in real brains?

a) Implementation of information processing.

About the biological implementation of the mental aspect of information processing in real brains, the computer model of the mind does not (and in its orthodox form of functionalism does not want to) provide any theory. Its vocabulary stays on the level of the mind and relies on observations of the non-invasive disciplines of psychology and linguistics. How cerebral network activity could run the algorithms of the mind remains completely unexplained. Accordingly, the computational theory of mind also cannot offer any bridge laws in order to link its vocabulary of mental algorithms to the vocabulary of single cell physiology (Fig. 2C).

In this respect, connectionism is stronger. It adopts the concept of a neuron as the elementary network units from single cell physiology and shows that information processing actually can be implemented using networks of artificial neurons. The principles of network activation in the model are the equivalent to a bridge law between single cell activity and network activity. Thus, the emergence of information processing from network activity would be explained. However, connectionism severely suffers from the fact that no rules exist how to infer a higher level of emergence from the laws for the parts of a system. As the level of single cells does not imply the principles of emergence on the network level, connectionism necessarily depends on speculative assumptions about wiring rules and reward mechanisms. Being dependent on such ad hoc hypotheses, models of neural networks are not decisive. A modern branch of connectionism, called “computational neuroscience”, strictly tries to use only experimental data to implement “neuromorphic network” models of information processing which fit the best way possible to neurophysiological observations (Sejnowski et al., 1988). It aims for a “true” model of information processing in the brain in contrast to just conceivable or computationally possible other models. However, even the most biologically accurate neural network model, as long it is fed with input from the level of single cell physiology, cannot generate by itself the rules of networks and thus continues to depend on hypothetical assumption. As a consequence, the main problem for connectionism is that multiple realizability is still possible. Still neural networks of different architecture can solve a given task of information processing or be tuned to good agreement with neurophysiological observations. In such cases it is not obvious which of the possible models is closest to the real brain’s architecture and function.

Taken together, both theories are unsuccessful in predicting which kind of emergent properties of network activity implement information processing in the brain.

b) Implementation of qualitative consciousness.

About qualitative consciousness as the second basic emergent property of the mind (Fig. 1) both, computational theory of mind and connectionism, widely stay silent. Associated with the name of Baars, cognitive science started to deal with consciousness (Baars, 1988). However, his “Global Workspace Theory”, which is closely related to models of working memory, is concerned only with the functional aspect of consciousness, showing that in this model the existence of consciousness can improve information processing. It misses the qualitative dimension. Other attempts were made by cognitive scientists to explain qualitative consciousness as a sort of meta-representation of representations (Carruthers, 2008), but adding additional algorithmic layers of symbolic (self-) reference of the same kind does not explain the emergence of qualitative consciousness. Paraphrasing the “Chinese Room argument” by Searle, the qualitative aspect of consciousness cannot be the result of a calculation, not even of the most sophisticated one (Searle, 1980, 1992). Concerning consciousness, connectionism has nothing to add. It can offer the implementation of more sophisticated algorithms, but no concept for an additional mechanism of emergence.

As a consequence, neither theory of the mind introduced here provides cogent predictions for the study of network activity with respect to either the emergence of information processing or qualitative consciousness.

2.2.2 Paradigmatic preoccupation

Why do I claim then that this theoretical background is a confinement for experimental research on network activity? In the worst case, the abovementioned theories should be useless for design of experiments and methods, maybe not helpful in the context of research, but neutral. My answer is that they have led to a “paradigmatic preoccupation” which implicitly confines the kind of questions asked in the labs. As hypothetical models with intrinsic logical plausibility they have taken the position of the missing emergent phenomena on the network level in the model of the real brain (Fig. 2C). The resulting illusion is that the middle level gap is filled. Only one level of emergence seems to be left to be described in order to explain information processing in the mind. This illusion masks the perception that there may be several emergent levels missing in the model of brain functions (Fig. 2C vs. 2B). This, in turn, might diminish the efforts of researchers, who are engaged in the field of invasive brain research, to identify the missing levels of emergence and to find bridge laws. In this way theories, which initially were designed to learn more about the brain and the mind, seem to have caused axiomatic assumptions and thereby to distract researchers who set out to find the actual mechanisms.

The statement that there is this “paradigmatic preoccupation” in the community of neuroscientists clearly has to be labeled as my personal impression. Nevertheless, the conclusions I will draw from this might be helpful for the theoretical background of future network studies.

The credo of the preoccupied view of network activity in a short form could be, "Electrophysiological activity, including somatodendritic integration of synaptic inputs and action potentials, distributed over a network of neurons which are coupled by plastic synapses is sufficient to implement the emergence of information processing in the brain. Consciousness might be a meta-calculation on top of an unknown hierarchy of information processing, being based on electrophysiological activity as well, and representing selected information." I call Koch as a witness for the first sentence: „Unless some discovery dramatically changes the way neurobiologists view the way individual nerve cells work, action potentials traveling along axons and triggering synaptic events are *the* canonical means of quickly disseminating information within nervous tissue.“ (Koch, 2004, p. 36). In more detail, important elements of this often unsaid credo are the following.

Restriction to neurons. In line with connectionism, neuroscientists have a biased view to the parenchyma of the central nervous system. The definition that "Neurons are the atoms of perception, memory, thought, and action, and the synaptic connections among them shape and guide how individual cells are transiently assembled into the larger coalitions that generate perception" (Koch, 2004, p. 22) is shared by most neuroscientists today. I claim that this strong focus on the activity of neurons can mask crucial activity in additional cell types.

Restriction to electrophysiological activity, action potentials, and synaptic conductances. The computer-related theories of mind focus on the electrical phenomenon of the membrane potential. They suppress the possibility that other measurements like the concentration of molecules could carry information as well. Integrate-and-fire calculations are assumed to be the only relevant emergent phenomenon on the level of networks in the brain. Action potentials and their timing are assumed to be sufficient to implement digital information processing and even consciousness. The only open question seems to be which temporal relations of spiking patterns are essential to constitute the neural code (coincidence? synchronization? bursts? oscillation?) (Dayan and Abbott, 2001; Crick and Koch, 2003, p. 34).

Without historical proof, I think the success of the Hodgkin and Huxley paradigm of neurons as electronic circuits (Hodgkin and Huxley, 1952) supports a computer-centered model of the brain. Cells as the constituting components of brains are electrical circuits. The components of computers are electrical circuits. The basic unit of information in a computer is a binary digit, and neurons exhibit action potentials as binary states. How could a network of neurons be something else than a complex parallel computer? And if the algorithm which the mind uses to calculate has to be changed, e.g. after learning, adjustments of the synaptic weights in the axo-dendritic circuits will do the job. This is at least a standard conceptual framework for invasive research on network activity in the brain.

Restriction to one type of all-purpose neurons, exclusion of pathway coding. Integrate-and-fire models of neurons curtail the diversity of differentiated cell types. All neurons are considered equal. Only two types of neurons, excitatory and inhibitory ones seem to be enough. Differences in firing frequencies and transfer functions are the only properties needed to provide the basis for all emergent phenomena which might arise from network activity. Pathway coding of information, which is fully accepted for the peripheral nervous system, is rarely included in models of the central nervous system. As a consequence, multiple realizability of information processing still seems to be possible.

Restriction to “a single computational layer” of emergence. The paradigm of the computational theory of mind that the brain is a universal Turing machine suggests that there is only one level of emergence between single cell physiology and the mind, a level of computation, which the brain needs to solve all tasks of information processing. Once the single-layer mechanism of how calculation emerges is found, all computational abilities of the brain are expected to be explained, the middle level gap would be filled (cf. Fig 2C). The computational theory of mind virtually occupied the space of the network level of theories: Single cell electrophysiology underlies abstract computational networks which underlie the mind. This view masks the possibility that the neurophysiological activity in the brain, which is necessary for information processing, itself might comprise several or even many additional levels of emergence (Fig. 2B/E). As discussed earlier, the idea that mental functions are based on single cells mediated by only one emergent level of intermediary processes seems obscure.

I claim that the paradigmatic preoccupation sets a double snare for neuroscientists. The discussion about the explanatory gap hides the problem of the middle level gap. And when the mid-level gap is analyzed, a single-level, computation-centered model of the mind fills in the imagination and prevents the appreciation of and search for multiple levels of emergence.

Restriction to “a single shared hierarchy of emergence” for information processing and consciousness. Due to their axioms, both, the computational theory of mind and connectionism speak about qualitative consciousness only in terms of some special kind of information processing. However, as long as qualitative consciousness is thought to be dependent on information processing, not only with regards to its content but also with regards to its existence, the possibility of largely independent implementations for both mental aspects based on distinct mechanisms of emergence cannot be explored.

In a nutshell, the paradigmatic preoccupation seems to restrict the directions in which the experimental search on network activity is allowed to go on, thereby possibly delaying the progress of neuroscience.

2.3 Towards a less biased view of network activity

In contrast to the progress which established paradigms suggest, invasively validated models of real network activity are still in their infancy. Network neuroscience is in a pre-paradigmatic phase in the Kuhnian sense (Kuhn, 1962). In the following I will accentuate the need for a less restricted framework for the theoretical background of experiments on network activity. To find new anchor points for the detection of emergent mechanisms, the paradigmatic preoccupation should be given up in favor of a new impartiality of thinking. However, the price for letting go established doctrines and accepting that network research still is in the stage of “immature science” is high. But so is the benefit. The price is to lose the vocabulary of the purely electrical model of network activation, with electricity being a comfortably understood part of physics, and a computer-based model of information processing. The benefit is the freedom to make new and unconventional assumptions and to perform new kinds of experiments. If prematurely cemented models of network activity are put aside, conflicting models could be more liberally allowed to coexist until one earns the most credit of evidence. All aspects of the field could be assigned the same level of preliminary justification again. As a consequence, experimental research would not be less theory-laden, but the range of allowed theories which are applied would be increased.

2.3.1 Systematizing the search for correlates between brain and mind

In order to “free” network research, just qualifying old paradigms, of course, is not enough. In the following I try to sketch an unbiased framework for research on network activity. The boundaries of this framework have to be wider than the ones of the abovementioned paradigms, but they should not be arbitrary.

I propose to define the following boundaries as a less biased but systematic experimental guideline:

1) *All kinds* of low-level activities with appropriate time scales have to be checked to be a correlate of a mental activity.

2) *All kinds* of simultaneous mental activities have a correlate on lower emergent levels of the brain.

My approach builds on a method of Crick and Koch (Koch, 2004), which they use to investigate consciousness, and augments it. Therefore I will introduce their method first in a short outline.

The search for a neural correlate of consciousness.

A trivial consequence of physical monism is that changes in the mental domain must have a neurophysiological correlate on the lower levels of network activity. The whole can only change with its parts. Crick and Koch apply this rule to qualitative consciousness and can take the credit for re-promoting the issue of looking for low-level correlates of consciousness as a research program in the scientific community. They call attention to the fact that there must not only be correlates of information processing in the domain of network activity but also correlates of consciousness: "At any moment consciousness corresponds to a particular type of activity in a transient set of neurons that are a subset: of a much larger set of potential candidates." (Crick and Koch, 1990). Taking into consideration that there might be accompanying cerebral activity which is not directly needed for consciousness, their refined definition of the "neural correlate of consciousness" (NCC) is now "the minimal set of neuronal events and mechanisms jointly sufficient for a specific conscious percept" (Koch, 2004, p.16). From the observation that the content of consciousness excludes other conscious content at the same time, they predict that competing coalitions of neurons correlate to the specific content of consciousness (Crick and Koch, 2003).

Crick and Koch themselves point out that finding a full description of the NCC on the network level would not yet be equivalent to an explanation of qualitative consciousness. Repeating what I said about the explanatory gap, it would be only the first step, minimizing the "explanatory distance" from the insurmountable incommensurability between single cell activity and consciousness, which it is at present, shrinking it to a manageable explanatory distance between an elaborated model of network activity and consciousness. On this basis still the discovery of bridge laws would be needed as a second step, converting temporal correlations into causal explanations of how qualitative consciousness as a system property emerges from the parts of the brain.

The important simplification and generalization of the proposal by Crick and Koch in contrast to the predominant paradigms is to limit the predictions to the notion that mental activity has a correlate on the network level which can be found experimentally, without *a priori* assumptions about the causal mechanism of emergence. The only axiom needed is based on the safe ground of physical monism: No mental action without physical action.

My approach of defining the boundaries for experimental research on network activity in general builds on the one of Crick and Koch but refines it by adding degrees of freedom which I think are necessary. The established part of the approach is to look for activity in cellular networks of the brain which correlates with activity of the mind. The first important but simple refinement which I promote is to expand the search space.

1) *All kinds* of low-level activities with time scales corresponding to mental events have to be checked to be a correlate of a mental activity.

All types of low-level activity have to be taken into account as possible correlates. Crick and Koch made their choice about what they expect as a correlate in experimental studies, namely action potentials. Action potentials are the correlate of both, information processing and consciousness (Koch, 2004). I am seeking to widen the horizon and to add other types of activity in the experimental search for the correlate of mental activity (see below in chapter 2.3.2).

The second refinement is based on the fact that different mental activities go on in the brain at the same time. I think it is not possible in an experiment to look for a segregated correlate of consciousness without dealing with the simultaneously changing correlates of different kinds of information processing.

2) *All kinds* of simultaneous mental activities have a correlate on lower emergent levels of the brain.

In the following I will exemplify these principles.

2.3.2 Including all types of low-level activity into the search space

In the context of low-level correlates for mental brain functions I want to define “activity” in a very general way as any change of any property in time. Information processing as mental function is necessarily linked to such activity as it implies the transition from one pattern encoding information to a subsequent pattern encoding processed information. Without paradigmatic specifications, any change in the parts of the system or lower levels of emergence could be the correlate for a change in the higher levels, as long as the time scale is comparable. This generalization is important. In this widened view, every dynamic property at hand has to be seen as possible carrier of information. Which kinds of changes occur in the brain? Potential candidates for the correlation with mental activity, simply because they are dynamic in time, are electrophysiological, biochemical, structural, and pathway activities.

Include all types of electrophysiological activity.

Electrophysiological activity is certainly part of the core activity. It is probably the only type of activity which is able to recruit distant cells into active assemblies. Action potentials are fast and robust signals between cells and areas of the brain. The debate about action potentials is mainly centered around the question in which way they encode information. Is the “neural code” in the mean frequency of firing cells? In the timing of single spikes? In the temporal correlation between spikes – within one cell or between cells? In the coincidence of spikes? In the relation of a given spikes to a global rhythm? In the selection of active cells? (Dayan and Abbott, 2001,

p. 34). In any case, the paradigmatic focus still lies on action potentials, i.e. on suprathreshold activity and its spread in the network via fast synaptic interactions. However, action potentials are not the only type of electrical activity. Information might be encoded in the analog domain of subthreshold activity, too. Subthreshold activity, for example, is sufficient to trigger the opening of ion channels in cell membranes (Berger, 2007). Field theories claim that the spatial structure of the electrical field as a whole, generated by all electrically active cells, contains information (McFadden, 2002) e.g. in form of voltage objects (Markram, 2005; cited in Markram, 2006).

Include emergent electrophysiological states. Furthermore, besides fast synaptic activity, more attention should be paid to the potential of intrinsic conductances. A key input might switch a cell into a different state which is maintained with the aid of intrinsic conductances for a longer time scale in comparison to the instantaneous summation of synaptic input. Such persistent states add an important degree of freedom to information encoding. A switch between functional states of a cell provides conditioned probabilities, changing the rules for electrophysiological integration and action potential generation. Given intrinsic state A, the output of a cell due to synaptic input might be completely different from the output which the cell generates given intrinsic state B. States also might indicate the result of a network calculation without being dependent on the presence of reverberating action potentials. There are specialized cell types, for example, which can change the state of large networks of cells. Neurogliaform cells have an inhibitory effect on a cortical volume of $\sim 300\mu\text{m}^3$, mediated by the dense axonal arborization of this cell type, which lasts for several hundred milliseconds (Szabadics et al., 2007) and resulting in a sustained inhibitory effect on the whole network. Similarly, hormones and neuromodulators can change the excitability of neurons and the correlated firing probability dramatically, probably without eliciting a single action potential.

Biochemical activity. Going beyond electrophysiological activity there are also dynamic biochemical changes in the brain which might convey information. Fluctuating concentrations of calcium ions in the intracellular space, for example, or the extracellular concentrations of neurotransmitters. Such biochemical changes are often investigated only with regard to their influence on the electrophysiological activity. However, they might be the correlate of information processing itself. Therefore the calcium transients revealed by CASD imaging might be a valuable correlate of activity on higher levels of emergence, beyond its function as an indirect indicator of action potentials.

Structural activity. Finally, there is structural low-level activity in the brain. Following excitatory and inhibitory input to cells, intracellular signal transduction cascades are started which cause genomic and non-genomic effects. Intracellular signaling switches on and off molecular pathways which lead to covalent alterations and conformational changes of proteins, structural

modifications of synapses, changes in the cytoskeleton, and altered gene expression. The elaborate theory for the correlate of consciousness by Penrose and Hameroff considers structural activity as crucial. It builds on quantum activity in the cytoskeleton (Hameroff and Penrose, 1996). In general, there might be unknown molecular machines in the intracellular or the extracellular compartment which store or process local information on fast timescales. As the influx of calcium into neurons is tightly connected with electrophysiological activity, maybe unknown calcium binding proteins are part of such molecular machines. The activation of one molecular pathway in contrast to another also might encode information.

2.3.3 Considering all types of mental activity

Recent models of the mind comprise an inner representation of the external world as well as an inner representation of the self with location of the self in the map of the external world (Hesslow, 2002; Grush, 2004). The internal, combined world- and self-model is not a copy of the physical world, but a purposeful representation of it. The aspect of physical interaction with the environment including sensory feedback of motor action-induced effects has a strong weight. Using terms promoted by Varela, in this “embodied” or “enactive” model of the mind (e.g. Thompson and Varela, 2001) again large parts of information processing remain unconscious whereas other parts of the world model are prepared for consciousness. The world model is maintained intrinsically and only updated by sensory input from moment to moment. Its maintenance does not depend on continuous sensory input. An example from daily life: If one closes the eyes, the mental representation of the room in which the person is in stays intact, although the exact position might get lost after a while without sensory update. Preemptive assumptions and guesses about the environment and its changes, taken from experiences which are retrieved from long-term memory, reduce the requirement of complete sensory information and thus speed up the “refresh rate” of the world model.

In this view, there are two sources of information which are fed into the world-model. First, the internally constructed representation of the world, based on long-term memory and working memory. Second, sensory input which is used to modify the model. The internal world model has several representational dimensions. A bodily dimension (What is the spatial environment of the body? Which objects are within reach? Which options are there to manipulate them?), a cognitive dimension (What is the current topic of thoughts, intentions, motivation and plans?), and a social dimension (What is the current social environment, the social hierarchy, the social role one is in at the moment?).

The activity of place cells seems to be a confirmed correlate for the self-localizing part of the world model (Nakazawa et al., 2004; McNaughton et al., 2006). Bodily illusions and artificial out-of-body-experiences impressively prove its existence (Blanke et al., 2002; Blanke and Metzinger, 2009).

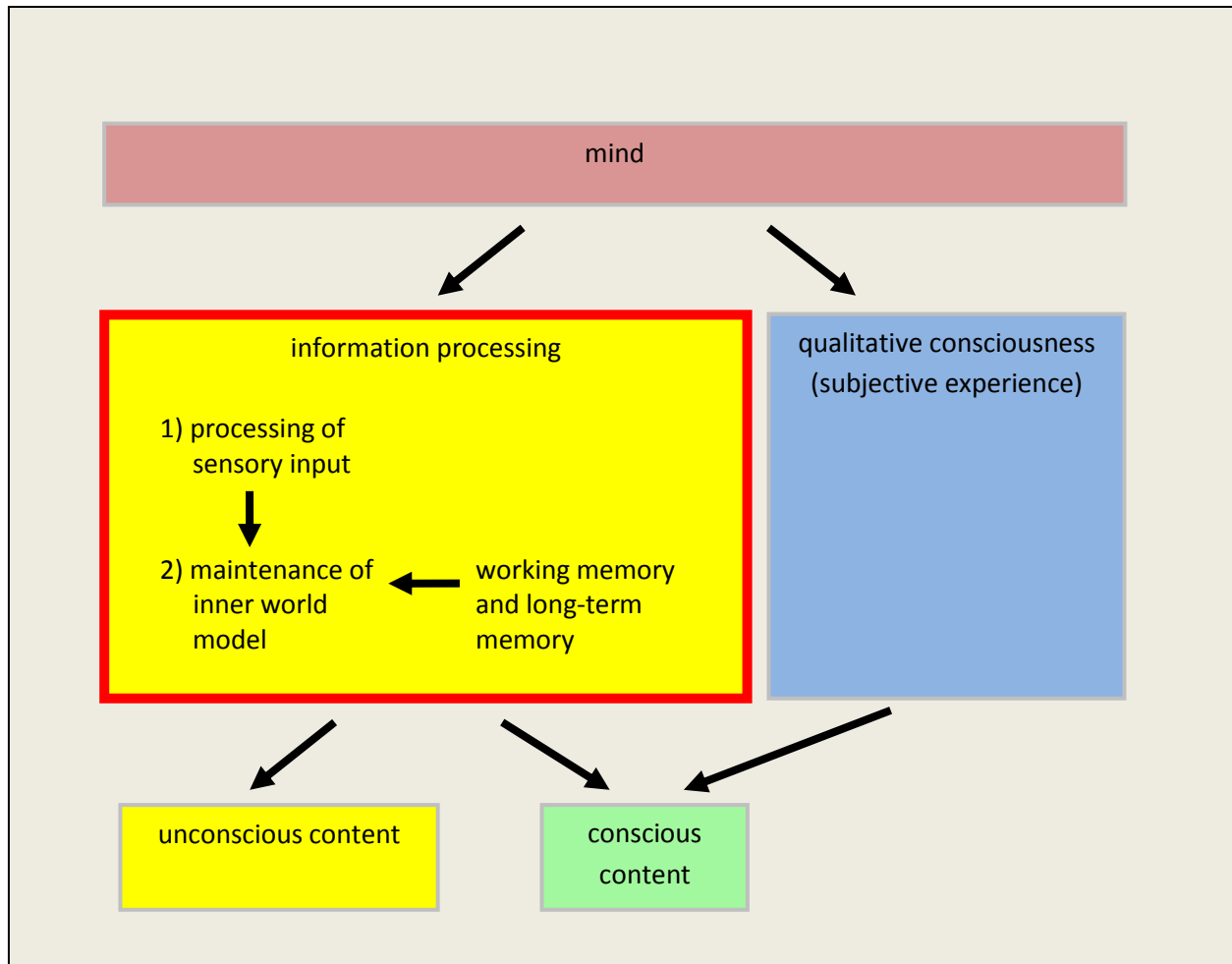


Fig. 3. Several types of information processing have to be expected to run at the same time.

This figure is an augmented copy of Fig. 1. There are at least two different streams of information, which are simultaneously processed from moment to moment by an awake mind. One is the sensory input coming in from the external world. The other is a constantly updated inner representation of the world (including the self in this world and expectations of what is likely to happen next), maintained by working (short-term) memory and retrievals from long-term memory. The sensory input updates the inner model of the world.

This more detailed view on the mind implies that there is more than one source of activity related to information processing (Fig. 3).

Variety of correlations.

In this expanded scenario, not only all low-level activity with appropriate time scale might be a correlate of a given mental function, but also all kinds of mental functions have to have a low-level activity correlate. At the same time, in an awake human being, there coexist at least a "correlate of information uptake from sensory input", a "correlate of information retrieval from memory", a "correlate of maintenance of the inner world representation", a "correlate of qualitative consciousness", and a "correlate of memory formation" (cf. Fig. 5). Even if action potentials are absolutely necessary to recruit distant populations of brain cells into the emergent mechanisms for mental functions, other types of low-level activity might be involved on a local basis.

Taken together, accepting the augmented pool of low-level activity in the network as the basis for emergent functions and accepting that several mental sub-functions have low-level correlates at the same time, enlarges and systematizes the framework for experimental research. Given a mental function which is to be explored, all low-level parameters should be screened without bias for being a correlate of this mental function. Given the experimental observation of a specific kind of low-level activity, one has to ask to which mental task it belongs and all mental functions have to be taken into account. As emergent subsystems of the mind are present at the same time, it is a demanding task for invasive experimental research on network activity to identify the low-level correlates and to distinguish between them in terms of the mental function they serve.

The weight of activity related to sensory input vs. activity related to internal world representation.

In the light of the theory of a permanently maintained internal world model as a core mental function (Fig. 3), there must be correlating low-level activity which is not related to sensory input from the external world. In associative areas, the main part of ongoing activity might be caused by the maintenance of the internal world model and activity correlating to the sensory update might be only a small fraction. However, even within primary sensory parts of the cortex, population activity might be predominantly caused by intrinsic, or top-down, information processing and only being modulated when sensory stimuli are applied. This issue is important mainly for in vivo experiments. Recent in vivo results show that sensory input is at least not the only source of information processing as activity in primary sensory areas can be recorded in the absence of stimuli (Crochet and Petersen, 2006; Poulet and Petersen, 2008). In vitro results indicate that network activity patterns in primary sensory areas are quite

stereotyped and are hardly influenced by artificial sensory input, suggesting a predominant role for intrinsically generated and maybe world-model-related activity (Maclean et al., 2005).

Infrastructural activity.

Whereas any emergent activity must have a correlate on a lower level, there could be low-level activity without any emergent function, too. For example, plain turn-over of membrane lipids is activity without correlation to mental functions. Such infrastructural activity might include the electrophysiological domain and might not carry information nor generate consciousness, but could be needed for one or both of them, providing the system with stability on a middle level of emergence. Infrastructural activity might provide the basic operational mode of the system. It might be of the same low-level kind as correlate activity, let's say there might be spikes which have a stabilizing function for network activity without containing information themselves. In terms of information theory such activity would simply be called noise. It might be demanding to tell infrastructural activity apart from correlate activity (cf. Stein et al., 2005). Which part of observed activity provides just infrastructure for emergent mental functions and which part correlates with content which the network is processing at present? What is carrier, what is message? A technological analogy might be the difference between charges in a power supply unit of a computer not carrying information and charges in the transistors doing so, both in the eyes of an alien who tries to reverse engineer the machine. Besides the correlate of a permanently maintained inner model of the external world, infrastructural activity, if it exists, is already the second kind of low-level activity present in a resting brain which is not exposed to sensory stimuli.

Considering different branches of emergence for information processing and consciousness.

What is the difference between the neurophysiological correlate of unconscious information processing and conscious information processing? Information processing is one emergent property of the brain. Qualitative consciousness is most probably a different one (Searle, 1980). While the result of an information processing event might attract attention and recruit consciousness (e.g. in the case of perceiving a threat), it is unlikely that the emergence of consciousness is the result of pure information processing. The fact that information can be processed without becoming conscious supports the hypothesis that there are two different subsystems in the brain which separately constitute the emergence of information processing and qualitative consciousness (Fig. 4). If there are two separate hierarchies of emergence for both functions of the mind, they could also be based on different kinds of low-level activity. Like the emergent property of a car to be driveable, by analogy, is based on a different subsystem than its emergent property to play music. As a speculative assignment, action potential activity might be the correlate of information processing and decide which cell population is recruited into the active assembly, whereas activity of an intracellular, calcium-triggered molecular machinery in dendrites might be the "extra ingredient" (Chalmers, 1995) responsible for the

emergence of consciousness. Such considerations can support experiments which address the question as to which changes occur whenever content-representing activity becomes conscious in addition.

The idea of two branches of emergence is contrary to the hypothesis of strong artificial intelligence that computers will be conscious when calculations become sufficiently complex. Creating a conscious machine then means to duplicate whatever physical processes (and emergent stages) the brain goes through to cause consciousness (Searle, 1992).

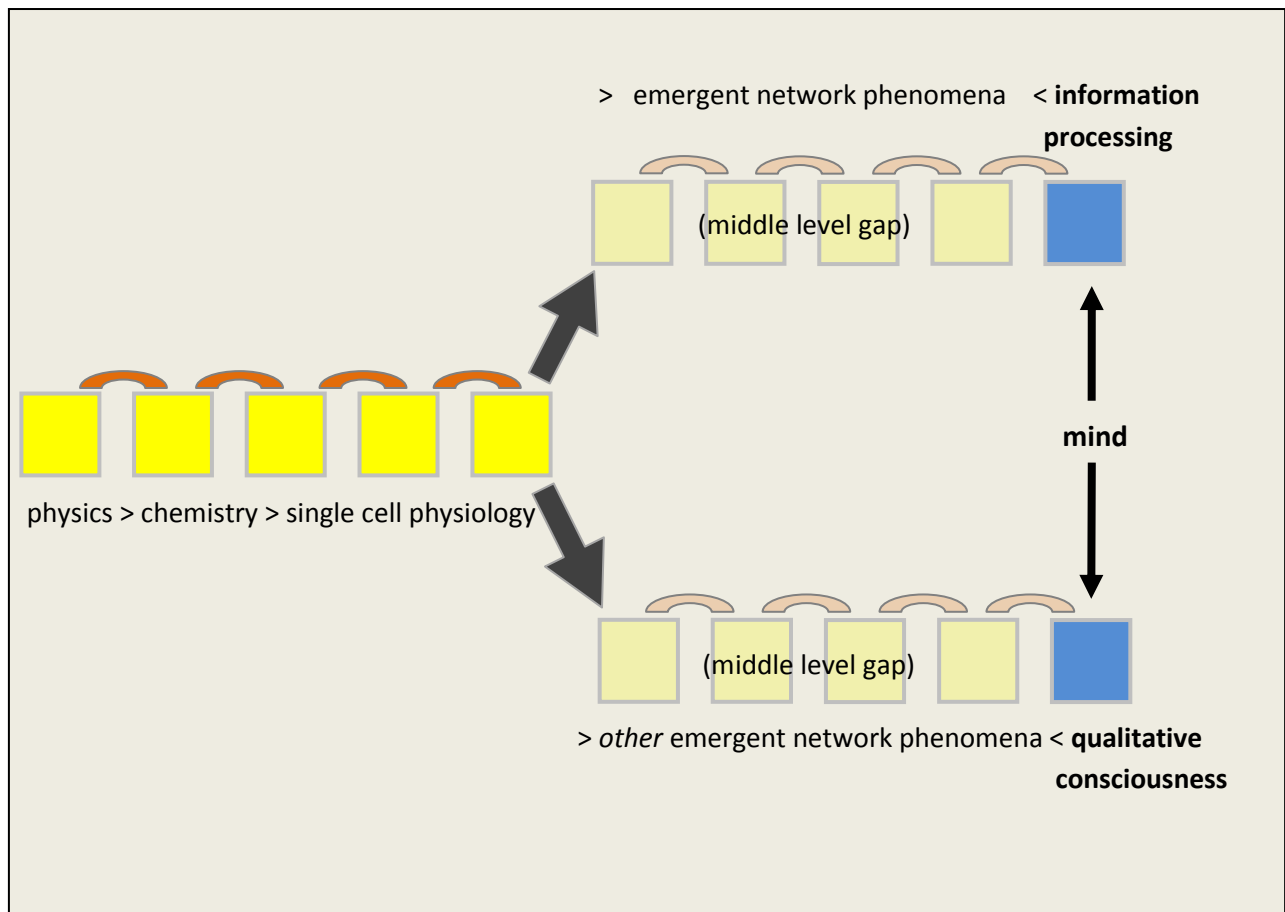


Fig. 4. Different mechanisms for information processing and qualitative consciousness?

The basic functions of the mind, content-related information processing and qualitative consciousness might emerge in the brain by means of two different subsystems of network activity.

Understanding in which respect these mechanisms differ from each other would complete the explanatory model of the mind.

Expecting more than one step of emergence correlated with network activity.

The computational model of the mind suggests that there is only one level of emergence missing in the hierarchy of emergent properties. If the mechanism of computation were found, the mind would be reduced to the brain. In contrast to this assumption, it is unknown how many levels of emergence the brain actually employs to provide information processing and consciousness. The explanatory distance between the behavior of single cells and mental functions indicates more than one such level of emergence within the domain of network activity. The existence of several anatomical scales from microcircuits, cortical layers, columns, areas and systems supports this idea as structures can be expected to be related to functions.

The real number of emergent levels again is important for the interpretation of experimental results. As the activity of single cells, activation of assemblies, and coactivation of cerebral systems might reflect different levels of emergence within the machinery of the mind.

Including other cell types.

Organisms in general do not waste energy. According to recent findings, the cerebral cortex contains as many glial cells as neurons (Azevedo et al., 2009), and older publications even state a ratio of 10:1 in favor of glial cells (References in [Azevedo et al., 2009]). This indicates that glial cells are functionally important. Their acknowledged role is that they are involved in the support of neuronal metabolism. However, they are also electrically excitable. They modulate synaptic transmission directly (Araque and Perea, 2004). They release neurotransmitters and modulate neuronal baseline excitability (Volterra and Meldolesi, 2005; Fellin et al., 2004). Following depolarization they show calcium transients (Nimmerjahn et al., 2004). With an unbiased approach, one has to ask which other non-electrical signals underlying information processing or consciousness might be generated by glial cells.

Including pathway coding.

In the theory of connectionism, neurons are exchangeable modules in a calculating network. There is information in the weights of synapses, but there is no information in the selection of specific kinds of neurons. The variety of differentiated cell types is not considered. Due to this reason, multiple realizability still holds for connectionism. However, according to localized fMRI signals, information in the brain seems to be encoded in the population of activated cells. Pathway coding, which is fully accepted in the peripheral nervous system, is present in the central nervous system, too, and should be taken into account more consistently. Pathway coding means that it actually does matter which cell population exhibits an activity pattern. Information in the brain is not copied from one location to another, but the recruitment of additional cell assemblies already implies a transformation of information into the next state. Pathway coding might be especially important in the context of the correlate of consciousness. fMRI studies support empirically that experiencing certain qualia comes along with increased activity of specific brain areas. It has been shown that the additional qualia which people with

synesthesia experience following an external stimulus are associated with derivations of the architecture of long-range fibers, resulting in a recruitment of areas of the brain which do not respond to the same stimulus in non-synesthetes (Sperling et al., 2006; Weiss and Fink, 2009). Thus, consciousness originates where the related content is encoded. It is not a copy of information which is made conscious elsewhere in an area specialized for the generation of consciousness. If the variety of qualia cannot be the result of calculations, they must be based on molecular differences between cell types in different networks, which means that they must be based on pathway coding. Networks generating different qualia might also use different temporal spiking codes for this task, but there is no evidence for crucial differences in rhythms or frequencies in primary sensory areas associated with different qualia.

I dare to predict that the emergence of different qualia of consciousness eventually will be explained with the morphological differences of brain areas as described by Brodmann (Brodmann, 1909).

Figure 5 summarizes and exemplifies the central idea of this chapter, showing which combinations of low-level activity and mental function have to be considered in the field of invasive research on network activity. The finer the discrimination of mental activity, the finer the discrimination of cell types, and the more complete the knowledge about intracellular molecular pathways as part of the structural category of low-level activity will be, the more complete this map of mental activities and their neurophysiological correlates will become. The explanatory distance between the mind and the physical brain will be lowered and an explanation of the mental in terms of the physical might come within our grasp.

low-level activity correlate of mental function (in neurons and glial cells)				
mental function:	electrophysiology: synaptic integration	electrophysiology: intrinsic states	short-term biochemical	structural
information processing: sensory input	✓	?	?	?
information processing: retrieval from long-term memory	?	?	?	?
information processing: internal world model	✓	?	?	?
qualitative consciousness	✓	?	?	?
long-term memory formation	✓	?	✓	✓
other function:				
“infrastructural” activity	✓ / ?	?	?	✓

Fig. 5. The proposed framework for mental functions and their low-level correlates

This mapping of low-level activity as correlate for different types of mental activity reflects predominant paradigms with the emphasis on electrophysiological activity and shows where experimental research should make efforts to look for matches as well.

Legend: ✓ = generally accepted within paradigms

 ? = not known or generally not discussed within paradigms

3 Chapter summary and aim of my PhD work

In chapter I.1 we have seen that the identification and description of emergent mechanisms within the domain of cerebral network activity is *the* prerequisite for a unifying model of brain and mind which explains mental functions in terms of physical events.

In chapter I.2 I have argued that knowledge about emergent network phenomena is vague and that the progress of network neuroscience might profit from an unbiased view on low-level correlates of mental functions besides the development of new techniques.

The overall aim of the experimental studies I did during my PhD work was to add to the knowledge about network activity in the mammalian brain. I contributed to four different published/submitted studies which either quantify spontaneous network activity in vitro or improve the methods for research on network activity, or both. The accessibility of structures, the stability of recordings, and the options of pharmacological manipulations of network activity are limited in vivo. Handling is much easier and more experimental possibilities are available in preparations of isolated brain tissue in vitro. However, some physiologically relevant activity must be preserved in the preparation.

For all projects described in this thesis, we used the brain of rodents (mice or rats) which serve as model animals for the taxonomic class of mammals.

The broader context of the studies will be presented briefly in outlines in Chapter II, but details and discussions are given only in the respective publication.

The introduction about the philosophy of neuroscience (Chapter I) is the summary of thoughts I developed during my PhD work and is intended to be an “intellectual tool” for network research of its own.

II Guide to publications

Publication 2 and the first part of publication 1 provide new experimental protocols to study network activity in vitro. The second part of publication 1 shows an application of the developed method in the context of intracellular signal integration. Publication 3 calibrates techniques of fluorescent dye imaging. Publication 4 aims at revealing mechanisms of long-lasting inhibitory activity on the single cell level and the resulting effect on the level of network activity. A 5th project on mechanisms of bistable upstate/downstate network activity was in preparation when this thesis was finished and will be published elsewhere.

- Publication 1 -

“Somatodendritic Integration under Increased Network Activity in Layer 5 Pyramidal Cells of the Somatosensory Cortex”

Florian B. Neubauer & Thomas Berger (2008). *Pflügers Archiv* 455:1063-1079.

In this study we address the problem that acute slice preparations of the neocortex maintained in standard bath solutions exhibit almost no spontaneous network activity. Although electrophysiological activity can be evoked artificially in the brain slice by electrical stimulation, this activity usually dies out on a short timescale because the cells are not sufficiently excitable to sustain network activity. Spontaneous activity, in contrast, would arise and spread based on physiological mechanisms which would be also present in the living animal. One reason for the lack of self-sustained network activity in vitro is that axons which mediate neuromodulatory input from subcortical areas are cut away. In this study, we established means to pharmacologically mimic the depolarizing effect of subcortical neuromodulatory systems in cortical slices. As a result, the excitability and spontaneous electrophysiological activity of neocortical neurons in vitro increases and reaches values comparable to those reported in awake animals. In addition, we apply this method to investigate somatodendritic signal integration in vitro, comparing standard conditions to our enhanced network activity.

Taken together we established a method which allows for studying spontaneous activity at the level of single cells or networks of cells in well-accessible cortical slices.

Somatodendritic integration under increased network activity in layer 5 pyramidal cells of the somatosensory cortex

Florian B. Neubauer · Thomas Berger

Received: 10 July 2007 / Revised: 17 August 2007 / Accepted: 10 September 2007 / Published online: 20 October 2007
© Springer-Verlag 2007

Abstract Integrative properties of single neurons have been extensively studied in acute brain slices. However, these preparations are characterized by extremely low levels of synaptic and action potential activity. In comparison to *in vivo*, reduced intracortical input and lack of subcortical modulation increase the effective difference between mean membrane potential and spiking threshold, preventing self-sustained network activity *in vitro*. To elicit an increased and stable network activity (INA) *in vitro* comparable to that found in awake animals, we mimicked subcortical cholinergic and serotonergic inputs using carbachol or barium alone or in combination with serotonin in layer 5 pyramidal cells in slices of mouse somatosensory cortex. INA is primarily induced by a modulation of intrinsic conductances resulting in a depolarization of the membrane potential. We studied the impact of INA on synaptic and somatodendritic integration using extracellular stimulation and dendritic calcium imaging. Synaptic inhibition is strengthened due to an increased driving force for chloride. The critical frequency at which somatic action potentials induce a dendritic calcium action potential is lowered. Simultaneous inhibitory synaptic input is powerful enough to suppress dendritic calcium action potential generation. Pharmacologically induced INA enables the study of neuronal integration in well-accessible cortical slices within an active network.

Keywords Network activation · Neuromodulation · Cholinergic modulation · Serotonergic modulation · Somatosensory cortex · Dendrite · Patch clamp · Calcium-sensitive dye imaging

Introduction

Integration in cortical neurons depends on the spatiotemporal distribution of intracortical and subcortical inputs, the leak conductances determining passive membrane properties, and the active conductances generating the output signal of the neuron [30, 46]. In brain slice preparations, the ability to integrate synaptic input and to generate action potentials is, in general, retained. However, the drive of intracortical ionotropic and subcortical modulatory inputs is dramatically minimized due to the cut of long-range axons innervating the cortex. Together, these changes result in a considerably more hyperpolarized resting membrane potential with low variability in comparison to *in vivo* recordings [38]. Nevertheless, slice preparations are widely used for the study of functional cellular properties due to an ideal accessibility and visibility. Measurements in awake animals, in contrast, face technical obstacles. There, it is impossible to investigate integrative properties with the same ease, precision, and stability as *in vitro*. Given this dilemma, a method that establishes integrative properties based on increased network activity (INA) in the slice preparation is highly desirable.

Modulatory input from cholinergic neurons from the brainstem and the basal forebrain is a well-known mechanism for the activation of thalamic and cortical networks, respectively, during the awake state [12, 35, 36, 57]. The depolarizing action of acetylcholine on neocortical neurons is associated with a rise in cell input resistance due to the

Electronic supplementary material The online version of this article (doi:10.1007/s00424-007-0350-z) contains supplementary material, which is available to authorized users.

F. B. Neubauer · T. Berger (✉)
Institute of Physiology, University of Bern,
Bühlplatz 5,
3012 Bern, Switzerland
e-mail: berger@pvl.unibe.ch

blockade of resting potassium conductances [23, 24]. Serotonergic input is another strong source of subcortical activation [48].

A well-suited cell type to study integration along the somatodendritic axis is the layer 5 pyramidal cell of the somatosensory cortex. This cell type is characterized by two distinct action potential initiation zones [42]. The somatic initiation zone generates sodium action potentials that backpropagate into the dendrite [50]. The dendritic initiation zone triggers high-threshold calcium action potentials [26]. Both initiation zones interact. Temporal coincidence of a backpropagated somatic action potential and distal dendritic activation is the most likely event to generate a calcium action potential [27]. In contrast, concomitant dendritic GABAergic input is a powerful mechanism to prevent dendritic calcium events (so-called veto effect [27]).

We investigate here the possibility of inducing, in an *in vitro* preparation, an increased tonic activity level similar to that found in awake animals. Firstly, criteria are defined for such a state, which we name “increased network activity” (INA). Then, three different pharmacological approaches are tested to generate INA in layer 5 pyramidal cells in acute slices of the somatosensory cortex of juvenile mice. Mimicking subcortical input, we were successful in inducing INA. This is mainly based on a depolarization mediated by the modulation of intrinsic conductances. We employ INA to study somatodendritic interaction and the associated veto effect of inhibitory interneurons. Taken together, INA is a promising novel tool to study cortical integration in an acute brain slice preparation under restored network activity.

Material and methods

Slice preparation Postnatal day 12 to 30 DDY mice were killed by decapitation, following the guidelines of the veterinary office of the canton Bern. Their brains were rapidly removed and immersed in ice-cold artificial cerebrospinal fluid (ACSF). INA was investigated in thalamocortical slices [2] (Figs. 1, 2, 3, 4, 5, 6, and 7) of the somatosensory cortex of P12- to P18-old mice. Dendritic activity was studied in parasagittal slices from P27 to P30 mice (Figs. 8 and 9). Four-hundred-micrometer-thick slices were cut on a vibratome (Microm HM 650 V; Walldorf, Germany), incubated at 35°C for 30 min, and afterwards left at room temperature until the transfer to the recording chamber.

Patch-clamp recordings Pyramidal cells in layer 5 of the somatosensory cortex were visualized by infrared differential interference contrast videomicroscopy. Current-clamp whole-cell recordings were obtained from the soma of one or two neurons simultaneously. Two BVC-700A amplifiers

were used (Dagan, Minneapolis, MN, USA). Electrodes were made from borosilicate glass tubing with resistances of 4–8 M Ω when filled with intracellular solution. All experiments were done at 33°C. Data were low-pass filtered at 3 kHz using the internal two-pole Bessel filter of the amplifiers and sampled at 5–10 kHz. Capacitance compensation and bridge balance were properly adjusted. Liquid junction potentials were left uncorrected. Only neurons with a mean membrane potential more negative than –60 mV were recorded [mean membrane potential was -67.9 ± 5.6 mV, mean \pm standard deviation (SD), $n=54$ cells]. Signals were digitized and stored using Clampex 9 and analyzed off-line with Clampfit 9 (Axon Instruments, Union City, CA, USA). Extracellular stimulation was done using patch pipettes filled with ACSF as monopolar stimulation electrodes.

Electrophysiological data analysis The input resistance was obtained under different pharmacological conditions by a linear fit of the slope of a current–voltage curve. For this curve, a set of steady-state membrane potential values induced by 1-s-long hyperpolarizing current injections was used. The time constant was obtained from a monoexponential fit of the membrane potential decay at the offset of such a hyperpolarizing current pulse. The SD sigma of the membrane potential was obtained in the following way: Shifts in long recordings (up to 10 min) of the membrane potential were compensated and a histogram of the resulting trace was fitted with a Gauss function in Clampfit. With this procedure, membrane potential deflections during action potentials did not have an impact on sigma, while changes in excitatory postsynaptic potential (EPSP) and inhibitory postsynaptic potential (IPSP) activity did (see Figs. 1b and 2b). Sigma was used for comparison of the variability of the membrane potential under different pharmacological conditions. When parameter changes are presented as percent of control, the control values were obtained from the identical cells prior to pharmacological modulation. Pooled data are expressed as mean \pm SD. Raw data were compared for statistical significance using a paired *t* test. Significance level was set at $p \leq 0.05$ (* in Table 1), and $p \leq 0.01$ was indicated in Table 1 with **.

Calcium epifluorescence imaging To monitor changes in the intracellular calcium concentration related to dendritic calcium events in layer 5 pyramidal cells ([39]; our Figs. 8 and 9), the potassium salt of the high-affinity calcium-sensitive dye Oregon Green 488 BAPTA-1 (OGB-1; Molecular Probes, Eugene, OR, USA) was applied to the cell via the intracellular patch pipette solution. Filling the complete somatodendritic compartment took about 40–50 min. The light source was a 75 W Xenon short arc

lamp in a Deltaram V monochromator (PTI, Lawrenceville, NJ, USA). Changes in epifluorescence were imaged with a Zeiss objective (40 \times , 0.8 numerical aperture). A low-resolution (80 \times 80 pixel), fast (500 Hz) CCD camera (Redshirt NeuroCCD, RedShirtImaging, Fairfield, CT, USA) running under computer control (Neuroplex software) was used to image changes in fluorescence in a 250 \times 250- μ m field of view covering the distal dendrite around about 625 μ m from the soma (Figs. 8 and 9). The following filter set for OGB-1 was in use: dichroic mirror 510 nm, emission filter BP540/25 nm. Excitation via the monochromator was at 470/6 nm.

Chemicals and solutions Slices were continuously superfused with an ACSF containing (in mM): 125 NaCl, 25 NaHCO₃, 2.5 KCl, 1.25 NaH₂PO₄, 2 CaCl₂, 1 MgCl₂, and 20 glucose, bubbled with 95% O₂ and 5% CO₂. To induce INA in the slice preparation, we used three different approaches. (a) α -Latrotoxin (600–900 pM) and pardaxin (1–2.7 μ M) were added to the extracellular solution. (b) A modified extracellular solution (mACSF) was used with the following altered concentrations (in mM): 5 or 6.25 KCl, 1.5 CaCl₂, and 0.5 MgCl₂, compared to 2.5, 2, and 1 in ACSF, respectively. (c) The nonhydrolyzable acetylcholine analog carbachol (20 μ M) or barium (20–100 μ M) as a blocker of inwardly rectifying potassium currents, as well as serotonin (10–20 μ M), were added to the extracellular solution. Pipette solution contained (in mM): 135 K-gluconate, 5 KCl, 10 ethylene glycol bis(2-aminoethyl ether)-*N,N,N',N'*-tetraacetic acid (EGTA), 10 4-(2-hydroxyethyl)-1-piperazineethanesulfonic acid (HEPES), 4 Mg-ATP, 0.3 Na₂-GTP, and 10 Na₂-phosphocreatine, pH adjusted to 7.25 with KOH. In combined patch-clamp and calcium imaging experiments, the pipette solution contained no EGTA, but in addition 100 μ M OGB-1. The following antagonists were added to the extracellular solutions: D-2-amino-5-phosphonovalerate (D-APV) 50 μ M, and 6-cyano-7-nitroquinoxaline-2,3-dione (CNQX) 10 μ M. Pardaxin and α -latrotoxin were from Alomone (Jerusalem, Israel) and all other chemicals were from Sigma (St. Louis, MO, USA) or Tocris (Ellisville, MO, USA).

Results

Definition of increased network activity

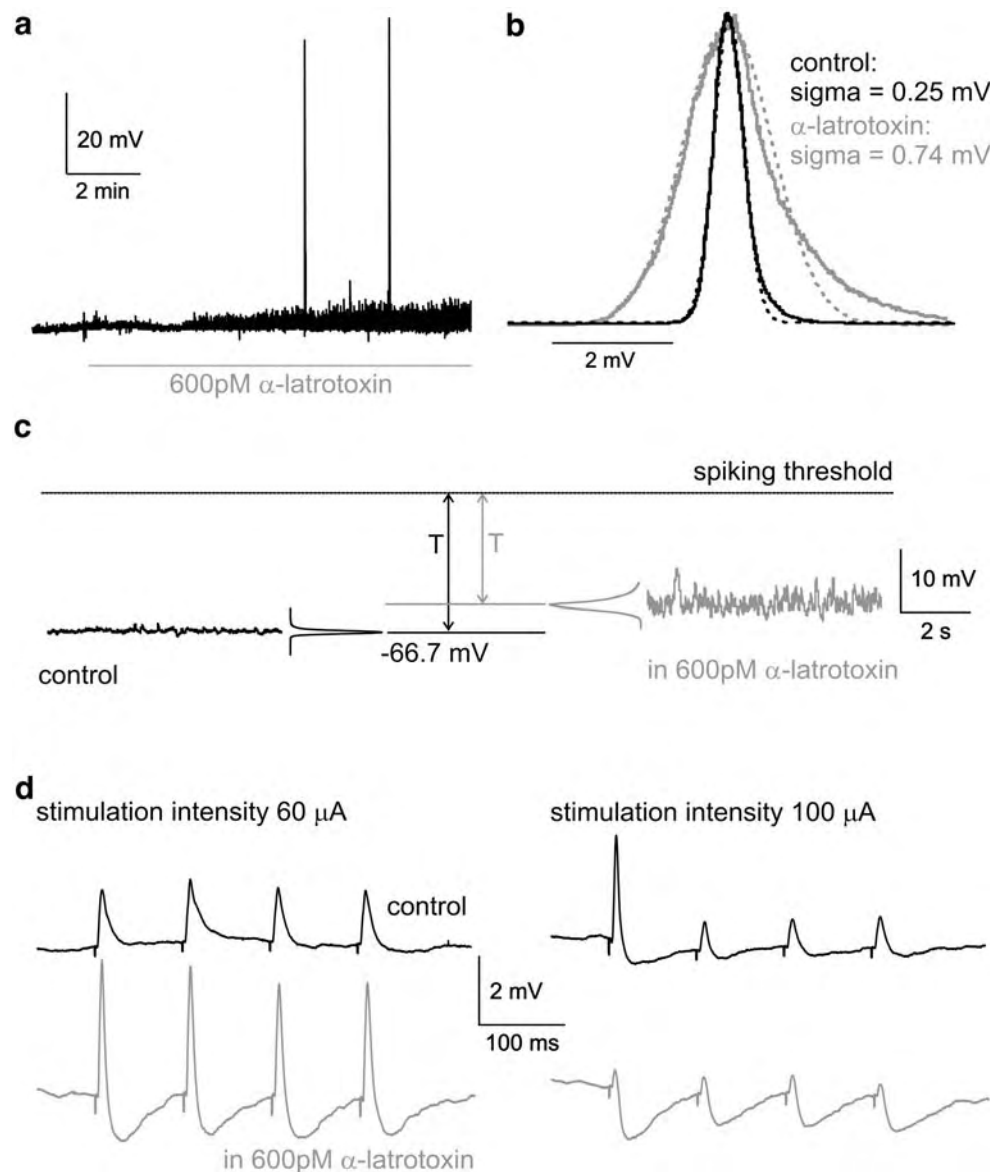
For the specification of INA, we rely on parameters obtained in acute brain slice preparations and awake animals. In the literature there is consent that cells in vivo are depolarized in comparison to the in vitro situation and

that the amplitude of membrane potential (Vm) fluctuations is much higher [4, 10, 11, 15, 29, 33, 34, 41, 49] (reviewed in Destexhe et al. [14]). The spiking rate of a neuron is proportional to the probability of the Vm to cross the spiking threshold. This probability in turn depends on two factors, the difference between the mean Vm and the spiking threshold and the amplitude of actual Vm deflections. As a first criterion for INA, we use the “effective difference” between mean Vm and spiking threshold, which is the controlling variable for the rate of spiking [1]. This effective difference is defined as the absolute difference between mean Vm and spiking threshold in millivolts divided by the SD of the Gaussian-fitted Vm distribution. We refer to this difference as T/σ , with T for the difference between mean Vm and threshold and σ for the SD [1] (Figs. 1b,c and 2b,c). It expresses the depolarization needed to evoke an action potential as a multiple of the SD of Vm. The smaller the difference between mean Vm and the spiking threshold and the higher the Vm fluctuations are, the lower T/σ is and the more likely the generation of action potentials is. In the standard in vitro preparation incubated in ACSF, the value for T/σ is 71.6 ± 37.8 (Table 1), while the values in awake animals were estimated from the literature to be in a range of about 1 to 12 [4, 10, 11, 15, 29, 33, 34, 41, 49]. Our first criterion for INA demands that the T/σ value obtained for a particular pharmacological condition reaches the range of twice the low T/σ values found in awake animals, i.e., smaller than 24. The second criterion is that electrophysiological behavior reached a sustainable steady state. If both criteria are fulfilled, the induced conditions are called INA.

Activation of the presynaptic release machinery using α -latrotoxin or pardaxin

In an isolated slice preparation, long-range afferents are cut, and this leads to the hypothesis that lacking synaptic drive is the predominant reason for the increased T/σ in vitro. Assuming this, a promising technical approach for the induction of INA is the activation of the presynaptic release machinery, while leaving postsynaptic receptors unaffected by the activation protocol itself. Such changes in the synaptic release probability can be obtained with toxins like α -latrotoxin [9, 16, 40] and pardaxin [28]. Application of 600 or 900 pM α -latrotoxin (concentration range see Capogna et al. [9] and Henze et al. [21]) resulted in a significantly increased SD of the membrane potential distribution (σ) to $187 \pm 63.8\%$ of the control value (mean \pm SD), reflecting an increased synaptic input to the cells under study ($p=0.04$; $n=5$ cells; Fig. 1a–c, Table 1). However, the mean membrane potential of the cells was not significantly depolarized ($p=0.65$; $n=5$ cells; Fig. 1a,c).

Fig. 1 Effects of α -latrotoxin on membrane potential and synaptic transmission. **a** Bath application of 600 pM α -latrotoxin (depicted by the gray line) to a layer 5 pyramidal cell results in increased membrane potential fluctuations and rare action potentials. **b** Histograms of membrane potential distribution during control and α -latrotoxin (black and gray solid curves, respectively) were normalized and fitted with Gauss functions (dotted curves) to obtain the SD sigma. **c** Analysis of membrane potential recordings under control (black trace, left part) and during α -latrotoxin (gray trace, right part). Due to sparse depolarization under α -latrotoxin, even increased synaptic drive is not sufficient to bridge the remaining difference T between the mean membrane potential and the spiking threshold. **d** Activation of synaptic input by extracellular stimulation in layer 2. Under control conditions, a train of four pulses (400 μ s duration, 60 or 100 μ A amplitude, 10 Hz, 30 trials averaged) evokes either EPSPs (60 μ A) or EPSP–IPSP sequences (100 μ A) (black traces). With α -latrotoxin, synaptic transmission is strengthened, resulting in larger EPSPs and IPSPs in comparison to control (60 μ A). At stronger stimulation intensity (100 μ A), strengthened inhibition is masking EPSPs. Mouse P18



Action potentials occurred only at a very low level (range 0 to 0.12 Hz, median 0 Hz). Input resistance and membrane time constant were not significantly changed (Table 1). The obtained values for depolarization and sigma resulted in an effective difference between V_m and spiking threshold T/σ of 35.3 ± 23.6 ($p=0.03$; $n=5$ cells; Fig. 1c), about half the value calculated for the control condition (71.6 ± 37.8 , $n=43$). However, the increase in V_m fluctuations under α -latrotoxin was still insufficient to bridge the distance between V_m and spiking threshold as depicted in Fig. 1c.

To check the ability of the system to perform classical synaptic transmission, a patch pipette filled with extracellular solution was placed in layer 2 and used for extracellular stimulation. Four stimuli (400 μ s duration, 60 or 100 μ A amplitude, 10 Hz frequency) evoked 1.5- to 2-mV-large EPSPs in standard ACSF. At higher stimulation

intensities, disynaptic IPSPs could be seen (Fig. 1d). Addition of 600 pM α -latrotoxin increased the EPSP amplitude at lower stimulation intensities, but these EPSPs were shortened due to a pronounced disynaptic inhibition. Because the membrane potential was only slightly depolarized and the input resistance was unchanged, the increased EPSPs and IPSPs suggest that α -latrotoxin improves the synaptic transmission in our preparation. Such an effect may be due to the presynaptic calcium increase following incorporation of α -latrotoxin channels in the membrane [20]. With increasing stimulation intensities, inhibition became so prominent that the EPSPs were nearly abolished. This might be explained by the fact that the local circuitry in the cortex is dominated by inhibitory synapses and, at higher stimulation intensities, more and more neighboring interneurons are recruited (Fig. 1d).

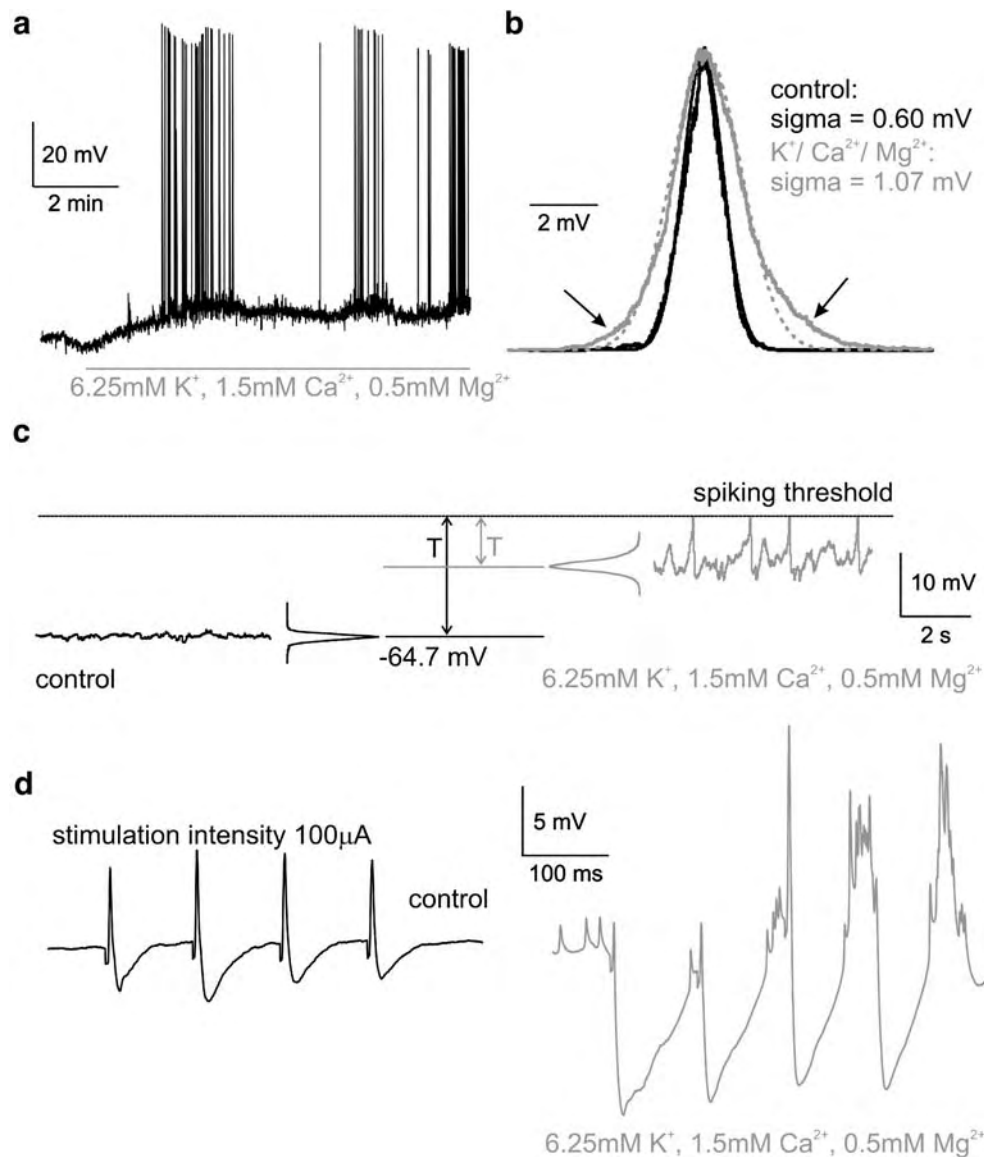


Fig. 2 Effects of increased extracellular potassium and decreased calcium and magnesium concentrations on membrane potential and synaptic transmission. **a** Extracellular concentrations of KCl, CaCl₂, and MgCl₂ were changed to 6.25, 1.5, and 0.5 mM (mACSF), compared to 2.5, 2, and 1 mM, respectively, in standard ACSF. The membrane potential of a layer 5 pyramidal cell is shown under control and during mACSF (depicted by the *gray line*). The cell depolarizes by 17.1 mV, sigma increases, and the neuron starts to generate action potentials at a mean frequency of 0.9 Hz. **b** Histograms of the membrane potential distribution in standard ACSF (control) and mACSF (*black and gray solid curves*, respectively) were normalized and fitted with Gauss functions (*dotted curves*) to obtain the sigma

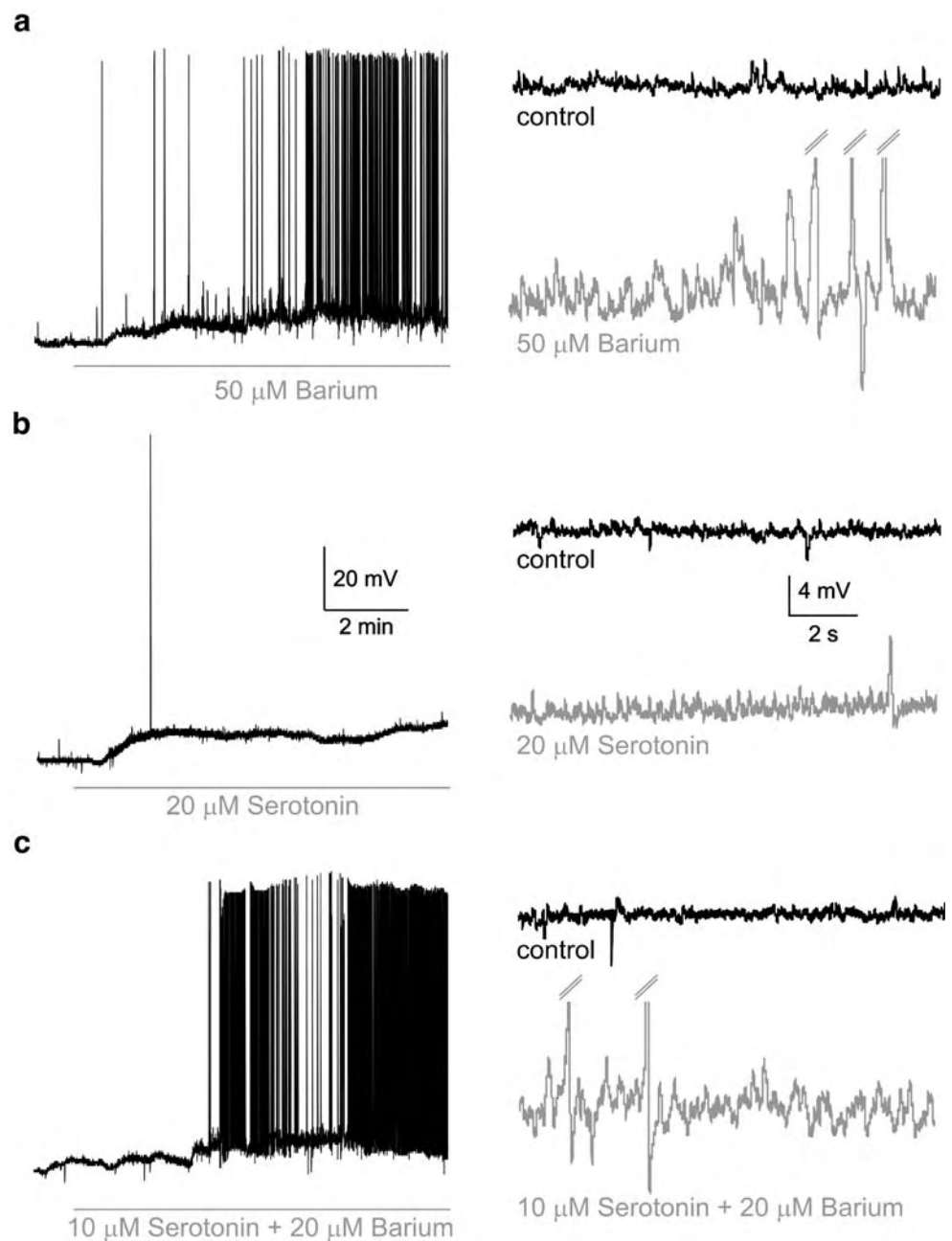
values given. Deflections of the membrane potential from a Gaussian-distributed behavior due to spikes and afterhyperpolarizations (*arrows*) are neglected by this fitting procedure and do not influence sigma. **c** Analysis of recording under control (*black trace*) and under mACSF (*gray trace*). The differences T between mean V_m and the spiking threshold reflect sufficient depolarization and synaptic drive under mACSF for the generation of action potentials. Spikes are truncated. **d** Activation of synaptic input by extracellular stimulation in layer 2 (400 μ s duration, 100 μ A amplitude, 10 Hz, 30 trials averaged) under control conditions evokes EPSP-IPSP sequences (*black trace*). In mACSF, the cell depolarizes, action potentials can be seen, and IPSPs become much larger. Mice P16 (**a–c**) and P15 (**d**)

Pardaxin at concentrations of 1 or 2.7 μ M (concentration range see Henze et al. [21]) resulted in comparable effects. The neurons depolarized slightly but significantly by 3.3 ± 2.4 mV ($p < 0.01$; $n = 8$ cells). Sigma increased to $141 \pm 34.1\%$ of control ($p < 0.01$; $n = 8$). The obtained reduction of T/σ to 59.7 ± 45.2 with pardaxin was not significant

($p = 0.07$, $n = 5$ cells), and there was no spiking. Input resistance and membrane time constant did also not show significant changes under pardaxin (Table 1).

Recordings with α -latrotoxin and pardaxin were stable and lasted for 60 min (median; range 50–120 min), meeting the second criterion for INA, stability in time. However, T/σ

Fig. 3 Cholinergic and serotonergic activation depolarizes the cells and increases the synaptic drive of the network. Application of 50 μM barium (**a**), 20 μM serotonin (**b**), or 10 μM serotonin plus 20 μM barium (**c**) all depolarize the cells and lead to action potential generation (*left part*). An increased sigma reflects the increased synaptic drive under these conditions (*right part*; here, action potentials are truncated). Membrane potentials: **a** control: -66.0 mV; 50 μM barium: -59.0 mV. **b** Control: -65.2 mV; 20 μM serotonin: -60.1 mV. **c** Control: -68.2 mV; 10 μM serotonin + 20 μM barium: -62.5 mV. Mice P14 (**a–c**)



values obtained with exclusive activation of the presynaptic release machinery were far away from the T/σ value defined in the first criterion (i.e., below 24). Therefore, this pharmacological approach failed to induce INA.

Activation with increased extracellular potassium and decreased calcium and magnesium concentrations

A modified ionic composition of the extracellular medium could be an alternative method to obtain INA. Extracellular potassium concentration was raised to 5 or 6.25 mM, while the calcium and magnesium concentrations were lowered to

1.5 and 0.5 mM, respectively (mACSF; compare Berger et al. [6] and Silberberg et al. [47]). In contrast to α -latrotoxin and pardaxin, mACSF containing 6.25 mM potassium led to a pronounced depolarization of the cells under study by 18.4 ± 11.1 mV ($p < 0.01$; $n = 8$ cells). The median of the spiking frequency was 1.15 Hz (range 0 to 13.0 Hz; $n = 8$). Sigma increased to $256.6 \pm 71.5\%$ of the control value ($p = 0.02$; $n = 6$ cells; Fig. 2b,c). This increase was not due to the presence of action potentials because sigma values were obtained from Gaussian-fitted histograms rejecting action potentials (Fig. 2b). In comparison to α -latrotoxin, the spiking threshold was reached in mACSF primarily due to a

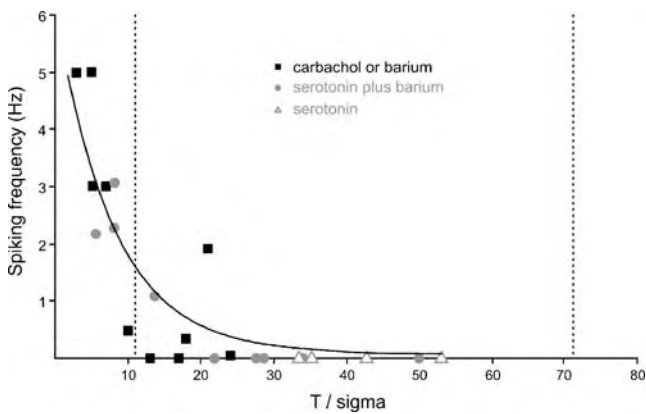


Fig. 4 INA is characterized by the reduction of the effective difference between mean membrane potential and spiking threshold. Plot of the spiking frequency against the effective difference between mean membrane potential and spiking threshold (T/σ). Data from 23 cells under INA were fitted logarithmically (black line). Mimicking subcortical input with cholinergic or mixed cholinergic–serotonergic activation induces INA with low T/σ values in comparison to the mean control value of 71.6 (right dashed line). Under INA, the T/σ values are similar to those found in the awake animal, and the highest spiking frequency is 5 Hz. The left dashed line depicts the highest T/σ values described in awake animals

strong depolarization and a concomitant high sigma (Fig. 2c). T/σ was reduced to 15.8 ± 8.7 ($p < 0.01$; $n = 6$), reaching a similar range as observed in vivo. Input resistance and membrane time constant were significantly decreased in mACSF (Table 1). mACSF with 5 mM potassium instead of 6.25 mM had similar but weaker effects (Table 1).

Extracellular stimulation induced EPSPs (not shown) and, at higher stimulation intensities, sequences of EPSPs with disynaptic IPSPs (Fig. 2d). In mACSF, the EPSP component became smaller while the IPSP component increased in amplitude. This may be simply explained by the fact that the cell's membrane potential approached the reversal potential for the cationic AMPA receptors while the driving force for GABAergic conductances increased.

The critical disadvantage of mACSF was the short duration and insufficient stability of the emerging activity (with 5 and 6.25 mM potassium). Neurons often continued to depolarize without reaching a new stable steady-state activity level. After a relatively short time (median 30 min; range 20–100 min; $n = 20$ cells), they were inactivated by

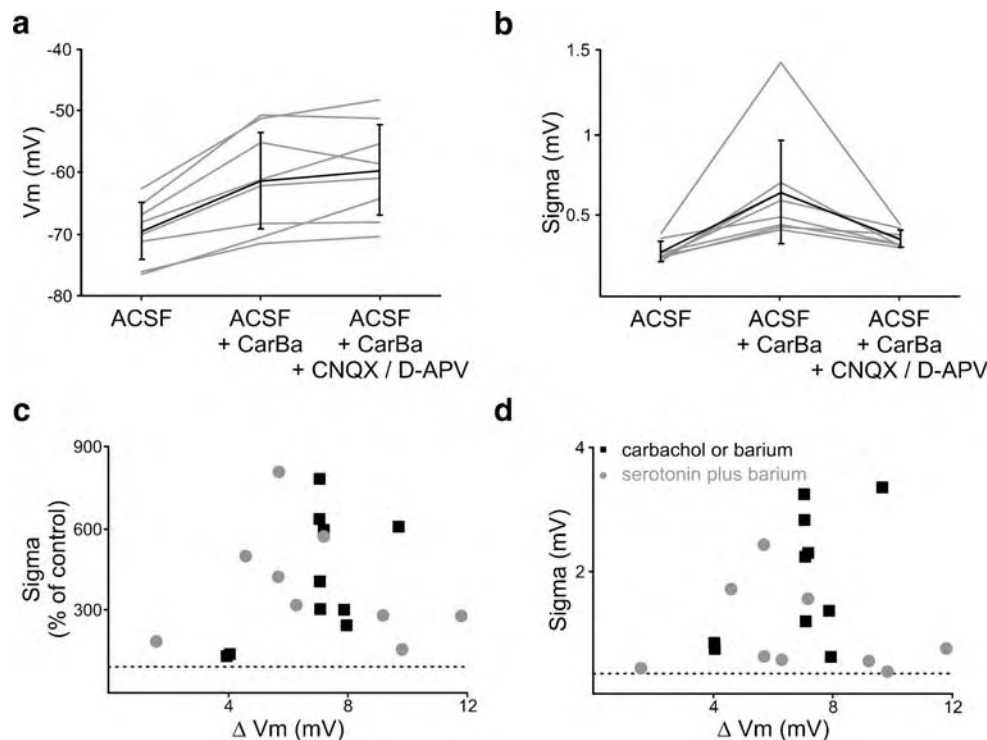
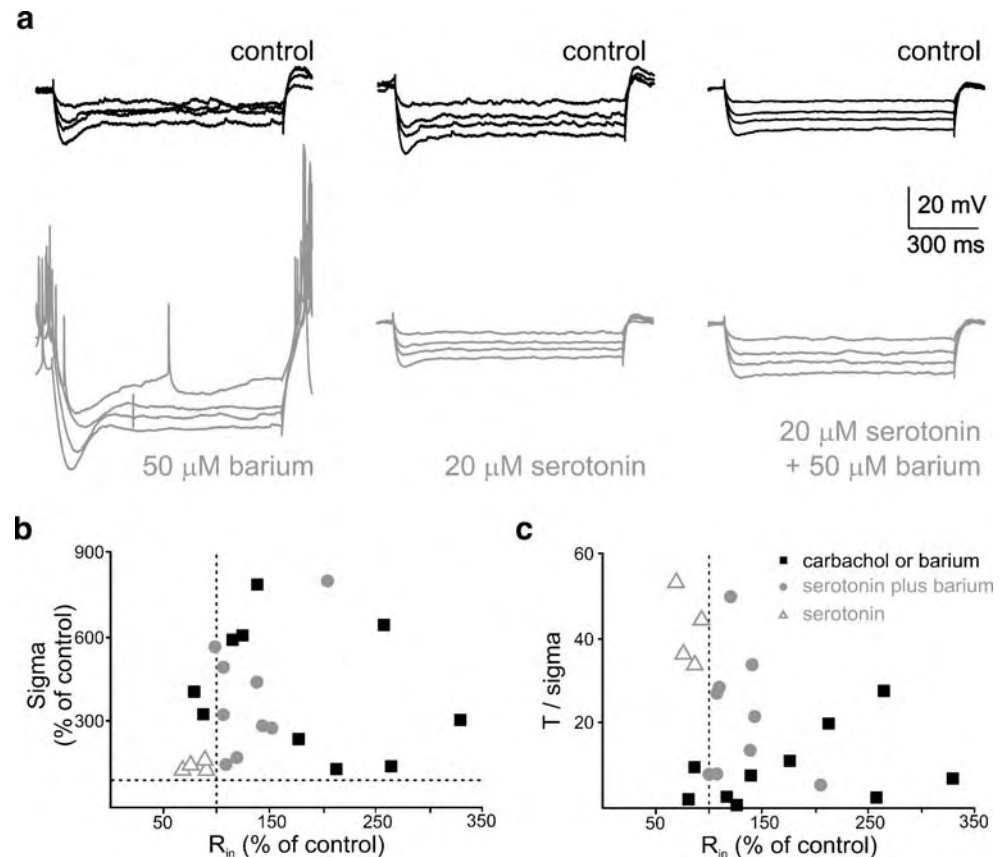


Fig. 5 Depolarization during INA is due to modulation of intrinsic conductances and not due to excitatory synaptic drive in the network. **a** The membrane potential of eight cells in ACSF, ACSF plus 20 μ M carbachol or 50 μ M barium (ACSF + CarBa, cholinergic activation), and ACSF + CarBa plus 10 μ M CNQX/50 μ M D-APV. The cells depolarize under ACSF + CarBa. This depolarization is not reversed under ACSF + CarBa + CNQX/D-APV. Single-cell values in gray, mean \pm SD in black. **b** Plot of sigma under the same pharmacological conditions. Sigma increases under ACSF + CarBa, but this increase is

reversed under ACSF + CarBa + CNQX/D-APV. **c** Plot of the changes in sigma against the changes in membrane potential in 19 cells. A stronger depolarization of the cells under study is not correlated with an increased synaptic drive of the surrounding network reflected in sigma. **d** Plot of absolute values of sigma against the changes in membrane potential. The cells analyzed for **c** and **d** are identical to those in Fig. 4, except for serotonin. Dashed lines show the control level in ACSF

Fig. 6 Sigma and T/σ are not correlated with input resistance. **a** The input resistance was monitored with current injections between -100 and -400 pA. 50 micromoles of barium increases the input resistance, while 20 μM of serotonin lower it. A mixture of serotonin and barium results in an intermediate effect. **b** The plot of changes in sigma against changes in input resistance does not show a correlation. **c** Also, the plot of T/σ against changes in input resistance does not show a correlation. The cells analyzed are identical to those in Fig. 4. Dashed lines show the control level in ACSF. Mice P14 (**a**, left and middle part) and P15 (**a**, right part)



depolarization and ceased to generate action potentials. Activation with increased extracellular potassium and decreased calcium and magnesium concentrations resulted in a sufficient but only transient decrease of T/σ . Thus, these conditions did not result in INA.

Modulation of cholinergic and serotonergic conductances establishes stable and reversible increased network activity

Subcortical serotonergic and cholinergic fibers trigger wakefulness and responsiveness of cortical neurons to sensory stimuli, forming part of the ascending arousal system [37, 48]. We mimicked the cholinergic input using bath application of carbachol, an acetylcholine analog, or barium, a specific blocker of inward rectifier potassium channels [54]. These are downstream targets of the cholinergic action [23, 31]. Alternatively or in addition we applied serotonin, which acted in our system via an activation of persistent sodium channels (supplementary Fig. 1). We used the following pharmacological conditions: (a) cholinergic activation, 20 μM carbachol, 50 μM barium, or 100 μM barium; (b) serotonin 20 μM ; and (c) mixed activation, 10 μM serotonin plus 20 μM barium or 20 μM serotonin plus 50 μM barium. Data sets for the action of carbachol ($n=2$ cells), 50 μM barium ($n=4$ cells), or 100 μM barium ($n=4$ cells) showed comparable steady-

state effects on passive membrane properties. Therefore, they were pooled using the term “cholinergic activation” despite the fact that the blocking effect of barium on inwardly rectifier potassium channels might not reflect the full range of acetylcholine effects. We also pooled the values for mixed activation via different concentrations of serotonin and barium.

In all three pharmacological conditions, neurons depolarized, sigma increased, and the effective difference between mean V_m and spiking threshold was reduced, but the extent of these changes was different for the different pharmacological interventions (Figs. 3 and 4; Table 1). Using cholinergic activation, the cells depolarized by 9.5 ± 6.7 mV ($p < 0.01$; $n=10$ cells) and sigma increased to $420.4 \pm 207.4\%$ of control ($p < 0.01$; $n=10$; Fig. 3a; Table 1). T/σ was reduced to 12.0 ± 12.0 ($p < 0.01$; $n=10$). Spiking activity was seen with a median of 0.42 Hz (range $0-5.0$ Hz; $n=10$). In contrast to barium, carbachol initially hyperpolarized the cells for 2–3 min before reaching the depolarized steady-state level. In addition, the carbachol effect was the only one that was not fully reversible (not shown). Serotonergic activation alone resulted in weaker effects. The change of V_m of 3.3 ± 2.9 mV was not significant ($p=0.37$; $n=4$ cells). The change in sigma to $184.4 \pm 32.0\%$ of control was significant ($p=0.011$; $n=4$ cells; Fig. 3b; Table 1), and T/σ was decreased to

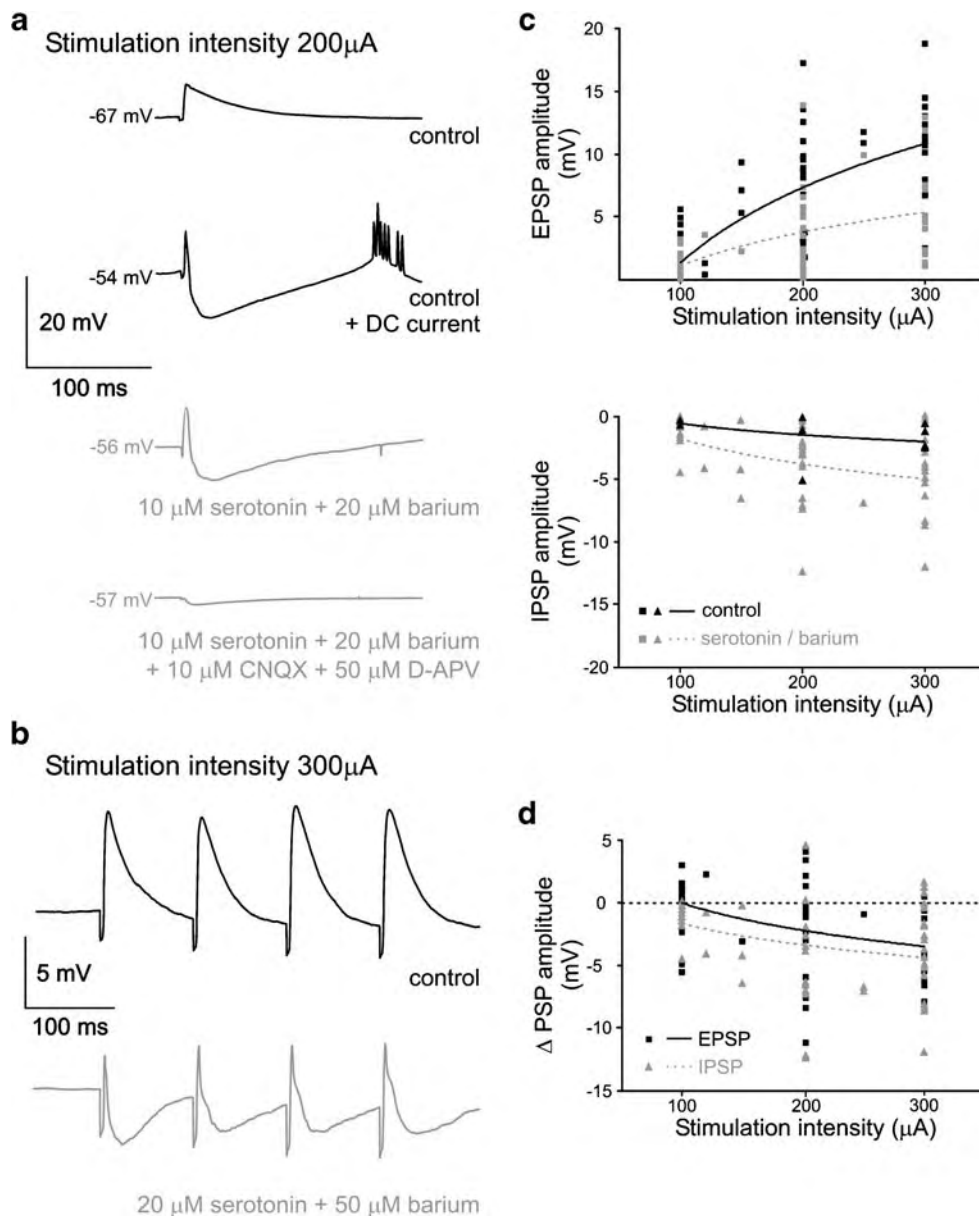


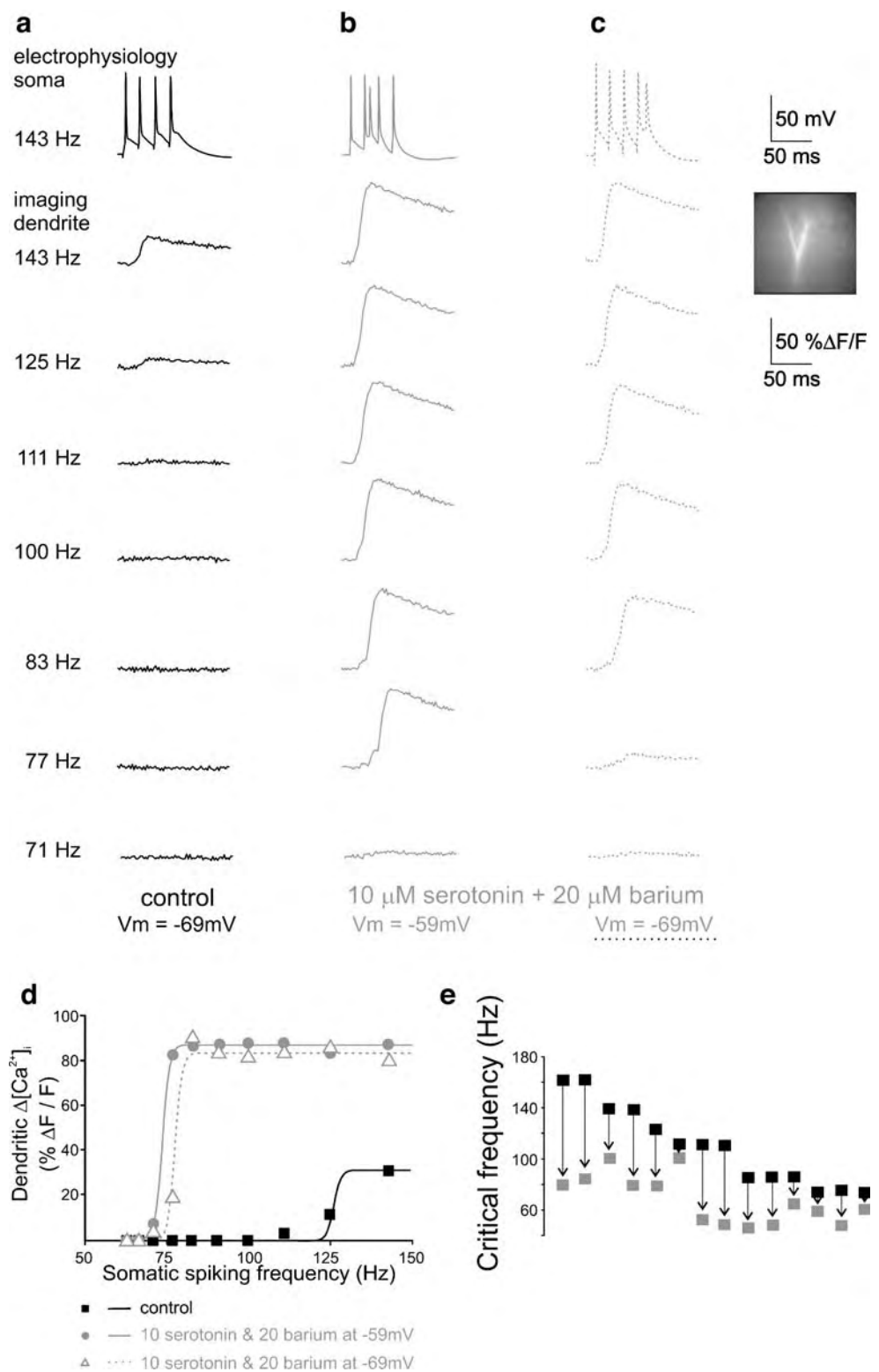
Fig. 7 INA increases the driving force for inhibitory inputs. **a** Activation of synaptic input by extracellular stimulation in layer 2 (400 μs duration, 200 μA amplitude, 10 trials averaged; *uppermost trace*). Under control conditions, an EPSP is evoked. At a depolarized membrane potential due to DC current injection, a diphasic response with an EPSP and an additional inhibitory component is observed (*second trace from top*). Mixed cholinergic–serotonergic activation depolarizes the cell and stimulation results in a comparable EPSP–IPSP sequence (*third trace from top*). Additional application of CNQX and D-APV results in the disappearance of all synaptic activity except a tiny monosynaptic inhibitory activity (*trace on bottom*). **b** A train of four pulses (400 μs duration, 300 μA amplitude, 10 Hz, 30 trials

averaged) evokes EPSPs under control conditions (*black trace*). Under mixed cholinergic–serotonergic activation, the evoked EPSPs are curtailed by disynaptic IPSPs (*gray trace*). **c** EPSP and IPSP amplitudes are plotted as a function of the stimulation intensity. *Solid black symbols* give the amplitude under control, *bordered gray symbols* depict the amplitude during mixed cholinergic–serotonergic activation. Curves are logarithmic fits of the data sets. **d** Changes in EPSP and IPSP amplitude following the switch to mixed cholinergic–serotonergic activation. EPSP changes are depicted as *black rectangles*, IPSP changes as *triangles*. A negative value means a decrease in EPSP size but an increase in the IPSP size. Mice P27 (**a**), P15 (**b**)

41.1 ± 7.7 ($p < 0.01$; $n = 4$ cells; Fig. 4). Spiking could not be observed under serotonin. Mixed serotonergic–cholinergic activation led to comparable effects on membrane potential depolarization and fluctuation in comparison to cholinergic activation alone. Cells depolarized by $10.0 \pm$

5.1 mV ($p < 0.01$; $n = 9$ cells) and sigma increased to $404.3 \pm 221.7\%$ of control ($p < 0.01$; $n = 9$; Fig. 3c; Table 1). The effective difference to spiking threshold T/σ decreased to 22.0 ± 14.7 ($p < 0.01$; $n = 9$; Fig. 4). Spiking activity was seen at 0.1 Hz (median; range 0 to 3.1 Hz; $n = 9$).

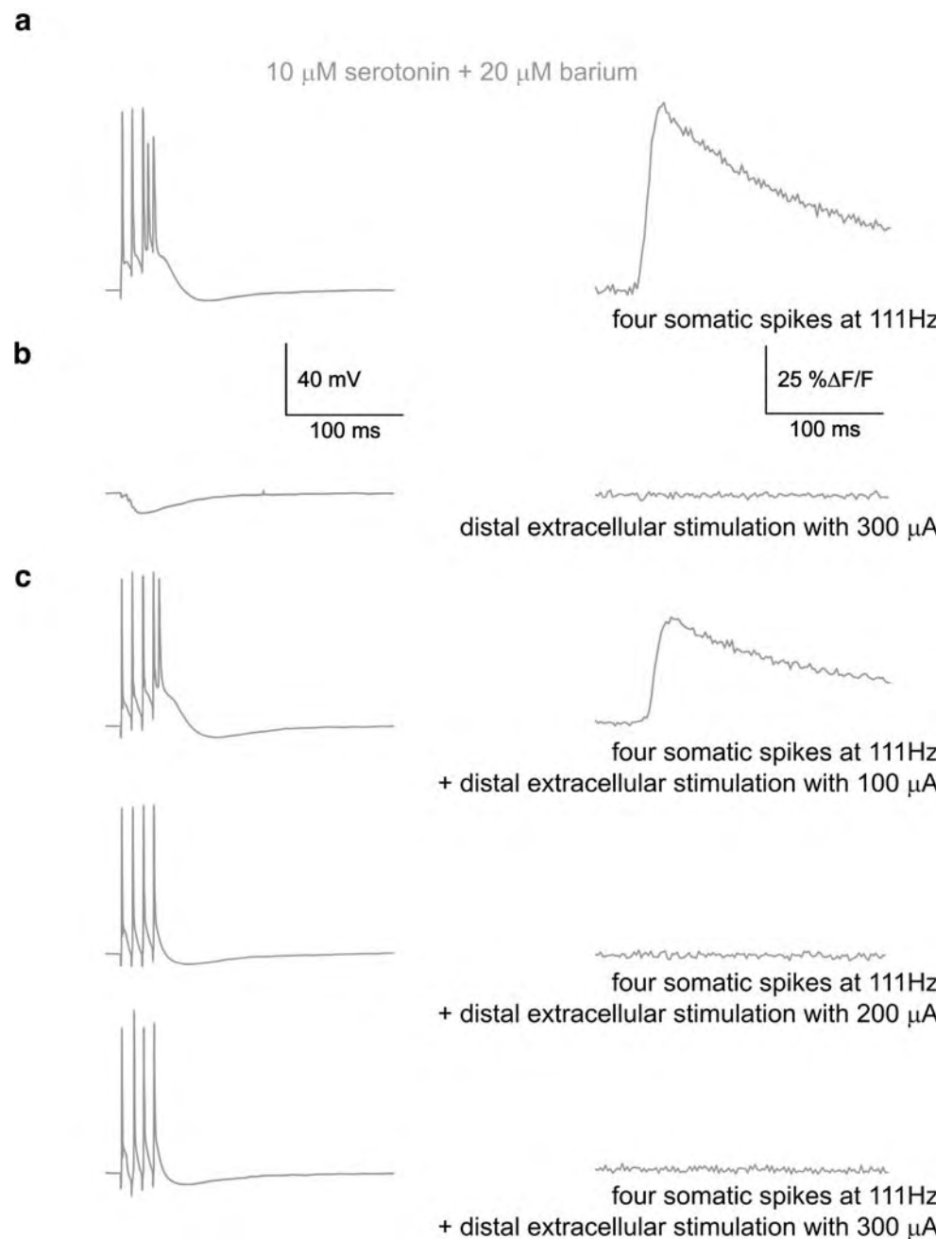
Fig. 8 INA decreases the critical frequency for dendritic calcium action potentials. The ability of layer 5 pyramidal cells to generate dendritic calcium action potentials was studied with four induced somatic action potentials at different frequencies. **a–c** Somatic membrane potential (*first row*, single trials). At the branchpoint of the distal apical dendrite (625 μm from the soma; see *inset*) changes in intracellular calcium concentration were imaged as changes in the fluorescence of the high-affinity calcium dye OGB-1 (following rows). Averaged signals from 10 trials, taken from a 100- μm segment of the dendrite. Electrophysiology and imaging are not aligned. **a** Below the so-called critical frequency (here 125 Hz), no dendritic calcium transients are visible under control conditions. **b** Mixed cholinergic–serotonergic activation depolarizes the cell. In addition, the critical frequency is decreased to 77 Hz and the amplitude of calcium events increases to 263% of control. **c** Repolarization of the somatic membrane potential with DC current injection to the control value changes the amplitude of dendritic calcium events and the critical frequency only marginally. **d** For the cell shown in **a–c**, the evoked changes of the calcium concentration in the dendrite are plotted against the frequency of induced somatic action potentials. During INA, calcium transients increase and the critical frequency is lowered. **e** For 14 cells, the shift in the critical frequency under INA is shown. Mouse P27 (**a–d**)



Thus, the strongest depolarizing effects and the largest increase in network synaptic drive were observed with cholinergic or mixed serotonergic–cholinergic activation, while serotonin alone had minor effects. For cholinergic or

mixed serotonergic–cholinergic activation, T/σ was in the requested range of values (Fig. 4), and electrophysiological behavior was stable and did not limit recording time. Thus, we refer to these conditions as INA.

Fig. 9 During INA, the GABAergic veto effect is present. To test if distal GABAergic input is able to suppress dendritic calcium action potentials (veto effect), we simultaneously evoked both signals during mixed cholinergic–serotonergic activation. *Left column*, somatic membrane potential (single trials); *right column*, imaged dendritic calcium changes (averaged from 10 trials, taken from a 100- μm segment of the dendrite). **a** Four somatic action potentials at 111 Hz evoke a dendritic calcium event that is accompanied by a somatic afterdepolarization with overlying additional spikes. **b** Distal extracellular stimulation at 300 μA evokes an IPSP, which does not show up at all in the calcium signal. **c** The combination of four somatic spikes at 111 Hz with a distal extracellular stimulation at 100 μA still results in a dendritic calcium event but with a reduced amplitude in comparison to somatic spikes alone. The somatic afterdepolarization is still present. Increasing the extracellular stimulation intensity to 200 and 300 μA results in the disappearance of the dendritic calcium signal and the somatic afterdepolarization. Mouse P27



Depolarization due to modulation of intrinsic conductances is the main factor for increased network activity

Depolarization of the neurons could be caused either by the modulation of intrinsic leak conductances that hyperpolarize the cells under control conditions or by a net excitatory synaptic drive emerging from the surrounding network. To get an estimate for the importance of the synaptic drive for depolarization during INA, we activated the network with 20 μM carbachol or 50 μM barium and then blocked synaptic conductances with 10 μM CNQX and 50 μM D-APV. Under these conditions, depolarization had an

amplitude of $128.1 \pm 41.4\%$ of the depolarization seen with carbachol or barium alone (difference not significant, $p=0.19$; $n=8$ cells; Fig. 5a). Sigma under carbachol or barium plus CNQX/D-APV was markedly reduced in comparison to carbachol or barium ($62.0 \pm 17.3\%$; $p<0.01$; $n=8$ cells; Fig. 5b). That it was still larger in comparison to the control value in ACSF ($133.0 \pm 25.6\%$; $p=0.012$) might be attributed to inhibitory input or to excitatory neurotransmitters other than glutamate. Next, we plotted the depolarization of a given cell against its sigma, either against the percentage of the control value (Fig. 5c) or against its absolute value (Fig. 5d), and found no

Table 1 Electrophysiological properties of layer 5 pyramidal cells under different pharmacological conditions

	ΔV_m (mV) (mean \pm SD)	T (mV) (mean \pm SD)	σ (mV) (range, median)	σ (% of control) (mean \pm SD)	T/σ (mean \pm SD)	Spiking frequency (Hz) (range, median)	R_{in} (% of control) (mean \pm SD)	τ (% of control) (mean \pm SD)
ACSF (control)	0 $n=54$	25.3 \pm 7.4 $n=54$	0.17–0.92, 0.35 $n=43$	100 $n=43$	71.6 \pm 37.8 $n=43$	0 $n=54$	100 $n=54$	100 $n=54$
LTX	2.5 \pm 3.0 $n=5$	29.5 \pm 10.4 $n=5$	0.49–1.86, 0.94 $n=5$	187 \pm 63.8 $n=5$	35.3 \pm 23.6* $n=5$	0–0.12, 0 $n=5$	109 \pm 27.7 $n=5$	94 \pm 8.5 $n=5$
PDX	3.3 \pm 2.4** $n=8$	25.8 \pm 11.1 $n=5$	0.28–0.76, 0.345 $n=8$	141 \pm 34.1** $n=8$	59.7 \pm 45.2 $n=5$	0–0.05, 0 $n=8$	95 \pm 26.8 $n=6$	95 \pm 29.6 $n=8$
5 K ⁺	13.3 \pm 5.6** $n=12$	17.2 \pm 3.3** $n=12$	0.73–2.23, 0.8 $n=5$	222.8 \pm 94.4* $n=5$	18.7 \pm 7.5** $n=5$	0–15.3, 0.2 $n=12$	72.3 \pm 38.0* $n=12$	63.9 \pm 22.9** $n=12$
6.25 K ⁺	18.4 \pm 11.1** $n=8$	15.6 \pm 2.7** $n=8$	0.5–2.02, 1.24 $n=6$	256.6 \pm 71.5* $n=6$	15.8 \pm 8.7** $n=6$	0–13.0, 1.15 $n=8$	79.3 \pm 28.5* $n=8$	51.3 \pm 21.4** $n=8$
CarBa	9.5 \pm 6.7** $n=10$	10.9 \pm 7.0** $n=10$	0.55–3.35, 1.16 $n=10$	420.4 \pm 207** $n=10$	12.0 \pm 12.0** $n=10$	0–5.0, 0.42 $n=10$	174.8 \pm 71.0** $n=10$	168.5 \pm 53.8** $n=10$
Ser	3.3 \pm 2.9 $n=4$	16.1 \pm 2.2* $n=4$	0.32–0.46, 0.405 $n=4$	184.4 \pm 32.0* $n=4$	41.1 \pm 7.7** $n=4$	0–0.01, 0 $n=4$	77.5 \pm 8.5 $n=4$	91.6 \pm 7.3 $n=4$
SerBa	10.0 \pm 5.1** $n=9$	13.8 \pm 2.4** $n=9$	0.34–2.41, 0.52 $n=9$	404.3 \pm 221** $n=9$	22.0 \pm 14.7** $n=9$	0–3.1, 0.1 $n=9$	127.2 \pm 32.4** $n=9$	139.1 \pm 21.8** $n=9$
Estimated ranges in vivo	–	2–30	1.4–12	–	<1–12	0.06–45	–	–

The parameters input resistance, membrane time constant, and mean spiking rate are not part of the INA definition. We include them to provide a more complete picture of the induced conditions. The in vivo values for T and σ were given in or had to be estimated from figures in Baranyi et al. [4], Chen and Fetz [10], Crochet and Petersen [11], DeWeese and Zador [15], Lee et al. [29], Margrie et al. [33], Matsumura et al. [34], Rudolph et al. [41], and Steriade et al. [49]. Spiking frequencies were taken from Chen and Fetz [10], Crochet and Petersen [11], DeWeese and Zador [15], Margrie et al. [33], Rudolph et al. [41], Steriade et al. [49], and Woody et al. [57].

ΔV_m change in membrane potential; T difference between mean membrane potential and spiking threshold; σ SD of the Gaussian-fitted membrane potential distribution; R_{in} input resistance; τ membrane time constant; ACSF control conditions in standard ACSF; LTX α -latrotoxin; PDX pardaxin; 5 K⁺ mACSF with 5 mM KCl, 1.5 CaCl₂, 0.5 mM MgCl₂; 6.25 K⁺ mACSF with 6.25 mM KCl, 1.5 CaCl₂, 0.5 mM MgCl₂; CarBa cholinergic activation with carbachol or barium; Ser serotonin; SerBa mixed cholinergic–serotonergic activation with barium and serotonin

*0.01 < p \leq 0.05; ** p \leq 0.01

correlation. These findings supported an intrinsic origin of the depolarization, while the synaptic network drive had no relevant effect in this preparation.

To test how changes of passive membrane properties due to cholinergic and serotonergic activation may influence σ or T/σ , we evaluated the changes in input

resistance related to the pharmacological intervention. Cholinergic activation resulted in an increase in input resistance to 174.8 \pm 71.0% of control (p < 0.01; n = 10 cells; Fig. 6a left part; Table 1). In contrast, serotonergic activation did not change input resistance significantly (77.5 \pm 8.5% of control; p = 0.12; n = 4 cells; Fig. 6a middle

part). With a mixed serotonergic–cholinergic activation, the value for input resistance was between that for purely serotonergic or cholinergic activation ($127.2 \pm 32.4\%$ of control, $p < 0.01$, $n = 9$ cells; Fig. 6a right part). Membrane time constant was changed accordingly in all conditions (Table 1).

Next, we checked whether changes in input resistance were related to changes in sigma or T/σ . A plot of both parameters did not give any correlation (Fig. 6b,c). This suggests that network activity reflected by sigma and the ability to generate INA (low T/σ) did not depend on a net change of input resistance. As a consequence, the resulting depolarization must have been the primary factor that drove the cells and the network.

Increased network activity augments the driving force for inhibitory inputs

Comparable to α -latrotoxin and mACSF (Figs. 1d and 2d), we tested how INA changes synaptic integration using extracellular stimulation (Fig. 7). EPSPs were markedly reduced in amplitude (70% of control) and duration under cholinergic or serotonergic–cholinergic activation (stimulation intensity 100–300 μA ; 59 data points obtained in 17 cells; Fig. 7a–d). These changes were accompanied by the appearance of an inhibitory disynaptic activity in 15 out of 17 cells (Fig. 7a, second trace from bottom). In 2 out of 17 cells, the disynaptic component was excitatory (not shown). The inhibitory component was nearly exclusively due to disynaptic activation because only a minor part was present under 10 μM CNQX and 50 μM D-APV (Fig. 7a, trace on bottom). The inhibitory disynaptic response could be mimicked if the cells were depolarized under control conditions by DC current injection to values obtained with serotonin plus barium (Fig. 7a, second trace from top). This suggests a role of the modified driving forces for chloride, potassium, and cationic conductances of GABA_A, GABA_B, and AMPA receptors, respectively, under INA.

Increased network activity boosts dendritic calcium events

To study dendritic activity in layer 5 pyramidal cell under INA, we prepared parasagittal slices from P27 to P30 mice ($n = 14$ cells). Comparing the properties of INA following serotonergic–cholinergic activation, differences between cells from the P14–P15 and the P27–P30 age groups are not significant. In the P27–P30 age group, sigma has a range of 0.37–0.85 mV with a median of 0.54 mV. T is 14.2 ± 5.6 mV (13.8 ± 2.4 mV in P14–P15 cells; $p = 0.78$), while T/σ is 27.7 ± 11.8 (22.0 ± 14.7 in P14–P15 cells; $p = 0.12$). Dendritic calcium events are best evoked due to a combined somatic and dendritic activation, suggesting that they need coincident input arriving at different cortical

layers to occur [27]. However, somatic action potentials alone can also induce dendritic calcium activity if they surpass a so-called critical frequency [7, 25]. Four somatic action potentials were induced at different frequencies, and the presence of a consecutive dendritic event was seen as an afterdepolarization in the somatic trace ($n = 14$ cells, not shown). In six cells, this was combined with a detection of the distal dendritic calcium signal using epifluorescence imaging (Fig. 8). We found a critical frequency of 120.8 ± 11.0 Hz under control (Fig. 8a), which was reduced to 59.8 ± 5.0 Hz in serotonergic–cholinergic INA (Fig. 8b, d, e), reflecting $57.0 \pm 4.1\%$ of control ($n = 14$ cells). In seven cells under serotonergic–cholinergic activation, DC current was injected to hyperpolarize the somatic membrane back to the value recorded under control conditions (Fig. 8c, d). Then, the critical frequency was unchanged and did not increase to the values found under control (compare Berger et al. [7] and Larkum et al. [25]).

Under increased network activity the GABAergic veto effect is still intact

A prominent feature of dendritic calcium events is their strong control via distal GABAergic inputs (veto effect [27, 39]). Therefore, we investigated the effects of distal dendritic stimulation on a dendritic calcium event evoked under serotonergic–cholinergic INA with four somatic action potentials (Fig. 9). Somatic activity beyond the critical frequency evoked a dendritic calcium transient (Fig. 9a, dendritic imaging data in the right part), which was accompanied by a strong somatic afterdepolarization and overlying action potentials (Fig. 9a, somatic membrane potential in the left part). Distal extracellular stimulation alone evoked a hyperpolarization-dominated postsynaptic response, which was, of course, not correlated to a calcium signal (Fig. 9b). In eight cells, concomitant and increasing extracellular stimulation abolished the somatic afterdepolarization, as well as the calcium event (Fig. 9c). Thus, also under conditions of a facilitated initiation of dendritic calcium events, distal inhibitory input is powerful enough to stop this activity.

Discussion

Definition of increased network activity

Acute slice preparations are the ideal system for electrophysiological studies of single cells and optical imaging in the cerebral cortex, as they provide major methodological advantages. All layers can be targeted. A high degree of visibility allows the recording from selected cell types and cellular compartments. Direct access enables local extracel-

lular drug application and absence of movement provides stable recordings. The physiological relevance of *in vitro* measurements, however, is limited due to altered integrative properties of the system. Here, we show that INA can be evoked in a stable and fully reversible manner in acute brain slices mimicking subcortical input. This enables a sophisticated level of investigation of neuronal integration at subcellular resolution, which is not feasible in the awake animal.

The first criterion of our definition of INA considers the probability of V_m to reach the spiking threshold. All studies using intracellular recordings in awake animals indicate low T/σ values in a range between 1 and 12 (estimations from Baranyi et al. [4], Chen and Fetz [10], Crochet and Petersen [11], DeWeese and Zador [15], Lee et al. [29], Margrie et al. [33], Matsumura et al. [34], Rudolph et al. [41], and Steriade et al. [49]). In contrast, standard slice preparations are characterized by an extreme increase of T/σ (to about 100, Destexhe et al. [14]; to 71.6, this study). The underlying mechanism is a consistently lowered σ in the slice situation (0.18 mV, Paré et al. [38]; 0.35 mV, this study) in comparison to the non-anesthetized animal (σ of about 2 mV [14]), and a much more hyperpolarized V_m *in vitro* (T of about 20 mV, Destexhe et al. [14]; 25.3 mV, this study). An apparent advantage of the T/σ parameter is the possibility of distinguishing intense subthreshold integration from only minute subthreshold activity (Fig. 4). If V_m values are not Gaussian-distributed, e.g., in cases of a highly coincident synaptic drive (auditory cortex [15]), the probability of action potentials might transiently be higher than indicated by T/σ .

Our two criteria for INA (see “Results” section) consider (a) the low T/σ values *in vivo* and (b) the fact that induced network activity should always be sustainable. One can argue that the action potential rate should also be included in the definition of INA. However, the literature is quite contradictory with respect to the spiking frequency in awake animals. Recordings of cortical cells reveal large differences in spiking frequencies (range 0.06–45 Hz [10, 11, 15, 33, 41, 49, 57]) that seem not to be due to different recording techniques [56]. Because of this disagreement, we do not include spiking rates in the definition of INA. In contrast, the T/σ paradigm even provides a possible explanation for differing rates of spiking *in vivo*. At the low T levels observed *in vivo*, slight changes of σ are sufficient to cause quite heterogeneous spiking frequencies.

Depolarization via modulated intrinsic conductances is the key mechanism for increased network activity

Large T/σ values in the untreated cortical slice normally prevent action potential output, while the pre-

served connectivity in this preparation in general is sufficient to generate network activity [32, 47, this study]. As active membrane properties are intact *in vitro*, two possible factors remain that can be responsible for the enormous T/σ and the electrophysiological quiescence in the slice: lack of synaptic drive and alteration of passive membrane properties. During INA, synaptic drive mediated by ionotropic conductances for sure contributes to the reduction of T/σ , as σ is increased in all cells under study and is in the range found in nonanesthetized animals (mean 1.16 mV for cholinergic and 0.52 mV for serotonergic–cholinergic activation, compared to about 2 mV *in vivo* [14]). However, it was not clear whether the increase of σ and the reduction of T were correlated phenomena. Blocking excitatory synaptic transmission under INA, we find that the depolarization remains while σ approaches the control values seen in ACSF. This means that the modulation of intrinsic conductances provides a sufficient degree of depolarization on the basis of which suprathreshold integration of synaptic input can take place. Taken together, the depolarization during INA seems to be due to the modulation of intrinsic conductances and does not depend on a net excitatory synaptic drive.

The input resistance is a passive membrane property that could determine the impact of synaptic input on V_m and σ . On the one hand, depolarizing synaptic activity is able to lower the input resistance of cortical neurons *in vivo* [13, 14]. On the other hand, depolarizing events can also reliably be associated with an increase in input resistance if intrinsic conductances come into play that counteract the shunting effect of synaptic input [56]. In our study, INA is accompanied by an increased input resistance, but this increase is correlated neither with σ nor with T/σ . Therefore, an increase of input resistance is not a prerequisite for the induction of INA. This finding is supported by our experiments with a changed ionic composition of the extracellular solution (mACSF). In this case, low T/σ values and an elevated spiking rate are associated with a markedly decreased input resistance. Thus, low T/σ values can be obtained under conditions that include either an increase or a decrease of input resistance. The possible independence of network activity from input resistance is further corroborated by the study of Steriade and coworkers [49], which shows that comparable spiking rates can be observed at very different levels of input resistance. During wakefulness, the input resistance in cortical cells is almost doubled in comparison to the depolarizing phase of slow wave sleep, while the spiking rate is even lower. As we have discussed above, INA depends on the depolarization of neurons, which is mainly based on the tuning of intrinsic leak conductances and only to a minor degree, if at all, on a modification of input resistance.

Cholinergic modulation of the cortical function is complex [31]. m1 Muscarinic acetylcholine receptors inhibit G protein-coupled inwardly rectifying potassium channels (GIRK channels [22]) while m2 receptors activate them. Accordingly, muscarinic activation of the cortex can lead either to excitatory phenomena like gamma oscillations [8] or dampening effects, e.g., on synaptic integration in pyramidal cell dendrites [17, 44]. Using carbachol, Vm depolarization and an increase in input resistance are consistent with the blocking effect of acetylcholine on resting potassium conductances [23]. With barium, we specifically select the effect on inwardly rectifying potassium channels [54]. Barium has comparable effects to acetylcholine, and their effects are not additive [23]. In this study, carbachol and barium have comparable effects, and cells are pooled.

Serotonin has been shown to have several effects on cortical cells via ionotropic and metabotropic receptors. It activates GIRK channels in layer 5 pyramidal cells of the somatosensory cortex via 5-HT1A receptors [54]. However, this effect is delayed during development [45] and, therefore, may be of less importance at the age range studied here. 5-HT2 receptors have been shown to activate the persistent sodium current in spinal cord motoneurons [18]. The persistent sodium conductance is an important factor for the excitability of layer 5 pyramidal cells in the somatosensory cortex [3]. Using voltage-clamp recordings in layer 5 pyramidal cells, we find that serotonin indeed activates the persistent sodium current (supplementary Fig. 1). This effect can explain the depolarization under serotonin seen in the present study.

In vitro, long-range afferents of both kinds, ionotropic and subcortical neuromodulatory ones, are severed due to the slice preparation. Pure activation of the presynaptic release machinery using α -latrotoxin or pardaxin is ineffective in providing INA, indicating that the lack of ionotropic input is not the main reason for the silent state in slice preparations. Proper subthreshold activity is not sufficient to push Vm to threshold as long as cells stay locked in an unphysiological hyperpolarization. Our findings suggest that the in vitro slice preparation mainly lacks subcortical neuromodulatory input providing depolarization. Restoring this input is sufficient for the generation of INA.

Synaptic and somatodendritic integration in layer 5 pyramidal cells under increased network activity

The apical dendrite of layer 5 pyramidal cells of the somatosensory cortex is actively taking part in the integration of synaptic input. Generation of calcium action potentials in the distal dendrite is regulated by synaptic and intrinsic conductances. Inhibitory synaptic drive via GABA receptors impairs the initiation of dendritic calcium events

(veto effect [39]). Dendritic calcium spikes may result from the interaction of sensory and associative signals [27]. In addition, resting conductances like Ih [5, 7] and GIRK [55] separate somatic and dendritic initiation zones electrotonically. The effectiveness of boosting and dampening conductances is dramatically influenced by changes in the actual membrane potential and in the passive membrane properties. Unfortunately, the knowledge about the interactions in the dendrite primarily derives from recordings in untreated slices where passive membrane properties are altered. In vivo, dendrites of layer 2/3 and layer 5 pyramidal cells are able to generate so-called complex action potentials [19, 26, 53, 58], which seem to be the correlate of calcium events observed in vitro. There is, however, not a one-to-one relationship between dendritic calcium event and somatic action potential burst [19]. Such observations cannot be addressed in detail due to the limitations of in vivo experiments. Therefore, it is highly desirable to study dendritic phenomena under well-manageable conditions with INA.

Here, we show that distal extracellular stimulation under INA is dominated by disynaptic inhibition, which dramatically curtails the evoked EPSP. This strengthened inhibition is primarily due to an increased driving force for chloride, while the driving force for the cationic glutamatergic conductance is diminished. At lower stimulation intensity (100 μ A), the size of the EPSPs is almost the same under INA and control (Fig. 7d). Thus, it seems unlikely that there is an additional direct effect of INA on the release probability of excitatory synapses. The depolarized conditions in vivo may therefore result in a comparably pronounced inhibitory action. The overall control of inhibitory synaptic conductances over excitatory ones is expected to be strengthened (see Schiller et al. [42]), as well as thalamocortical feedforward inhibition [52] and, in particular, the dendritic veto effect [27]. Therefore, we studied the changes in dendritic excitability under INA. Compared to standard in vitro conditions, we find a strong decrease in the frequency of somatic action potentials critical for the induction of dendritic calcium action potentials and an increase of the amplitude of the dendritic calcium response. In contrast to the effect of GABAergic synaptic inhibition, this facilitation is not compensated by somatic hyperpolarizing DC current injection. Thus, it does not seem to be a depolarization of the dendritic initiation zone that decreases the critical frequency but a modulation of the input resistance and membrane time constant. Alternatively, an insufficient space-clamp of the dendritic initiation zone may cause the failure to prevent dendritic calcium action potentials (but see Berger et al. [7]). Our data suggest that blocking dendritic GIRK channels with carbachol or barium prolongs the membrane time constant of dendrites and thereby facilitates dendritic electrogenesis.

Activation of persistent sodium currents via serotonin may ease action potential backpropagation and further favor calcium spikes [43, 51]. In spite of the facilitated dendritic excitability, boosted disynaptic inhibition is strong enough to prevent calcium spikes. These experiments show that, in the somatosensory cortex, the veto effect first described in vitro [27] is present under INA levels.

Acknowledgements We thank Drs. Alain Destexhe, Michele Giugliano, Serge Korogod, Matthew Larkum, and Hans-R. Lüscher for useful discussions and comments on earlier versions of the manuscript. This work was supported by the Swiss National Foundation (Grant 3100-107529/1) and the Novartis Foundation for Medical-Biological Research.

Disclosures There are no conflicts of interest.

References

- Abeles M (1982) Local cortical circuits—an electrophysiological study. Springer, Berlin Heidelberg New York
- Agmon A, Connors BW (1991) Thalamocortical responses of mouse somatosensory (barrel) cortex in vitro. *Neuroscience* 41:365–379
- Aracri P, Colombo E, Mantegazza M, Scalmani P, Curia G, Avanzini G, Franceschetti S (2006) Layer-specific properties of the persistent sodium current in sensorimotor cortex. *J Neurophysiol* 95:3460–3468
- Baranyi A, Szente MB, Woody CD (1993) Electrophysiological characterization of different types of neurons recorded in vivo in the motor cortex of the cat. II. Membrane parameters, action potentials, current-induced voltage responses and electrotonic structures. *J Neurophysiol* 69:1865–1879
- Berger T, Larkum ME, Lüscher HR (2001) High I_h channel density in the distal apical dendrite of layer V pyramidal cells increases bidirectional attenuation of EPSPs. *J Neurophysiol* 85:855–868
- Berger T, Lüscher HR, Giugliano M (2006) Transient rhythmic network activity in the somatosensory cortex evoked by distributed input in vitro. *Neuroscience* 140:1401–1413
- Berger T, Senn W, Lüscher HR (2003) Hyperpolarization-activated current I_h disconnects somatic and dendritic spike initiation zones in layer V pyramidal neurons. *J Neurophysiol* 90:2428–2437
- Buhl EH, Tamas G, Fisahn A (1998) Cholinergic activation and tonic excitation induce persistent gamma oscillations in mouse somatosensory cortex in vitro. *J Physiol* 513:117–126
- Capogna M, Gähwiler BH, Thompson SM (1996) Calcium-independent actions of alpha-latrotoxin on spontaneous and evoked synaptic transmission in the hippocampus. *J Neurophysiol* 76:3149–3158
- Chen D, Fetz EE (2005) Characteristic membrane potential trajectories in primate sensorimotor cortex neurons recorded in vivo. *J Neurophysiol* 94:2713–2725
- Crochet S, Petersen CC (2006) Correlating whisker behavior with membrane potential in barrel cortex of awake mice. *Nat Neurosci* 9:608–610
- Descarries L, Gisiger V, Steriade M (1997) Diffuse transmission by acetylcholine in the CNS. *Prog Neurobiol* 53:603–625
- Destexhe A, Pare D (1999) Impact of network activity on the integrative properties of neocortical pyramidal neurons in vivo. *J Neurophysiol* 81:1531–1547
- Destexhe A, Rudolph M, Pare D (2003) The high-conductance state of neocortical neurons in vivo. *Nat Rev Neurosci* 4:739–751
- DeWeese MR, Zador AM (2006) Non-Gaussian membrane potential dynamics imply sparse, synchronous activity in auditory cortex. *J Neurosci* 26:12206–12218
- Grasso A, Alema S, Rufini S, Senni MI (1980) Black widow spider toxin-induced calcium fluxes and transmitter release in a neurosecretory cell line. *Nature* 283:774–776
- Gulledge AT, Stuart GJ (2005) Cholinergic inhibition of neocortical pyramidal neurons. *J Neurosci* 25:10308–10320
- Harvey PJ, Li X, Li Y, Bennett DJ (2006) 5-HT₂ receptor activation facilitates a persistent sodium current and repetitive firing in spinal motoneurons of rats with and without chronic spinal cord injury. *J Neurophysiol* 96:1158–1170
- Helmchen F, Svoboda K, Denk W, Tank DW (1999) In vivo dendritic calcium dynamics in deep-layer cortical pyramidal neurons. *Nat Neurosci* 2:989–996
- Henkel AW, Sankaranarayanan S (1999) Mechanisms of alpha-latrotoxin action. *Cell Tissue Res* 296:229–233
- Henze DA, McMahon DB, Harris KM, Barrionuevo G (2002) Giant miniature EPSCs at the hippocampal mossy fiber to CA3 pyramidal cell synapse are monoquantal. *J Neurophysiol* 87:15–29
- Hill JJ, Peralta EG (2001) Inhibition of a Gi-activated potassium channel (GIRK1/4) by the Gq-coupled m1 muscarinic acetylcholine receptor. *J Biol Chem* 276:5505–5510
- Krnjevic K, Pumain R, Renaud L (1971a) Effects of Ba^{2+} and tetraethylammonium on cortical neurones. *J Physiol* 215:223–245
- Krnjevic K, Pumain R, Renaud L (1971b) The mechanism of excitation by acetylcholine in the cerebral cortex. *J Physiol* 215:247–268
- Larkum ME, Kaiser KM, Sakmann B (1999a) Calcium electrogenesis in distal apical dendrites of layer 5 pyramidal cells at a critical frequency of back-propagating action potentials. *Proc Natl Acad Sci USA* 96:14600–14604
- Larkum ME, Zhu JJ (2002) Signaling of layer 1 and whisker-evoked Ca^{2+} and Na^+ action potentials in distal and terminal dendrites of rat neocortical pyramidal neurons in vitro and in vivo. *J Neurosci* 22:6991–7005
- Larkum ME, Zhu JJ, Sakmann B (1999b) A new cellular mechanism for coupling inputs arriving at different cortical layers. *Nature* 398:338–341
- Lazarovici P, Lelkes PI (1992) Pardaxin induces exocytosis in bovine adrenal medullary chromaffin cells independent of calcium. *J Pharmacol Exp Ther* 263:1317–1326
- Lee AK, Manns ID, Sakmann B, Brecht M (2006) Whole-cell recordings in freely moving rats. *Neuron* 51:399–407
- London M, Häusser M (2005) Dendritic computation. *Annu Rev Neurosci* 28:503–532
- Lucas-Meunier E, Fossier P, Baux G, Amar M (2003) Cholinergic modulation of the cortical neuronal network. *Pflügers Arch* 446:17–29
- Maclean JN, Watson BO, Aaron GB, Yuste R (2005) Internal dynamics determine the cortical response to thalamic stimulation. *Neuron* 48:811–823
- Margrie TW, Brecht M, Sakmann B (2002) In vivo, low-resistance, whole-cell recordings from neurons in the anaesthetized and awake mammalian brain. *Pflügers Arch* 444:491–498
- Matsumura M, Cope T, Fetz EE (1988) Sustained excitatory synaptic input to motor cortex neurons in awake animals revealed by intracellular recording of membrane potentials. *Exp Brain Res* 70:463–469
- McCormick DA (1989) Cholinergic and noradrenergic modulation of thalamocortical processing. *Trends Neurosci* 12:215–221
- McCormick DA, Prince DA (1986) Mechanisms of action of acetylcholine in the guinea-pig cerebral cortex in vitro. *J Physiol* 375:169–194

37. Miller DB, O'Callaghan JP (2006) The pharmacology of wakefulness. *Metabolism* 55(Suppl 2):S13–S19
38. Paré D, Shink E, Gaudreau H, Destexhe A, Lang EJ (1998) Impact of spontaneous synaptic activity on the resting properties of cat neocortical pyramidal neurons in vivo. *J Neurophysiol* 79:1450–1460
39. Perez-Garci E, Gassmann M, Bettler B, Larkum ME (2006) The GABAB1b isoform mediates long-lasting inhibition of dendritic Ca^{2+} spikes in layer 5 somatosensory pyramidal neurons. *Neuron* 50:603–616
40. Petrenko AG (1993) Alpha-Latrotoxin receptor. Implications in nerve terminal function. *FEBS Lett* 325:81–85
41. Rudolph M, Pospischil M, Timofeev I, Destexhe A (2007) Inhibition determines membrane potential dynamics and controls action potential generation in awake and sleeping cat cortex. *J Neurosci* 27:5280–5290
42. Schiller J, Schiller Y, Stuart G, Sakmann B (1997) Calcium action potentials restricted to distal apical dendrites of rat neocortical pyramidal neurons. *J Physiol* 505:605–616
43. Schwandt PC, Crill WE (1995) Amplification of synaptic current by persistent sodium conductance in apical dendrite of neocortical neurons. *J Neurophysiol* 74:2220–2224
44. Seeger T, Alzheimer C (2001) Muscarinic activation of inwardly rectifying K^+ conductance reduces EPSPs in rat hippocampal CA1 pyramidal cells. *J Physiol* 535:383–396
45. Sickmann T, Alzheimer C (2003) Short-term desensitization of G-protein-activated, inwardly rectifying K^+ (GIRK) currents in pyramidal neurons of rat neocortex. *J Neurophysiol* 90:2494–2503
46. Sidiropoulou K, Pissadaki EK, Poirazi P (2006) Inside the brain of a neuron. *EMBO Rep* 7:886–892
47. Silberberg G, Wu C, Markram H (2004) Synaptic dynamics control the timing of neuronal excitation in the activated neocortical microcircuit. *J Physiol* 556:19–27
48. Steriade M, McCarley R (2005) *Brain control of wakefulness and sleeping*. Plenum, New York
49. Steriade M, Timofeev I, Grenier F (2001) Natural waking and sleep states: a view from inside neocortical neurons. *J Neurophysiol* 85:1969–1985
50. Stuart GJ, Sakmann B (1994) Active propagation of somatic action potentials into neocortical pyramidal cell dendrites. *Nature* 367:69–72
51. Stuart GJ, Sakmann B (1995) Amplification of EPSPs by axosomatic sodium channels in neocortical pyramidal neurons. *Neuron* 15:1065–1076
52. Sun QQ, Huguenard JR, Prince DA (2006) Barrel cortex microcircuits: thalamocortical feedforward inhibition in spiny stellate cells is mediated by a small number of fast-spiking interneurons. *J Neurosci* 26:1219–1230
53. Svoboda K, Denk W, Kleinfeld D, Tank DW (1997) In vivo dendritic calcium dynamics in neocortical pyramidal neurons. *Nature* 385:161–165
54. Takigawa T, Alzheimer C (1999) G protein-activated inwardly rectifying K^+ (GIRK) currents in dendrites of rat neocortical pyramidal cells. *J Physiol* 517:385–390
55. Takigawa T, Alzheimer C (2003) Interplay between activation of GIRK current and deactivation of I_h modifies temporal integration of excitatory input in CA1 pyramidal cells. *J Neurophysiol* 89:2238–2244
56. Waters J, Helmchen F (2006) Background synaptic activity is sparse in neocortex. *J Neurosci* 26:8267–8277
57. Woody CD, Swartz BE, Gruen E (1978) Effects of acetylcholine and cyclic GMP on input resistance of cortical neurons in awake cats. *Brain Res* 158:373–395
58. Zhu Y, Zhu JJ (2004) Rapid arrival and integration of ascending sensory information in layer 1 nonpyramidal neurons and tuft dendrites of layer 5 pyramidal neurons of the neocortex. *J Neurosci* 24:1272–1279

- Publication 2 -

“Reassembling a System from the Sensor to Cerebral Representation: The Olfactory System In Vitro”

Foivos Markopoulos, Florian B. Neubauer, Thomas Berger & Alessandra L. Scotti (2008).
Neuroscience 156:1048-1063.

When sensory information reaches the brain it has already been processed on its way from the sensory receptor via relay neurons to the primary sensory area in the cortex related to the sensory system. To capture the full mechanisms of information processing in the brain, it would be very useful to know in which form the information is encoded at the point in time when the cortex becomes involved. However, neuronal activity at this stage, distributed over axons from the last subcortical station to the cortex, is not accessible *in vivo*. The second publication to which I contributed describes for the first time an *in vitro* preparation of a complete mammalian sensory system, the olfactory system. The preparation includes the full sensory pathway of a postnatal mouse, i.e. the olfactory epithelium, the olfactory bulb, and the olfactory cortex. The olfactory epithelium which contains the sensory receptors is disrupted from the olfactory bulb during the initial slicing. Therefore the system has to be grown in a slice culture. The olfactory epithelium reestablishes its axonal connectivity to the olfactory bulb over culturing time, guided by intrinsic growth factors. Olfactory bulb and olfactory cortex, in contrast, are obtained in a common single slice preparation and therefore their mutual connections are preserved from the beginning. According to immunohistochemical staining, the olfactory epithelium has re-innervated the olfactory bulb and its axons find their way to their postsynaptic partners, the mitral cells in the bulb, after 3 weeks of co-culturing. Now the olfactory pathway is available for studies *in vitro* with maximum accessibility. By means of artificial electrical stimulation and calcium-sensitive dye imaging we show that excitatory neuronal connectivity is intact between the olfactory epithelium and the olfactory bulb as well as between the olfactory bulb and the olfactory cortex. An outlook of this project for the future is to improve the system further so that odorants as natural stimuli could be used and to describe in detail the resulting activity patterns in the olfactory bulb and in the cortex. As a culture system, this preparation is limited in terms of equivalency to the anatomical structure *in vivo*. However, basic mechanisms of information processing in the olfactory network should be much easier to study with single cell resolution in this preparation than *in vivo*.

REASSEMBLING A SYSTEM FROM THE SENSOR TO CEREBRAL REPRESENTATION: THE OLFACTORY SYSTEM *IN VITRO*

F. MARKOPOULOS,^{a1} F. B. NEUBAUER,^b T. BERGER^{b2}
AND A. L. SCOTTI^{a3*}

^aInstitute of Anatomy, CH3012 Bern, Switzerland

^bInstitute of Physiology of the University of Bern, CH-3012 Bern, Switzerland

Abstract—An odorant's code is represented by activity in a dispersed ensemble of olfactory sensory neurons in the nose, activation of a specific combination of groups of mitral cells in the olfactory bulb and is considered to be mapped at divergent locations in the olfactory cortex. We present here an *in vitro* model of the mammalian olfactory system developed to gain easy access to all stations of the olfactory pathway. Mouse olfactory epithelial explants are cocultured with a brain slice that includes the olfactory bulb and olfactory cortex areas and maintains the central olfactory pathway intact and functional. Organotypicity of bulb and cortex is preserved and mitral cell axons can be traced to their target areas. Calcium imaging shows propagation of mitral cell activity to the piriform cortex. Long term coculturing with postnatal olfactory epithelial explants restores the peripheral olfactory pathway. Olfactory receptor neurons renew and progressively acquire a mature phenotype. Axons of olfactory receptor neurons grow out of the explant and rewire into the olfactory bulb. The extent of reinnervation exhibits features of a postlesion recovery. Functional imaging confirms the recovery of part of the peripheral olfactory pathway and shows that activity elicited in olfactory receptor neurons or the olfactory nerves is synaptically propagated into olfactory cortex areas. This model is the first attempt to reassemble a sensory system in culture, from the peripheral sensor to the site of cortical representation. It will increase our knowledge on how neuronal circuits in the central olfactory areas integrate sensory input and counterbalance damage. © 2008 IBRO. Published by Elsevier Ltd. All rights reserved.

Key words: calretinin, GAP43, OMP, Oregon Green-BAPTA, Reelin.

The olfactory system recognizes, discriminates and elaborates volatile chemicals in our environment. Odorant molecules are detected in the nose by the specialized receptor neurons of the olfactory epithelium (OE) located in the roof of each nostril. Olfactory receptor neurons (ORNs) transduce the chemical signals into electrical signals that are conveyed by their axons through the ethmoidal cribriform plate in the anterior skull base to the olfactory bulbs. The principal neurons of the main olfactory bulb (MOB), the mitral cells, send their axons through the lateral olfactory tract (LOT) to target the piriform cortex (Pir), the primary olfactory cortex. Both the LOT and the Pir extend along the most anterior basal portion of the forebrain (Shipley et al., 2004).

An odorant's code is represented by activity in a dispersed ensemble of ORNs in the nose and by activation of a specific combination of glomeruli in the MOB. The high degree of convergence in the MOB allows the amplification of many weak signals, optimizing sensitivity to the generally low concentrations of odorants. Intrabulbar circuits involving two main classes of interneurons, periglomerular and granule cells, provide additional processing of olfactory inputs. Compared with the large amount of data available on ORN function and on the activity of the MOB network (Lledo et al., 2005), studies focusing on the primary olfactory cortex are less numerous, due to the difficulty to access this ventrally located region *in vivo*. Thus, knowledge on the cortical representation of odors and on the network characteristics of the primary and associational olfactory cortical areas remains incomplete. There is recent evidence that input from one particular odorant receptor is mapped at divergent locations in the cortex and that different odorant receptors are represented in overlapping cortical areas (Zou et al., 2005). Brain slices that include olfactory cortical areas are used for *in vitro* electrophysiological and imaging studies and have provided valuable information on the network and cellular properties of these regions. These preparations, however, generally disrupt the peripheral olfactory pathway and rarely preserve the MOB (Litaudon et al., 1997; Demir et al., 2001; Balu et al., 2007). Whole brain preparations including the MOB and the Pir and perfused through the vessels are used for functional investigations (Uva et al., 2006) and have been recently further improved to maintain both the peripheral and central olfactory pathway (Ishikawa et al., 2007). This approach facilitates access to the LOT and the Pir that line the base of the skull and respects at the same

¹ Upcoming address (from October 1, 2008): Department of Molecular and Cellular Biology, Harvard University, 16 Divinity Avenue, Cambridge MA 02138, USA.

² Present address: Institute for Physiology and Pathophysiology, University of Mainz, Duesbergweg 6, D-55128 Germany.

³ Present address: Department of Medicine, Anatomy Unit, University of Fribourg, Rte A.Gockel 1, CH-1700 Fribourg, Switzerland.

*Corresponding author. Tel: +41-26-300-85-09.

E-mail address: alessandra.scotti@unifr.ch (A. L. Scotti).

Abbreviations: AON, anterior olfactory nucleus; APir, anterior piriform cortex; AP5, 2-amino-5-phosphonvaleric acid; BrdU, bromo-deoxyuridine; CNQX, 6-cyano-7-nitroquinoxaline-2,3-dione; CR, calretinin; DAB, diaminobenzidine; Dil, 1,1'-dioctadecyl-3,3',3'-tetramethylindocarbocyanine perchlorate; DIV, days *in vitro*; GAP43, growth associated protein 43; GFP, green fluorescent protein; LECx, lateral entorhinal cortex; LOT, lateral olfactory tract; MEM, minimal essential medium; MOB, main olfactory bulb; NMDA, N-methyl-D-aspartic acid; OB, olfactory brain; OE, olfactory epithelium; OMP, olfactory marker protein; ORN, olfactory receptor neuron; P, postnatal day; PBS, phosphate buffer saline; Pir, piriform cortex; PPir, posterior piriform cortex.

time the integrity of this sensory system. Nevertheless, it remains technically demanding and limited to acute studies.

The mammalian olfactory system is also a very valuable model for the investigation of neuronal regeneration and axonal growth in its peripheral part. In fact, ORNs are short-lived cells periodically replaced by stem cells located in the basal layer of the OE (Weiler and Farbman, 1997; Beites et al., 2005; Mombaerts, 2006). After damage to the OE or transection of the olfactory nerves the ORNs reconstitutes, the axons regrow, eventually reinnervating the olfactory bulb. Such repair potential compensates for the extremely exposed location of olfactory sensory neurons cell bodies within the nasal cavities (Graziadei and Graziadei, 1979; Graziadei and Monti Graziadei, 1980). Afferent sensory input determines numerous properties of target CNS neurons. As known for other sensory systems (Kupfer and Palmer, 1964; Born and Rubel, 1985), cellular phenotypes in the MOB are profoundly altered following olfactory deafferentation and functional recovery following reinnervation is partial (Schwob et al., 1999; Christensen et al., 2001; Schwob, 2005; Mombaerts, 2006). Numerous subtle changes are also observed in the MOB in response to sensory deprivation, not solely during the critical postnatal period of input dependent maturation (Liu et al., 1999; Matsutani and Yamamoto, 2000; Couper Leo and Brunjes, 2003) but also in the adult animal (Hamilton et al., 2008). There is general belief that both sensory deprivation and denervation must also secondarily affect the synaptic landscape of those olfactory cortex regions receiving a direct MOB input. Knowledge on local adjustments of neurochemical characteristics and on the extent of synaptic remodeling in these regions in response to altered sensory input is growing but still limited, due to methodological and technical constraints (Best and Wilson, 2003; Franks and Isaacson, 2005; Kim et al., 2006).

We present here an *in vitro* model of the mammalian olfactory system developed to gain easy access to all stations of the olfactory pathway. The *in vitro* transfer of the

olfactory system consists in coculturing olfactory epithelial explants with a brain slice that includes the MOB and olfactory cortex areas. We provide evidence for the maintenance of the central olfactory pathway in this slice culture and show that the peripheral olfactory pathway reconstitutes and recovers function over a prolonged time in coculture. This coculture approach represents the first attempt to completely restore a sensory system. It makes possible to investigate how neuronal circuits in the MOB and the olfactory cortex integrate sensory input and adapt to degenerative change and repair damage in a culture environment.

EXPERIMENTAL PROCEDURES

Animals

Balb/c mice ($n=70$) were provided by the central animal facilities of the University of Bern. Olfactory marker protein-green fluorescent protein (OMP-GFP) mice ($n=7$) provided by Dr. Strotmann (University of Hohenheim, Germany), were used for additional experiments (Potter et al., 2001) and their breeding was performed by mating homozygous animals. Mice were kept on a 24 h day-night cycle with free access to food and water. All experiments were performed in accordance with the Swiss animal protection laws and with formal approval of the cantonal review board on animal experiments. All experiments conformed to international guidelines on the ethical use of animals. Efforts were made to minimize the number of animals used and their suffering.

Cultures

The slices and tissue explants were cultured at the air–liquid interface on hydrophilized PTFE membrane of 0.4 μm pore size (Millicel-CM of 4.5 mm frame height, Millipore, MA, USA). Tissues were maintained in 100% humidity in air with 5% CO_2 , at 37 °C for 1–3 weeks.

Preparation of the olfactory brain slice (OB slice). Mice from postnatal days 5 to 7 (P5–7) were killed by decapitation and the brain was rapidly dissected out of the skull and placed in a culture dish filled with cooled dissection medium (4 °C). Tissue dissection and sectioning were carried out under sterile conditions. The two hemispheres were cut apart along the midsagittal plane and

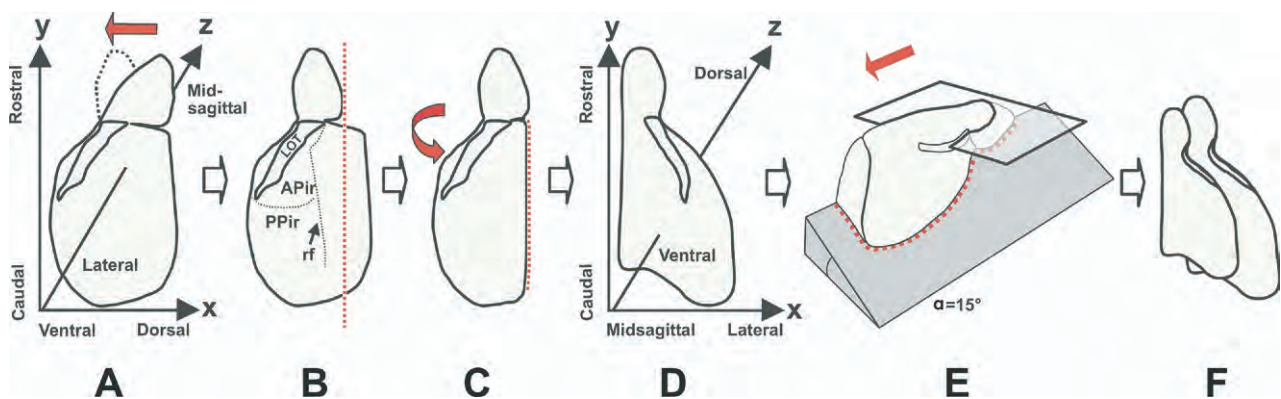


Fig. 1. Preparation of the OB slice. The reorientation approach consists in sliding down the olfactory bulb toward the ventral surface of the brain hemisphere and tilting the brain hemisphere laterally along the rostrocaudal axis. The intact olfactory bulb is first aligned to a horizontal plane at about -5 mm from bregma by a cut through the dorsal forebrain (A, B). The trimmed hemisphere is then tilted laterally relative to the rostrocaudal axis (C, D) and the surface (red dotted line in B, C and E) is glued on a 15° socket. Sectioning as indicated by the red arrow in E, yields two slices (400 μm thick, F), that include the MOB, the LOT and the Pir. Black dotted lines on the hemisphere drawing in B mark the rhinal fissure (rf) and the border between the APir and PPir. Drawings are not scaled.

treated independently. The olfactory bulb was gently pulled down from dorsal to ventral (Fig. 1A) to the level of the LOT and of the Pir. The dorsal forebrain was trimmed away 5 mm above the rhinal fissure to obtain a plane surface (Fig. 1B) that was glued on a socket tilted 15° from the horizontal plane (Fig. 1C–E). Serial 400 μm thick sections were cut with a vibrating microtome (HM 650 V, Microm, Germany) starting from the ventral surface of the brain. Among the four to five slices obtained from each tissue block, only two presented the MOB, the LOT and the Pir aligned, the limiting factor being the thickness of the LOT (see Results section for details). Sections were immediately transferred onto a Millicel-CM insert flooded with dissection medium. The medium was gently removed to let the slices lie on the membrane and the insert was then placed in a culture dish (30 mm) filled with 1 ml of equilibrated culture medium and placed in the incubator.

Preparation of OE explants. P5–7 mice were killed by decapitation. After skin removal, the heads were placed under the stereomicroscope, cut approximately midsagittally and the nasal septum was removed to reveal the turbinates. The olfactory mucosa covering the ethmoturbinate was carefully peeled off the cartilage, transferred to a culture dish filled with cooled dissection medium and further trimmed into small 2 mm \times 1 mm fragments. For cultures of the isolated OE, four to six explants were then transferred to a Millicel-CM insert. For coculturing, two OE explants were placed in front of the MOB of the OB slice at a distance of 0.5–1 mm. Preparation of OE explants for the cocultures always occurred on the same day as the brain slice preparation. Plating of the explants followed maximal 2 h after the plating of the brain slices.

Culture method and media composition. The dissection medium consisted of minimal essential medium (MEM with Hanks' salts and Hepes, without NaHCO_3 ; AppliChem, Darmstadt, Germany) with 5.5 mM D-glucose at pH 7.3. The culture medium (pH 7.35) consisted of 25% MEM, 25% basal medium Eagle (BME with Earle's salts, GIBCO, Scotland, UK), 25% heat inactivated normal horse serum (NHS, GIBCO) adjusted to a final concentration of D-glucose of 7.5 mM. Both media were supplemented with 2 mM Glutamax I (GIBCO) and 1000 U/ml streptomycin and 1000 $\mu\text{g}/\text{ml}$ penicillin (GIBCO). About 50% of the culture media volume was changed three times per week.

Fixation of cultures. Cultures (days *in vitro* (DIV) 2 to DIV5=24, DIV7=112, DIV10=22, DIV12 to DIV14=26, DIV18 to DIV21=14) were first washed with 0.013 M phosphate buffer saline (PBS) pH 7.4 and then fixed with 4% paraformaldehyde in PBS, at 4 °C and left in fixative overnight. Fixation was performed on the Millicell-CM inserts, leaving the tissues adhered on the membrane. After fixation, each membrane was cut out of the insert frame, trimmed and the membrane/tissue ensemble was treated as one unit (Gong et al., 1996).

Tracing experiments. To trace mitral cell projections to the olfactory cortex, 1,1'-diocetadecyl-3,3',3'-tetramethylindocarbocyanine perchlorate (DiI) carbocyanine crystals (Molecular Probes, Leiden, Netherlands) were placed along the mitral cell layer of DIV2 cocultures under stereomicroscopic control. The living cocultures were then observed under the fluorescence microscope to follow up tracing progress, fixed at DIV7, and mounted on slides to collect further images. Alternatively, DiI tracing was performed on cultures fixed at DIV7. After application of the crystals, the samples were kept in 2% PFA, in a humidified chamber, for 3–4 weeks.

Proliferation and differentiation essays. For bromo-deoxyuridine (BrdU) pulse-labeling, tissues were incubated with culture medium containing 10 mM BrdU (Sigma-Aldrich, Schnellendorf, Germany) for 48 h, either from DIV2 to DIV4 or from DIV5 to DIV7. Then the cultures were either rinsed and immediately fixed or

subjected to two changes of 1 h each with fresh culture medium, to wash out the BrdU, and were cultured for further 7–14 days.

Morphological analysis

Balb/c mice aged P5 to P7 ($n=3$) were deeply anesthetized by i.p. injection (100 $\mu\text{l}/100$ g body weight) of prequillan (0.5 mg/ml), xylapan (5 mg/ml) and narketan (50 mg/ml) and transcardially perfused with 4% paraformaldehyde in 0.1 M phosphate buffer, pH 7.4. Brains were left in the same fixative overnight (4 °C), then trimmed and oriented as described (Fig. 1) on the tilted socket. Serial (40 μm thick) sections were obtained with the vibrating microtome, mounted on slides and further processed for histology to essay the cellular architecture of the Pir and confirm the orientation of LOT fibers at this postnatal age. In addition, 400 μm thick OB slices, sectioned from unfixed brains, were immersion fixed for 48 h and processed for DiI tracing as described in the previous section.

Immunocytochemistry. All steps were conducted at room temperature on fixed, free floating culture samples or brain sections unless otherwise stated. PBS was used for dilutions and rinses between incubation steps. A tissue permeabilization step with 0.4% Triton X-100 (90 min) and a blocking step with 2% normal goat serum or normal donkey serum (90 min) preceded overnight incubation of primary antibodies. To facilitate binding of the antibody against BrdU with its epitope, samples were treated with 0.2 M HCl for 30 min at 37 °C to denaturate DNA and then rinsed in 0.1 M sodium borate, pH 8.5 (15 min at room temperature). Primary antibodies were diluted in 2% normal sera as follows: mouse anti-Reelin 1:1000 (Chemicon, MA, USA), mouse anti-calretinin (CR) 1:5000 (Swant, Bellinzona, Switzerland), rabbit anti-calbindin 1:5000 (Swant), mouse anti-Smi32 1:100 (Sternberger, MD, USA), rabbit anti-growth associated protein 43 (GAP43) 1:1000 (Chemicon), mouse anti PSA-NCAM 1:2000 (Chemicon), guinea-pig anti-doublecortin 1:5000 (Chemicon), goat anti-olfactory marker protein (OMP) 1:5000 (kindly provided by F. L. Margolis, University of Maryland, Baltimore, MD, USA), sheep anti BrdU 1:2000 (Abcam, Chembridgeshire, UK). For single labeling, we adopted the biotin streptavidin method. Biotinyll-conjugated secondary antibodies (Jackson Immunoresearch Europe, Suffolk, UK) and streptavidin-conjugated horseradish peroxidase (Vector, CA, USA) were both diluted 1:200, incubated 90 min each and visualized with diaminobenzidine (DAB) and hydrogen peroxide. Fluorochrome-conjugated reagents were adopted for multiple labelings. Rhodamine (TRITC)-conjugated or fluorescein (FITC)-conjugated secondary antibodies (Jackson Immunoresearch, multiple labeling grade) were diluted 1:100 and applied for 90 min. For triple labeling, a biotinyll-conjugated secondary antibody (1:200) was simultaneously incubated with the fluorochrome-conjugated ones. Alexa Fluor 633-conjugated streptavidin diluted 1:200 (Molecular Probes) followed in an additional incubation step (90 min). Mounted sections and cultured tissue stained by the DAB method were coverslipped with Kaiser's glycerol gelatin (Merck, Darmstadt, Germany). Fluorescently labeled sections and cultures were coverslipped with 80% (v/v) glycerol and 2% paraphenyl diamine in 0.1 M phosphate buffer, pH 8.6. To avoid squeezing and the related displacement of tissue elements during coverslipping, the culture samples were embedded within a plastic frame of approximately 300 μm height glued on the mounting glasses.

Microscopy. Fluorescent samples were viewed with an inverted microscope (Axiovert, Zeiss) equipped for epifluorescence and laser scanning microscopy (LSM 510 Meta, Zeiss). Confocal images were collected as z stacks of min three and max 100 sections of 1–1.5 μm optical thickness. FITC was excited by the Ar laser (488 nm) and its emission band filtered between 505 and 530 nm. TRITC was excited by the He–Ne laser (543 nm) and the

emission band filtered between 560 and 615 nm. Alexa Fluor 633 was excited by the second He–Ne line (633 nm) and its emission long pass filtered between 638 and 756 nm. Image processing was performed with the public domain Java-based Image J software and consisted mainly of sigma filtering, γ adjustment and of maximum intensity z projections of consecutive slices. Histological stains and DAB-reacted sections were examined with light microscopes equipped with standard (Leica) or differential interference contrast optics (Olympus) and digital cameras (Colorview IIIu, Olympus). Adobe Photoshop was used to assemble single images to collages and CorelDRAW was used to assemble images and collages into figures.

Functional analysis

Calcium imaging was adopted to measure functional activity in the olfactory system cocultures (DIV7 and DIV19–21). The samples were transferred to the bath chamber of the imaging microscope and superfused with artificial cerebrospinal fluid (ACSF) which was saturated with 95% O₂ and 5% CO₂ (pH 7.4) and contained 125 mM NaCl, 25 mM NaHCO₃, 25 mM glucose, 2.5 mM KCl, 1.25 mM NaH₂PO₄, 2 mM CaCl₂, 1 mM MgCl₂. Experiments were carried out at room temperature. The acetoxymethyl ester form of the calcium-sensitive dye Oregon Green 488 BAPTA-1 (OGB-1 AM; Molecular Probes) was dissolved, applied and trapped into the intracellular compartment as previously described (Berger et al., 2007). Briefly, a pipette with a tip diameter of 16–22 μ m was back-filled with 20 μ l OGB-1 AM (400 μ M) and connected with air-filled flexible tubing to a 50 ml syringe. Pressure was manually applied and the dye was injected at multiple sites into the MOB and the Pir of OB slices under visual control. In cocultures, we avoided touching the OE explants with the pipette tip and used the same device to gently superfuse instead the OE with the dye. Extracellular stimulation of ORNs was performed with a bipolar platinum/iridium electrode (type CE2C550; FHC) inserted into the OE. A train of 20 pulses per stimulation (intensity range 50–200 μ A, duration 400 μ s, frequency 100 Hz) was delivered to the tissue. The resulting changes in fluorescence of OGB-1 reflected changes of the intracellular calcium concentration. OGB-1 was excited with a 100 W halogen light source (band pass filter 480–530 nm, dichroic mirror 505 nm) and its emission collected through a 535–540 nm band pass. Images were acquired with a Zeiss Axioskop microscope (4 \times , 0.13 NA Olympus optics) equipped with a 80 \times 80 pixel CCD camera (RedShirt NeuroCCD, RedShirtImaging) running at a frame rate of 500 Hz. Pixel size was 52 \times 52 μ m. The Neuroplex software (RedShirtImaging) was used for the camera control, data acquisition and data analysis. To correct for spatial differences in staining intensity, the change of fluorescence (ΔF) recorded from each pixel was divided by the resting light intensity (F_0) from the same pixel under fluorescence excitation when no stimulation was applied. Background fluorescence from the specimen in the absence of specific excitation was subtracted from both resting and stimulated frames, prior to signal normalization. The resulting response amplitudes were expressed as $\Delta F/F_0$ in percent. For each stimulation condition, 10 trials were averaged. A temporal median filter was applied to improve the signal to noise ratio. For the peak images, a spatial center weight filter was additionally applied. After imaging, selected cocultures were fixed and processed for immunocytochemistry as described above.

RESULTS

A slice preparation that includes the MOB and the olfactory cortex and preserves mitral cell axon projections

Our first concern in transferring the olfactory system into the culture dish was to avoid the coculturing of the isolated

tissue elements (i.e. MOB and Pir) containing the second order and third order neurons of the olfactory pathway. Thus, we first developed a brain slice that includes the MOB and the Pir and preserves the mitral cell axons within the LOT. It is difficult to obtain the MOB and the Pir on the same section since they are quite distant from each other in both the conventional sagittal and horizontal planes. Horizontal sections cut through the brain tilted to the midline have yielded a slice preparation of the Pir reported to preserve the connectivity along its rostrocaudal extent. The MOB, however, is not included in this slice preparation (Demir et al., 2001). Recently, Balu et al. (2007) have obtained a horizontal slice including the MOB, the anterior olfactory nucleus (AON) and a portion of the anterior piriform cortex (APir) to investigate the top-down inputs onto granule cells.

Our reorientation approach combines these two methods and consists in sliding down the olfactory bulb toward the ventral surface of the brain and tilting the brain hemisphere laterally along the rostrocaudal axis. As shown in Fig. 1A–C, the olfactory bulb is left intact and aligned to a horizontal plane at about –5 mm from bregma by a cut through the dorsal forebrain (see horizontal section 8, www.mbl.org/atlas232/; Rosen et al., 2000). However, sections obtained starting from the ventral surface of the hemisphere parallel to this horizontal level did not longitudinally cut the LOT through its whole rostrocaudal extent. Therefore we tilted the trimmed brain hemisphere relative to the rostrocaudal axis (Fig. 1D–E). We sectioned brains of juvenile and adults brains with different tilt angles and processed them for histology to evaluate the orientation of LOT fibers: a tilt angle of 15° gave the best results and also allowed us to obtain two slices per hemisphere (not shown). We confirmed to best preserve the LOT fiber orientation also in postnatal mice. The first olfactory slice obtained (OB slice, see Fig. 6) resembles a plain horizontal section through the olfactory cortical areas at about –8.5 mm from bregma (horizontal section 14, www.mbl.org/atlas232/) but rostrally includes a small tangential cut through the MOB. Fig. 2A–B shows an overview of the second of the two slices obtained from a P6 brain, as it appears when immediately fixed after sectioning (Fig. 2A) or following 1 week of culturing (Fig. 2B). This section level approximately corresponds to bregma –8 mm (horizontal section 13, www.mbl.org/atlas232/) and includes the LOT with the underlying APir, the posterior Pir (PPir) and the lateral entorhinal cortex (LECx). This section is rostrally connected to a large and rather symmetrical MOB section which also presents the medial AON. Note that, in contrast with the strictly horizontal atlas sections we refer to, the two OB slice levels were both lacking the olfactory tubercle because of the tilt. The regions are difficult to recognize in the cultured section, due to the flattening of the tissue but can still be distinguished at higher magnification and upon specific labeling of fiber tracts and neuronal types (Fig. 2D, F and Fig. 3).

To prove the connectivity between the MOB and the Pir in such preparation we needed to demonstrate that a large amount of mitral cell axons can be traced on their course

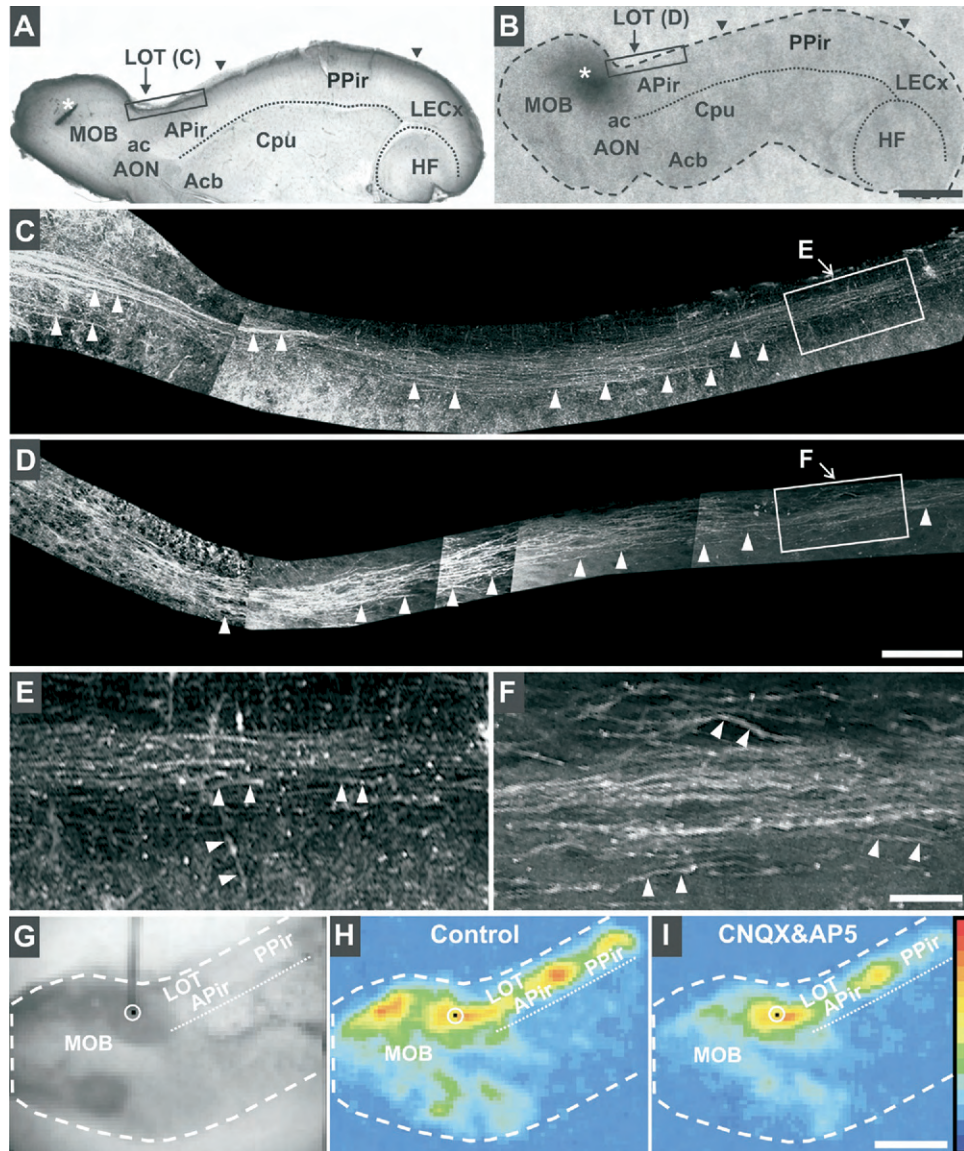


Fig. 2. Mitral cell projections to the Pir are maintained in the OB slice. (A, B) Overview of the second of the two slices obtained from a P6 brain as it appears when immediately fixed after sectioning (A) or after 1 week in culture (B). This section level approximately corresponds to bregma -8 mm (see Results) and includes the LOT (arrows) with the underlying APir, the PPIr and the LECx. Such section is connected to a MOB section and also includes the medial AON. The outline of the cultured section (dashed lines in B) and borders between regions (arrowheads and stippled lines) are less distinguishable at low magnification, due to the flattening of the tissue (B). White asterisks indicate the application site of Dil crystals. Ac: anterior commissure; Acb, accumbens; Cpu: caudate putamen; HF: hippocampal formation. (C) Collage reconstruction of the frame in A. Dil fluorescence can be recognized in numerous bundles of fibers coursing within the LOT of the OB slice. Fibers are oriented parallel to the plane of the section and can be followed for long stretches in rostrocaudal direction (arrowheads). Fluorescence becomes less intense with increasing distance from the MOB (boxed area) but can still be distinguished in fibers at further magnification (arrowheads in E). (D) Collage reconstruction of the frame in B. No major changes are detected when the tracing experiment is carried out after 1 week of culturing. The fibers appear slightly less bundled but are oriented longitudinally and quite abundant. Pale fluorescence in the caudal part of the LOT (boxed area) is clearly recognizable as axon bundles when observed at higher magnification (arrowheads in F). (E–I) Calcium imaging to study the function of the central olfactory pathway. (G) Bright field image of a DIV7 OB slice. The white circle indicates the position of the stimulating electrode in the MOB. (H, I) Epifluorescence calcium imaging. Activity is color coded whereby a larger increase in the intracellular calcium is coded in red. (H) Stimulation of the caudal and lateral mitral cell layer causes a rise in the intracellular calcium locally at the electrode position (black dot) and also caudally in the APir and PPIr. Additional activation occurs in the MOB anterior to the stimulation site. Activation maximum corresponds to dF/F_0 (%) = 8.02. (I) Blockage of glutamatergic receptors by bath application of CNQX and AP5 prevents postsynaptic calcium increases and isolates the presynaptic component of the imaged activity at the site of stimulation (black dot). Note the discrete CNQX and AP5 insensitive area in the APir. Scale bars = 1 mm (A, B); 100 μ m (C, D); 25 μ m (E, F); 1 mm (G–I).

through the LOT to the olfactory cortical areas. We adopted the lipophilic tracer Dil and placed dye crystals on the olfactory bulb in proximity of the mitral cell bodies (Fig.

2A, B). To compare the amount of fibers present in the brain slice preparation before plating with those detectable in culture, OB slices were traced after sectioning (Fig. 2A,

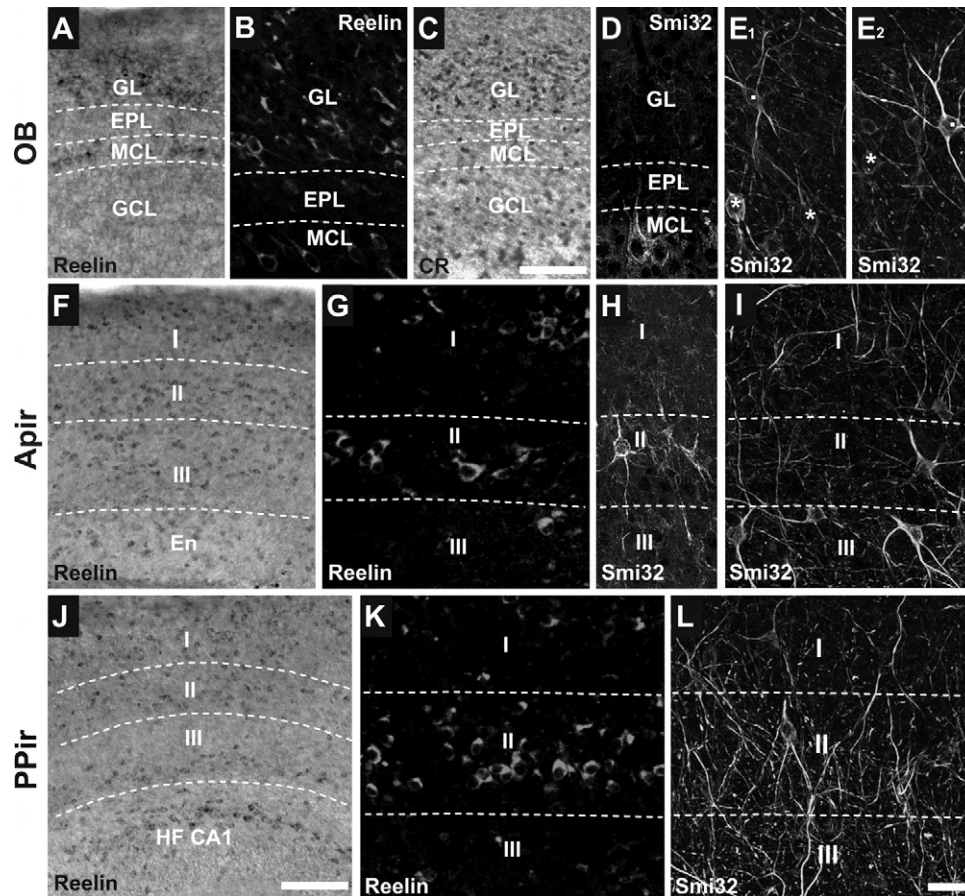


Fig. 3. Organotypicity is preserved in the MOB and Pir areas of the OB slice. (A–E) At DIV7, Reelin labeling in the MOB (A) is limited to two bands of cells alternating with pale regions. The superficial cell band resembles the glomerular layer (GL) and includes Reelin positive cells of different size and labeling intensity (A, B). The deeper cell band (A) consists of one or two rows of large neurons which appear as mitral cells at larger magnification (B). (C) CR immunoreactivity is dense within the glomerular layer of the DIV7 MOB. In addition, loosely scattered CR containing neurons appear in the granule cell layer (GCL, compare with A). The CR content in mitral cell bodies is variable at this age in culture and therefore the mitral cell layer (MCL) is difficult to distinguish (compare with Fig. 7D). (D) A subset of mitral cells labeled with Smi32 in the MOB of a P8 mouse. (E₁–E₂) Smi32 expression is maintained in the cultured MOB and allows us to visualize the orientation of the dendrites of mitral (asterisks) and tufted cells (dots). EPL: external plexiform layer. (F–L) Characteristics of Pir areas in an OB slice cultured for 1 week. In the APir, numerous interneurons scattered throughout layers 1 (I) to 3 (III) contain Reelin (F–G). (H) Smi32 distributes in a group of second layer (II) interneurons in the PPir of a P7 mouse. (I) Smi32 expression is also maintained in this region upon culturing. Apical dendrites of labeled interneurons stretch and eventually ramify into the molecular layer of the APir. (J–L) Reelin distributes in interneurons also throughout the PPir (J). In addition, it is particularly abundant within the cell band of layer 2 (II, K). Smi32-labeled dendrites are numerous and vertically oriented in this area (L). En: endopiriform nucleus; HF CA1: hippocampal formation, field CA1. Dashed lines mark borders between layers. Scale bars=100 μm (A, C); 50 μm (B, D, E, G–I, K, L); 200 μm (F, J).

C, E) and 1 week of culturing (Fig. 2B, D, F). Numerous fibers course through the deep layers of the MOB (not shown) and bundle into a fiber tract at the border between the MOB and the APir. Fibers are oriented parallel to the plane of the section and can be followed for long stretches in rostrocaudal direction (Fig. 2C, E). No major changes are detected after 1 week of culturing: the fibers appear slightly less bundled at the border between the MOB and the olfactory cortex but are oriented longitudinally and quite abundant over the APir (Fig. 2D, F). The higher fluorescence intensity observed in the cultured specimen may rather depend on the thickness differences between the two tissues and the related variance in the diffusion of the dye along the membranes than on a real increase in the amount of fibers with culturing.

We adopted the calcium imaging technique to provide evidence that the central olfactory pathway is functional in the OB slice preparation. We studied the extent of triggered activity in the Pir in response to a direct stimulation of the mitral layer of the MOB. Fig. 2G shows an OB slice cultured for DIV7 with the stimulating electrode positioned in the caudal and lateral part of the mitral cell layer. The rise in intracellular calcium that reflects the stimulus evoked depolarization occurs locally, at the electrode position, and extends caudally to the APir and PPir (Fig. 2H). The calcium response triggered in the Pir is to a large extent synaptically mediated, since it disappears upon pharmacological blockade of glutamatergic receptors of the AMPA and *N*-methyl-D-aspartic acid (NMDA) type by bath application of 6-cyano-7-nitroquinoxaline-2,3-dione

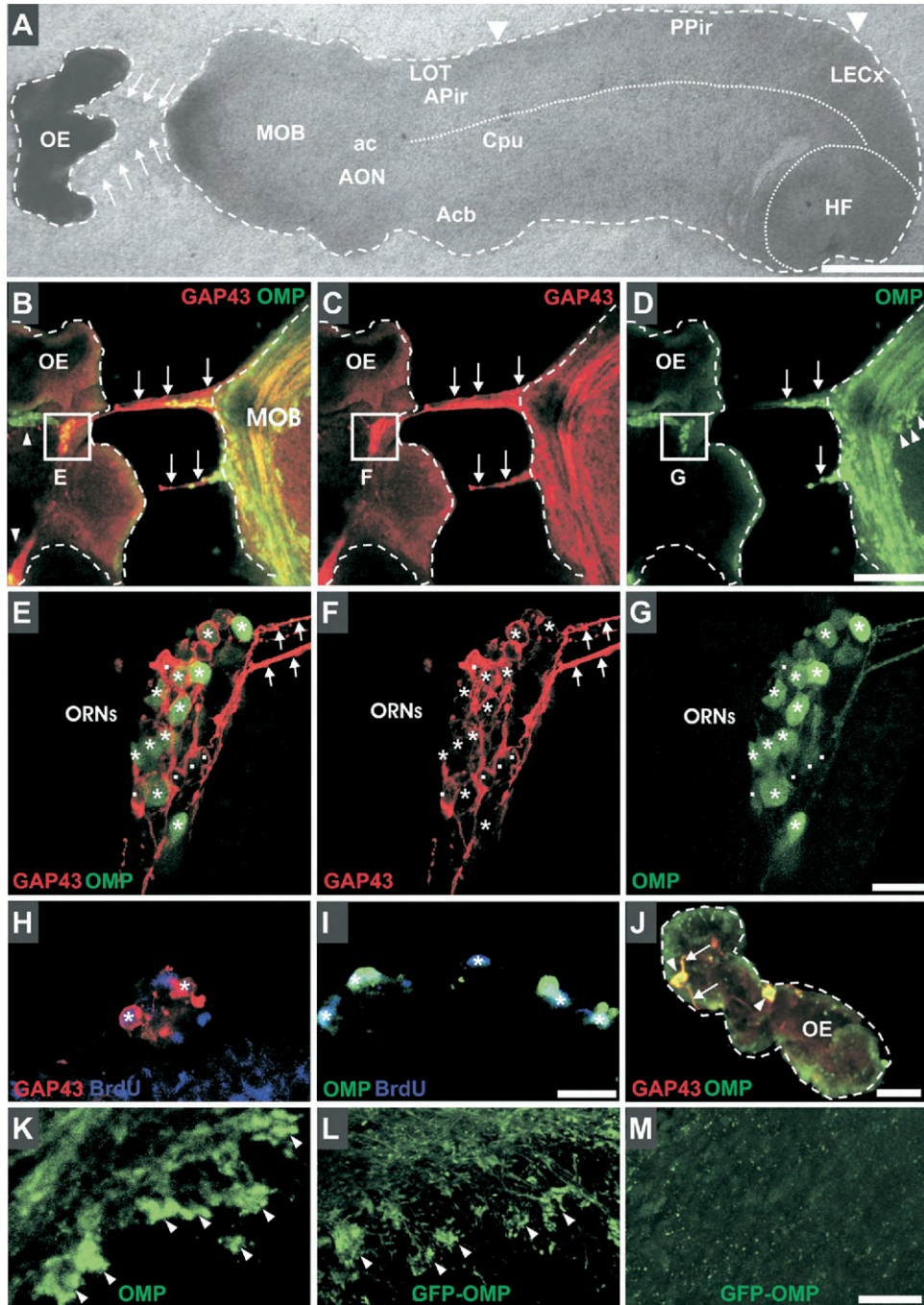


Fig. 4. Axons regrow from the OE onto the OB slice. (A) Overview of a DIV7 coculture. The borders of the explanted OE and of the OB slice with the Millipore membrane are marked by dashed lines. Tissue bridges (arrows) connecting the two cocultured regions are visible at this magnification and with bright field optics. For further abbreviations see Fig. 2. (B–D) Higher magnification of the growth zone between the OE explant and the MOB in another DIV7 coculture double labeled with antibodies recognizing the ORN markers GAP43 (red label) and OMP (green label). Three irregularly shaped spots of immunoreactivity can be seen in the OE on the overlay image (arrowheads and frame in B). One of these spots mostly contains OMP (B, D). The other two zones exhibit both markers, though to a different extent (C, D). Note the discrepancy between the scarce OMP content of the tissue bridges (arrows) and the abundant OMP labeling on the MOB (B–D). (E–G) Detail of the frame on the OE in B–D. The higher magnification reveals the immunoreactive zone as a cluster of ORNs. Most ORNs express GAP43 and a large subset contains both markers (asterisks). Note that OMP distributes in both the nucleus and the cytoplasm of these neurons. Dots mark neurons that only contain GAP43. (H) Detail of a DIV12 cluster of ORNs reacted with antibodies against BrdU and GAP43. BrdU-labeled nuclei belong to cells which underwent mitosis between 5 and 7 DIV. Asterisk marks a 5–7 day old cell expressing GAP43. (I) Detail of a 21 DIV cluster of ORNs double labeled for BrdU and OMP. The BrdU-labeled nuclei belong to 17–19 day old cells that more often express OMP at this age (asterisk). (J) Overview of a representative OE explant dissected from postnatal mice (P5–P8), cultured alone for DIV7 and double labeled for GAP43 and OMP. Discrete clusters of ORNs can be visualized (arrowheads) but the characteristic outgrowth of processes outside the tissue border (dashed lines) is lacking. Axon bundles, when detectable, remain within the tissue (arrows). (K) MOB of a cocultured OB slice at DIV7. Detail of the border zone between the olfactory nerve

(CNQX) and 2-amino-5-phosphonovaleric acid (AP5). Local presynaptic activity at the stimulation site is not affected by these drugs. These results confirm the presence of largely intact mitral cell projections to the target olfactory areas. Additional activity which is insensitive to CNQX and AP5 is often observed (Fig. 2H, I) and may reflect a discrete retrograde activation of fibers originating in the Pir.

Thus, we can make use of a slice preparation that includes the olfactory bulb and the olfactory cortex and preserves great part of the mitral cell projections to the olfactory cortex also if cultured.

We carried out additional morphological characterization of the OB slice to ensure that principal neurons, interneurons and the layering of the MOB and Pir are maintained in culture. Fig. 3A–C shows details of the MOB in OB slices cultured for 1 week. Reelin immunocytochemistry was used to evaluate the layering of this region. Reelin is known to distribute in the cell bodies of mitral and tufted cell and is also abundant in superficial short axon interneurons located at the inner border of the glomerular layer. Moreover, Reelin is faintly expressed in periglomerular neurons and is absent from granule interneurons in mice (Alcantara et al., 1998; Ramos-Moreno et al., 2006; Herrmann et al., 2007). In the MOB of cultured OB slices, Reelin labeling is limited to two bands of cells alternating with pale regions. The superficial cell band resembles the glomerular layer and includes Reelin positive cells of different size and labeling intensity, the most intensely labeled ones being those located at its inner border (Fig. 3A). The deeper cell band is thinner, consisting of one or two rows of large neurons which appear as mitral cell at larger magnification (Fig. 3A, B). Taken together the Reelin labeling corresponded to the distribution of Reelin mRNA in the olfactory bulb of 1-week-old mice described by Alcantara et al. (1998). To visualize more interneurons and the mitral cells we adopted an antibody against the calcium binding protein CR (Wouterlood and Hrtig, 1995). CR is known to be expressed in numerous periglomerular neurons and also in a subset of granule neurons located within the superficial half of the granule cell layer (Herrmann et al., 2007). CR immunoreactivity is dense within the glomerular layer of the DIV7 MOB, as observed for Reelin. In addition, loosely scattered positive neurons appear in the granule cell layer (Fig. 3C). The CR content in mitral cell bodies is variable and difficult to distinguish in the MOB at this age in culture. It can be recognized, though, in few cell bodies at higher magnification (not shown for DIV7, but see Fig. 7D). To better visualize mitral cells we adopted the antibody Smi32 that recognizes nonphosphorylated high-molecular-weight neurofilaments. Compared with other cytoskeleton markers which label neuronal cell bodies and their processes, we preferred Smi32 because it is distributed in distinct subsets of neurons throughout the brain

(Lopez-Picon et al., 2003) and selectively labels a subset of mitral cells in the MOB (Fig. 3D). Smi32 containing mitral and tufted cells are also well visible in the cultured MOB. Their dendritic processes appear properly oriented and extend toward the superficial layers of the MOB (Fig. 3E).

Reelin and Smi32 were also used to essay the organotypicity of the olfactory cortical areas in the cultured OB slice. The Pir areas exhibit particularly high levels of Reelin that distributes in numerous interneurons and principal neurons (Ramos-Moreno et al., 2006). Such characteristic distribution pattern is well maintained *in vitro* (Fig. 3F–G, J–K). In the APir, Reelin is expressed in numerous interneurons scattered throughout the layers (Fig. 3F–G). Smi 32 is present in a heterogeneous subset of interneurons of the second layer and of the pyramidal layer (third layer) in the APir (Fig. 3H) and PPIr of 1-week-old mice (not shown) and seems to maintain its distribution pattern *in vitro*. While Reelin distribution is limited to the neuronal cell body, the Smi32 labeling reveals the orientation of the dendrites of these neurons: some course horizontally or to deeper layers and other dendrites stretch and eventually ramify into the molecular layer of the APir (Fig. 3I). Fig. 3J–L illustrates the distribution of Reelin and Smi32 in the PPIr, cultured for about 1 week. Reelin containing neurons are abundant in the superficial molecular layer and in the cell band in layer 2 of the PPIr (Fig. 3J–K) and less numerous in the deeper layers. Smi32 containing dendrites are more numerous and more regularly vertically oriented in this area (Fig. 3L).

We can thus conclude that the layering and the characteristic neuronal populations of both the olfactory bulb and of the Pir in the OB slice are maintained under our culture conditions.

The peripheral olfactory pathway *in vitro*: renewal and differentiation of ORNs and reinnervation pattern of the MOB

As a next step we cocultured the new OB slice preparation with the OE to restore *in vitro* the peripheral olfactory pathway. We dissected fragments of the olfactory mucosa from mice (P5–P7) and plated one or two OE explants in front of the MOB. The gap between the OE and the target tissue varied between 0.5 and 1 mm. Tiny tissue bridges generally appear between the OE explants and the MOB within DIV3 and seem to connect the two tissues by DIV7. Since the tissue processes can be well recognized at low magnification and with simple optics, their growth can be easily followed up at regular intervals e.g. during the medium changes (Fig. 4A). While small appendices attaching to the substrate grow on the whole circumference of the OE explants, tissue bridges are notably observed only in the gap between the OE and the MOB.

layer and the glomerular layer corresponding to the frame in D. OMP immunoreactive axon terminals distribute in a glomerular-shaped fashion (arrowhead). (L, M) The same zone as it appears if the OB slice is cultured isolated for DIV7 (L) and DIV14 (M), respectively. The tissue is from a P6 OMP-GFP mouse. The green fluorescence reflects GFP expression under the OMP promoter. Intrinsic GFP fluorescence labels olfactory axon terminals and is maintained in the deafferented glomeruli (arrowheads) for about 1 week (L). Complete resorption of olfactory axon terminals that were lesioned during dissection is accomplished by DIV14 (M). Scale bars=1 mm (A); 200 μ m (B–D, J); 20 μ m (E–I); 50 μ m (K–M).

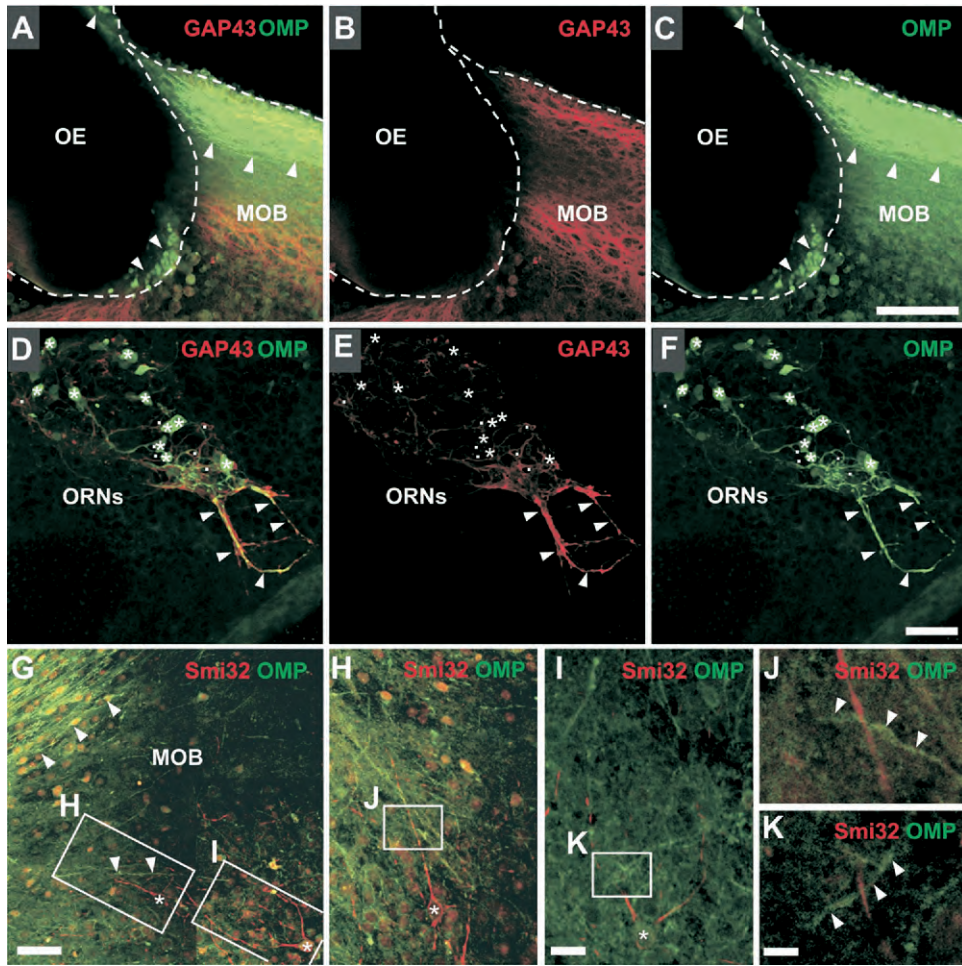


Fig. 5. Long term culturing. Maturation of OMP expression and termination pattern of ORNs axons within the MOB of DIV 21 cocultures. (A–C) Overview of DIV21 cocultures labeled for GAP43 and OMP. The relative expression of the two markers has changed: in the OE, clusters of ORNs (arrowheads) exhibit dense OMP labeling at this age in culture. The OE explant and MOB often attach to each other with long term culturing, so that the borders (dashed lines) and the axon connections between the tissues cannot be discerned. Within the MOB, OMP-labeled fibers are concentrated to discrete superficial regions (arrowheads) and show little overlap with the strong and homogeneous GAP43 immunoreactivity. Note that the termination pattern of putative ORN axons is not clustered into glomerular like structures 1 week after resorption of the lesioned terminal arborizations (see also Fig. 4K–M). (D–F) Detail of a cluster of ORNs in an OE explant cultured for 20 DIV and stained for GAP43 and OMP. The majority of the ORNs are OMP immunoreactive (asterisks). GAP43 is almost absent from the cell body of ORNs (dots) but it is still present in part of the outgrowing axon bundles (arrowheads), where it largely colocalize with OMP. (G–K) Termination pattern of OMP-labeled ORN axons within the depths of the MOB. (G–I) Z projection of stacks of eight consecutive images of ca 1.5 μm optical thickness immunolabeled for OMP and smi32. Numerous axons (arrowheads) leave the dense OMP-labeled outermost superficial zone of the MOB (G) to course through the deeper layer amid smi32 positive structures. Asterisks mark cell bodies of putative mitral cells (H and I). (H, I) OMP-labeled fibers and puncta appear numerous in proximity of dendrites of smi32-labeled mitral cells. (J, K) Single optical slice images corresponding to the boxed areas in H and I, respectively, showing details of mitral cell dendrites crossed by OMP labeled ORN axons carrying varicosities (arrowheads). Scale bars=100 μm (A–C); 40 μm (D–F); 50 μm (G); 20 μm (H, I); 5 μm (J, K).

Fig. 4B–D shows a higher magnification of the growth zone between OE explant and MOB in a coculture double labeled with antibodies recognizing the GAP43 and the OMP. GAP43 is a cytosolic protein kinase C substrate that is anchored to the cell membrane and regulates the actin cytoskeleton. GAP43 is abundantly expressed in growing axons of the peripheral and CNS during development, maintained in selected brain structures in the adult and reinduced during nerve regeneration. It is expressed in differentiating ORNs and their growing axons within the olfactory mucosa. OMP instead is highly restricted to mature olfactory neurons in all vertebrates from amphibians to

humans (Margolis et al., 1991). At DIV7 the two markers appear differently distributed within the OE explant and the tissue bridges. In contrast, their distribution over the superficial layer of the MOB is quite similar (Fig. 4B–D). Partially overlapping, dense GAP43 and OMP immunoreactive spots of irregular shape can be distinguished at low magnification in the OE explants. Zooming in allows to identify these discretely distributed immunoreactive zones as clusters of cells (Fig. 4B–G). At DIV7 the majority of cells within the clusters express GAP43 and a large subset contains both GAP43 and OMP. The OMP labeling is always well visible, being distributed in both the nucleus

and the cytoplasm of these cells (Fig. 4E–G). Cell clusters exhibiting an intense OMP signal and a rather faint cytoplasmic GAP43 content were rare in DIV7 cocultured OE explants (Fig. 4B–D). At this age *in vitro* we regularly observe GAP43 immunoreactive, axon-like processes originating from cells within the clusters and converging into bundles within the tissue bridges which connect the OE with the MOB of the OB slice. The OMP immunoreactivity instead, though strong within the cell bodies, is less intense within the axon-like processes and discontinuous along the fiber bundles of the tissue bridges (Fig. 4C–D). Both clusters and fiber bundles are also labeled by antibodies recognizing the polysialylated neuronal cell adhesion protein or doublecortin (not shown). These proteins are also known as alternative markers for maturing neurons (von Bohlen und Halbach, 2007).

Based on their homogeneous phenotype, the regular presence of processes and considering the variable expression of OMP, GAP43 and other typical markers we thus conclude that islands of ORNs are scattered over the OE explant and start to make connections with the MOB under our culture conditions.

A prerequisite for long term survival of ORNs in the cultured OE is the maintenance *in vitro* of proliferating cells that can renew them. In fact, ORNs regularly undergo programmed cell death and are continuously replaced by cell division of stem cells and neuronal progenitors (Beites et al., 2005). Moreover, differentiated ORNs are known to undergo retrograde degeneration upon transection of the olfactory nerves (Graziadei and Graziadei, 1979; Schwob, 2005). To provide evidence that ORNs within clusters are born in culture we applied BrdU for 48 h to mark dividing cells in the OE explants and carried out a differentiation essay. Fig. 4H shows a detail of a DIV12 cluster of ORNs double labeled with antibodies recognizing BrdU and GAP43. BrdU-labeled nuclei belong to cells which underwent mitosis between DIV5 and DIV7. One of these 5–7 day old cells expresses GAP43 at this age. In a DIV21 OE explant instead, 17–19 day old cells more frequently co-express OMP (Fig. 4I).

In an additional set of experiments we compared the phenotype of the cocultured OE explants with that of OE alone. Fig. 4J shows a representative overview of an OE explant cultured alone for DIV7 and double labeled for GAP43 and OMP. Clusters of ORN can be regularly spotted and the distribution patterns of the two markers do not significantly differ from those described above for the cocultured OE explants. Surprisingly, ORN axons fail to grow out of the tissue and to bundle on the membrane when OE explants dissected from postnatal mice (P5–P7) are cultured alone.

Taking these results together, we have evidenced so far that in postnatal OE explants, ORNs renew, differentiate to some extent and send their axons out to reach the MOB in an apparently target dependent manner. We noted, however, that the intense OMP immunoreactivity of the fiber bundles coursing through the MOB superficial layer (Fig. 4D) and distributing in numerous glomerular like structures (Fig. 4D, K) is in contrast with the faint OMP

labeling in the OE and in the axon bundles connecting the tissues. The OMP positive fibers within the MOB may thus not completely correspond to those originating in the OE explant. To test this hypothesis we examined OMP expression in the MOB of OB slices cultured in absence of the OE explants. To simultaneously exclude a possible unspecific binding of the OMP antibody to this reorganizing tissue we adopted transgenic mice expressing GFP under the OMP promoter (Potter et al., 2001). A detail of the superficial zone of the MOB in such isolated OB slice cultures is shown in Fig. 4L and M at DIV7 and DIV14, respectively. Intrinsic putative olfactory axon fibers with their characteristic glomerular like termination pattern persist in the MOB during the first week of cultivation and gradually disappear between DIV8 and DIV14.

We therefore conclude that the new ORN axons growing into the MOB cannot be distinguished from the lesioned ones that are being resorbed before the end of the second week *in vitro*. We then labeled with GAP43 and OMP DIV21 cocultures to study changes in 1) the long-term, relative expression of the two markers in ORNs and 2) the extent of olfactory axons innervating the MOB at this age (Fig. 5A–F). The OE explant and the OB of numerous cocultures appear almost attached to each other at DIV21 so that the axon bundles connecting the tissues cannot be discerned. Clusters of ORN neurons on the OE appear to contain more OMP than GAP43 at this age (Fig. 5A–C). At higher magnification GAP43 is almost absent from the cell body of ORNs but is abundant instead in the outgrowing axon bundles, where it appears to colocalize with OMP (Fig. 5D–F). The OMP labeling within the MOB is more concentrated to discrete regions. This is compatible with the assumption that OMP stains specifically for newly generated ORN axons at this time of cultivation *in vitro*. Interestingly, however, coalescence of OMP-labeled terminal axons into glomerular-like structures is lacking in DIV21 cocultures (Fig. 5A–C).

To test as to whether ORN axons target mitral cell dendrites despite the lack of glomerular organization of the two synaptic partners we investigated DIV21 cocultures stained with OMP and smi32, which detects a subset of mitral cells in the MOB (Fig. 6G–K). Several OMP positive ORN axons leave the bundles of the superficial newly formed olfactory nerve layer within the MOB. They course toward the depth of the MOB (Fig. 6G–I), crossing and coming into close contacts with dendrites of mitral cells in a zone corresponding to the original glomerular and external plexiform layer (Fig. 5J–K).

Thus, despite the little progress in reconstitution of glomeruli at this age most ORN axons have acquired a mature OMP immunoreactive phenotype and show a certain degree of target specificity onto dendrites of mitral cells.

The extent of functional recovery following olfactory bulb reinnervation

We adopted the calcium imaging technique to verify the extent of functional recovery achieved by the newly formed connections between OE explants and the MOB. In addi-

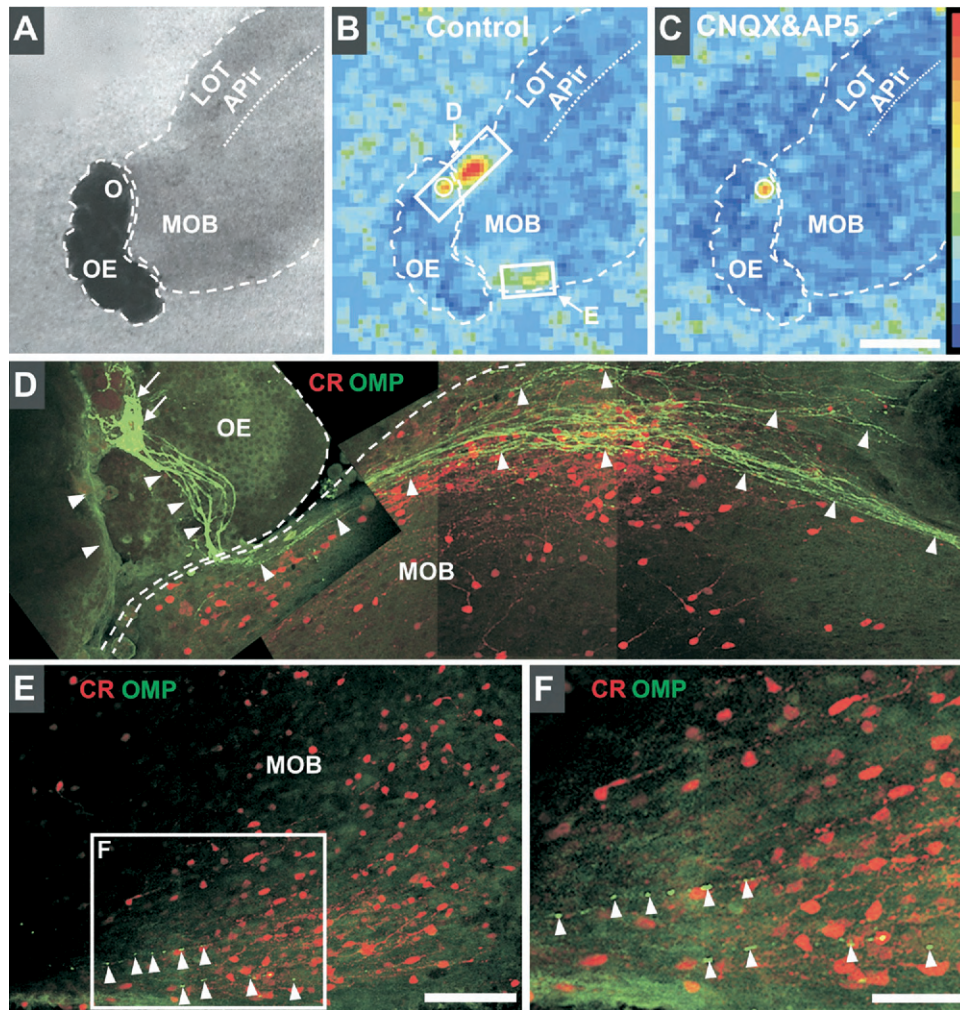


Fig. 6. Functional imaging after repair of the peripheral olfactory pathway: the activity in the MOB. Calcium imaging responses monitored in the reinnervated MOB after stimulation of the OE. A culture period of DIV21 is necessary to have functional ORN synapses in the MOB. (A) Bright field image of the recorded area showing the position of the stimulating electrode (white circle) in the OE of a DIV21 coculture. (B, C) Epifluorescence calcium imaging. The red color codes for the largest increase in intracellular calcium. (B) Stimulation in the OE results in a local calcium response at the electrode position and activation in two distinct areas in the MOB. One intense calcium response occurs near the stimulation site (D). The second calcium response within the MOB is faint and located far away (E). A calcium response in the Pir cannot be elicited in this coculture. Activation maximum corresponds to dF/F_0 (%) = 0.63. (C) Blockage of glutamatergic receptors by CNQX and AP5 prevents postsynaptic calcium increases in the MOB. However, local activity in the OE remains unaffected. (D–F) Post hoc morphological analysis of the areas within the frames shown in B. (D) An intensely OMP-labeled cluster of ORN (arrows) is located underneath the stimulation electrode. Numerous OMP positive axon bundles (arrowheads) can be followed as they cross the gap and reach the activated zone in the MOB. Numerous CR immunoreactive, small-sized interneurons intermingle with the axon bundles in the same area. (E) CR positive cells are also numerous in the second distant zone of evoked MOB activity. Here, however, the amount of OMP-labeled fibers is rather low (arrowheads). (F) Larger magnification of the frame in E. Only few isolated OMP positive axons and puncta can be resolved (arrowheads). Scale bars = 1 mm (A–C); 100 μ m (D, E); 50 μ m (F).

tion we wanted to investigate whether the flow of information to the olfactory cortex also restores along with the reinnervation of the MOB.

For this purpose we used 12 independent cocultures: four DIV7 and eight DIV18–21. Fig. 6A–C representatively shows the response of the OE and the MOB to electrical OE stimulation in a DIV21 coculture. The response in the OE occurs in immediate proximity of the stimulating electrode, and resembles in shape the ORN clusters we observed by immunolabeling. A calcium response can be regularly elicited in the OE of DIV18–21 cocultures and it is accompanied by a response of variable intensity in the

MOB (Figs. 6B; 7B, F), in 87.5% (seven out of eight) of the samples tested. In younger cocultures, however the success rate is low. Only 12.5% (one out of eight) of the samples tested exhibit response in the MOB, either because the OE response cannot be elicited or because the synaptically evoked response is lacking (not shown). The calcium response triggered in the MOB by the OE stimulation is discrete and most intense in proximity of the stimulation electrode. Sometimes additional faint calcium responses can be simultaneously detected in distant regions within the MOB (Fig. 6B). The activity triggered in the MOB is synaptically mediated since it disappears upon

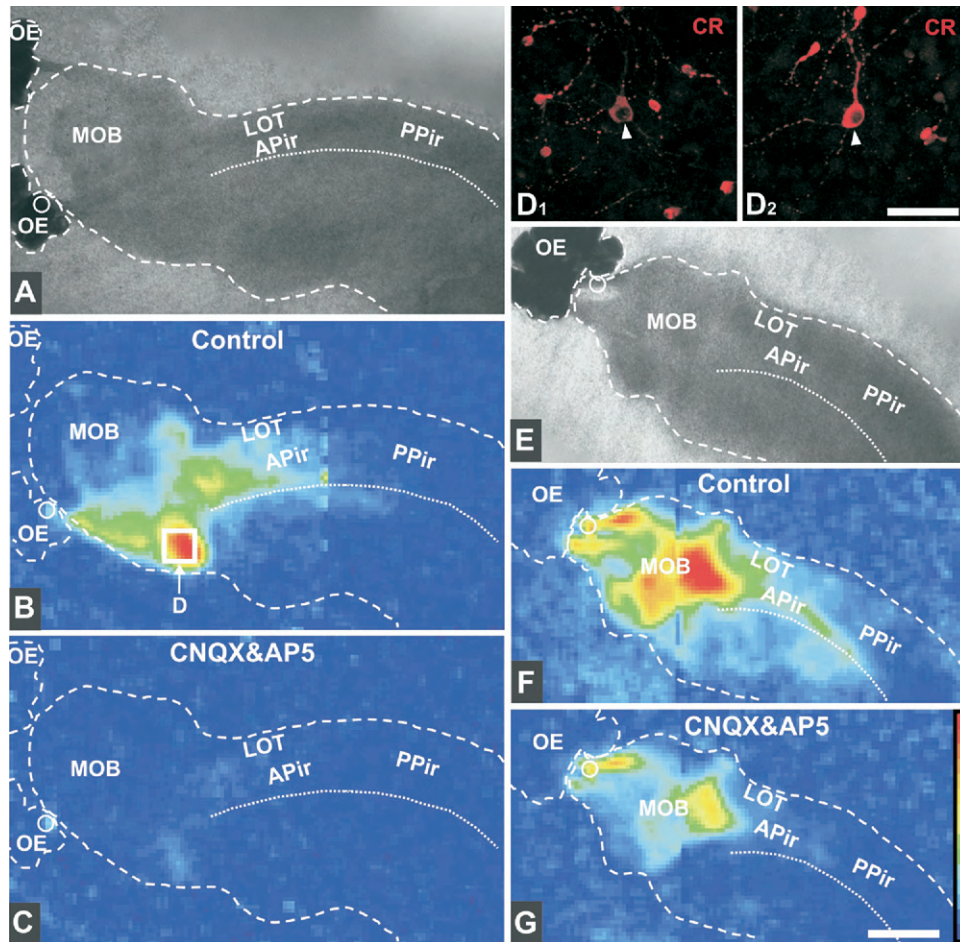


Fig. 7. Functional imaging after repair of the peripheral olfactory pathway: the activity in the Pir. (A) Bright field picture of the imaged area of a DIV21 coculture illustrating the position of the stimulation electrode (white circle). (B, C) Epifluorescence calcium imaging: the red color codes for the largest increase in intracellular calcium. (B) OE stimulation triggers a local calcium increase in the OE at the electrode position and a faint calcium response in the superficial MOB, just opposite to the stimulation site. A larger calcium response is also triggered in a discrete spot in the depth of the MOB, distant from the stimulation site. Simultaneously, a calcium response occurs in the APir of this coculture. Activation maximum corresponds to dF/F_0 (%) = 3.83. (C) Application of CNQX and AP5 prevents postsynaptic calcium increases in both the OB and the APir but leaves the OE local activation unaffected. (D₁, D₂) Details of the area boxed in B. Post hoc morphological analysis reveals the presence of large CR immunoreactive mitral cells (arrowheads) and interneurons within the area of peak calcium response. (E) Bright field picture of the imaged area in F–G. In this coculture the stimulating electrode was placed in the superficial layer of the MOB (white circle). (F, G) Epifluorescence calcium imaging. Red codes for the largest increase in intracellular calcium. (F) Stimulation in the MOB, within the area targeted by the ORN axons triggers large calcium responses located near the stimulation site and within the center of the MOB. Simultaneously, there is a calcium response in the APir as well as more caudally, in the PPir. Activation maximum corresponds to dF/F_0 (%) = 5.66. (G) Blockade of glutamatergic transmission is effective in the Pir but incomplete in the MOB. Scale bars = 1 mm (A–C, E–G); 50 μ m (D₁, D₂).

pharmacological blockade of glutamatergic synapses by application of CNQX and AP5. The presynaptic activity of the putative ORN clusters in response to OE stimulation is not affected by the application of the AMPA and NMDA receptor blocking drugs (Fig. 6C). Propagation of the calcium response into the olfactory cortex area is variable and could not be elicited in this coculture (compare Figs. 6 and 7).

Post hoc morphological analysis of the recorded coculture shows the presence of a large OMP-labeled cluster of ORNs underneath the stimulation electrode (Fig. 6D). Numerous OMP positive axon bundles leave the ORN cluster and can be followed as they cross the small gap between the tissues, reach the MOB and course through its superficial layers for quite long stretches (Fig. 6D). The micro-

scopic analysis of the second distant calcium response evidences a lower amount of OMP-labeled fibers in this zone (Fig. 6E–F). The CR antibody was adopted here to visualize as many neuronal elements within the MOB as possible. Numerous CR-labeled small neurons, resembling periglomerular cells are scattered amid the ORN axon fibers in the superficial layers of the MOB. No significant differences in the density of neurons can be detected between the two responsive areas (Fig. 6D–F). Thus, the differences in intensity between calcium responses in the MOB correlate with the distance from the stimulating electrode and rather depend on the overall extent of ORN fibers reaching the target.

Synaptic propagation of the activity to the olfactory cortex area was observed only in cocultures of approxi-

mately DIV21. The success rate was 50% (four of eight), due to the variability in the intensity of the MOB calcium response triggered by OE stimulation. Fig. 7 shows two examples of the variable extent of activity recorded in the Pir in response to the stimulation of ORNs. The coculture in Fig. 7A–C exhibits a faint calcium response in the superficial MOB just opposite the stimulated ORNs, which extends to the center of the MOB and the APir. An intense calcium response occurs in MOB, deeper and more distant from the OE stimulation site. Pharmacological blockade of glutamate receptors by CNQX and AP5 is effective, confirming the postsynaptic nature of the response in both the MOB and the Pir. Post hoc immunolabeling for OMP and CR confirmed the presence of ORN fibers innervating the superficial MOB (not shown). Confocal microscopic examination of the zone of peak calcium response reveals the presence of large CR containing neurons resembling mitral cells (Fig. 7D₁–D₂). These data suggest that an OE-evoked calcium response in the Pir can only be expected if MOB deep layers harboring mitral cells are sufficiently active.

To stimulate more effectively the MOB we placed the electrode on the superficial layer of the MOB, within the area targeted by the ORN axons. An example of the response obtained is shown in Fig. 7E–F. Large calcium responses occur near the stimulation site and involve the center of the MOB, corresponding to the granule cell layer. Simultaneous activation of the APir and a faint calcium response more caudally into the PPir can be recognized. Blockade of glutamatergic transmission is effective in the Pir but incomplete in the MOB, where part of the deeper layers remains insensitive. This may depend on the activation of putative local inhibitory circuits within the MOB via top down afferents. The large and almost generalized activity evoked in the MOB under these conditions suggests that more mitral cells can be recruited, provided the extent of the ORN fibers stimulated is increased. Despite sufficient connectivity between the MOB and its target cortical areas (compare with Fig. 2G–H), the level of activation in the Pir triggered by stimulation of the restored olfactory axon projections remains moderate. Thus, the termination pattern of olfactory axons within the MOB *in vitro*, the extent of reinnervation and of functional recovery, rather exhibit features of a postlesion recovery (Christensen et al., 2001; Schwob, 2005; Mombaerts, 2006).

DISCUSSION

Establishing a slice that preserves the central olfactory pathway

We present here a novel brain slice which we call OB slice because it includes the MOB and the Pir and preserves mitral cell axons within the LOT. Our preparation method is based on recent work by Demir et al. (2001) and Balu et al. (2007) and is the first attempt to transfer the central relay stations of the olfactory pathway into an organotypic culture system.

The central olfactory pathway is well established at birth: mitral cells are among the first neurons appearing in

the MOB at E12 and principal neurons of the Pir are born at about the same time (Schwob and Price, 1984). Mitral cell axons shortly retain their navigational potential after birth: they can grow again into their target if the LOT is transected during the first postnatal week (Grafe, 1983). Since axons of mitral cells can be traced from the MOB through the LOT into the Pir of the OB slice without differences before and after 1 week in culture, we conclude that they are rarely transected during the preparation and do not undergo relevant degenerative or regenerative changes upon culturing.

The layering and the characteristic neuronal populations present in the P5–P7 MOB and Pir are maintained in the OB slice upon culturing. We adopted Reelin as a marker for glomerular layer interneurons and mitral cells of the MOB (Alcantara et al., 1998; Ramos-Moreno et al., 2006; Herrmann et al., 2007). CR was used to detect granular and periglomerular interneurons (Herrmann et al., 2007) and as an alternative marker of mitral and tufted cells (Wouterlood and Hrtig, 1995) in the MOB. To visualize dendrites, we preferred Smi 32 to other cytoskeleton markers because it selectively labels a subset of mitral cells in the MOB (Lopez-Picon et al., 2003). The expression pattern of Reelin in the Pir at DIV7 in culture does not even differ much from that of mature animals (Ramos-Moreno et al., 2006; A. L. Scotti, personal communication). Only the cell dense molecular layer—still rich with Reelin positive Cajal Retzius cells—reminds of the early postnatal cortex (D'Arcangelo et al., 1997). The distribution of Smi 32 labeling in the Pir of OB slice is also comparable to that found in the 1-week-old mouse.

In conclusion, we can make use of a slice that includes the central olfactory pathway and maintains numerous morphological characteristics of second and third order neurons of the OB when cultured.

Cocultures of OE explants and OB slice: ORNs regenerate, mature and rewire

Dissociated ORNs are difficult to maintain in culture (McEntire and Pixley, 2000). Instead, ORNs of embryonal (MacDonald et al., 1996; Gong et al., 1996; Goetze et al., 2002; Hamlin et al., 2004) or postnatal (Kanaki et al., 2000; Josephson et al., 2004) OE explant cultures can better regenerate. In fact the stem cell niche is better maintained in OE explants, thus enabling long term culturing (Beites et al., 2005).

Regeneration and differentiation of ORNs also occur under our culture conditions. BrdU positive nuclei appear GAP43 immunoreactive 1 week after the BrdU exposure, indicating that ORNs are born *in vitro*. In DIV7 cultures, GAP43 often colocalizes with OMP, the marker of differentiated ORNs. Similarly to what generally occurs *in vivo* during development (Kim and Greer, 2000), GAP43 expression has subsided by the end of the third week *in vitro* and most ORNs are now OMP immunoreactive. The density and distribution of OMP positive ORN clusters do not differ between postnatal OE explants grown isolated or in coculture. In fact, OMP expression in the OE is independent of the contact of ORN axons with the MOB (Schwob

et al., 1992; Gong et al., 1996). The ORNs we detect are discretely distributed in clusters (Goetze et al., 2002), as if only few stem cells would survive at randomly distributed locations and start to proliferate. We thus assume that ORNs derived from an island of preserved stem cells may represent a clonal population sharing the same receptor and zonal characteristics.

When the OE is cocultured with the OB slice, axon outgrowth regularly occurs, in agreement with previous reports of OE–MOB cocultures (Kanaki et al., 2000; Josephson et al., 2004; Storan and Key, 2004). Axons course in direction of the MOB within tissue bridges resembling the glial migratory mass that forms between the nasal pit and the rostral surface of the telencephalon during embryonic development. ORN axons navigate following this glial path of ensheathing cells born in the OE and migrating toward the telencephalon (Treloar et al., 1996). If ensheathing cells fail to migrate, olfactory axons do not grow out, whorling in the OE explant (Tisay and Key, 1999). Establishment of the migratory mass depends on chemotropic molecules released by the brain tissue (Liu et al., 1995) as well as on the chemical composition of the extracellular matrix substrate (Tisay and Key, 1999). As reported for embryonal OE explants by Storan and Key (2004), who also adopted uncoated Millipore membranes for culturing, we could detect ORN axon bundles by GAP43 and OMP immunocytochemistry in our isolated OE explants, but never observed axons grow out of the tissue. Other literature data reporting olfactory axon outgrowth from OE explants in absence of the MOB (Gong et al., 1996; Goetze et al., 2002; Hamlin et al., 2004) are only apparently contradictory: in fact the laminin these authors use as substrate powerfully promotes ensheathing cell migration (Treloar et al., 1996) and may suffice in guiding glia out of the explant resulting in ORN axon outgrowth.

Thus, our coculture system supports regeneration and differentiation of ORNs in the OE explants and also enables navigation of ORN axons onto the MOB of the OB slice.

Cocultures of OE explants and OB slice: ORNs target specificity despite lack of glomeruli

In mice, *in vivo*, ORN axons start to grow into the MOB at ca. E 14 and then coalesce into protoglomeruli during late embryonal development. Axodendritic synapses between ORNs and mitral cells are present at this stage but the targeted mitral cell dendrites are rudimental and do not drive the process (Mombaerts, 2006). Partitioning of mitral cell dendrites into the definitive glomerular cores is accomplished only by P7. By this time, more juxtglomerular cells have settled in the zone and the dendrodendritic glomerular shell gets into shape (Bailey et al., 1999; Treloar et al., 1999).

A cell dense superficial zone resembling the glomerular layer exists in the MOB of the OB slice at DIV7. After 21 days of coculturing with OE explants, the glomerular layer has changed into a loose cellular lamina traversed by numerous bundles of OMP immunoreactive ORN axons accumulating in the newly formed olfactory nerve layer above it. Organization of these axon bundles into glomeruli seems not progressed enough by DIV21 under our culture

conditions. However, small axon bundles can be followed below the olfactory nerve layer as they course amid numerous cell bodies and dendrites within the MOB of the OB slice. OMP immunoreactive punctates on dendrites of mitral cells and of interneurons suggest a certain degree of target specific reconnection, despite the absence of glomerular organization.

Lack of a defined glomerular layer is often described in OE–MOB cocultures. Kanaki et al. (2000) report the absence of morphologically recognizable glomeruli in the MOB of DIV7 cocultures despite a successful functional proof of reconnection. Also Storan and Key (2004) refer to the general absence of distinct glomerular formation in their DIV7 cocultures. Since well-formed OMP expressing glomeruli can be occasionally detected in DIV28 cocultures (Josephson et al., 2004) it is possible that formation of glomeruli ensues upon prolonged culturing.

Thus, once separated, OE and MOB (of both embryonic and postnatal origin) are not able to properly reconstruct glomeruli in their new *in vitro* environment, despite morphological or/and functional evidence for target specificity (Kanaki et al., 2000; Josephson et al., 2004; Storan and Key, 2004).

Dissection and transfer in culture of postnatal OE and OB tissue attempts to study repair strategies, because it is a lesion of an embryonally formed connection. In the adult, *in vivo*, the glomerular scaffold is not lost following olfactory nerve transection or OE damage (Graziadei and Monti Graziadei, 1980; Schwob et al., 1999; Christensen et al., 2001). In contrast, to repair *in vitro* a lesion of the peripheral olfactory pathway set postnatally, the deafferented glomeruli disassemble and the rewiring seems to resume embryonic development. Such a difference may well reflect a dedifferentiation trend intrinsic to the culture system but also indicates that repair strategies may change with age. In this respect, it is tempting to speculate that the failure of restoration of rhinotopy and receptotopic glomerular convergence often observed in the adult (Christensen et al., 2001; Schwob, 2005; Mombaerts, 2006) may be related to the persistence of the glomerular scaffold. Data on the response of the MOB glomerular layer during rewirement of ORN axons in postnatal mice *in vivo* may help to better define the limits of this coculture approach.

Functional integrity of the organotypic olfactory system

The study of the cellular basis of sensory processing is hampered by several drawbacks. The most critical ones are the bad accessibility and visibility of the structures to be studied and the impossibility to have all involved structures from the sensor in the periphery up to the cortical representation areas in one preparation. With regard to the olfactory system the only successful example up to now is a whole brain preparation perfused through the vessels that preserves the OE, the MOB and the Pir *in situ* and is used for acute functional investigations (Ishikawa et al., 2007). We show for the first time the combined culturing of the peripheral and the central parts of the olfactory system. Such *in vitro* olfactory system gives for the first time the

possibility to activate peripheral olfactory sensors and to explore the response of central neurons at different level of cortical integration.

We adopted the calcium imaging technique to prove the functional integrity of our OE–OB cocultures because it allows detecting activity at different locations in the culture avoiding multiple electrode recording. Changes in the intracellular calcium concentration reflect the suprathreshold activity in neuronal cell bodies. Thus, areas lightening up in these experiments are those where synaptic activation induces spiking activity, while the regions where synaptic input is insufficient to induce action potentials cannot be detected (Berger et al., 2007). It is also important to note that calcium imaging does not distinguish between action potential activity in principal cells and inhibitory neurons.

The MOB–Pir axonal connection is functional in our novel OB slice preparation. Extracellular electrical stimulation of the mitral cell layer in cultures stained with a calcium sensitive dye induces increases in the intracellular calcium concentration in both MOB and Pir. The rise in intracellular calcium reflects the suprathreshold activity in the cell bodies of MOB and Pir neurons that follows excitation via glutamatergic synapses of the AMPA and NMDA type (Berger et al., 2007). When the OB slice is cocultured with OE explants, the function of the OE–MOB–Pir pathway recovers in a time dependent manner along with the rewiring between OE explants and the MOB. A significant increase in the MOB activity accompanies the maturational changes observed between the first and the third week of coculturing, similar to what is reported in the literature (Kanaki et al., 2000; Josephson et al., 2004; Muramoto et al., 2006). In analogy, functional responses in the Pir upon stimulation of the OE are more readily detected upon long term coculturing in our system.

The calcium-evoked response in the rewired peripheral olfactory pathway is limited to the electrically stimulated cluster of ORNs within the OE and to circumscribed zones within the superficial layer of the MOB which appear as focal glomerular activity. Assuming that the stimulated ORNs are clonal and share the same receptor, it is tempting to speculate that such focal MOB response may indicate that a certain degree of receptor topography is maintained. Thus, while immunofluorescence labels all ORN fibers in the MOB and can only indicate whether their termination pattern is specific, functional imaging of homogeneous groups of ORNs provides additional information on their putative positional specificity.

The Pir does not regularly respond when a single ORN cluster in the OE explant is triggered. To stimulate a discrete OE cluster means to activate a putatively clonal population of ORNs. It is possible that the resulting activity in the olfactory cortex may not reach the spike threshold. The calcium-evoked response in the Pir is regular instead and extends into the PPir when stimulation is applied at the tip of the connecting bridge on the MOB olfactory nerve layer. Assumed all ingrowing axons are activated at this position, these data show that a critical mass of ORNs and the activity of more mitral cells within the deep layer of the MOB are necessary to efficiently evoke spiking activity in the Pir areas.

CONCLUSION

In conclusion, our coculture system is characterized by a sufficient connectivity not only between ORN and MOB neurons but also to the higher order neurons in the olfactory cortex. Further studies *in vitro* and *in vivo* are required to determine to which extent the functional responses of this *in vitro* olfactory system can be considered as a model for postlesional olfaction disorders.

Acknowledgments—Financial support was granted by the Swiss National Science Foundation (3100A0100549/1 to A.L.S., 3100-107529/1 to T.B. and 3100A0105822 to Daniel Studer), the Novartis Foundation for Medical Biological Research (04B47 to A.L.S.), the Swiss 3R Research Foundation (288/04 to A.L.S. and 06A04 to T.B.) and the Institute of Anatomy of the University of Bern.

OMP-GFP mice pairs were kindly donated by Dr. Jörg Strotmann (University of Hohenheim, Germany) with the permission of Prof. Peter Mombaerts (Rockefeller University, New York, NY, USA). We are grateful to H. R. Lüscher, P. S. Eggli, and G. Herrmann for discussion and to C. Nitsch for critical reading of the manuscript.

This work is included in the PhD thesis of F.M. submitted to the graduate school for cellular and biomedical sciences of the University of Bern.

REFERENCES

- Alcantara S, Ruiz M, D'Arcangelo G, Ezan F, de Lecea L, Curran T, Sotelo C, Soriano E (1998) Regional and cellular patterns of reelin mRNA expression in the forebrain of the developing and adult mouse. *J Neurosci* 18:7779–7799.
- Bailey MS, Puche AC, Shipley MT (1999) Development of the olfactory bulb: evidence for glia-neuron interactions in glomerular formation. *J Comp Neurol* 415:423–448.
- Balu R, Pressler RT, Strowbridge BW (2007) Multiple modes of synaptic excitation of olfactory bulb granule cells. *J Neurosci* 27:5621–5632.
- Beites CL, Kawachi S, Crocker CE, Calof AL (2005) Identification and molecular regulation of neural stem cells in the olfactory epithelium. *Exp Cell Res* 306:309–316.
- Berger T, Borgdorff A, Crochet S, Neubauer FB, Lefort S, Fauvet B, Ferezou I, Carleton A, Lüscher HR, Petersen CC (2007) Combined voltage and calcium epifluorescence imaging *in vitro* and *in vivo* reveals subthreshold and suprathreshold dynamics of mouse barrel cortex. *J Neurophysiol* 97:3751–3762.
- Best AR, Wilson DA (2003) A postnatal sensitive period for plasticity of cortical afferents but not cortical association fibers in rat piriform cortex. *Brain Res* 961:81–87.
- Born DE, Rubel EW (1985) Afferent influences on brain stem auditory nuclei of the chicken: neuron number and size following cochlea removal. *J Comp Neurol* 231:435–445.
- Christensen MD, Holbrook EH, Costanzo RM, Schwob JE (2001) Rhinotomy is disrupted during the re-innervation of the olfactory bulb that follows transection of the olfactory nerve. *Chem Senses* 26:359–369.
- Couper Leo JM, Brunjes PC (2003) Neonatal focal denervation of the rat olfactory bulb alters cell structure and survival: a Golgi, Nissl and confocal study. *Brain Res Dev Brain Res* 140:277–286.
- D'Arcangelo G, Nakajima K, Miyata T, Ogawa M, Mikoshiba K, Curran T (1997) Reelin is a secreted glycoprotein recognized by the CR-50 monoclonal antibody. *J Neurosci* 17:23–31.
- Demir R, Haberly LB, Jackson MB (2001) Epileptiform discharges with *in-vivo*-like features in slices of rat piriform cortex with longitudinal association fibers. *J Neurophysiol* 86:2445–2460.
- Franks KM, Isaacson JS (2005) Synapse-specific downregulation of NMDA receptors by early experience: a critical period for plasticity of sensory input to olfactory cortex. *Neuron* 47:101–114.

- Goetze B, Breer H, Strotmann J (2002) A long-term culture system for olfactory explants with intrinsically fluorescent cell populations. *Chem Senses* 27:817–824.
- Gong Q, Liu WL, Srodon M, Foster TD, Shipley MT (1996) Olfactory epithelial organotypic slice cultures: a useful tool for investigating olfactory neural development. *Int J Dev Neurosci* 14:841–852.
- Grafe MR (1983) Developmental factors affecting regeneration in the central nervous system: early but not late formed mitral cells reinnervate olfactory cortex after neonatal tract section. *J Neurosci* 3:617–630.
- Graziadei GA, Graziadei PP (1979) Neurogenesis and neuron regeneration in the olfactory system of mammals. II. Degeneration and reconstitution of the olfactory sensory neurons after axotomy. *J Neurocytol* 8:197–213.
- Graziadei PP, Monti Graziadei GA (1980) Neurogenesis and neuron regeneration in the olfactory system of mammals. III. Deafferentation and reinnervation of the olfactory bulb following section of the fila olfactoria in rat. *J Neurocytol* 9:145–162.
- Hamilton KA, Parrish-Aungst S, Margolis FL, Erdelyi F, Szabo G, Puche AC (2008) Sensory deafferentation transsynaptically alters neuronal GluR1 expression in the external plexiform layer of the adult mouse main olfactory bulb. *Chem Senses* 33:201–210.
- Hamlin JA, Fang H, Schwob JE (2004) Differential expression of the mammalian homologue of fasciclin II during olfactory development *in vivo* and *in vitro*. *J Comp Neurol* 474:438–452.
- Herrmann G, Hlushchuk R, Baum O, Scotti AL (2007) Nitric oxide synthase protein levels, not the mRNA, are downregulated in olfactory bulb interneurons of reeler mice. *J Chem Neuroanat* 33:87–96.
- Ishikawa T, Sato T, Shimizu A, Tsutsui K, de Curtis M, Iijima T (2007) Odor-driven activity in the olfactory cortex of an *in vitro* isolated guinea pig whole brain with olfactory epithelium. *J Neurophysiol* 97:670–679.
- Josephson EM, Yilma S, Vodyanoy V, Morrison EE (2004) Structure and function of long-lived olfactory organotypic cultures from postnatal mice. *J Neurosci Res* 75:642–653.
- Kanaki K, Sato K, Kashiwayanagi M (2000) Functional synapse formation between rat olfactory receptor neurons and olfactory bulb neurons *in vitro*. *Neurosci Lett* 285:76–78.
- Kim H, Greer CA (2000) The emergence of compartmental organization in olfactory bulb glomeruli during postnatal development. *J Comp Neurol* 422:297–311.
- Kim HH, Puche AC, Margolis FL (2006) Odorant deprivation reversibly modulates transsynaptic changes in the NR2B-mediated CREB pathway in mouse piriform cortex. *J Neurosci* 26:9548–9559.
- Kupfer C, Palmer P (1964) Lateral geniculate nucleus: Histological and cytochemical changes following afferent denervation and visual deprivation. *Exp Neurol* 9:400–409.
- Litaudon P, Datiche F, Cattarelli M (1997) Optical recording of the rat piriform cortex activity. *Prog Neurobiol* 52:485–510.
- Liu KL, Chuah MI, Lee KK (1995) Soluble factors from the olfactory bulb attract olfactory Schwann cells. *J Neurosci* 15:990–1000.
- Liu N, Cigola E, Tinti C, Jin BK, Conti B, Volpe BT, Baker H (1999) Unique regulation of immediate early gene and tyrosine hydroxylase expression in the odor-deprived mouse olfactory bulb. *J Biol Chem* 274:3042–3047.
- Lledo PM, Gheusi G, Vincent JD (2005) Information processing in the mammalian olfactory system. *Physiol Rev* 85:281–317.
- Lopez-Picon FR, Uusi-Oukari M, Holopainen IE (2003) Differential expression and localization of the phosphorylated and nonphosphorylated neurofilaments during the early postnatal development of rat hippocampus. *Hippocampus* 13:767–779.
- MacDonald KP, Murrell WG, Bartlett PF, Bushell GR, Mackay-Sim A (1996) FGF2 promotes neuronal differentiation in explant cultures of adult and embryonic mouse olfactory epithelium. *J Neurosci Res* 44:27–39.
- Margolis FL, Verhaagen J, Biffo S, Huang FL, Grillo M (1991) Regulation of gene expression in the olfactory neuroepithelium: a neurogenetic matrix. *Prog Brain Res* 89:97–122.
- Matsutani S, Yamamoto N (2000) Differentiation of mitral cell dendrites in the developing main olfactory bulbs of normal and naris-occluded rats. *J Comp Neurol* 418:402–410.
- McEntire JK, Pixley SK (2000) Olfactory receptor neurons in partially purified epithelial cell cultures: comparison of techniques for partial purification and identification of insulin as an important survival factor. *Chem Senses* 25:93–101.
- Mombaerts P (2006) Axonal wiring in the mouse olfactory system. *Annu Rev Cell Dev Biol* 22:713–737.
- Muramoto K, Huang GZ, Taniguchi M, Kaba H (2006) Functional synapse formation between cultured rat accessory olfactory bulb neurons and vomeronasal pockets. *Neuroscience* 141:475–486.
- Potter SM, Zheng C, Koos DS, Feinstein P, Fraser SE, Mombaerts P (2001) Structure and emergence of specific olfactory glomeruli in the mouse. *J Neurosci* 21:9713–9723.
- Ramos-Moreno T, Galazo MJ, Porrero C, Martinez-Cerdeno V, Clasca F (2006) Extracellular matrix molecules and synaptic plasticity: immunomapping of intracellular and secreted Reelin in the adult rat brain. *Eur J Neurosci* 23:401–422.
- Rosen GD, Burstein D, Galaburda AM (2000) Changes in efferent and afferent connectivity in rats with induced cerebrocortical microgyria. *J Comp Neurol* 418:423–440.
- Schwob JE (2005) Restoring olfaction: a view from the olfactory epithelium. *Chem Senses* 30:1131–1132.
- Schwob JE, Szumowski KE, Stasky AA (1992) Olfactory sensory neurons are trophically dependent on the olfactory bulb for their prolonged survival. *J Neurosci* 12:3896–3919.
- Schwob JE, Youngentob SL, Ring G, Iwema CL, Mezza RC (1999) Reinnervation of the rat olfactory bulb after methyl bromide-induced lesion: timing and extent of reinnervation. *J Comp Neurol* 412:439–457.
- Schwob JE, Price JL (1984) The development of lamination of afferent fibers to the olfactory cortex in rats, with additional observations in the adult. *J Comp Neurol* 223:203–222.
- Shipley MT, Ennis M, Puche A (2004) Olfactory system. In: *The rat nervous system* (Paxinos G, ed), pp 922–964. London: Elsevier Academic Press.
- Storan MJ, Key B (2004) Target tissue influences the peripheral trajectory of mouse primary sensory olfactory axons. *J Neurobiol* 61:175–188.
- Tisay KT, Key B (1999) The extracellular matrix modulates olfactory neurite outgrowth on ensheathing cells. *J Neurosci* 19:9890–9899.
- Treloar HB, Nurcombe V, Key B (1996) Expression of extracellular matrix molecules in the embryonic rat olfactory pathway. *J Neurobiol* 31:41–55.
- Treloar HB, Purcell AL, Greer CA (1999) Glomerular formation in the developing rat olfactory bulb. *J Comp Neurol* 413:289–304.
- Uva L, Strowbridge BW, de Curtis M (2006) Olfactory bulb networks revealed by lateral olfactory tract stimulation in the *in vitro* isolated guinea-pig brain. *Neuroscience* 142:567–577.
- von Bohlen und Halbach O (2007) Immunohistological markers for staging neurogenesis in adult hippocampus. *Cell Tissue Res* 329:409–420.
- Weiler E, Farbman AI (1997) Proliferation in the rat olfactory epithelium: age-dependent changes. *J Neurosci* 17:3610–3622.
- Wouterlood FG, Hrtig W (1995) Calretinin-immunoreactivity in mitral cells of the rat olfactory bulb. *Brain Res* 682:93–100.
- Zou Z, Li F, Buck LB (2005) Odor maps in the olfactory cortex. *Proc Natl Acad Sci U S A* 102:7724–7729.

- Publication 3 -

“Combined Voltage and Calcium Epifluorescence Imaging In Vitro and In Vivo Reveals Subthreshold and Suprathreshold Dynamics of Mouse Barrel Cortex”

Thomas Berger, Aren Borgdorff, Sylvain Crochet, Florian B. Neubauer, Sandrine Lefort, Bruno Fauvet, Isabelle Ferezou, Alan Carleton, Hans-Rudolf Lüscher & Carl C. H. Petersen (2007).

Journal of Neurophysiology 97:3751-3762.

Two of the most dynamic low-level correlates of brain functions are the membrane potential and the intracellular concentration of calcium. Both can be imaged optically by the introduction of fluorescent probes into brain preparations. Voltage-sensitive dyes (VSD) insert into the plasma membrane and change their fluorescence intensity dependent on the potential across the lipid bilayer. Fluorescent calcium-sensitive dyes (CASD) respond rapidly and selectively to changes in the cytosolic free calcium ion concentration. Publication 3 is a methodological study in the field of optical imaging and consists in a precise evaluation of the kind of the signals which are obtained with commonly used voltage-sensitive dyes and calcium-sensitive dyes. We combine epifluorescence VSD and CASD imaging with whole cell recordings of the membrane potential to allow a quantitative comparison of what is measured using fluorescent dyes. We recorded VSD and CASD signals in three different experimental conditions, in single cells, in brain slices, and in vivo. Our findings indicate that VSD signals predominantly report subthreshold activity and CASD report suprathreshold activity.

Combined Voltage and Calcium Epifluorescence Imaging In Vitro and In Vivo Reveals Subthreshold and Suprathreshold Dynamics of Mouse Barrel Cortex

Thomas Berger,^{1,3} Aren Borgdorff,¹ Sylvain Crochet,¹ Florian B. Neubauer,³ Sandrine Lefort,¹ Bruno Fauvet,¹ Isabelle Ferezou,¹ Alan Carleton,² Hans-Rudolf Lüscher,³ and Carl C. H. Petersen¹

¹Laboratory of Sensory Processing and ²Flavour Perception Group, Brain Mind Institute, Ecole Polytechnique Federale de Lausanne, Lausanne; and ³Institute of Physiology, University of Bern, Bern, Switzerland

Submitted 6 November 2006; accepted in final form 10 March 2007

Berger T, Borgdorff A, Crochet S, Neubauer FB, Lefort S, Fauvet B, Ferezou I, Carleton A, Lüscher H-R, Petersen CC. Combined voltage and calcium epifluorescence imaging in vitro and in vivo reveals subthreshold and suprathreshold dynamics of mouse barrel cortex. *J Neurophysiol* 97: 3751–3762, 2007. First published March 14, 2007; doi:10.1152/jn.01178.2006. Cortical dynamics can be imaged at high spatiotemporal resolution with voltage-sensitive dyes (VSDs) and calcium-sensitive dyes (CaSDs). We combined these two imaging techniques using epifluorescence optics together with whole cell recordings to measure the spatiotemporal dynamics of activity in the mouse somatosensory barrel cortex in vitro and in the supragranular layers in vivo. The two optical signals reported distinct aspects of cortical function. VSD fluorescence varied linearly with membrane potential and was dominated by subthreshold postsynaptic potentials, whereas the CaSD signal predominantly reflected local action potential firing. Combining VSDs and CaSDs allowed us to monitor the synaptic drive and the spiking activity of a given area at the same time in the same preparation. The spatial extent of the two dye signals was different, with VSD signals spreading further than CaSD signals, reflecting broad subthreshold and narrow suprathreshold receptive fields. Importantly, the signals from the dyes were differentially affected by pharmacological manipulations, stimulation strength, and depth of isoflurane anesthesia. Combined VSD and CaSD measurements can therefore be used to specify the temporal and spatial relationships between subthreshold and suprathreshold activity of the neocortex.

INTRODUCTION

Many computations in the neocortex are thought to occur on the millisecond timescale within maps composed of cortical columns. Most current techniques to investigate cortical processing offer limited spatial resolution because of the low density of recording electrodes or theoretical difficulties of defining the signal sources. Optical methods, however, offer both sufficient temporal and spatial resolution for real-time analysis of cortical processing.

Two of the most dynamic parameters in the active brain are membrane potential (V_m) and intracellular calcium concentration ($[Ca^{2+}]_i$). Both of these can be imaged optically by the introduction of fluorescent probes into the brain. Voltage-sensitive dyes (VSDs) insert into the plasma membrane and change their fluorescence intensity dependent on the potential

across the lipid bilayer. Previous studies recorded VSD signals in invertebrate preparations (Antic and Zecevic 1995; Salzberg et al. 1973), from cultured cells (Bullen and Saggau 1998), brain slices (Antic et al. 1999; Contreras and Llinas 2001; Laaris and Keller 2002; Petersen and Sakmann 2001), and in vivo (Borgdorff et al. 2007; Civillico and Contreras 2006; Derdikman et al. 2003; Ferezou et al. 2006; Grinvald et al. 1984; Kleinfeld and Delaney 1996; Petersen et al. 2003a,b; Shoham et al. 1999). The VSD JPW1114 (also known as di-2-ANEPEQ) has proven useful as a dye for intracellular application in individual nerve cells, allowing the spatiotemporal analysis of electrical signaling in dendrites (Antic and Zecevic 1995; Antic et al. 1999). The VSD RH1691 is optimized for in vivo measurements (Shoham et al. 1999) and, when topically applied to the neocortex, it can resolve cortical activity with millisecond and subcolumnar resolution (Grinvald and Hildesheim 2004). Fluorescent calcium-sensitive dyes (CaSDs) such as Fluo-3 and Oregon Green BAPTA-1 (OGB-1) have been developed that respond rapidly and selectively to changes in the cytosolic free calcium ion concentration (Tsien 1980). CaSDs can be applied extracellularly in a membrane-permeable ester form, which is subsequently cleaved intracellularly by esterases releasing the functional fluorescent CaSD (Tsien 1981). Recently, network activity was imaged with CaSD both in brain slices and in the intact brain (Borgdorff et al. 2007; Kerr et al. 2005; Nimmerjahn et al. 2004; Ohki et al. 2005; Peterlin et al. 2000; Stosiek et al. 2003; Wachowiak and Cohen 2001; Yaksi and Friedrich 2006).

In this study, we combined epifluorescence VSD and CaSD imaging together with whole cell (WC) V_m recordings to allow a quantitative comparison of what is measured using these techniques, focusing on their application to the study of the mouse barrel cortex (Petersen 2003; Woolsey and Van der Loos 1970). We recorded VSD and CaSD signals in three different experimental conditions: in single cells, in brain slices, and in vivo. In single cells, we studied the dynamic range of VSDs and CaSDs during controlled membrane potential changes. In the barrel cortex in vitro, we characterized the link of the VSD and CaSD signals to sub- and suprathreshold electrophysiological network activity and thereafter studied the spatial spread of synaptic activity and action potentials. We next transferred these methods to make in vivo optical measurements of activity in layer 2/3 barrel cortex of anesthetized mice, analyzing both the evoked and the spontaneous spatiotemporal dynamics of the VSD and CaSD signals. The data are

Address for reprint requests and other correspondence: C. Petersen, Laboratory of Sensory Processing, Brain Mind Institute, SV-BMI-LENS, Station 15, Ecole Polytechnique Federale de Lausanne, CH-1015 Lausanne, Switzerland (E-mail: carl.petersen@epfl.ch).

consistent with VSD signals reporting predominantly sub-threshold activity and CaSD reporting suprathreshold activity.

METHODS

All experiments were carried out in accordance with the Swiss Federal Veterinary Office.

Voltage-sensitive dye biophysics

Defolliculated *Xenopus* oocytes were incubated for about 30 min in 1.6 mM RH1691 (Optical Imaging, Rehovot, Israel) dissolved in a solution containing (in mM): 135 NaCl, 5 KCl, 5 HEPES, 1.8 CaCl₂, and 1 MgCl₂ (pH 7.3 with NaOH). The oocyte was transferred to the recording bath filled with a standard ND96 *Xenopus* oocyte medium containing (in mM): 96 NaCl, 2 KCl, 5 HEPES, 1.8 CaCl₂, and 2 MgCl₂ (pH 7.4 with NaOH). Two microelectrodes filled with 2 M KCl were used to voltage-clamp the oocyte using an Axoclamp 2B amplifier (Axon Instruments, Union City, CA). A computer running Igor Pro (WaveMetrics, Lake Oswego, OR), interfacing with an ITC-18 board (Instrutech, Port Washington, NY), not only controlled the command potential but also sampled the achieved membrane potential at 20 kHz. The oocyte membrane was imaged using an Olympus BX51WI microscope equipped with an Olympus $\times 20$ 0.95 numerical aperture (NA) objective. Excitation light from a 100 W halogen lamp with a shutter (Uniblitz, Vincent Associates, Rochester, NY) was band-pass filtered (630/30 nm) and reflected toward the sample by a 650 nm dichroic mirror. Emitted fluorescence was long-pass filtered (665 nm) and imaged using a MiCam Ultima camera (SciMedia, Irvine, CA). Fluorescence measurements were synchronized to electrophysiology through TTL pulses. In one set of experiments the membrane potential was stepped from a holding potential of -60 mV to test membrane potentials (-100 to $+40$ mV in 20 mV steps) for 200 ms periods and fluorescence changes were recorded at 10 ms frame rates (Fig. 1A). For each oocyte fluorescence signals from 10 to 20 trials were averaged. Fluorescence signals were integrated across the field of view (FOV) containing 100×100 pixels covering roughly $300 \times 300 \mu\text{m}$. This spatial averaging and averaging across different trials was carried out using the MiCam Ultima analysis software. The fluorescence time-course traces were subsequently exported to Igor Pro (WaveMetrics) for further analysis, where the data from six oocytes were combined and a polynomial bleaching curve was subtracted. In a separate set of experiments fluorescence was sampled at 1 ms time resolution while membrane potential was repeatedly alternated from -60 to 40 mV every 10 ms for 1 s (Fig. 1B). For each oocyte fluorescence signals from 10 trials were averaged and then the response to each of the 100 voltage steps was further averaged. Data from six oocytes were combined. The change in fluorescence, given throughout the paper, is normalized to resting fluorescence ($\Delta F/F_0$), i.e., as the change divided by the fluorescence before stimulation (Figs. 1–5, 6A, and 7) or without spontaneous ongoing activity (Fig. 6, B and C).

Brain slice preparation

Parasagittal or thalamocortical slices (300 or 400 μm thick, respectively) (Agmon and Connors 1991) of the somatosensory cortex were prepared using a vibratome from 14- to 29-day-old C57BL/6J mice in ice-cold artificial cerebrospinal fluid (ACSF) containing (in mM): 125 NaCl, 25 NaHCO₃, 25 glucose, 2.5 KCl, 1.25 NaH₂PO₄, 2 CaCl₂, and 1 MgCl₂ bubbled with 95% O₂-5% CO₂ (pH 7.4). Slices were incubated at 35°C for 30 min and then left at room temperature until recording.

In vitro cellular imaging

Current-clamp recordings in the whole cell mode of the patch-clamp technique were obtained from the somata of neurons in acute

slices of the barrel cortex with Multiclamp 700A (Axon Instruments) or BVC-700A (Dagan, Minneapolis, MN) amplifiers. Patch pipettes were made from borosilicate glass with resistances of 3–7 M Ω filled with the following solution (in mM): 135 K-gluconate, 5 KCl, 10 HEPES, 4 Mg-ATP, 0.3 Na₂-GTP, and 10 Na₂-phosphocreatine (pH 7.3 with KOH). The pipette contained in addition either 200 μM of the CaSD Oregon Green 488 BAPTA-1 potassium salt (Takechi et al. 1998) (OGB-1, Molecular Probes, Eugene, OR), 0.9–5.5 mM of the VSD JPW1114 (di-2-ANEPEQ, Molecular Probes) or 6.8 mM of the VSD RH1691. Stock solutions of these dyes were prepared in pipette solution. JPW1114 and RH1691 were added only in the 4 μl backfill of the pipette, whereas its tip was filled with 1 μl of dye-free solution to prevent staining of the slice with expelled VSD. However, no functional VSD signals could be recorded using RH1691 applied intracellularly. Current injections into the cell under study with exponentially shaped rise and decay (“alpha currents”) induced both inhibitory and excitatory postsynaptic potential (IPSP and EPSP, respectively)–like membrane voltage deflections and action potentials (Fig. 1, D and F). Alternatively, synaptic potentials around action potential threshold were evoked with extracellular stimulation using an ACSF-filled pipette. Corresponding changes in fluorescence were imaged with a Zeiss Axioskop 2FS+ microscope [$\times 40$ 0.8 NA objective; 75-W xenon short-arc lamp; Deltaram V monochromator (PTI, Lawrenceville, NJ)]. A low-resolution (80 \times 80 pixel), fast (1–2 kHz) CCD camera (Redshirt NeuroCCD, RedShirtImaging, Fairfield, CT) running under computer control (Neuroplex software) was used to image changes in fluorescence in the FOV covering the soma and proximal dendrites (Fig. 1, D and F). All experiments were done at 35°C. The following filter sets were used: for OGB-1, excitation filter BP470/20 nm, dichroic mirror 510 nm, emission filter BP540/25 nm; for JPW1114, excitation filter BP520/20 nm, dichroic mirror 580 nm, emission filter LP590 nm; for RH1691, excitation filter BP630/30 nm, dichroic mirror 650 nm, emission filter LP665 nm.

In vitro network imaging

Stock solutions (10 mM) of the acetoxymethyl (AM) ester forms of OGB-1 (OGB-1 AM; Molecular Probes) or Fluo-3 (Biotium, Hayward, CA) were made in 80% fresh DMSO/20% pluronic acid and diluted 1:19 in a Ringer solution containing (in mM): 135 NaCl, 5 KCl, 5 HEPES, 1.8 CaCl₂, and 1 MgCl₂. The final solution (500 μM) was vortexed, sonicated, aliquoted, and stored in the freezer. The AM ester solution (10 μl) was sucked into an oil-filled application pipette (tip diameter 15–25 μm). To obtain even staining of the approximately $900 \times 900\text{-}\mu\text{m}$ cortical region of interest, the AM ester was injected into the slice at six to ten locations in the barrel cortex in parasagittal slices under visual control. In thalamocortical slices, the AM ester was applied with the same technique to label the entire layer 4 barrel cortex. OGB-1 AM was used throughout this study except in a few experiments involving the thalamocortical slice preparation, where both OGB-1 AM and Fluo-3 AM were used. The changes resulting from pharmacological manipulations were similar between OGB-1 and Fluo-3, so the data were pooled. Subsequently, the VSD RH1691 was applied to the slice surface at 1.6 mM in Ringer solution for approximately 1 min. Extracellular stimuli (duration 500 μs ; stimulation intensity range 15–500 μA ; normally two to three times threshold, i.e., 50 μA) were delivered to a layer 4 barrel using a Ringer solution–filled patch pipette (Fig. 2, A and B). In the thalamocortical preparation, a bipolar stimulation electrode was used to activate the ventral posterior medial (VPM) nucleus at 1.7- to 6-fold the threshold value for cortical activity, i.e., 200–400 μA (Fig. 2E). Imaging techniques for in vitro networks were as described earlier, except a wider FOV of the barrel cortex was imaged using either an Olympus BX51WI microscope ($\times 20$ 0.95 NA objective; 100 W halogen lamp) or a Zeiss Axioskop 2FS+ microscope ($\times 10$ 0.3 NA objective; 75 W xenon short-arc lamp; Deltaram V monochromator). In thalamocortical slices, we used $\times 4$ 0.13 NA (visual field 4.4×4.4

mm) or $\times 10$ 0.3 NA objectives (visual field 1.8×1.8 mm) (Zeiss Axioskop FS microscope; 100 W halogen lamp). Recording of OGB-1 and RH1691 fluorescence was interleaved. VSD and CaSD signals in thalamocortical slices from 6 to 25 trials were averaged to improve the signal-to-noise ratio. In some experiments, we combined imaging with somatic whole cell recordings of neurons in layer 2/3 (Fig. 2, A–D). Biocytin (2 mg/ml) was routinely included in the patch pipette solution to facilitate morphological analysis of the neurons.

In vivo imaging

C57BL/6J mice aged postnatal day (P) 21 to P25 were anesthetized with urethane (1.5 mg/g body weight; Figs. 4–6, Supplementary Fig. S1)¹ or isoflurane (0.5–2%; Fig. 7). Paw withdrawal, whisker movement, and eye blink reflexes were largely suppressed. A heating blanket maintained the rectally measured body temperature at 37°C. The skin overlying the somatosensory cortex was removed. The head of the mouse was glued to a metal head plate and fixed. In a first step, the location of C2 whisker representation was mapped by intrinsic optical imaging. The cortical surface was visualized through the intact skull covered with Ringer solution sealed with a glass coverslip. The surface blood vessels were visualized using light at 530 nm to enhance contrast. The illumination was switched to 630 nm for functional imaging. The reflected light was imaged using a Quicam CCD camera (Q-imaging; 10-Hz frame rate, 800×800 pixels covering approximately 2.5×2.5 -mm area). Image acquisition by a Firewire and stimulus control of the piezo by an ITC18 board were governed by custom routines running in Igor Pro. To avoid interference with VSD signals in the intrinsic imaging experiments described in Supplementary Fig. 1, we illuminated at 700 nm and to obtain the same FOV as the VSD imaging, we also imaged the intrinsic signals using a MiCam Ultima camera (20-Hz frame rate, 100×100 pixels covering a 2×2 -mm area). Alternating sweeps were imaged with or without stimuli delivered to the C2 whisker. Stimuli were applied at 10 Hz for 4 s and repeated 7 to 15 times with a 120 s interval. The intrinsic signal was quantified as the difference in the reflected light on stimulus compared with a 4 s time interval immediately before. The local signal was mapped onto the blood vessel pattern to guide surgery for the craniotomy (ranging in size from 1×1 to 3×3 mm), which was performed with extreme care so as not to damage the cortex, especially during removal of the dura. RH1691 was topically applied to the exposed cortex and allowed to diffuse into the cortex for about 40 min. Subsequently, unbound dye was washed away. OGB-1 AM was injected into layer 2/3 at multiple locations by a glass pipette connected to a hydraulic micromanipulator, avoiding blood vessels (about 50 nl of a 500 μ M or 1 mM solution per injection site). Fluorescence from the esterase-cleaved OGB-1 AM increased gradually over time and stabilized 1 h after injection as previously reported (Stosiek et al. 2003). Fluorescence at an injection site covered a circular area with half-maximal values at 330 ± 70 μ m diameter.

The cortex was covered with 1% agarose and a coverslip placed on top to stabilize the cortex. The excitation light was focused onto the cortical surface with a 25 mm Navitar video lens (or 50 mm Nikon lens). Fluorescence was collected by the same optical pathway but without reflection of the dichroic mirror, long-pass or band-pass filtered, and focused onto the camera by another 25 mm Navitar lens (or 135 mm Nikon lens). The voltage-sensitive dye was excited with 630 nm light emitted by light-emitting diodes (LEDs, L630, Epitex, Kyoto, Japan), reflected using a 655 nm dichroic mirror and long-pass filtered (>665 nm). Alternatively the RH1691 was illuminated with an electronically shuttered 100 W halogen lamp and directed onto the sample using fiber-optic light guides. The OGB-1 was excited either with 490/15 nm LEDs (L490-06U, Epitex) or by an electronically shuttered halogen lamp, reflected with a 500 nm dichroic mirror, and emitted fluorescence collected after band-pass filter 535/15 nm. Brief

backward deflections of the C2 whisker were delivered using a computer-controlled piezoelectric bimorph. The time course and amplitude of stimuli were recorded approximately 1 mm away from the skin with an optical displacement sensor (Philtec D64-0QT4, Philtec, Annapolis, MD). Images were recorded at frame rates ranging from 200 to 1,000 Hz using either a CCD camera (RedShirtImaging; Figs. 4, 5, and 7) or a dual camera MiCAM Ultima (BrainVision, Tokyo, Japan; Fig. 6 and Supplementary Fig. S1) for simultaneous measurements. Images were analyzed off-line using custom-written routines in Igor Pro.

Autofluorescence of the unstained brain was negligible (accounting for $<1\%$ of the resting fluorescence) at the wavelengths used to excite RH1691 fluorescence. However, there was considerable autofluorescence (accounting in some experiments for $>80\%$ of the resting fluorescence) of the brain at the wavelengths at which the CaSD was imaged. This autofluorescence was subtracted from the collected CaSD images to specifically measure the CaSD fluorescence signal. VSD and CaSD signals were quantified as $\Delta F/F_0$ to correct for differences in the spatial distribution of the fluorescent dye. In some experiments, imaging sweeps were triggered at a fixed point of the electrocardiogram. The C2 whisker was deflected on alternate sweeps. Unstimulated trials were subtracted from trials with stimuli and many trials (15–60) were averaged. This analysis procedure aims to reduce both heart beat-related imaging artifacts, bleaching artifacts, and the contribution of spontaneous cortical activity. A range of stimulation strengths differing in deflection amplitude, velocity, and acceleration were studied.

No evoked signals (at the wavelengths used for intrinsic, VSD, or CaSD measurements) were detected in control experiments where the cortex was not stained with dye, but identical brief single C2 whisker stimuli were applied. The brief single-whisker stimuli that we applied thus did not produce measurable intrinsic signals originating from the optical properties of the neocortex (Grinvald et al. 1986; Shibuki et al. 2003).

Statistical tests

Data are expressed as means \pm SE and were tested for statistical significance using Student's *t*-test or ANOVA.

RESULTS

VSD fluorescence correlates linearly with V_m

Our first goal was to characterize the relationship between membrane potential changes and fluorescence changes under controlled conditions. We applied the VSD RH1691 to voltage-clamped *Xenopus* oocytes and found linear submillisecond changes in fluorescence with respect to V_m ($n = 6$ oocytes; Fig. 1, A–C). However, we were unsuccessful in our attempts to obtain functional fluorescence signals from single neurons labeled with RH1691. As a positive control for our experimental procedures, we introduced the VSD JPW1114 into individual layer 2/3 neurons in brain slices of the mouse barrel cortex by the patch pipette during WC recordings. VSD fluorescence (Fig. 1, D and E) linearly followed both sub- and suprathreshold changes in neuronal V_m induced by alpha currents ($n = 9$ cells). In agreement with previous studies (Antic and Zecevic 1995; Antic et al. 1999), these data indicate that VSD fluorescence (from both RH1691 and JPW1114) correlates linearly with V_m at sub-millisecond precision.

CaSD signals reflect action potential firing

Having found a linear relationship of V_m and VSD fluorescence in individual cells, we next investigated the behavior of

¹ The online version of this article contains supplemental data.

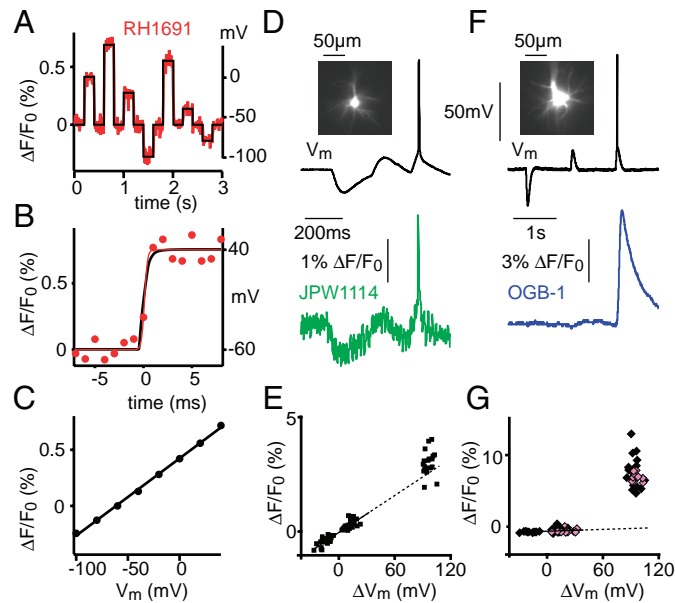


FIG. 1. Voltage-sensitive dye (VSD) fluorescence correlates linearly with membrane potential (V_m), whereas calcium-sensitive dye (CaSD) signals are dominated by action potentials (APs) with little contribution of subthreshold events. **A:** VSD RH1691 was applied at 1.6 mM extracellularly to *Xenopus* oocytes and fluorescence was imaged during 2-electrode voltage clamp. Voltage steps (black trace, V_m) evoked fluorescence changes (red trace, $\Delta F/F_0$). **B:** fluorescence changes recorded at high temporal resolution followed V_m with submillisecond precision ($\Delta F/F_0$, red data points; solid red line shows a sigmoidal fit to the fluorescence data yielding a time constant 0.15 ms; V_m , black line). **C:** RH1691 fluorescence changes were linearly correlated with V_m with a slope of 0.7% $\Delta F/F_0$ per 100 mV. **D:** whole cell recordings of neurons were performed in acute brain slices with 1.8 mM of the VSD JPW1114 included in the backfill of the patch pipette. Dye diffused into the cell during recording (inset shows fluorescence image). Hyperpolarizing and depolarizing alpha current injections mimicked both inhibitory and excitatory postsynaptic potentials (IPSPs and EPSPs, respectively) and evoked spikes recorded in the whole cell V_m trace (black trace). Corresponding changes in the JPW1114 fluorescence were measured over the proximal dendritic arbor of the cell. JPW1114 fluorescence (green trace) closely follows V_m . **E:** plot of JPW1114 fluorescence changes vs. ΔV_m . Subthreshold $\Delta F/F_0$ values were obtained at the peak of the IPSP or EPSP from low-pass (100-Hz) filtered traces, whereas suprathreshold values were obtained from unfiltered traces. A linear fit of the subthreshold values (3.1% $\Delta F/F_0$ per 100 mV) was extrapolated and crossed also the data points for APs, thereby reflecting a linear relationship over the whole activation range. **F:** 200 μ M of the CaSD OGB-1 was included in the pipette solution and V_m (black trace) was changed by injecting hyperpolarizing or depolarizing alpha currents. Large calcium signals (blue trace) were recorded only after APs and not in response to subthreshold V_m changes. **G:** plot of changes in OGB-1 fluorescence as a function of ΔV_m . $\Delta F/F_0$ values of somatic CaSD signals (blue trace) were measured from low-pass filtered traces at the peak of the calcium response, which was delayed by 15 ms relative to the V_m peak. A linear fit of the subthreshold values was extrapolated toward higher ΔV_m values and did not cross the data points for APs, thereby reflecting a steplike relationship between $\Delta F/F_0$ and ΔV_m . This plot contains points attributed to both alpha current injection (black, data from 11 cells) and extracellular synaptic stimulation (magenta, data from 8 cells).

CaSD fluorescence with respect to membrane potential changes. CaSD OGB-1 was loaded intracellularly into single layer 2/3 neurons in brain slices of the mouse barrel cortex during WC recordings. V_m changes were evoked either with alpha current injection (Fig. 1F and black data points in Fig. 1G) or through synaptic potentials evoked by an extracellular electrical stimulus (magenta data points in Fig. 1G). Subthreshold V_m changes evoked only small fluorescence signals, but an action potential (AP) was followed immediately by a prominent CaSD signal with a prolonged time course (half-width of

231 \pm 19 ms; n = 11 cells) largely determined by calcium buffers (Helmchen et al. 1996). Threshold synaptic stimulation evoked some trials with subthreshold V_m responses and small CaSD responses ($\Delta F/F_0$ = 0.13 \pm 0.10%; n = 8 cells) and other trials in which an AP was triggered together with a large CaSD response ($\Delta F/F_0$ = 7.3 \pm 0.2%; n = 8 cells). In good agreement with previous studies (Kerr et al. 2005; Peterlin et al. 2000; Stosiek et al. 2003; Svoboda et al. 1997; Yaksi and Friedrich 2006), our data therefore indicate that CaSD signals predominantly reflect APs, with only a minor contribution from subthreshold potentials (2 \pm 1%; n = 8 cells; calculated as the ratio of the subthreshold calcium signal $\Delta F/F_0$ = 0.13 relative to the suprathreshold calcium signal, $\Delta F/F_0$ = 7.3).

Cortical spatiotemporal dynamics of VSD and CaSD signals in vitro

After delineating the behavior of VSD and CaSD at a cellular level, we next investigated how their fluorescence signals compared when applied to the study of neuronal networks in vitro. Brain slices of the mouse somatosensory barrel cortex were labeled with VSD RH1691 by topically applying the dye to the slice surface. CaSD OGB-1 was injected into multiple locations across the cortical area of interest in its AM ester form and nearly 1 h later cells were strongly labeled (Stosiek et al. 2003). In some experiments, the imaging was combined with WC recordings of V_m from neurons in layer 2/3. The imaged area covered three to four barrel columns and spanned from cortical layer 2 to layer 5. Neuronal network activity was evoked with a stimulation electrode in a layer 4 barrel and the time course quantified in layer 2/3 (Fig. 2, A–C). Compared with the VSD signal, the CaSD signal was roughly 20 times larger (peak amplitude $\Delta F/F_0$ VSD 0.34 \pm 0.07%, n = 9; CaSD 8.3 \pm 2.2%, n = 13); in four experiments only CaSD and not VSD signals were imaged) and lasted about five times longer than the VSD signal (half-width VSD 35.5 \pm 3.1 ms, n = 9; CaSD 181 \pm 14 ms, n = 13).

Pharmacological manipulations were carried out to explore the underlying nature of these signals. Bath application of the ionotropic glutamate receptor antagonists D-2-amino-5-phosphonovaleric acid (D-APV, 50 μ M) and 6-cyano-7-nitroquinoxaline-2,3-dione (CNQX, 10 μ M) blocked WC responses and VSD signals (1.3 \pm 0.8% of control; n = 9 slices) (Fig. 2, C and D). This suggests that the VSD response almost exclusively reflects postsynaptic potentials (PSPs). In contrast to the profound block of the VSD response, adding D-APV/CNQX reduced the peak of the CaSD response to only 56.3 \pm 6.9% of the control value (n = 6 slices; Fig. 2, C and D). This reveals that the CaSD signal evoked by local electrical stimulation is not driven primarily by synaptic potentials. Additional application of 1 μ M tetrodotoxin (TTX) abolished all responses (WC recording, VSD and CaSD) (Fig. 2, C and D). Evoked V_m and CaSD signals were not changed by blockade of metabotropic glutamate receptors [500 μ M (*S*)- α -methyl-4-carboxyphenylglycine (MCPG); peak CaSD response was 92.6 \pm 3.2% of control; n = 7] or the endoplasmic reticulum calcium ATPase (5 μ M thapsigargin; peak CaSD response was 101.7 \pm 6.0% of control; n = 5). These results indicate that the entire CaSD signal is thus mediated by action potential firing. The fraction of the CaSD signal that is sensitive to ionotropic glutamate receptor antagonists likely reflects APs in postsynaptic cells

driven by synaptic potentials. The majority of the CaSD signal (which is not blocked by D-APV/CNQX) is likely evoked by the direct stimulation of APs in neurons with axons near the stimulation electrode.

To separate the stimulation site from the measuring location and, in addition, to excite the cortical network in a more physiological manner, we prepared thalamocortical slices (Agmon and Connors 1991), with CaSD injected into the barrel cortex (Fig. 2E). Stimulation of the VPM nucleus of the thalamus evoked calcium signals in the connected layer 4 barrels (Beierlein et al. 2002; MacLean et al. 2005). These thalamically evoked responses were almost completely abolished by blockade of postsynaptic ionotropic glutamate receptors. We found that bath application of 50 μ M D-APV and 10 μ M CNQX reduced the peak of the thalamic evoked cortical CaSD response to $7.6 \pm 1.6\%$ of the control response ($n = 10$ slices; Fig. 2E). These calcium transients are therefore not

mediated by signals in the thalamic axons, but instead are likely to relate primarily to cortical action potentials evoked after the release of glutamate from the thalamocortical synapses.

Consistent with our cellular measurements (Fig. 1), these data from neuronal networks suggest that VSD signals measure predominantly PSPs and that CaSD signals measure local AP activity. We therefore applied these two optical techniques to image the spatiotemporal dynamics of subthreshold and suprathreshold activity evoked by electrical stimulation of a layer 4 barrel in the mouse somatosensory cortex (Fig. 3; Supplemental Movie 1). Excitation began in the stimulated layer 4 barrel, then spread in a columnar fashion into layer 2/3, and finally into neighboring columns. In layer 2/3 of the neighboring barrel column, the VSD response was reduced to $71.7 \pm 9.3\%$ ($n = 9$ slices) and the CaSD response was reduced to $25.5 \pm 4.0\%$ ($n = 13$ slices) of the peak response in the stimulated layer 4 barrel ($P = 0.0001$; Fig. 3C). These data likely reflect a signaling sequence that begins with the stimulation of APs in layer 4 evoking PSPs in the columnar layer 2/3 through the strong axonal projection from layer 4 to layer 2/3 (Laaris and Keller 2002; Petersen and Sakmann 2001; Wirth and Lüscher 2004). If in turn the layer 2/3 neurons fire APs, then these will evoke PSPs across a large area of cortex through the extensive horizontal axonal arborizations of the layer 2/3 pyramidal neurons (Petersen et al. 2003a). The VSD signal therefore spreads further than the CaSD signal, which remains more tightly localized to the stimulus location. These results are consistent with the hypothesis that VSD images PSPs, which originate from neurons firing APs localized close to the stimulating electrode and are imaged with CaSD.

In vivo VSD and CaSD imaging of neocortical sensory processing

To investigate the spatiotemporal dynamics of sensory processing evoked by whisker deflection, we recorded VSD RH1691 and CaSD OGB-1 signals in vivo from layer 2/3 of the barrel cortex of anesthetized mice. The staining and imaging

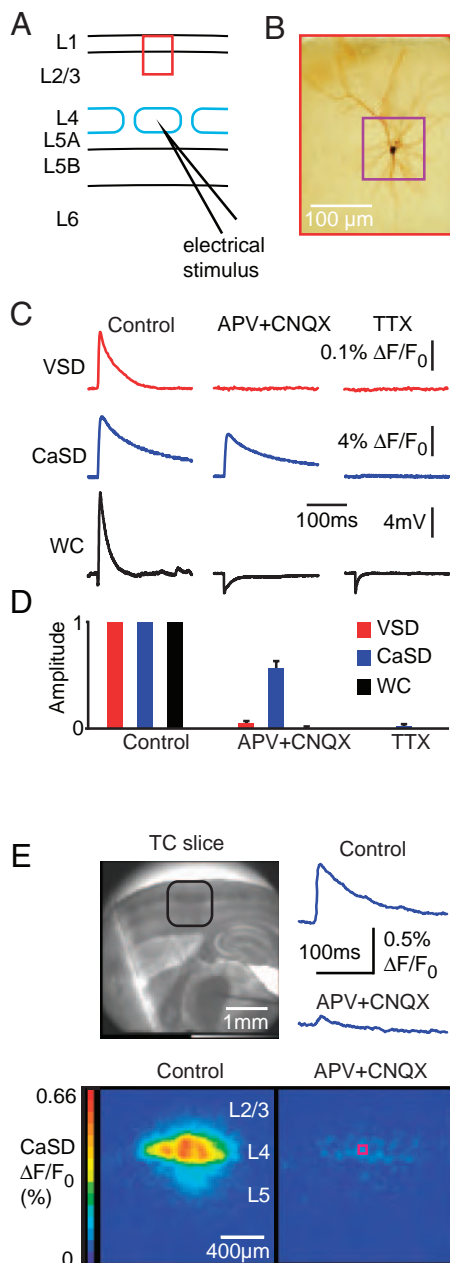


FIG. 2. Kinetic and pharmacological profile of electrically evoked VSD and CaSD signals in the mouse barrel cortex and thalamocortical neuronal network in vitro. *A*: schematic drawing of the recording arrangement. An extracellular electrical stimulus was delivered to a layer 4 barrel in a parasagittal slice labeled with VSD RH1691 and CaSD OGB-1. A whole cell (WC) recording from a layer 2 neuron was performed simultaneously with imaging. *B*: example membrane potential recordings in *C* relate to the biocytin-filled layer 2 neuron and the $100 \times 100\text{-}\mu\text{m}$ purple square is the area from which the fluorescence changes in *C* were quantified. *C*: stimulation in the layer 4 barrel evoked changes in fluorescence relating to network depolarization and changes in V_m of the layer 2 cell monitored by WC recording. Stimulus was repeated 10–25 times under different pharmacological conditions: control, D-2-amino-5-phosphonovaleic acid (D-APV, 50 μ M)/6-cyano-7-nitroquinoxaline-2,3-dione (CNQX, 10 μ M), and tetrodotoxin (TTX, 1 μ M). *D*: normalized amplitudes of the evoked VSD, CaSD, and WC signals across all experiments are shown for the different conditions. VSD and WC responses were completely blocked by D-APV/CNQX, whereas the majority of the CaSD response remained intact. Under TTX, all responses were completely blocked. *E*: CaSD was injected into layer 4 of the barrel cortex of thalamocortical slices (brightfield image, top left). Thalamic stimulation evoked cortical CaSD signals, which were quantified in layer 4 (bottom left image with color-coded response amplitude; field of view (FOV) indicated by black outline in the brightfield image). Cortical CaSD signals could be blocked by bath application of D-APV/CNQX (bottom right image and top right traces quantified from area outlined by the magenta square).

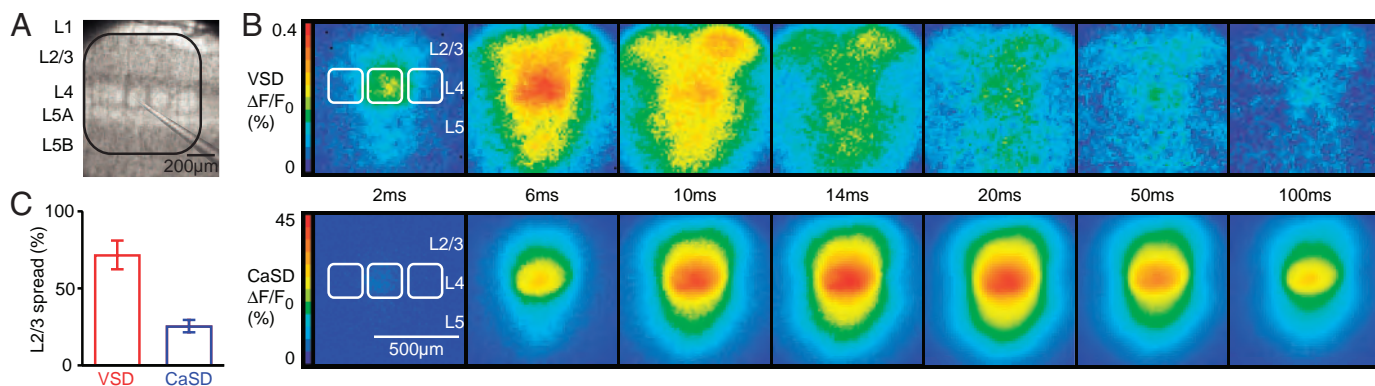


FIG. 3. Spatiotemporal dynamics of electrically evoked VSD and CaSD signals in the mouse barrel cortex neuronal network in vitro. *A*: brightfield micrograph of a parasagittal mouse somatosensory cortical slice showing the position of the stimulation electrode in a selected layer 4 barrel (same slice as *B*). Area enclosed by the black line reflects the FOV of the high-speed camera. Cortex within the FOV was evenly stained with VSD RH1691 and CaSD OGB-1 AM. *B*: cortical spatiotemporal dynamics of the VSD and CaSD signals evoked by a layer 4 barrel stimulation. VSD signal starts early after stimulation at 0 ms and spreads to both supra- and infragranular layers, where it also propagates laterally to neighboring columns. CaSD signal in contrast is slower with respect to both rise and decay and remains more localized. *C*: spatial spread of the VSD and CaSD signals was quantified in layer 2/3 of the neighboring column relative to the signal evoked in the stimulated layer 4 barrel.

procedures did not alter cortical sensory processing as assessed by intrinsic optical imaging (Supplementary Fig. 1; Slovín et al. 2002). The in vivo VSD and CaSD fluorescence measurements were combined with WC recordings targeted to layer 2/3 neurons in the C2 barrel column ($n = 7$ cells, each in a different mouse). The optical signals were quantified over a barrel-sized area, immediately surrounding the recorded neuron. The C2 whisker was deflected in a highly controlled manner and each whisker deflection measured with an optical displacement sensor. Layer 2/3 neurons typically responded with large subthreshold V_m depolarizations accompanied by APs on some trials (Fig. 4, *A–E*; peak whisker deflection averaged across the seven experiments was $33 \pm 1 \mu\text{m}$). The time course of the VSD signal closely followed V_m changes both in individual experiments (Fig. 4, *A–C*) and in the traces computed by averaging across the seven experiments (Fig. 4, *D* and *E*). Our in vivo VSD measurements thus reflect the mean V_m changes of layer 2/3 neurons. These V_m changes in response to whisker stimulation were almost entirely dominated by subthreshold activity. Comparing averages of raw V_m with averages of median-filtered V_m (the median filter used was adjusted in a way that APs were specifically removed) showed that APs made very little impact on the averaged evoked V_m response (Fig. 4*D*).

The CaSD signal evoked by whisker deflection also showed a rapid onset, but it was somewhat delayed relative to the VSD signal (difference 2.9 ± 1.2 ms; $n = 11$ animals, $P = 0.019$). The CaSD signal lasted longer than the VSD signal (222 ± 26 vs. 97 ± 11 ms half-width). The delayed calcium response can relate to the fact that the neurons first need to depolarize through summation of PSPs before reaching AP threshold. In our WC recordings the delay between PSP onset and the first occurring AP was 7.7 ± 2.6 ms ($n = 7$ cells, range 0.9–21.7 ms). The correlation of single-cell V_m and the VSD signal suggests that, on the scale of a single barrel, many neurons behave in a similar subthreshold manner.

Similar to our observations in vitro (Fig. 2, *C–E*), we found that topical application of $500 \mu\text{M}$ D-APV and $125 \mu\text{M}$ CNQX to the cortical surface blocked the sensory response measured with both CaSD and VSD after a 10 min wash-in period (Fig. 4, *F* and *G*). Both VSD and CaSD therefore predominantly

measure the local cortical processing of sensory information rather than axonal signals from long-range (e.g., thalamocortical or corticocortical) inputs.

CaSD and VSD spatiotemporal dynamics

Different stimulation strengths evoked different temporal and spatial patterns of activity and an example experiment is shown in Fig. 5, *A–C*. At low stimulation strength (peak whisker displacement amplitude $14 \mu\text{m}$) localized VSD responses could be observed without any CaSD signal (Fig. 5*A*). This likely reflects subthreshold potentials in layer 2/3 neurons without evoking APs. In contrast, at an intermediate stimulation strength (peak whisker displacement amplitude $18 \mu\text{m}$), the VSD signal spreads and a localized CaSD signal was recorded (Fig. 5*B*). The spreading VSD signal likely results from AP firing of layer 2/3 neurons in the C2 barrel column evoking PSPs on target cells distributed across the extensive lateral axonal arborizations of the L2/3 pyramidal neurons. A stronger stimulus (peak whisker displacement amplitude $26 \mu\text{m}$) evoked spreading VSD and CaSD signals (Fig. 5*C*). The horizontal spread of VSD and CaSD signals evoked by C2 whisker stimulation was quantified in seven experiments by comparing the peak amplitude of evoked responses in the C2 barrel column relative to a location about $500 \mu\text{m}$ away. The VSD signal evoked by an intermediate whisker stimulus ($19 \pm 3 \mu\text{m}$) was reduced to $34 \pm 3\%$ and the CaSD response was reduced to $14 \pm 2\%$ ($n = 7$, $P < 0.01$). Increasing stimulation strength increased both the amplitude and spread of the evoked responses. Doubling whisker deflection amplitude ($38 \pm 4 \mu\text{m}$) increased peak responses in the C2 barrel column to $161 \pm 8\%$ for VSD and to $259 \pm 52\%$ for CaSD. In a region about $500 \mu\text{m}$ away from the C2 barrel column, the VSD response amplitude was reduced to $59 \pm 4\%$ and the CaSD signal was reduced to $28 \pm 5\%$ ($n = 7$, $P < 0.001$). In vivo CaSD signals evoked by sensory stimuli thus remain significantly more localized compared with the VSD signals, which can spread over large cortical areas. These results are consistent with small suprathreshold receptive fields reflected in localized CaSD signals and larger subthreshold receptive fields (Brecht et al. 2003; Moore and Nelson 1998; Petersen and

Diamond 2000; Wilent and Contreras 2005; Zhu and Connors 1999) imaged as spreading VSD signals.

Cortical responses evoked by identical whisker stimuli are highly variable from trial to trial (Arabzadeh et al. 2005; Crochet and Petersen 2006). An interaction of ongoing spontaneous activity with the evoked response can largely account for the response variability, with small responses, both in terms of PSPs and APs, being evoked during spontaneous depolarizations (Petersen et al. 2003b; Sachdev et al. 2004). To investigate the single-trial variability of the evoked responses, we made simultaneous fluorescence measurements of VSD and CaSD signals using two cameras. Single-sweep simultaneous

VSD and CaSD recordings revealed strong variability in both optical signals (Fig. 6A, $n = 7$ mice). The sensory-evoked CaSD and VSD response amplitudes covaried trial by trial, with small CaSD signals accompanying small VSD signals and large CaSD signals accompanying large VSD signals. These results are consistent with both evoked APs (reflected in the CaSD signal) and evoked PSPs (reflected in the VSD signal) competing with the spontaneous activity (Petersen et al. 2003b; Sachdev et al. 2004). The spontaneous activity itself, occurs as propagating waves, which are nearly simultaneous in CaSD and VSD signals (Fig. 6B; Supplemental Movie 2). Topical application of 500 μM D-APV and 125 μM CNQX to the cortical surface after 10 min blocks this spontaneous activity as measured by both VSD and CaSD (Fig. 6, C and D). These spontaneous fluorescence changes similar to the evoked sensory responses are thus also dominated by local cortical activity rather than long-range axonal signals.

Deep isoflurane anesthesia suppresses CaSD signals more than VSD signals

We were interested to see whether further experimental conditions could be found that would affect the CaSD and the VSD responses differently, in addition to the effect of varying stimulus strength described earlier. Striking differences were found between the two optical signals measured under different levels of anesthesia. We imaged both CaSD and VSD responses under different concentrations of isoflurane and found that VSD responses were relatively little affected by depth of anesthesia (Ferezou et al. 2006), whereas CaSD responses were strongly suppressed by anesthesia (Fig. 7A). Deep (1.5–2%) isoflurane anesthesia reduced the whisker-evoked response amplitude to $85.7 \pm 13.5\%$ for VSD and to $33.4 \pm 6.8\%$ for

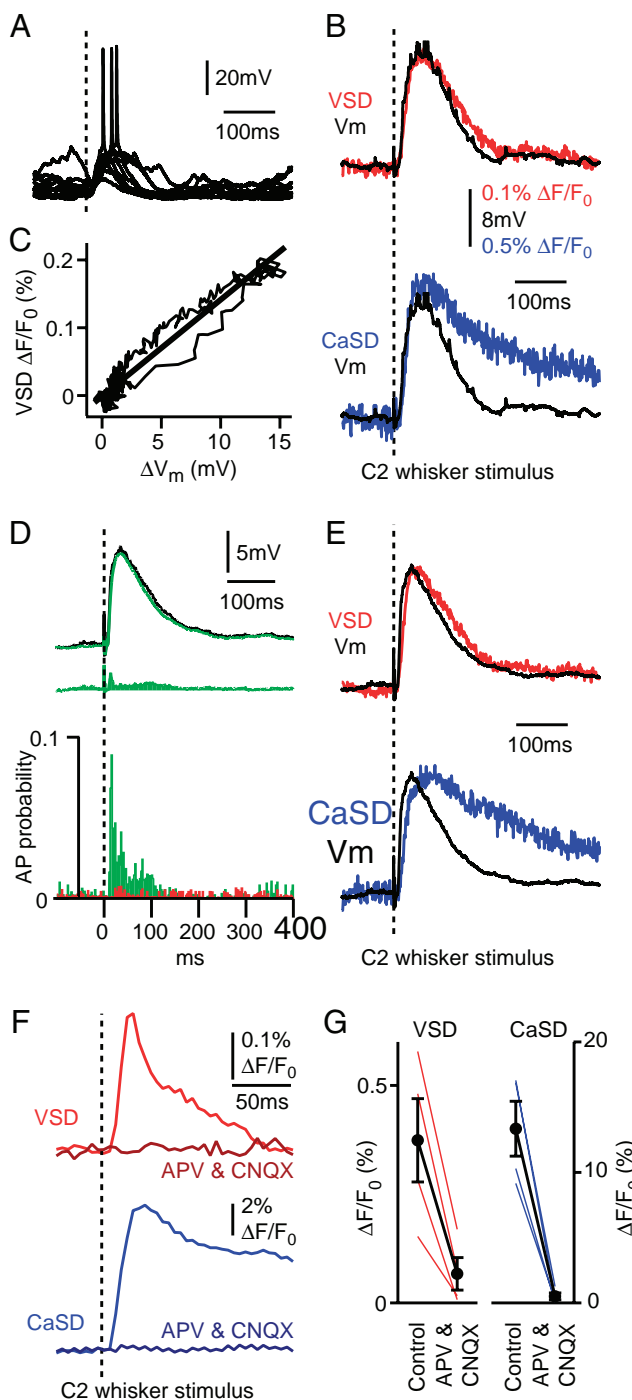


FIG. 4. Combined VSD and CaSD imaging in vivo in the mouse somatosensory barrel cortex. *A*: WC recording from a layer 2/3 neuron located in the C2 barrel column. C2 whisker was briefly deflected at the time indicated by the dotted line with a peak stimulus amplitude of 33 μm . Ten superimposed sweeps are shown. A depolarizing sensory response is consistently observed that is dominated by subthreshold depolarization. In 3 sweeps APs were evoked. *B*: VSD RH1691 and the CaSD OGB-1 responses were measured in the C2 column during the WC recording. Superimposed time courses of the averaged VSD response (red trace, above) and the averaged V_m (black trace). Averaged CaSD OGB-1 response (blue trace, below) has slower kinetics; for comparison the V_m trace (black trace) is superimposed. *C*: averaged VSD signal plotted as a function of change in membrane potential (ΔV_m) for this cell indicated a close to linear relationship. *D*: averaged V_m (black trace) changes recorded in 7 cells located in layer 2/3 of the C2 barrel column in 7 different mice. Responses were evoked by C2 whisker stimulus (mean peak stimulus amplitude $33 \pm 1 \mu\text{m}$) and recorded simultaneously with the imaging. Superimposed green trace is the result of median filtering to remove APs from the V_m traces. APs make very little impact on the averaged V_m trace. Differences between the averaged original data and the averaged median filtered data are shown in the solid green plot below. Peristimulus time histogram (PSTH, below) averaged across all 7 cells shows when APs were evoked in the WC recordings on trials with (green bars) or without (red bars) whisker stimulus. Firing rate is plotted as the probability of an AP being evoked per stimulus per 2.5-ms time-bin. *E*: averaged across all experiments, the time course of the VSD response (red trace, above) with the V_m (black trace) superimposed. Averaged across all experiments, the time course of the CaSD response (blue trace, below) with the V_m trace (black trace) superimposed. *F*: an example experiment showing that the topical application of 500 μM D-APV and 125 μM CNQX to the cortical surface blocked the sensory-evoked responses measured with both VSD and CaSD. *G*: summary data for experiments involving pharmacological blockade of ionotropic glutamate receptors show that peak response amplitudes of both CaSD and VSD sensory-evoked signals were strongly reduced ($n = 4$).

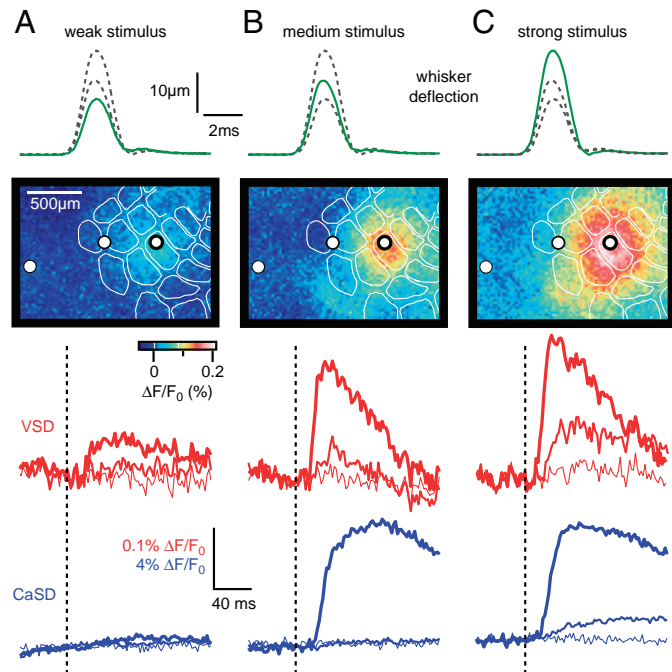


FIG. 5. Spatial spread of sensory responses evoked by different stimulation strengths imaged *in vivo* with VSD and CaSD. *A*: both the temporal and spatial dynamics of the signals depend on stimulus strength. *Top*: time course of the C2 whisker stimulus measured by an optical displacement sensor about 1 mm from the base of the whisker. Color-coded images show temporally averaged VSD responses evoked by the whisker stimulus. Barrel map derived from cytochrome oxidase staining and aligned using the blood vessel pattern is superimposed in white on the VSD images. Three locations where CaSD was injected in this experiment are indicated in thick (C2 barrel column), medium (between α and B1 barrel columns), and thin circles (dysgranular zone). Time course of VSD signals (red traces) and CaSD signals (blue traces) were calculated within a radius of about 150 μm centered on these locations and the thickness of the traces codes the location. At low stimulus strengths there is no CaSD signal and only a localized VSD response can be observed. *B*: at intermediate stimulus strengths the VSD response spreads and a localized CaSD response is recorded. *C*: at high stimulus strengths both VSD and CaSD signals spread. These results demonstrate qualitatively different processing regimes in the barrel cortex.

CaSD relative to the responses recorded at low (0.5–1%) concentrations of isoflurane (Fig. 7*B*). Because our results suggest that the VSD signals reflect subthreshold V_m changes and CaSD reflects suprathreshold signaling (Figs. 1–5), these data then suggest that increasing isoflurane concentration strongly reduces AP firing with a much smaller effect on subthreshold PSPs. To test whether these observations hold true at the level of individual neurons, we made whole cell V_m recordings to study evoked responses at different concentrations of isoflurane. Some cells responded with only subthreshold PSPs (Fig. 7*C*) and others also fired APs (Fig. 7*D*). Deep isoflurane anesthesia reduced PSP amplitude to $73.8 \pm 9.5\%$ ($n = 8$) and reduced evoked AP activity to $2.0 \pm 2.2\%$ ($n = 5$) of the evoked response recorded under light isoflurane anesthesia (Fig. 7*E*). Increased isoflurane anesthesia therefore slightly reduces evoked synaptic depolarization of cortical neurons and strongly reduces AP firing. The nonlinear threshold for AP initiation likely allows a small reduction in VSD signal and PSPs to be translated into a large reduction in CaSD signal and suprathreshold activity.

DISCUSSION

We have demonstrated that VSD and CaSD epifluorescence measurements can be combined to image the spatiotemporal dynamics of cortical activity both *in vitro* and *in vivo*. The VSD signal was found to correlate with subthreshold membrane potential changes and the CaSD signal reflected predominantly action potential firing. We therefore imaged *in vivo* VSD and CaSD to define the sub- and suprathreshold spatiotemporal dynamics in layer 2/3 of spontaneous activity and sensory processing evoked with different stimulus strengths and under different conditions of isoflurane anesthesia.

Imaging membrane potential with VSD and action potentials with CaSD

In vivo, the time course of the VSD RH1691 fluorescence followed V_m changes recorded in individual layer 2/3 neurons of mouse somatosensory barrel cortex (Fig. 4, *A–C*), similar to

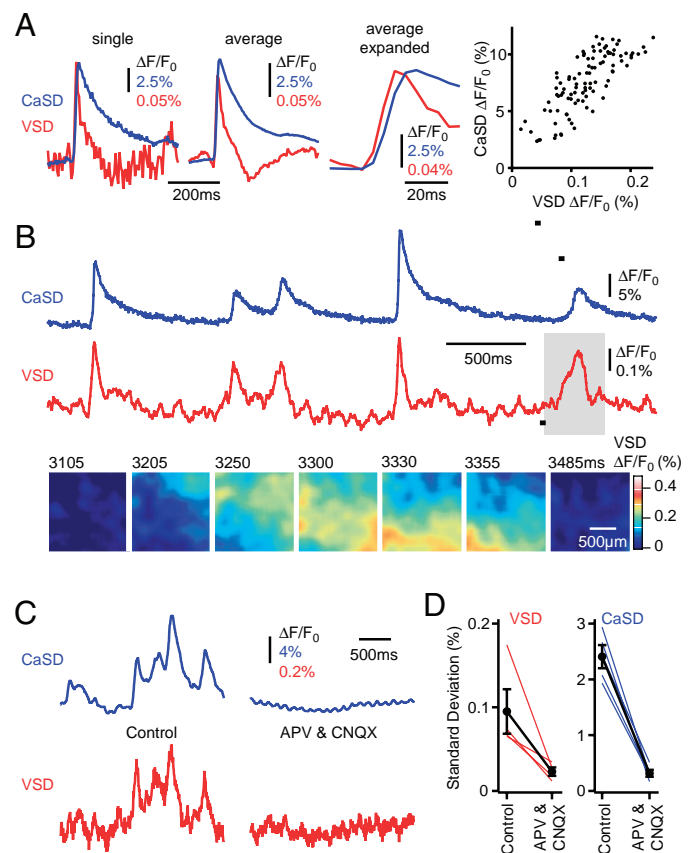


FIG. 6. Single-trial simultaneous VSD and CaSD imaging of evoked responses and spontaneous activity. *A*: example of the time course of a simultaneously recorded single trial VSD RH1691 and CaSD OGB-1 whisker-evoked response (far left). Average of 100 evoked responses (middle left). On an expanded temporal scale, the VSD response is observed to precede the CaSD response (middle right). Quantifying the peak evoked response amplitude on each individual trial indicates that the VSD and CaSD responses covary (far right). *B*: spontaneous activity was also closely correlated between VSD and CaSD signals. Spontaneous activity occurred as propagating waves (below, gaussian spatially filtered VSD images show the time period shaded in gray). *C*: example traces showing that the application of D-APV and CNQX to the cortical surface blocked spontaneous activity measured with both VSD and CaSD. *D*: spontaneous activity before and after application of 500 μM D-APV and 125 μM CNQX was quantified by calculating the SD of the fluorescence traces ($n = 4$).

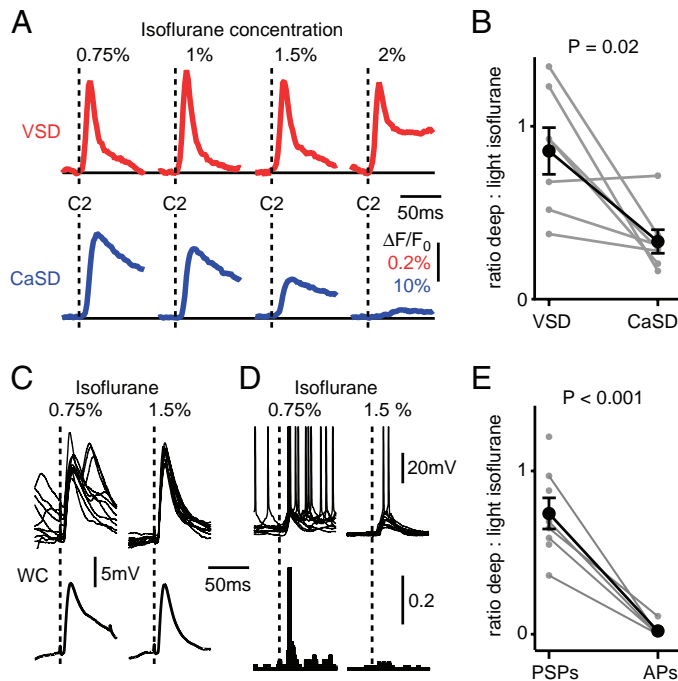


FIG. 7. Deep isoflurane anesthesia strongly suppresses evoked CaSD signals and APs with a smaller reduction in VSD signals and postsynaptic potentials (PSPs). *A*: increasing the isoflurane concentration in this example experiment did not change the peak VSD RH1691 signals evoked by whisker stimulation, but strongly reduced CaSD OGB-1 signals (each trace is an average of 10 trials). *B*: plot of the ratio of the peak response amplitude evoked during deep anesthesia (1.5–2% isoflurane) relative to light anesthesia (0.5–1% isoflurane) for VSD and CaSD signals (gray circles represent individual experiments with a line linking VSD and CaSD measurements; black circles show the average \pm SE, $n = 7$). VSD signal was weakly reduced during deep isoflurane anesthesia, whereas the CaSD response was strongly suppressed. *C*, *top*: 10 superimposed individual sweeps of evoked PSPs measured with a WC recording under 0.75% isoflurane (*left*) and 1.5% isoflurane (*right*). Increasing the concentration of isoflurane did not affect the amplitude of PSPs evoked by whisker stimulation (averaged sweeps below). *D*: in a different cell, which responded with suprathreshold activity to whisker deflection during light isoflurane anesthesia, the AP firing was almost abolished at deeper isoflurane anesthesia. Ten superimposed trials are shown (above) at 0.75% isoflurane (*left*) and 1.5% isoflurane (*right*). PSTH for this cell is plotted below, quantified as the probability of evoking an AP in a given 2-ms time bin. *E*: plot of the ratio of the evoked PSP amplitude and APs during deep isoflurane anesthesia (1.5–2%) relative to light isoflurane anesthesia (0.5–1%) (gray circles represent individual experiments). APs were not evoked in all neurons and a line links experiments where both PSPs and APs were recorded. Black circles show the average \pm SE; $n = 8$ PSPs; $n = 5$ APs. PSP amplitude is much less affected than AP firing by increasing isoflurane anesthesia, mirroring the strong reduction in CaSD signals with smaller effects on the VSD signals described earlier.

results described previously in rat barrel cortex (Petersen et al. 2003a,b) and mouse barrel cortex (Ferezou et al. 2006). Complete truncation of action potentials through median filtering makes only a small difference to the mean V_m trace (Fig. 4, *D* and *E*). Experimentally, it is therefore clear that APs contribute little directly to the ensemble network membrane potential changes. The absence of a substantial direct AP-related VSD signal, while imaging network activity, can also be understood in terms of the relative ensemble electrical impact of APs versus PSPs. A single AP in a single pyramidal neuron will directly cause a depolarization of approximately 1 cell \times 100 mV \times 1 ms (\approx 100 mV \cdot ms). However, the synaptic impact of this single AP on surrounding postsynaptic neurons in the

network is orders of magnitude larger, causing a network depolarization of approximately 1,000 cells \times 1 mV \times 25 ms (\approx 25,000 mV \cdot ms). The V_m changes observed in the averaged traces of the WC recording and the accompanying VSD signals are therefore dominated by subthreshold V_m changes. This situation applies to networks where neurons are on average far from threshold and require substantial depolarization to evoke an action potential. This is the case for both the in vitro and the in vivo measurements. The correlation of single-cell V_m and the VSD signal suggests that, on the scale of a single barrel, many neurons behave in a similar subthreshold manner and it is likely that specificity in encoding information arises from the subset of neurons that reach threshold to fire action potentials.

Because the VSD stains the brain tissue nonspecifically, changes in V_m of glial cells will also contribute to the fluorescence signals. However, this is likely to be a small effect because glial responses to direct neuronal transmitter release have small amplitudes as a result of the relatively high glial membrane conductance (Lin and Bergles 2004) and because glial VSD responses resulting from increased extracellular potassium concentrations have much slower kinetics (Konnerth et al. 1987).

CaSD signals require AP firing and reflect suprathreshold neuronal activity. In addition to the AP-evoked calcium signals, we found only a minor subthreshold contribution (estimated to be roughly 2% of the AP-evoked calcium signal in the cellular measurements; Fig. 1, *F* and *G*). The nonspecific loading with AM esters labels both neurons and glia, both of which might contribute to our calcium measurements. However, it was recently demonstrated that glial and neuronal calcium signals do not temporally correlate (Nimmerjahn et al. 2004) and that sensory-evoked glial calcium signals are nearly two orders of magnitude slower in onset and duration compared with neuronal calcium signals (Wang et al. 2006). The calcium signals evoked by sensory or electrical stimulation that we recorded are fast, linked to neuronal activity, and are thus unlikely to substantially involve glial calcium signals. We did not observe slow CaSD signals unrelated to VSD signals, although very slow signals are more difficult to detect and so may have gone unnoticed. We conclude that the CaSD signals we observed are likely to result predominantly from AP firing in neurons (Smetters et al. 1999). In particular, local action potential activity seems to play a dominant role for the calcium signal we measured, whereas long-range axonal signals from the thalamus or other cortical areas appear to make only a minor contribution (Figs. 2*E*, 4, *F* and *G*, and 6, *C* and *D*). In contrast, the VSD signal is driven by PSPs and dominated by changes in neuronal subthreshold V_m which it follows with millisecond precision. Although VSD and CaSD signals are clearly related, the highly nonlinear aspect of AP generation allows the two signals to be differentially manipulated.

Imaging sensory processing with VSD and CaSD

Whisker deflections evoke responses in the primary somatosensory barrel cortex, through a signaling pathway from the trigeminal nerve to the brain stem, and then to the thalamus, which provides input to the neocortex. Three qualitatively different processing modes of layer 2/3 barrel cortex were observed depending on the strength of the whisker stimulus. The weakest stimuli evoked localized

VSD signals without any CaSD signal, implying a localized subthreshold excitation without supragranular AP activity. Such a local subthreshold signal could modulate other inputs, for example, by summing with other sensory inputs from neighboring whiskers, other sensory modalities, or with top-down influences. Intermediate stimuli evoked propagating PSPs with localized suprathreshold signals in layer 2/3. In response to this intermediate stimulation strength, the sensory processing of the single whisker stimulus in terms of action potential activity is therefore restricted to the principal whisker barrel column, although the spreading subthreshold VSD signal would allow multiwhisker integration to occur. The strongest stimuli evoked propagating VSD and CaSD signals. Therefore even a single whisker, if deflected sufficiently strongly, can evoke a propagating wave of sensory responses involving regenerative AP firing. These data are in good agreement with receptive field analysis of individual neurons in layer 2/3 of barrel cortex, which are very broad at the subthreshold level, but show more tightly tuned suprathreshold classical receptive fields (Brecht et al. 2003; Moore and Nelson 1998; Petersen and Diamond 2000; Simons 1978; Wilent and Contreras 2005; Zhu and Connors 1999).

Deep isoflurane anesthesia strongly reduces evoked action potentials and CaSD signals

In a further test to probe the relationship of the VSD and CaSD signals, we found that the level of isoflurane anesthesia led to appreciable differences in the behavior of the two fluorescence signals. The VSD signals and PSPs were only weakly affected by increasing isoflurane concentration, whereas the CaSD signals and APs were strongly suppressed (Hentschke et al. 2005). Even small changes in subthreshold activity may strongly affect suprathreshold activity at low firing rate conditions (Brecht et al. 2003; Crochet and Petersen 2006). Thus the action of isoflurane is likely to reflect a small change in subthreshold activity that nonlinearly translates into a strong effect in action potential discharge. Equally, one can construct a membrane potential trajectory by summing either many or few excitatory and inhibitory synaptic inputs. It might therefore be possible to record a similar PSP resulting from sparse AP firing compared with higher levels of AP activity, simply by appropriately balancing excitation and inhibition. Finally, the large CaSD signal at low anesthesia might suggest that AP firing rates are considerably higher in awake mice than in mice under deep anesthesia. Independent of the underlying mechanisms, these results stress the importance of measuring with both dyes because together they give information, which imaging either dye alone could not provide. The nonlinear function linking V_m to firing rate makes it difficult to relate PSPs to APs at a network level. The combined imaging approach presented here is thus likely to be a useful experimental tool for many investigators probing cortical network properties and seeking to differentiate between sub- and suprathreshold effects of a specific manipulation.

Outlook and limitations

The current technique is attractive in that it is relatively simple, requiring only epifluorescence optics and a fast

camera. The data collected by this method demonstrate that CaSD and VSD signals can be recorded in the same preparation with millisecond time resolution and that they image different aspects of cortical function, with the VSD reflecting subthreshold PSPs and the CaSD being dominated by APs. Currently, these methods applied in vivo are well suited only for the study of supragranular layers because VSD RH1691 does not penetrate deeply into the cortex (Supplementary Fig. 1; Ferezou et al. 2006). Also the fluorescence excitation light is unlikely to penetrate substantially below the supragranular layers and indeed the blue light needed to excite OGB-1 will penetrate less deeply into the brain than the red excitation light for VSD RH1691. Equally, the clear correlation between the VSD signal and subthreshold activity that we observe in the neocortex may not hold true for other brain areas. In hippocampal Schaffer collaterals, a high degree of synchronized action potential activity results in the detection of the suprathreshold activity with VSDs (Grinvald et al. 1982). Comparably, highly synchronous spiking activity of thalamocortical axons traversing the striatum can be observed with RH1691 in thalamocortical slices after stimulation in the thalamus (Neubauer and Berger, unpublished observations). In the cortical gray matter, however, the part of the VSD signal related to spiking activity (compare Fig. 1D) is extremely small because only a small fraction of membranes experience an action potential, but all neuronal membranes experience subthreshold depolarization. Thus either dye alone (VSD or CaSD) does not seem to be well suited to reflect the complexity of electrical signals in the cortical network. The CaSD responses measured under our conditions with epifluorescence do not have a dynamic range that allows the detection of subthreshold activity and VSDs on the gray matter network level do not reflect AP activity. However, what initially seems to be a limitation turns into an advantage if both dyes are used together, as done in this study for the first time. A combined use of VSDs and CaSDs enables the simultaneous but separate study of synaptic and action potential activity in the barrel cortex.

Using two-photon microscopy combined with OGB-1 AM labeling, Kerr et al. (2005) previously described the detection and separation of local input and output activity in neocortex by imaging the fluorescence of a single dye. Fluorescence changes in the neuropil were suggested to relate to axonal calcium transients, which would reflect local synaptic input. Somatic fluorescence changes resulted directly from action potential discharge of the imaged neuron, which thus provided a measure of output. With epifluorescence optics, the calcium signals of incoming long-range axons do not seem to have a major impact on the overall calcium signal (Figs. 2E and 4, F and G). Thus the calcium signal in our study appears to reflect only the local action potential activity of the local cortical area imaged.

A disadvantage for the use of CaSDs in vivo (in contrast to VSDs) is the need to inject the AM ester dye. AM esters can be applied with pipettes into the brain but they stain only neurons in a small volume of about 300- μ m diameter (Stosiek et al. 2003). In a spatially restricted field of three cortical columns in a parasagittal slice, a complete staining can be achieved (Fig. 3), but even with many injections we were unable to obtain uniform staining of a complete cra-

niotomy measuring several millimeters in diameter. Our analyses of the spatial extent of CaSD signals *in vivo* (Fig. 5) was therefore limited to three well-defined separate injection spots across the cortical map. This spatially restricted labeling is of course true for both epifluorescence and two-photon imaging. However, two-photon imaging is generally applied at high magnification and correspondingly small fields of view, which can be stained easily with one AM ester injection (Kerr et al. 2005; Stosiek et al. 2003). The recent development of transgenic mice expressing genetically encoded calcium-sensitive fluorescent proteins may provide an approach to wide-field epifluorescence measurements of calcium signaling *in vivo* (Diez-Garcia et al. 2005; Hasan et al. 2004; Nagai et al. 2004). However, current data suggest that the genetically encoded calcium indicators are not sensitive to single action potentials (Polgruto et al. 2004). In the rodent somatosensory cortex, where low-frequency action potential firing was previously observed (both for spontaneous and evoked activity) (Brecht et al. 2003; Crochet and Peterson 2006), the genetically encoded calcium indicators might then miss the majority of activity.

Our approach of wide-field epifluorescence imaging of CaSDs and VSDs therefore appears to be a promising combination to study different aspects of cortical computation. Such simultaneous imaging of subthreshold and suprathreshold neuronal activity will help advance our understanding of sensory processing.

ACKNOWLEDGMENTS

We thank M. Larkum for useful discussions and comments on the manuscript. We are grateful to K. Geering for kindly providing *Xenopus* oocytes. We also thank C. Bichsel for excellent technical assistance.

Present address of A. Borgdorff: Pelvipharm SAS, Domaine CNRS, Bat 5, 1 Avenue de la Terrasse, 91190, Gif-sur-Yvette, France.

GRANTS

This work was supported by the Swiss National Foundation Grants 3100-061335.00, 3100-107529/1, and 3100-103832/1; Novartis Foundation for Medical-Biological Research; Silva Casa Foundation; and Leenaards Foundation.

REFERENCES

- Agmon A, Connors BW. Thalamocortical responses of mouse somatosensory (barrel) cortex *in vitro*. *Neuroscience* 41: 365–379, 1991.
- Antic S, Major G, Zecevic D. Fast optical recordings of membrane potential changes from dendrites of pyramidal neurons. *J Neurophysiol* 82: 1615–1621, 1999.
- Antic S, Zecevic D. Optical signals from neurons with internally applied voltage-sensitive dyes. *J Neurosci* 15: 1392–1405, 1995.
- Arabzadeh E, Zorzin E, Diamond ME. Neuronal encoding of texture in the whisker sensory pathway. *PLoS Biol* 3: e17, 2005.
- Beierlein M, Fall CP, Rinzel J, Yuste R. Thalamocortical bursts trigger recurrent activity in neocortical networks: layer 4 as a frequency-dependent gate. *J Neurosci* 22: 9885–9894, 2002.
- Borgdorff AJ, Poulet JFA, Petersen CCH. Facilitating sensory responses in developing mouse somatosensory barrel cortex. *J Neurophysiol* 97: 2992–3003, 2007.
- Brecht M, Roth A, Sakmann B. Dynamic receptive fields of reconstructed pyramidal cells in layers 3 and 2 of rat somatosensory barrel cortex. *J Physiol* 553: 243–265, 2003.
- Bullen A, Saggau P. Indicators and optical configuration for simultaneous high-resolution recording of membrane potential and intracellular calcium using laser scanning microscopy. *Pflügers Arch* 436: 788–796, 1998.
- Civillico EF, Contreras D. Integration of evoked responses in supragranular cortex studied with optical recordings *in vivo*. *J Neurophysiol* 96: 336–351, 2006.
- Contreras D, Llinas R. Voltage-sensitive dye imaging of neocortical spatio-temporal dynamics to afferent activation frequency. *J Neurosci* 21: 9403–9413, 2001.
- Crochet S, Petersen CCH. Correlating whisker behavior with membrane potential in barrel cortex of awake mice. *Nat Neurosci* 9: 608–610, 2006.
- Derdikman D, Hildesheim R, Ahissar E, Arieli A, Grinvald A. Imaging spatiotemporal dynamics of surround inhibition in the barrels somatosensory cortex. *J Neurosci* 23: 3100–3105, 2003.
- Diez-García J, Matsushita S, Mutoh H, Nakai J, Ohkura M, Yokoyama J, Dimitrov D, Knöpfel T. Activation of cerebellar parallel fibers monitored in transgenic mice expressing a fluorescent Ca²⁺ indicator protein. *Eur J Neurosci* 22: 627–635, 2005.
- Ferezou I, Bolea S, Petersen CCH. Visualizing the cortical representation of whisker touch: voltage-sensitive dye imaging in freely moving mice. *Neuron* 50: 617–629, 2006.
- Grinvald A, Anglister L, Freeman JA, Hildesheim R, Manker A. Real-time optical imaging of naturally evoked electrical activity in intact frog brain. *Nature* 308: 848–850, 1984.
- Grinvald A, Hildesheim R. VSDI: a new era in functional imaging of cortical dynamics. *Nat Rev Neurosci* 5: 874–885, 2004.
- Grinvald A, Lieke E, Frostig RD, Gilbert CD, Wiesel TN. Functional architecture of cortex revealed by optical imaging of intrinsic signals. *Nature* 324: 361–364, 1986.
- Grinvald A, Manker A, Segal M. Visualization of the spread of electrical activity in rat hippocampal slices by voltage-sensitive optical probes. *J Physiol* 333: 269–291, 1982.
- Hasan MT, Friedrich RW, Euler T, Larkum ME, Giese G, Both M, Duebel J, Waters J, Bujard H, Griesbeck O, Tsien RY, Nagai T, Miyawaki A, Denk W. Functional fluorescent Ca²⁺ indicator proteins in transgenic mice under TET promoter. *PLoS Biol* 2: 763–775, 2004.
- Helmchen F, Imoto K, Sakmann B. Ca²⁺ buffering and action potential-evoked Ca²⁺ signaling in dendrites of pyramidal neurons. *Biophys J* 70: 1069–1081, 1996.
- Hentschke H, Schwarz C, Antkowiak B. Neocortex is the major target of sedative concentrations of volatile anaesthetics: strong depression of firing rates and increase of GABA_A receptor-mediated inhibition. *Eur J Neurosci* 21: 93–102, 2005.
- Kerr JN, Greenberg D, Helmchen F. Imaging input and output of neocortical networks *in vivo*. *Proc Natl Acad Sci USA* 102: 14063–14068, 2005.
- Kleinfeld D, Delaney KR. Distributed representation of vibrissa movement in the upper layers of somatosensory cortex revealed with voltage-sensitive dyes. *J Comp Neurol* 375: 89–108, 1996.
- Konnerth A, Obaid AL, Salzberg BM. Optical recording of electrical activity from parallel fibres and other cell types in skate cerebellar slices *in vitro*. *J Physiol* 393: 681–702, 1987.
- Laaris N, Keller A. Functional independence of layer IV barrels. *J Neurophysiol* 87: 1028–1034, 2002.
- Lin SC, Bergles DE. Synaptic signaling between neurons and glia. *Glia* 47: 290–298, 2004.
- MacLean JN, Watson BO, Aaron GB, Yuste R. Internal dynamics determine the cortical response to thalamic stimulation. *Neuron* 48: 811–823, 2005.
- Moore CI, Nelson SB. Spatio-temporal subthreshold receptive fields in the vibrissa representation of rat primary somatosensory cortex. *J Neurophysiol* 80: 2882–2892, 1998.
- Nagai T, Yamada S, Tominaga T, Ichikawa M, Miyawaki A. Expanded dynamic range of fluorescent indicators for Ca²⁺ by circularly permuted yellow fluorescent proteins. *Proc Natl Acad Sci USA* 101: 10554–10559, 2004.
- Nimmerjahn A, Kirchhoff F, Kerr JND, Helmchen F. Sulforhodamine 101 as a specific marker of astroglia in the neocortex *in vivo*. *Nat Methods* 1: 31–37, 2004.
- Ohki K, Chung S, Ch'ng YH, Kara P, Reid RC. Functional imaging with cellular resolution reveals precise micro-architecture in visual cortex. *Nature* 433: 597–603, 2005.
- Peterlin ZA, Kozloski J, Mao BQ, Tsiola A, Yuste R. Optical probing of neuronal circuits with calcium indicators. *Proc Natl Acad Sci USA* 97: 3619–3624, 2000.
- Petersen CCH. The barrel cortex—integrating molecular, cellular and systems physiology. *Pflügers Arch* 447: 126–134, 2003.
- Petersen CCH, Grinvald A, Sakmann B. Spatiotemporal dynamics of sensory responses in layer 2/3 of rat barrel cortex measured *in vivo* by voltage-sensitive dye imaging combined with whole-cell voltage recordings and neuron reconstructions. *J Neurosci* 23: 1298–1309, 2003a.

- Petersen CCH, Hahn TTT, Mehta M, Grinvald A, Sakmann B.** Interaction of sensory responses with spontaneous depolarization in layer 2/3 barrel cortex. *Proc Natl Acad Sci USA* 100: 13638–13643, 2003b.
- Petersen CCH, Sakmann B.** Functionally independent columns of rat somatosensory barrel cortex revealed with voltage-sensitive dye imaging. *J Neurosci* 21: 8435–8446, 2001.
- Petersen RS, Diamond ME.** Spatial-temporal distribution of whisker-evoked activity in rat somatosensory cortex and the coding of stimulus location. *J Neurosci* 20: 6135–6143, 2000.
- Pologruto TA, Yasuda R, Svoboda K.** Monitoring neural activity and $[Ca^{2+}]$ with genetically encoded Ca^{2+} indicators. *J Neurosci* 24: 9572–9579, 2004.
- Sachdev RN, Ebner FF, Wilson CJ.** Effect of subthreshold up and down states on the whisker-evoked response in somatosensory cortex. *J Neurophysiol* 92: 3511–3521, 2004.
- Salzberg BM, Davila HV, Cohen LB.** Optical recording of impulses in individual neurons of an invertebrate central nervous system. *Nature* 246: 508–509, 1973.
- Shibuki K, Hishida R, Murakami H, Kudoh M, Kawaguchi T, Watanabe M, Watanabe S, Kouuchi T, Tanaka R.** Dynamic imaging of somatosensory cortical activity in the rat visualized by flavoprotein autofluorescence. *J Physiol* 549: 919–927, 2003.
- Shoham D, Glaser DE, Arieli A, Kenet T, Wijnbergen C, Toledo Y, Hildesheim R, Grinvald A.** Imaging cortical dynamics at high spatial and temporal resolution with novel blue voltage-sensitive dyes. *Neuron* 24: 791–802, 1999.
- Simons DJ.** Response properties of vibrissa units in rat SI somatosensory neocortex. *J Neurophysiol* 41: 798–820, 1978.
- Slovin H, Arieli A, Hildesheim R, Grinvald A.** Long-term voltage-sensitive dye imaging reveals cortical dynamics in behaving monkeys. *J Neurophysiol* 88: 3421–3438, 2002.
- Smetters D, Majewska A, Yuste R.** Detecting action potentials in neuronal populations with calcium imaging. *Methods* 18: 215–221, 1999.
- Stosiek C, Garaschuk O, Holthoff K, Konnerth A.** In vivo two-photon calcium imaging of neuronal networks. *Proc Natl Acad Sci USA* 100: 7319–7324, 2003.
- Svoboda K, Denk W, Kleinfeld D, Tank DW.** In vivo dendritic calcium dynamics in neocortical pyramidal neurons. *Nature* 385: 161–165, 1997.
- Takechi H, Eilers J, Konnerth A.** A new class of synaptic response involving calcium release in dendritic spines. *Nature* 396: 757–760, 1998.
- Tsien RY.** New calcium indicators and buffers with high selectivity against magnesium and protons: design, synthesis, and properties of prototype structures. *Biochemistry* 19: 2396–2404, 1980.
- Tsien RY.** A non-disruptive technique for loading calcium buffers and indicators into cells. *Nature* 290: 527–528, 1981.
- Wachowiak M, Cohen LB.** Representation of odorants by receptor neuron input to the mouse olfactory bulb. *Neuron* 32: 723–735, 2001.
- Wang X, Lou N, Xu Q, Tian G-F, Peng WG, Han X, Kang J, Takano T, Nedergaard M.** Astrocytic Ca^{2+} signalling evoked by sensory stimulation in vivo. *Nat Neurosci* 9: 816–823, 2006.
- Wilent WB, Contreras D.** Stimulus-dependent changes in spike threshold enhance feature selectivity in rat barrel cortex neurons. *J Neurosci* 25: 2983–2991, 2005.
- Wirth C, Lüscher HR.** Spatiotemporal evolution of excitation and inhibition in the rat barrel cortex investigated with multielectrode arrays. *J Neurophysiol* 91: 1635–1647, 2004.
- Woolsey TA, Van der Loos H.** The structural organisation of layer IV in the somatosensory region (SI) of the mouse cerebral cortex: the description of a cortical field composed of discrete cytoarchitectonic units. *Brain Res* 17: 205–242, 1970.
- Yaksi E, Friedrich RW.** Reconstruction of firing rate changes across neuronal populations by temporally deconvolved Ca^{2+} imaging. *Nat Methods* 3: 377–383, 2006.
- Zhu JJ, Connors BW.** Intrinsic firing patterns and whisker-evoked synaptic responses of neurons in the rat barrel cortex. *J Neurophysiol* 81: 1171–1183, 1999.

- Publication 4 -

“Modulation of Network Activity through GABA_B receptor-mediated Tonic Inhibition in the Rat Medial Prefrontal Cortex *In Vitro*”

Ying Wang, Kay Thurley, Florian B. Neubauer & Hans-Rudolf Lüscher (submitted).

A given neurotransmitter can elicit effects on postsynaptic cells on different time scales. Besides the rate at which a neurotransmitter is removed from its receptor by cleavage or reuptake, specific properties of the receptor molecules influence the duration of neurotransmitter activity. Ionotropic receptors, which mediate a fast onset of the effect upon transmitter binding by opening ion channels, come in a variety of isoforms which provide different affinity and kinetics of inactivation. Metabotropic receptors act via signal transduction cascades, which can tune the duration of transmitter effects over a wide range. In the case of the inhibitory neurotransmitter γ -aminobutyric acid (GABA), short-living effects on the postsynaptic membrane potential which follow the time course of synaptic events have been termed “phasic inhibition” whereas effects lasting longer than that have been termed “tonic inhibition”. Tonic inhibition lowers the baseline of excitability of neurons, reducing their availability for being recruited into an active assemblies in the network. Therefore tonic inhibition also affects the intensity and characteristics at the level of network activity. It has been shown previously that GABA elicits tonic inhibition via high-affinity isoforms of ionotropic GABA_A receptors.

Publication 4 employs electrophysiological recordings, CASD epifluorescence imaging, and pharmacological tools in a preparation of the medial prefrontal cortex in vitro

1) to reveal that metabotropic GABA_B receptors are a second source for tonic inhibition besides the known GABA_A effects.

2) to classify the downstream ion channels which mediate GABA_B-dependent tonic inhibition.

3) to show the impact of GABA_B-dependent tonic inhibition on the excitability of layer 2/3 pyramidal cells.

4) to quantify the effect which this reduced excitability of single cell has on network activity, measured either as the frequency of EPSCs impinging on a single neuron or as the duration and spatial extent of spontaneous network upstates.

Taken together, the results show that ambient GABA can induce a tonic inhibition via GABA_B receptors, which is powerful enough to modulate the excitability of single neurons as well as the states of cortical activity.

Modulation of network activity through GABA_B receptor-mediated tonic inhibition in the rat medial prefrontal cortex *in vitro*

*Ying Wang, Kay Thurley, Florian B. Neubauer & Hans-Rudolf Lüscher**

Department of Physiology, University of Bern, Switzerland

Running head: Tonic GABA_B inhibition in PFC

Address for correspondence: Hans-Rudolf Lüscher
Department of Physiology
University of Bern
Bühlplatz 5
CH-3012 Bern/Switzerland
e-mail: luescher@pyl.unibe.ch

Number of figures: 8

Number of tables: 0

Number of pages: 46

Abstract:

GABA is known to mediate tonic inhibition via extrasynaptic GABA_A receptors. In this paper we demonstrate that a tonic GABA_B receptor-dependent outward current is present in L2/3 pyramidal cells of rat medial prefrontal cortex *in vitro* and leads to a tonic inhibition of the neurons. It has been reported that postsynaptic GABA_B receptors mediate their effects via G protein-coupled inwardly rectifying potassium (GIRK) channels. We also found GABA_B receptor-dependent currents to be in part GIRK channel-mediated. However, a second non-GIRK channel component was present in our experiments. Furthermore, we found tonic GABA_B currents to co-exist with tonic GABA_A currents, when ambient GABA levels were increased to concentrations found *in vivo* and/or GABA uptake was blocked. Evaluating the impact of GABA_B receptor-mediated tonic current on the excitability of pyramidal neurons, we found that GABA_B receptor activation shifts the input-output function to the right without affecting its slope. Electrophysiological recordings and epifluorescence Ca²⁺-imaging experiments indicated that GABA_B receptor-mediated tonic inhibition is capable of regulating network activity, as seen in the frequency of EPSCs impinging on a neuron and the duration and spatial extent of network upstates. These results show that ambient GABA via GABA_B receptors can induce a tonic inhibition, which is powerful enough to modulate neuronal excitability, neural networks and thus behaviorally relevant states of cortical activity.

Keywords: GABA_B receptor, GABAergic modulation, Tonic inhibition, Up- and downstate activity, GIRK channels

Introduction

GABA (γ -aminobutyric acid) is the main inhibitory transmitter in the mammalian central nervous system. Apart from phasic inhibitory signals, GABA mediates tonic inhibition via extrasynaptic GABA receptors activated by ambient GABA in the extracellular space. Classically, tonic inhibition was reported to be GABA_A-mediated (Brickley et al. 1996; Stell and Mody 2002). It operates on a very slow time scale and can modulate neuronal excitability with profound consequences on network behavior (Semyanov et al. 2004).

Postsynaptic GABA_B receptors are metabotropic receptors. They activate G protein-coupled inwardly rectifying potassium channels (GIRKs or Kir-3) leading to hyperpolarization of the neurons (Cruz et al. 2004; Cryan and Kaupmann 2005; Labouebe et al. 2007; Lüscher et al. 1997). Recent ultrastructural studies demonstrated that most postsynaptic GABA_B receptors are located extrasynaptically and are likely to be activated by ambient GABA arising from “spill-over” at highly active adjacent synapses and being “pooled” under regulation of GABA-uptake back into neurons and glial cells (Kulik et al. 2006; Kulik et al. 2003). Single action potentials in GABAergic cortical neurogliaform cells can generate GABA_B-mediated IPSPs in postsynaptic cells (Price et al. 2005; Tamás et al. 2003) and single inhibitory axons in the cerebellar glomerulus are capable of activating GABA_B receptors and in turn suppress excitatory transmission (Mitchell and Silver 2000).

GABA_B receptors mediate inwardly rectifying K⁺-currents, when activated by the GABA_B agonist baclofen at micro-molar concentrations (Cruz et al. 2004).

Hence postsynaptic GABA_B receptors are in a position to substantially affect neuronal excitability and network activity. To our knowledge, no postsynaptic GABA_B receptor-mediated tonic inhibition has been reported so far in the acute slice preparation of rat brains *in vitro*. However, there is evidence for presynaptic GABA_B receptor-mediated tonic inhibition (Lei and McBain 2003; Liu et al. 2006). In addition, activation of extrasynaptic GABA_B receptors has profound consequences for rhythmic activity, e.g., in the hippocampus (Brown et al. 2007; Scanziani 2000) and the olfactory bulb (Karpuk and Hayar 2008).

In this paper we demonstrate a tonic outward current mediated by GABA_B receptors in L2/3 pyramidal cells of rat medial prefrontal cortex (mPFC) *in vitro*. Activation of the tonic GABA_B current shifted the current-frequency relationship of these neurons to higher rheobase current and had a profound impact on network activity in the rat mPFC slice. In particular, we investigated the effect of GABA_B receptor-mediated tonic inhibition on up- and downstate activity. This slow oscillatory network behavior is characterized by periods of membrane depolarization due to augmented synaptic activity, called upstates, that alternate with hyperpolarized periods, called downstates (Shu et al. 2003). Up- and downstate activity is observed *in vivo* during slow-wave sleep and under anesthesia (Cowan and Wilson 1994; Luczak et al. 2007; Metherate and Ashe 1993; Steriade et al. 1993) and has been reproduced in cortical slices, where it was investigated electrophysiologically (Sanchez-Vives and McCormick 2000) and with calcium imaging (MacLean et al. 2005). We show that ambient GABA

via postsynaptic GABA_B receptors controls the duration and spatial extent of upstates.

Materials and Methods

Slice preparation and electrophysiology: All experimental procedures were performed according to the *Ethical Principles and Guidelines for Experiments on Animals* of the Swiss Academy of Medical Sciences. As described in Hempel et al. 2000, coronal slices of the rat brain (300 µm) (Microm HM 650V, Walldorf, Germany) containing the mPFC were prepared from Wistar rats of two different age groups (p28 to p36, mean: p32, n=99, and p10 to p14, mean: p12, n=17). Whole-cell patch-clamp recordings were made at 32°C from the soma of layer 2/3 neurons, visualized with IR-DIC contrast. Currents were amplified (Axonpatch 200A, Molecular Devices, USA), filtered (3 kHz) and digitized at 10 kHz with a Digidata 1322A A/D converter (Molecular Devices, USA) using Clampex 8.1 software (Molecular Devices, USA). Depolarizing current steps were used to characterize the firing properties of the cells in current clamp mode. Cells were voltage clamped at $V_h = -50$ mV. Holding voltage V_h was not corrected for liquid junction potential. Cell resistance and access resistance was monitored by means of a 200 ms negative voltage step at the beginning of each recording sweep. Holding current was calculated as the mean holding current of a 200 ms long measurement, repeated every second (or every two seconds in some experiments). Current changes due to drug application were quantified as the

difference between the mean of 60 to 120 steady state current measurements before and during drug application.

Focal extracellular electrical stimulation was accomplished with short voltage pulses delivered through a theta glass pipette filled with artificial cerebrospinal fluid (ACSF). Network activity was assessed by analyzing spontaneous excitatory postsynaptic currents (EPSCs) in long voltage clamp measurements at a holding potential $V_h = -70$ mV. For data analysis, Clampfit 9.2 (Molecular Devices, USA) was used. Spontaneous EPSCs were detected and analyzed using Mini Analysis Program (Synaptosoft, USA). Compiled data are expressed as mean \pm s.e.m. For statistical comparison of the means a two-sample *t*-test, assuming unequal variance was used. The Kolmogorov-Smirnov Test was used for comparing two cumulative frequency distributions of spontaneous EPSC amplitudes. For all tests the levels of significance are indicated as $p < 0.05$; *, $p < 0.01$; **, $p < 0.001$; ***.

Chemicals and solutions: Slices were continuously perfused with artificial cerebrospinal fluid (ACSF) containing (in mM) 125 NaCl, 25 NaHCO₃, 2.5 KCl, 1.25 NaH₂PO₄, 2 CaCl₂, 1 MgCl₂, and 25 glucose at a rate of 5 ml/min and continuously bubbled with 95% O₂ and 5% CO₂. In order to increase network activity in the brain slices, a modified ACSF (mACSF) was used in some experiments with the following composition (in mM): 125 NaCl, 25 NaHCO₃, 5.5 KCl, 1.25 NaH₂PO₄, 1.5 CaCl₂, 0.5 MgCl₂, and 25 glucose. Thick-walled borosilicate glass pipettes were filled with a solution containing (in mM) 130-K-

gluconate, 5 KCl, 10 HEPES, 4 ATP-Mg, 0.3 Na₂-GTP, and 10 Na₂-Phosphocreatin with pH adjusted to 7.3 with KOH. Electrode resistance was between 4 and 6 MΩ. In some experiments synaptic inputs were blocked by adding selective antagonists of ligand-gated channels to the bath (APV: 50 μM, CNQX: 10 μM, Gabazine: 10 μM). Kynurenate (1 mM) was used in 3 experiments instead of APV and CNQX. The selective GABA_B agonist baclofen was typically applied at a concentration of 25 μM. The potent and selective GABA_B antagonist CGP 52432 was used at a concentration of 1 or 5 μM. NO-711 was applied at a concentration of 2.5 or 10 μM to block the GAT1 GABA uptake transporter. All chemicals were purchased from Sigma, Merck or Tocris.

In 32 recordings, the pipette solution contained 2% biocytin for later reconstruction of the cell's morphology. The electrophysiological characterization of interneurons and pyramidal cells was confirmed morphologically in all these cases.

Measuring the input-output response: Current-clamp experiments on the input-output response function of mPFC L2/3 pyramidal neurons were performed, using stimulation currents, which were designed according to an Ornstein-Uhlenbeck stochastic process to mimic in-vivo synaptic barrage (for a detailed description see Rauch et al. 2003). Such currents are characterized by a Gaussian distribution with mean and a standard deviation, and by a correlation time. We fixed the correlation time to 3 ms in order to resemble fast excitatory and inhibitory synaptic inputs. We chose a standard deviation of 100 pA, which is

in a similar range used in other studies (Arsiero et al. 2007; Rauch et al. 2003; Thurley et al. 2008). The experimental protocol was as follows: Single stimulus trains had constant mean current and standard deviation and lasted 6 s. The frequency f of the neuronal response to such trains was calculated as the total number of action potentials divided by the stimulus duration. Recordings were not included in the analysis in case of considerable changes of spike amplitude and shape in the response (Rauch et al. 2003). Different trains were separated by 30-40 seconds, to let the cell recover from stimulation. At first, the mean input current m was increased stepwise from a sub-threshold value until the emission of a single or a few spikes, which gave the current threshold for spiking, i.e. the rheobase current (Rauch et al. 2003). Then, in the current interval between threshold and f - I curve saturation (Arsiero et al. 2007), stimuli with different mean were chosen and injected in random order to prevent temporal correlations. About 30% of the mean values were repeated once or twice. Recording such an f - I curve took about 10 minutes. After acquiring the control f - I curve, a second one was recorded with baclofen (25 μ M), and then one with CGP 52432 (1 μ M). Recordings started 3 min after the beginning of the bath application to ensure stable drug levels.

In addition to stimulating with noisy currents, the membrane resting potential and the access resistance were monitored by injection of a hyperpolarizing square pulse (100 ms, -50 to -150 pA) preceding each noisy stimulus train. Recordings were discontinued in case of large drifts, i.e.

membrane potential changes bigger than ± 3 mV, despite unmodified experimental conditions, or the series resistance exceeding 20 M Ω .

Large-field calcium-sensitive dye imaging:

Epifluorescence calcium sensitive dye imaging was used to quantify temporal and spatial properties of upstate activity in the prefrontal cortex (Berger et al. 2007).

Calcium-sensitive dye staining: Staining of the prefrontal cortex slices of p12-p14 old rats with the acetoxymethyl ester form of Oregon Green 488 Bapta-1 (OGB-1 AM; Molecular Probes) was done following an established protocol (Berger et al. 2007). Briefly, 50 μg of OGB-1 AM were solved in 5 μl of a fresh preparation of 80% DMSO / 20% pluronic acid F127 (w/v; Sigma). This lipophilic stock was diluted 1:19 in a HEPES buffered solution containing (in mM) 125 NaCl, 2.5 KCl, 10 HEPES. The final OGB-1 solution (~ 400 μM) was aliquoted and stored at -20 $^{\circ}\text{C}$. An application pipette with a tip diameter of 18-22 μm was back-filled with 20 μl of the OGB-1 solution and connected with air-filled flexible tubing to a 50 ml syringe. The dye was ejected at multiple sites into all layers of the prefrontal cortex by manual application of pressure under visual control.

Image acquisition: Spontaneous changes in epifluorescence reflecting upstate-dependent changes of the intracellular calcium concentration were imaged in a Zeiss Axioskop microscope (4x, 0.10NA Olympus optics; 100 W halogen lamp for excitation; filter set for OGB-1 imaging: excitation BP480/30 nm, dichroic 505 nm, emission BP535/40nm). For each pharmacological condition,

ten recordings of a length of one minute each were acquired at an imaging frame rate of 125 Hz with an 80 x 80 pixel CCD camera (Redshirt NeuroCCD, RedShirtImaging) running under Neuroplex software. The field of view was 4.2 x 4.2 mm (pixel size 52 x 52 μm).

Image pre-processing: Raw data were processed using custom MATLAB routines implementing the following steps. Emitted background fluorescence in the absence of fluorescence illumination (the “dark frame”) was subtracted from all frames of the recording. Bleaching was most prominent during the first 8s of recording and this initial period was therefore discarded. Pixels corresponding to the OGB-1-stained area of the cortex were identified applying a brightness threshold on a time-collapsed average image of the frame stack. The time course of each pixel was median filtered with a filter window size of 13 frames. Spatial differences in the staining intensity were corrected by normalizing the changes of fluorescence intensity over time ($\Delta F = F - F_0$) to the intensity of resting fluorescence (F_0) resulting in the time course of fluorescence intensity expressed as $\Delta F/F_0$. F_0 was defined as the 10th percentile of intensity values to be found within the time course of the individual pixel, based on average noise amplitude.

Upstate detection: For the detection of network calcium signals comprising several pixels and spanning several frames, an iterative thresholding approach was used. Threshold was set at 3.4 standard deviations with the exclusion of signal-containing frames. Consecutive suprathreshold frames were grouped into upstates. Upstates which were smaller than 5 pixels in a spatial cluster were

discarded. Incomplete upstates at the beginning and the end of a trace were also not considered in the analysis.

Upstate quantification: Duration, spatial area and the intensity of the detected upstates were calculated according to the following definitions. “Upstate duration” was measured as “onset-to-end-of-half-width”, i.e. from the first frame of a detected upstate until (and excluding) the frame after the peak in which the averaged signal fell below its half-maximal value for the first time. For this, the mean signal trace was calculated for all pixels which were suprathreshold at any time during the upstate. “Upstate area” represents the cumulative number of pixels which are active at any time during “upstate duration”. “Peak upstate intensity” was defined as the peak $\Delta F/F_0$ value of the averaged trace of the pixels belonging to “upstate area”. The baseline for calculating peak intensity was set at the lowest $\Delta F/F_0$ value found within “upstate duration”.

Results

First, we present experiments, in which we characterized baclofen induced outward currents in L2/3 pyramidal cells of the mPFC. Part of these outward currents was due to G protein-coupled inwardly-rectifying potassium (GIRK) channels. Similar tonic outward currents were present when we blocked GABA uptake and/or elevated ambient GABA levels. GABA_B receptor-dependent outward currents coexisted with GABA_A receptor-mediated tonic inhibition. In a second series of experiments, we focused on the impact of tonic GABA_B receptor-mediated inhibition on network activity in the mPFC slice. We started with demonstrating that postsynaptic GABA_B receptor activation shifts the input-output response functions of pyramidal cells to larger input currents, and finally performed experiments, illustrating how tonic inhibition effects upstate activity in the mPFC slice network.

L2/3 pyramidal cells in the mPFC display a baclofen-induced outward current in part reminiscent of a GIRK current: Bath application of baclofen, a selective GABA_B agonist, led to outward currents and a concomitant decrease of the input resistance in L2/3 pyramidal neurons of the rat mPFC (Fig. 1A1). These currents showed no or little desensitization after 2 to 10 min of continuous baclofen application. Bath application of the selective GABA_B antagonist CGP 52432 abolished the outward current completely, uncovering a small inward shift of the holding current which could partly be reversed by wash-out. The half

maximal effective concentration (EC_{50}) for baclofen was $0.967 \pm 0.17 \mu\text{M}$ ($n=8$, Hill-coefficient $h=1.00 \pm 0.04$, Fig. 1A4).

Blocking inwardly rectifying K^+ channels with $300 \mu\text{M}$ barium, we could revert the baclofen-evoked outward current below baseline levels and further reduce it with CGP 52432 (Fig. 1B). Blocking inwardly rectifying K^+ channels, including GIRK1/4 channels with tertiapin-Q ($0.5 \mu\text{M}$), we could reduce the baclofen-induced outward current by 40% (Fig. 1C). Increasing the concentration of tertiapin-Q to $1 \mu\text{M}$ did not change the effect ($n=5$, data not shown). There was always a barium-insensitive component of approximately 40% of the total baclofen-evoked current (Figs. 1D&E). Note that since GIRK1/4 currents and barium-insensitive currents together only account for 80% of the total baclofen-induced current, 20% remain unexplained.

The results so far clearly demonstrate that L2/3 pyramidal neurons of the mPFC contain $GABA_B$ receptors coupled to GIRK1/4 channels. In addition, the $GABA_B$ receptors couple to other, possibly potassium channels, whose molecular identities are not known.

Blockade of GABA-uptake reveals a tonic $GABA_B$ receptor-mediated inhibition: Application of CGP 52432 under control conditions elicited a small inward shift of holding current ($-4.2 \pm 3.1 \text{ pA}$, $n = 7$) which, however, was statistically not different from baseline values (Fig. 2A). This inward shift was significantly larger if the GAT1 GABA uptake inhibitor NO-711 was co-applied (Fig. 2B). Combined application of GABA ($3.3 \mu\text{M}$) and NO-711 resulted in a

slowly rising outward current, which could partly be reversed by the application of CGP 52432 (Fig. 2C). Figure 2D summarizes the findings for the CGP 52432 effects under different conditions. These experiments reveal a substantial GABA_B receptor-mediated tonic inhibition, provided that GABA uptake is inhibited and that the ambient GABA concentration is elevated. It has been suggested that CGP 52432 might act as an inverse agonist (Urwyler et al. 2005) and could thus reveal constitutive activity of the GABA_B receptor. However, the increase in the observed current due to increased extracellular GABA and/or the uptake inhibitor GAT-1 clearly indicate that ambient GABA concentration is responsible for the observed current.

Extracellular stimulation evokes a large, slow GABA_B receptor-mediated outward current: In order to elevate the concentration of ambient GABA to a level high enough for activating postsynaptic GABA_B receptors, we imitated network activity by extracellular stimulation at low frequency (see Fig. 3A and Materials and Methods). We used CNQX and APV to block excitatory synaptic transmission, and gabazine to block fast GABAergic inhibitory signals. A single electrical extracellular stimulus in layer 1, at approximately two times the threshold intensity to evoke a response, revealed a long-lasting, large outward current in L2/3 pyramidal cells (Fig. 3B&C). A train of 5 identical stimuli (70 Hz) increased this slow outward current by about a factor of 2 (Fig. 3D). Mean peak amplitude, half width, and time to peak were 193 ± 20 pA, 291.9 ± 21.9 ms, and 111.8 ± 8.2 ms, respectively (n=11 cells). Application of CGP 52432 or 300 μ M

barium to the bath abolished this outward current completely (Fig. 3E) suggesting, that moderate extracellular stimulation increases temporarily the concentration of ambient GABA to a level sufficient for strongly activating a GABA_B receptor-mediated outward current.

GABA_B and GABA_A receptor-mediated tonic inhibition coexist: The outward current evoked with GABA in the presence of NO-711 could only be partly reversed with CGP 52432. This observation suggests that both, GABA_B and GABA_A receptor-mediated tonic currents are involved. We confirmed this hypothesis by sequential application of CGP 52432 and gabazine after induction of the outward current with elevated ambient GABA in combination with GABA-uptake inhibitor (Fig. 4). Under this experimental conditions GABA_A receptor-mediated currents were not significantly smaller than GABA_B receptor-mediated currents (-15.1 ± 2.7 pA versus -22.4 ± 3.8 pA, $n=7$; $p>0.5$, t-test, Fig. 4B). In this set of experiments, excitatory synaptic transmission was blocked by the addition of CNQX and APV ($n=4$) or kynurebate ($n=3$). The CGP 52432-evoked inward shift of holding current was of similar amplitudes as without synaptic blockers (-22.4 ± 3.8 pA versus -20.0 ± 2.8 pA, see also Fig. 2C).

We demonstrated that tonic outward currents mediated by GABA_B receptors can be induced in the rat mPFC *in vitro*. However, the potential functional relevance of such a GABA_B receptor-mediated current remains open. We devoted the second part of the paper to this question.

GABA_B receptor activation shifts the input-output relationship of L2/3 pyramidal neurons: In a further series of experiments we studied the impact of tonic activation of GABA_B receptors onto the excitability of mPFC L2/3 pyramidal neurons. L2/3 pyramidal neurons were stimulated with noisy currents, which were designed to resemble the synaptic barrage that neurons receive *in vivo* (see Materials and Methods). We determined the input-output relationship (*f-I* curve) with and without drug application, by measuring the frequency of action potential discharge in response to different mean input currents (Fig. 5A gives an example). The first 1-2 seconds of the response of neocortical pyramidal neurons to long-lasting stimulation contain temporally variable components due to processes like spike frequency adaptation (La Camera et al. 2004; Rauch et al. 2003). After this initial phase the response stays quasi-stationary (see also Rauch et al. 2003 and Materials and Methods). Therefore we divided the neural response into two parts: a transient phase consisting of the first two seconds of the response and the subsequent part, which we refer to as “steady” state (Fig. 5A). The results were similar between transient phase and steady state - except for absolute firing frequencies, which were higher in the transient phase because of incomplete spike frequency adaptation. Baclofen shifted the *f-I* curve to higher current values but did not affect the slope. The shift could be reversed by application of CGP 52432 (Fig. 5A). Fitting the *f-I* curves with a threshold linear function, revealed a significant increase of the rheobase current with baclofen, i.e. the threshold current for spiking, which was measured from the x-intercept of the fitted *f-I* relationship and can be used as an estimate for the shift (Fig. 5B).

Baclofen also had effects on passive membrane properties (Fig. 5C). The membrane resting potential was significantly hyperpolarized (from -67.4 ± 2.3 mV to -73.8 ± 3.1 mV, $p < 0.05$, one-way ANOVA). The change of input resistance was not significant (124 ± 58 to 83 ± 41 M Ω , $p > 0.05$, one-way ANOVA). Again the effects were reversible by CGP 52432 application.

From the above experiments, it is conceivable that small changes in the excitability of single neurons due to changes in ambient GABA concentration via postsynaptic GABA_B receptor-mediated inhibition might have profound effects at the network level. The next two paragraphs describe experiments designed to substantiate this conjecture.

Tonic GABA_B receptor-mediated inhibition depresses network activity: We recorded spontaneous synaptic currents in single neurons for monitoring network activity. In order to increase network activity we superfused brain slices with a modified ACSF that contained elevated potassium, and reduced magnesium and calcium concentrations (mACSF: 5.5 mM K⁺, 1.5 mM Ca²⁺, 0.5 mM Mg²⁺; see also Materials and Methods). Pyramidal cells as well as fast-spiking interneurons were voltage clamped at $V_h = -70$ mV and the frequency of spontaneous EPSCs (i.e. fast inward currents that could be blocked by APV and CNQX, $n = 5$, data not shown) was analyzed under control conditions (i.e. mACSF), CGP 52432 and baclofen. Thirteen cells were from rats in the old age group (p29 to p33) and two cells from rats in the young age group (p10 and p12). Since there was no apparent difference between both age groups, we pooled the data. In a fast-spiking

interneuron, the mean EPSC frequency increased from 13.9 to 16.6 EPSCs/s with the addition of CGP 52432 (Fig. 6A). The distributions of EPSC frequencies were significantly different under control conditions and under CGP 52432 ($p < 0.001$, t-test, Fig. 6A, right panel). Applying baclofen to the bath solution decreased the EPSC frequency slightly below control conditions. The increase in the frequency of spontaneous EPSCs under CGP 52432 was seen in all cells irrespective of cell type (Fig. 6B). However, the overall frequency of EPSCs was in general higher in fast spiking interneurons ($n=7$, Fig. 6B, left panel) than in pyramidal cells ($n=8$, Fig. 6B, right panel). In 13 of 14 experiments, baclofen reduced the EPSC frequency below the control value recorded with mACSF, indicating that under elevated network activity, ambient GABA depresses overall network activity via GABA_B receptors. In principle, tonic activation of presynaptic GABA_B receptors could lead to the reduced network activity. If presynaptic GABA_B receptors are involved, we would expect an increase of the amplitude of spontaneous EPSCs with the application of CGP 52432. Comparing the cumulative EPSC amplitude distributions without and with CGP 52432 revealed a small although non-significant shift towards larger amplitudes ($n=13$ of 15, $p>0.5$, Kolmogorov-Smirnov test, Figs. 6C and D), which could be reversed with baclofen. We can therefore neither confirm nor exclude the co-activation of presynaptic GABA_B receptors in our experiments.

Blockade of GABA_B receptor-mediated tonic inhibition increases the duration of upstates: Using the mACSF, we evoked spontaneous up- and

downstate activity in brain slices of young rats (p10 to p14) (Neubauer and Berger 2008). In 14 of 17 experiments superfusion of the brain slice with mACSF lead to prominent up- and downstate activity in L2/3 and L5 pyramidal cells in the mPFC. In voltage-clamp recordings ($V_h = -70$ mV) these upstates were characterized by a transient large increase of the number of individual EPSCs, which in most cases summed up to a strong inward current (Figs. 7A&B). Control experiments in current clamp revealed periodic membrane potential fluctuations, sometimes with action potentials during periods of membrane depolarization reminiscent of upstates. The mean upstate duration was 674.5 ± 98 ms ($n = 9$ experiments) and the frequency of upstates was always below 1 Hz. Adding CGP 52432 increased the upstate duration on average by a factor of three to 1967.3 ± 440 ms ($n = 9$ experiments, see Fig. 7A). In each individual cell, the increase in upstate duration was statistically significant ($p < 0.01$, Fig. 7C). Upstates were abolished completely by the application of baclofen (Fig. 7A).

Large-field epifluorescence Ca^{2+} -imaging of the mPFC slice (see Materials and Methods) gave further evidence of a tonic $GABA_B$ receptor-mediated inhibitory effect on network activity. Upstate activity was recorded under control conditions (i.e. in mACSF), and CGP 52432 (Fig. 8). Upstates could be clearly assigned to one of two groups (Fig. 8K): (1) global or “large” upstates, extended over 95-100% of the analysis mask; (2) confined or “small” upstates were restricted to less than 20% of the analysis mask. The duration but not the peak intensity of large upstates increased significantly with the addition of CGP 52432 (Fig. 8K&L). Since the analysis was restricted to the mask area, a potential

increase in upstate area could not be detected. Neither duration, nor peak intensity, nor upstate area changed in the group of “small” upstates with the application of CGP 52432. Note that occasionally a second upstate started before the first one terminated (Figs. 8F&G); a behavior we also observed in the voltage clamp experiments reported above (Fig. 7B3, arrow).

Under baclofen “large” upstates were completely abolished; however, “small” upstates could still be seen (Figs. 8H&I). When calculating the mean $\Delta F/F_0$ for the small area of this upstate, the visibility of the signal increases (inset in Fig. 8I). Again, neither duration, nor peak intensity, nor upstate area changed in the group of “small” upstates with baclofen.

The significant increase in upstate duration of “large” upstates corroborates the similar finding in the voltage clamp experiments reported above. The observation that baclofen completely abolishes large upstates explains the absence of upstates with baclofen in the electrophysiological recordings, because it is unlikely that a neuron, which was randomly chosen for recording, takes part in one of the rare spatially restricted upstates (but see Fig. 7A). In summary then, GABA_B receptor-mediated tonic inhibition is capable of regulating the duration and size of individual upstates.

Discussion

In the first part of the paper we demonstrated a GABA_B receptor-mediated tonic current in pyramidal cells of the mPFC. Under the experimental conditions used, this current is comparable in strength to tonic GABA_A receptor-mediated currents observed in rat hippocampus, cerebellum, and somatosensory cortex (Brickley et al. 1996; Nusser and Mody 2002; Yamada et al. 2007), provided that the GAT1 inhibitor, NO-711, is present and extracellular GABA is elevated to *in vivo*-like concentrations. The second part of our experiments was devoted to elucidate the functional relevance of GABA_B receptor-mediated tonic inhibition. GABA_B receptor activation shifted the input-output relationship of L2/3 pyramidal neurons to larger input currents. Using electrophysiological recordings and epifluorescence Ca²⁺-imaging, we found that the blockade of GABA_B receptors increases the frequency of EPSCs impinging on a neuron and the duration of network upstates.

GABA_A and GABA_B receptor-mediated tonic inhibition: Our results demonstrate the coexistence of GABA_A and GABA_B receptor-mediated tonic inhibition in mPFC pyramidal cells of similar strength. Although we have not further analyzed the GABA_A receptor-mediated part, this finding adds to the numerous reports of tonic inhibition via GABA_A receptors (for review see Farrant and Nusser 2005).

About 60% of the total baclofen-induced GABA_B current was barium-sensitive in our experiments. Such a barium-sensitive component is in line with

other studies and mediated by GIRK channels (Lüscher et al. 1997). Using the specific blocker tertiapin-Q, we found the barium-sensitive component to be primarily due to currents that are mediated by GIRK1/4 channels. Still about one third of the barium-sensitive component or 20% of the total baclofen-induced current, respectively, remains unexplained. Moreover, an additional 40% of the total current was barium-insensitive and might, e.g., be due to the two-pore K⁺ channel family (Cruz et al. 2004).

While GIRK currents desensitize rapidly in dopaminergic neurons of the ventral tegmentum (Cruz et al. 2004), similar currents in mPFC pyramidal cells did in general not desensitize, being therefore well suited to mediate tonic inhibition.

Ambient GABA in vivo and in vitro: In order to persistently activate GABA_B receptors, GABA must be present at a sufficient concentration in the extracellular space. Estimated concentrations of ambient GABA vary between tens of nanomolar and few micromolar (Dalby 2000; Hernandez et al. 2003; Kennedy et al. 2002; Tossman et al. 1986). Recently, the ambient GABA concentration in primate PFC *in vivo* was measured to be $4.1 \pm 1.6 \mu\text{M}$ (Zhang et al. 2007). However, such high concentrations of ambient GABA cannot be expected in a brain slice, since these typically display very low spontaneous activity (Neubauer and Berger 2008). Therefore, we approximated the *in vivo* situation (Zhang et al. 2007), by adding GABA to the slice preparation and blocking GABA uptake – in order to keep the concentration of the added GABA constant. Under these

conditions, we found a substantial GABA_B receptor-mediated tonic inhibition of L2/3 mPFC pyramidal cells. Our approach is further justified, since the ambient extracellular GABA concentration found *in vivo* perfectly matches the EC₅₀ for GABA- and GABA_B agonist-induced currents. We found an EC₅₀ around 1 μM for baclofen-induced outward currents in L2/3 mPFC pyramidal neurons. This value is comparable to what is reported for other native GABA_B receptors (Bon and Galvan 1996; Cruz et al. 2004) and also closely matches the EC₅₀ for GABA-evoked GIRK currents in a heterologous expression system (Jones et al. 1998).

Phasic and tonic GABA_A receptor-mediated currents are highly correlated, suggesting that the main source of ambient GABA results from spill-over from vesicular synaptic release (Glykys and Mody 2007). GABA spill-over is also consistent with our finding that increasing neuronal activity with mACSF elevates ambient GABA sufficiently to exert tonic inhibition on network activity. In line with the idea of pooling ambient GABA, repetitive firing of groups of interneurons has been proposed to be necessary for the activation of extrasynaptic GABA_B receptors (Kim et al. 1997; Thomson and Destexhe 1999). Tight coupling between inhibition and excitation during spontaneous and sensory-evoked activity might facilitate ambient GABA accumulation (Okun and Lampl 2008). A second GABA source has been identified by Tamás and collaborators (Tamás et al. 2003). A subclass of GABAergic interneurons, the neurogliaform cells, is capable of mediating GABA_B receptor responses in pyramidal cells with single action potentials. These cells might even provide a spatially restricted compartment in which ambient GABA can modulate cellular excitability (Tamás

et al. 2003). In addition to synaptic release and spill-over into the extrasynaptic space, GABA might come from other sources like non-vesicular leakage (Rossi et al. 2003), glial cells (Kozlov et al. 2006; Rossi et al. 2003), or when the GAT1 does not remove GABA from the extracellular space but operates in the reverse direction (Wu et al. 2007).

Pre- versus postsynaptic effect of ambient GABA: From the voltage-clamp experiments presented in this paper, it appears that only postsynaptic GABA_B receptors are activated by GABA during states of high activity, since no effect could be detected on the amplitude of the spontaneous excitatory postsynaptic currents upon superfusion with the GABA_B receptor antagonist CGP 52432. However such an interpretation remains uncertain, because the dendritic arbor is poorly voltage-clamped and small EPSCs from synaptic contacts onto the dendrite might escape detection, and the experiments were not designed to perform a proper quantal analysis.

GABA_B receptor-mediated inhibition and the input-output relationship of L2/3 pyramidal neurons: GABA_B receptor activation shifted the input-output relationship of mPFC L2/3 pyramidal neurons in our experiments. Comparable results have been reported for inhibition mimicked by a constant conductance increase and fixed variability (Mitchell and Silver 2003), which is, in fact, similar to injecting noisy currents, as we did in our experiments. We conclude that GABA_B receptor-mediated tonic inhibition might act as a tonic shunting inhibition,

since it has additive (*f-I* curve shift, linear reduction of neuronal excitability) rather than multiplicative (gain change) effects (Holt and Koch 1997). The reduced excitability of single prefrontal neurons translates into lower overall network activity, as we will discuss in the next paragraph.

Consequence of GABA_B receptor-mediated tonic inhibition on network activity: GABA_B receptor-mediated influences on network activity have been mostly investigated in relation to rhythmic activity (Brown et al. 2007; Karpuk and Hayar 2008; Scanziani 2000). Activation of postsynaptic GABA_B receptors leads to a decrease in the frequency of oscillations in the hippocampus (Brown et al. 2007; Scanziani 2000) and the olfactory bulb (Karpuk and Hayar 2008).

We used two different approaches to investigate GABA_B effects on mPFC network activity. In both cases a bath solution, which more closely mimics cerebrospinal fluid, was used to increase the activity in the usually silent slice preparation (see Materials and Methods and Neubauer and Berger 2008). (1) To monitor ongoing excitatory network activity, we recorded spontaneous EPSCs from pyramidal cells as well as interneurons. Blocking GABA_B receptors increased the mean frequency of EPSCs in both, pyramidal as well as interneurons, revealing tonic GABA_B receptor-mediated inhibition. (2) We investigated up- and downstate activity which appears in the cortex *in vivo* as well as *in vitro* (Luczak et al. 2007; MacLean et al. 2005; Steriade et al. 1993; Steriade et al. 2001) in an oscillatory fashion (Compte et al. 2003; Sanchez-Vives and McCormick 2000). We focused on the properties of single upstates instead

of their rhythmic appearance. GABA_B receptor-blockade increased the duration of upstates that extend over large cortical areas.

In brain areas of high activity, ambient GABA might act as a negative feedback to limit spiking and probably the number of active neurons. This negative feedback provides a mechanism for controlling the duration of episodes of high neural activity, i.e. upstates. It is conceivable that upstates can only be initiated during episodes of low extracellular GABA concentration, exerting little or no tonic inhibition. As the activity increases during upstates, GABA is pooled in the extracellular space, GABA_B receptor-mediated tonic inhibition is increased and becomes relevant for terminating the episode of high activity. Then GABA is actively removed from the extracellular space by GABA transporters, which reduces tonic inhibition and allows for the initiation of another upstate.

The spatial extent of small upstates was about 100 μm in diameter in our experiments and was unaffected by tonic GABA_B receptor-mediated inhibition. We might therefore speculate that larger cortex areas need to be involved in order to increase the ambient GABA concentration to a level sufficient for activating GABA_B receptor-mediated inhibition. Such a hypothesis is in line with the studies on GABA_B-mediated influences on oscillatory network activity (Brown et al. 2007; Karpuk and Hayar 2008; Scanziani 2000).

We note that a negative feedback process similar to what we propose for GABA_B is also conceivable for GABA_A receptor-mediated tonic inhibition. Moreover, blocking GABA_B inhibition only lengthened upstates but did not prevent their cessation. Additional mechanisms might be involved in terminating

upstates (Compte et al. 2003; Sanchez-Vives and McCormick 2000; Timofeev et al. 2000).

In summary, our results, indicate that increases in network activity are self-limited by a concurrently rising ambient GABA concentration, which activates not only extrasynaptic GABA_A but also GABA_B receptors and in turn reduces the excitability of the neurons in the network. Therefore, GABA_B receptor-mediated tonic inhibition has a powerful effect onto neural networks and thus on behaviorally relevant states of cortical activity.

Acknowledgments: This work was supported by a grant from the Swiss National Science Foundation (3100A0-109305) to HRL. We would like to thank Drs. Benny Bettler, Matthew Larkum, and Christian Lüscher for critical reading of the manuscript.

Reference list

Arsiero M, Lüscher HR, Lundstrom BN, and Giugliano M. The impact of input fluctuations on the frequency-current relationships of layer 5 pyramidal neurons in the rat medial prefrontal cortex. *J Neurosci* 27: 3274-3284, 2007.

Berger T, Borgdorff A, Crochet S, Neubauer FB, Lefort S, Fauvet B, Ferezou I, Carleton A, Lüscher HR, and Petersen CC. Combined voltage and calcium epifluorescence imaging in vitro and in vivo reveals subthreshold and suprathreshold dynamics of mouse barrel cortex. *Journal of neurophysiology* 97: 3751-3762, 2007.

Bon C, and Galvan M. Electrophysiological actions of GABAB agonists and antagonists in rat dorso-lateral septal neurones in vitro. *British journal of pharmacology* 118: 961-967, 1996.

Brickley SG, Cull-Candy SG, and Farrant M. Development of a tonic form of synaptic inhibition in rat cerebellar granule cells resulting from persistent activation of GABAA receptors. *The Journal of physiology* 497 : 753-759, 1996.

Brown JT, Davies CH, and Randall AD. Synaptic activation of GABA(B) receptors regulates neuronal network activity and entrainment. *The European journal of neuroscience* 25: 2982-2990, 2007.

Compte A, Sanchez-Vives MV, McCormick DA, and Wang XJ. Cellular and network mechanisms of slow oscillatory activity (<1 Hz) and wave propagations in a cortical network model. *Journal of neurophysiology* 89: 2707-2725, 2003.

Cowan RL, and Wilson CJ. Spontaneous firing patterns and axonal projections of single corticostriatal neurons in the rat medial agranular cortex. *Journal of neurophysiology* 71: 17-32, 1994.

Cruz HG, Ivanova T, Lunn ML, Stoffel M, Slesinger PA, and Lüscher C. Bi-directional effects of GABA(B) receptor agonists on the mesolimbic dopamine system. *Nature neuroscience* 7: 153-159, 2004.

Cryan JF, and Kaupmann K. Don't worry 'B' happy!: a role for GABA(B) receptors in anxiety and depression. *Trends in pharmacological sciences* 26: 36-43, 2005.

Dalby NO. GABA-level increasing and anticonvulsant effects of three different GABA uptake inhibitors. *Neuropharmacology* 39: 2399-2407, 2000.

Farrant M, and Nusser Z. Variations on an inhibitory theme: phasic and tonic activation of GABA(A) receptors. *Nature reviews* 6: 215-229, 2005.

Glykys J, and Mody I. The main source of ambient GABA responsible for tonic inhibition in the mouse hippocampus. *The Journal of physiology* 582: 1163-1178, 2007.

Hempel CM, Hartman KH, Wang XJ, Turrigiano GG, and Nelson SB. Multiple forms of short-term plasticity at excitatory synapses in rat medial prefrontal cortex. *Journal of neurophysiology* 83: 3031-3041, 2000.

Hernandez LF, Segovia G, and Mora F. Effects of activation of NMDA and AMPA glutamate receptors on the extracellular concentrations of dopamine, acetylcholine, and GABA in striatum of the awake rat: a microdialysis study. *Neurochemical research* 28: 1819-1827, 2003.

Holt GR, and Koch C. Shunting inhibition does not have a divisive effect on firing rates. *Neural computation* 9: 1001-1013, 1997.

Jones KA, Borowsky B, Tamm JA, Craig DA, Durkin MM, Dai M, Yao WJ, Johnson M, Gunwaldsen C, Huang LY, Tang C, Shen Q, Salon JA, Morse K, Laz T, Smith KE, Nagarathnam D, Noble SA, Branchek TA, and Gerald C. GABA(B) receptors function as a heteromeric assembly of the subunits GABA(B)R1 and GABA(B)R2. *Nature* 396: 674-679, 1998.

Karpuk N, and Hayar A. Activation of postsynaptic GABAB receptors modulates the bursting pattern and synaptic activity of olfactory bulb juxtglomerular neurons. *Journal of neurophysiology* 99: 308-319, 2008.

Kennedy RT, Thompson JE, and Vickroy TW. In vivo monitoring of amino acids by direct sampling of brain extracellular fluid at ultralow flow rates and capillary electrophoresis. *Journal of neuroscience methods* 114: 39-49, 2002.

Kim U, Sanchez-Vives MV, and McCormick DA. Functional dynamics of GABAergic inhibition in the thalamus. *Science* 278: 130-134, 1997.

Kozlov AS, Angulo MC, Audinat E, and Charpak S. Target cell-specific modulation of neuronal activity by astrocytes. *Proceedings of the National Academy of Sciences of the United States of America* 103: 10058-10063, 2006.

Kulik A, Vida I, Fukazawa Y, Guetg N, Kasugai Y, Marker CL, Rigato F, Bettler B, Wickman K, Frotscher M, and Shigemoto R. Compartment-dependent colocalization of Kir3.2-containing K⁺ channels and GABAB receptors in hippocampal pyramidal cells. *J Neurosci* 26: 4289-4297, 2006.

Kulik A, Vida I, Lujan R, Haas CA, Lopez-Bendito G, Shigemoto R, and Frotscher M. Subcellular localization of metabotropic GABA(B) receptor subunits GABA(B1a/b) and GABA(B2) in the rat hippocampus. *J Neurosci* 23: 11026-11035, 2003.

La Camera G, Rauch A, Lüscher HR, Senn W, and Fusi S. Minimal models of adapted neuronal response to in vivo-like input currents. *Neural computation* 16: 2101-2124, 2004.

Labouebe G, Lomazzi M, Cruz HG, Creton C, Lujan R, Li M, Yanagawa Y, Obata K, Watanabe M, Wickman K, Boyer SB, Slesinger PA, and Lüscher C. RGS2 modulates coupling between GABAB receptors and GIRK channels in dopamine neurons of the ventral tegmental area. *Nature neuroscience* 10: 1559-1568, 2007.

Lei S, and McBain CJ. GABA B receptor modulation of excitatory and inhibitory synaptic transmission onto rat CA3 hippocampal interneurons. *The Journal of physiology* 546: 439-453, 2003.

Liu X, Tribollet E, and Raggenbass M. GABA(B) receptor-activation inhibits GABAergic synaptic transmission in parvocellular neurones of rat hypothalamic paraventricular nucleus. *Journal of neuroendocrinology* 18: 177-186, 2006.

Luczak A, Bartho P, Marguet SL, Buzsaki G, and Harris KD. Sequential structure of neocortical spontaneous activity in vivo. *Proceedings of the National Academy of Sciences of the United States of America* 104: 347-352, 2007.

Lüscher C, Jan LY, Stoffel M, Malenka RC, and Nicoll RA. G protein-coupled inwardly rectifying K⁺ channels (GIRKs) mediate postsynaptic but not

presynaptic transmitter actions in hippocampal neurons. *Neuron* 19: 687-695, 1997.

MacLean JN, Watson BO, Aaron GB, and Yuste R. Internal dynamics determine the cortical response to thalamic stimulation. *Neuron* 48: 811-823, 2005.

Metherate R, and Ashe JH. Ionic flux contributions to neocortical slow waves and nucleus basalis-mediated activation: whole-cell recordings in vivo. *J Neurosci* 13: 5312-5323, 1993.

Mitchell SJ, and Silver RA. GABA spillover from single inhibitory axons suppresses low-frequency excitatory transmission at the cerebellar glomerulus. *J Neurosci* 20: 8651-8658, 2000.

Mitchell SJ, and Silver RA. Shunting inhibition modulates neuronal gain during synaptic excitation. *Neuron* 38: 433-445, 2003.

Neubauer FB, and Berger T. Somatodendritic integration under increased network activity in layer 5 pyramidal cells of the somatosensory cortex. *Pflugers Arch* 455: 1063-1079, 2008.

Nusser Z, and Mody I. Selective modulation of tonic and phasic inhibitions in dentate gyrus granule cells. *Journal of neurophysiology* 87: 2624-2628, 2002.

Okun M, and Lampl I. Instantaneous correlation of excitation and inhibition during ongoing and sensory-evoked activities. *Nature neuroscience* 11: 535-537, 2008.

Price CJ, Cauli B, Kovacs ER, Kulik A, Lambolez B, Shigemoto R, and Capogna M. Neurogliaform neurons form a novel inhibitory network in the hippocampal CA1 area. *J Neurosci* 25: 6775-6786, 2005.

Rauch A, La Camera G, Lüscher HR, Senn W, and Fusi S. Neocortical pyramidal cells respond as integrate-and-fire neurons to in vivo-like input currents. *Journal of neurophysiology* 90: 1598-1612, 2003.

Rossi DJ, Hamann M, and Attwell D. Multiple modes of GABAergic inhibition of rat cerebellar granule cells. *The Journal of physiology* 548: 97-110, 2003.

Sanchez-Vives MV, and McCormick DA. Cellular and network mechanisms of rhythmic recurrent activity in neocortex. *Nature neuroscience* 3: 1027-1034, 2000.

Scanziani M. GABA spillover activates postsynaptic GABA(B) receptors to control rhythmic hippocampal activity. *Neuron* 25: 673-681, 2000.

Semyanov A, Walker MC, Kullmann DM, and Silver RA. Tonically active GABA A receptors: modulating gain and maintaining the tone. *Trends in neurosciences* 27: 262-269, 2004.

Shu Y, Hasenstaub A, Badoual M, Bal T, and McCormick DA. Barrages of synaptic activity control the gain and sensitivity of cortical neurons. *J Neurosci* 23: 10388-10401, 2003.

Stell BM, and Mody I. Receptors with different affinities mediate phasic and tonic GABA(A) conductances in hippocampal neurons. *J Neurosci* 22: RC223, 2002.

Steriade M, Nunez A, and Amzica F. A novel slow (< 1 Hz) oscillation of neocortical neurons in vivo: depolarizing and hyperpolarizing components. *J Neurosci* 13: 3252-3265, 1993.

Steriade M, Timofeev I, and Grenier F. Natural waking and sleep states: a view from inside neocortical neurons. *Journal of neurophysiology* 85: 1969-1985, 2001.

Tamás G, Lorincz A, Simon A, and Szabadics J. Identified sources and targets of slow inhibition in the neocortex. *Science* 299: 1902-1905, 2003.

Thomson AM, and Destexhe A. Dual intracellular recordings and computational models of slow inhibitory postsynaptic potentials in rat neocortical and hippocampal slices. *Neuroscience* 92: 1193-1215, 1999.

Thurley K, Senn W, and Lüscher HR. Dopamine increases the gain of the input-output response of rat prefrontal pyramidal neurons. *Journal of neurophysiology* 99: 2985-2997, 2008.

Timofeev I, Grenier F, Bazhenov M, Sejnowski TJ, and Steriade M. Origin of slow cortical oscillations in deafferented cortical slabs. *Cereb Cortex* 10: 1185-1199, 2000.

Tossman U, Jonsson G, and Ungerstedt U. Regional distribution and extracellular levels of amino acids in rat central nervous system. *Acta physiologica Scandinavica* 127: 533-545, 1986.

Urwyler S, Gjoni T, Koljatic J, and Dupuis DS. Mechanisms of allosteric modulation at GABAB receptors by CGP7930 and GS39783: effects on affinities and efficacies of orthosteric ligands with distinct intrinsic properties. *Neuropharmacology* 48: 343-353, 2005.

Wu Y, Wang W, Diez-Sampedro A, and Richerson GB. Nonvesicular inhibitory neurotransmission via reversal of the GABA transporter GAT-1. *Neuron* 56: 851-865, 2007.

Yamada J, Furukawa T, Ueno S, Yamamoto S, and Fukuda A. Molecular basis for the GABAA receptor-mediated tonic inhibition in rat somatosensory cortex. *Cereb Cortex* 17: 1782-1787, 2007.

Zhang X, Rauch A, Lee H, Xiao H, Rainer G, and Logothetis NK. Capillary hydrophilic interaction chromatography/mass spectrometry for simultaneous determination of multiple neurotransmitters in primate cerebral cortex. *Rapid Commun Mass Spectrom* 21: 3621-3628, 2007.

Figure 1:

Baclofen-induced currents in L2/3 pyramidal cells of rat mPFC consist of at least two different outward currents.

A1) The GABA_B agonist baclofen induced an outward current in an intrinsically bursting L2/3 pyramidal cell. The GABA_B antagonist CGP 52432 reversed the outward current leading to a small undershoot, which could partly be washed out. The change in input resistance during application of the drugs is shown below. Resting input resistance was 86 MΩ. A2) Biocytin-filled and reconstructed L2/3 pyramidal cell for the experiment shown on the left. A3) Bursting spike pattern at threshold DC current injection recorded from the cell shown in A2. A4) Concentration-response curve for the baclofen-induced outward current ($EC_{50} = 0.967 \pm 0.17 \mu\text{M}$, $h = 1.00 \pm 0.04$, $n = 8$). B) The baclofen-induced outward current can be blocked by the application of barium (Ba^{2+}), leading to a prominent undershoot. Additional application of CGP 52432 reveals a barium-insensitive current. C, left) The baclofen induced outward current could in part be reverted by the application of tertiapin-Q, a selective antagonist for the GIRK1/4 channel. C, right) Summary of the tertiapin-Q effect. Tertiapin blocked approximately 40% of the baclofen induced current. D) Barium-resistant current revealed by the application of baclofen together with Ba^{2+} . The barium-resistant current can be blocked by the addition of CGP 52432. E) Summary of currents evoked by baclofen, Ba^{2+} , and co-application of baclofen and Ba^{2+} . Concentrations were (in μM): Ba^{2+} , 300; baclofen, 25; CGP 52432, 1; tertiapin-Q, 0.5.

Figure 2:

The specific GAT1 GABA uptake inhibitor NO-711 reveals a tonic GABA_B receptor-mediated postsynaptic current.

A) Application of CGP 52432 reduces a persistent outward current in L2/3 pyramidal neurons revealing. The response to baclofen is not prevented by prior CGP 52432 application. B) A small tonic outward current is evoked by the application of NO-711, a specific GAT1 inhibitor. This outward current is blocked by the application CGP 52432. C) Combined application of GABA and NO-711 leads to a substantial outward current, which could in part be blocked by CGP 52432. The dotted line indicates interpolated missing data points. D) Summary of CGP 52432-evoked persistent inward shift of holding current in mPFC pyramidal cells in the absence of supplementary GABA and NO-711 (control), with NO-711 and with NO-711 plus GABA. Concentrations were (in μM): baclofen, 25; CGP 52432, 1; GABA, 3.3; NO-711, 2.5.

Figure 3:

Extracellular electrical stimulation evokes a GABA_B receptor-mediated outward current.

A) Schematic representation of the experimental arrangement. Voltage stimuli were delivered through a theta glass pipette filled with ACSF and positioned in L1. Stimulus intensity was approximately 2 times threshold and was identical for all experiments. Current signals were recorded from L2/3 pyramidal cells in voltage-clamp at $V_h = -50$ mV. B) Current trace evoked by a single stimulus. A fast inward current is followed by a fast outward current (see inset), and a long-lasting outward current. C) The fast, short-latency in- and outward currents were blocked by the application of CNQX and APV, and gabazine, respectively, leaving a long-lasting outward current. This suggests that the first two components were excitatory and GABA_A receptor-mediated inhibitory currents, respectively. D) A short burst of 5 stimuli (70 Hz) led to an increase of the late, long-lasting outward current. E) Peak amplitude (arrow in D) of the slow outward current as a function of time while stimulating with a burst of 5 stimuli at a repetition rate of 0.1 Hz. Application of CGP 52432 abolished this current completely. The washout progressed only slowly. Data was acquired in the presence of APV, CNQX and gabazine. The arrow marks the beginning of stimulation, which was retained for the remaining recording time. Concentrations were (in μ M): APV, 50; CGP 52432, 1; CNQX 10; gabazine, 10.

Figure 4:

Elevated GABA concentration induces a tonic current comprised of GABA_B and GABA_A components.

A) In the presence of GABA and NO-711 together with blockers of excitatory synaptic transmission with APV and CNQX application of CGP 52432 revealed a GABA_B receptor-mediated current. Addition of gabazine uncovered an additional component, which can be attributed to GABA_A receptor activation. Under these conditions both, the GABA_B and the GABA_A receptor-mediated currents are of similar amplitude (B). The amplitude of the baclofen-evoked current was measured from a baseline immediately before the application of baclofen. Concentrations were (in μM): APV, 50; baclofen, 25; CGP 52432, 1; CNQX, 10; GABA, 3.3; gabazine, 10; NO-711, 2.5.

Figure 5:

Tonic activation of GABA_B receptors shifts the input-output relationship of PFC L2/3 pyramidal neurons.

A) Example of the noisy stimulation current with a mean of 200 pA and standard deviation of 100 pA (*top*) and corresponding voltage traces before drug application (*2nd panel*) with baclofen (*3rd panel*) and with CGP 52432 (*4th panel*). The dashed vertical line divides response phases that were defined as transient and steady state responses. *Bottommost panels*: Mean firing rate f as a function of the mean input current m for control conditions, with baclofen and with CGP 52432. Curves are given for the transient phase at the beginning of the stimulation (*left*) and for the steady state response (*right*). The standard deviation (error bars) is given in case the stimulus was repeated at the particular mean value (30% of the values). Solid lines represent linear fits of the data. Rectangles mark values, belonging to the traces in the upper panels. B, C) Summary graphs for the changes of the rheobase current (firing threshold) (B), and the membrane resting potential (C) between control conditions and pharmacological treatment. The values for single cells are given as dots, corresponding values are connected by lines. Underlying bars are the mean values. Concentrations were (in μM): baclofen, 25; CGP 52432, 1; gabazine, 10.

Figure 6:

Blocking GABA_B receptors with CGP 52432 releases tonic inhibition of overall network activity.

A) *Left panel:* Frequency of spontaneous EPSCs are plotted against time recorded in voltage clamp ($V_h = -70$ mV) from a fast spiking interneuron in L2/3 in mACSF and in the presence of the GABA uptake inhibitor NO-711. Application of CGP 52432 increased the frequency of spontaneous EPSCs (green dots) over baseline levels (mACSF, red dots). Application of baclofen (blue dots) decreased the EPSC frequency slightly below baseline values. *Right panel:* distribution of the EPSC frequency in mACSF and with CGP 52432. B) Summary of experiments with 7 fast spiking interneurons (left panel, IN) and 8 pyramidal cells (right panel, PC). The mean frequency of EPSCs was higher in fast spiking neurons compared to pyramidal cells (note different scale of the y-axis in B). C) Examples of spontaneous EPSCs recorded from the fast spiking interneuron whose result is shown in (A) in mACSF (red), with CGP 52432 (green), and baclofen (blue). The corresponding cumulative EPSC amplitude distributions are shown in the right panel. Although a small right shift to larger EPSCs can be seen, it is not significant ($p > 0.5$, Kolmogorov-Smirnov test). D) Same as (C) but EPSCs recorded from a L2/3 pyramidal neuron. Note the lower frequency of the spontaneous EPSCs. Again, no significant difference in the two cumulative amplitude distributions can be found ($p > 0.05$, Kolmogorov-Smirnov test). Concentrations were (in μ M): baclofen, 25; CGP 52432, 5; NO-711, 2.5.

Figure 7:

Blocking GABA_B-mediated tonic inhibition increases the duration of upstates.

A) Upstate duration plotted against time. Under control conditions no upstates were detected. Superfusion with modified ACSF (mACSF, see Materials and Methods) led to prominent upstate activity. The duration of the upstates increased dramatically with the application of CGP 52432. Replacing CGP 52432 with baclofen abolished upstate activity (with 3 exceptions at the onset of washout) even though superfusion with mACSF continued. B) sample traces for the four time periods indicated by numbers in (A). Arrow in (B3) points to the onset of a new upstate without any delay. C) Summary diagram illustrating the increase in upstate duration for L2/3 (n=6, solid lines) and L5 pyramidal cells (n=3, dotted lines). The increase in upstate duration was statistically highly significant in each individual cell. Concentrations were (in μM): baclofen, 25; CGP 52432, 5.

Figure 8:

GABA_B receptor-mediated tonic inhibition determines the duration of upstates.

A) Bright field image of the mPFC in an acute slice preparation. B) Corresponding image of resting epifluorescence after dye injection. The blue rectangle (stippled) corresponds to the image rectangle shown in (C). C) Mask within which epifluorescence changes were analyzed; blue area was not considered in the analysis. D, F, H) Peak intensity maps for upstates under control conditions (D), with CGP 52432 (F), and with baclofen (H). The scale bar in (A) to (H) equals 1 mm. E, G, I) Corresponding mean $\Delta F/F_0$ traces during an imaging time period of 52 s. Arrows indicate the time points of the intensity maps on the left. The mean $\Delta F/F_0$ values are calculated across the entire mask shown in (C) resulting in a tiny change in the intensity profile for the small upstate in (arrow in I). The inset in (I) shows the mean intensity profile of the same upstate averaged over the actual upstate area shown in H (inset scale bars: 0.2 % $\Delta F/F_0$, 10 s). K, L, M) Summary results of 5 slices from 5 different animals. (K) Histogram of the size of the upstates recorded under control condition (mACSF, red) with CGP (green) and with baclofen (blue). The upstates were counted during the entire recording period of 520 s (see Materials and Methods). The histogram clearly reveals two populations of upstates, large and small ones. The large upstates completely disappear after the application of baclofen. The effect can be washed out (not shown). In (L) and (M) only large upstates were analyzed. Upstate duration increased significantly (L) while upstate peak intensity remained the same (M); one-way ANOVA. Neither duration, nor peak intensity, nor size of

the small upstates was affected by the pharmacological interventions. For his summary figure K, 212 upstates were analyzed during control condition, 168 with CGP, and 33 with baclofen. Concentrations were (in μM): baclofen, 25; CGP 52432, 5.

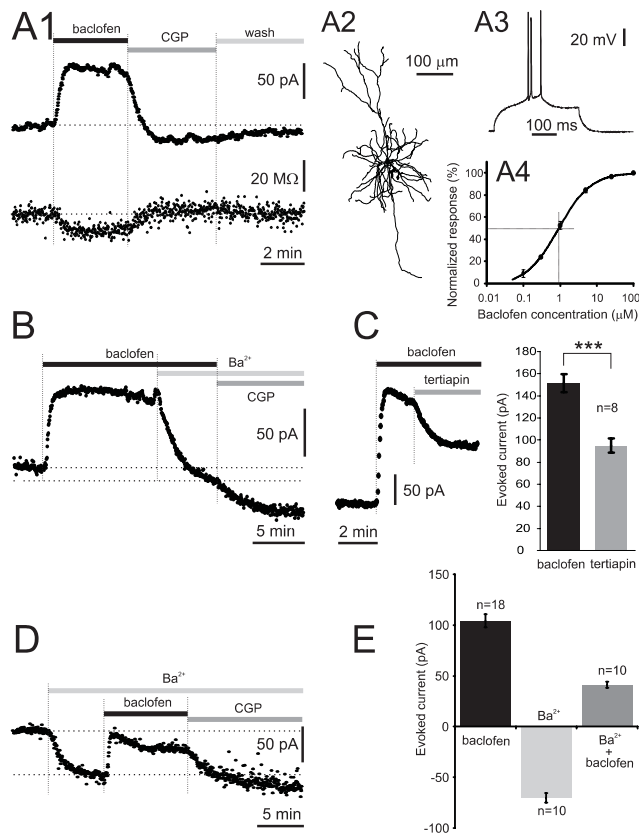


Figure 1
Wang et al.

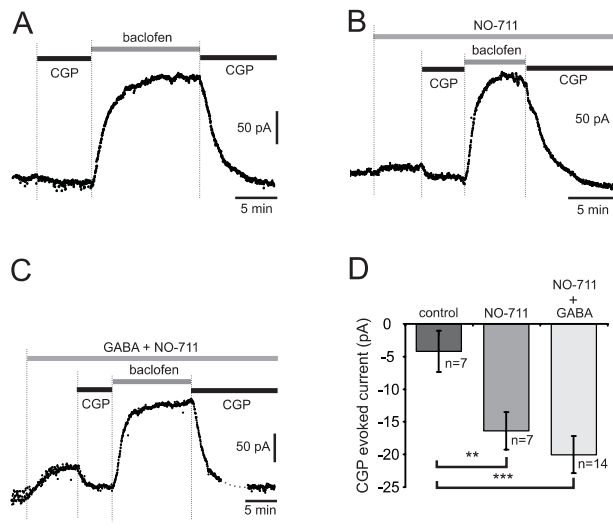


Figure 2
Wang et al.

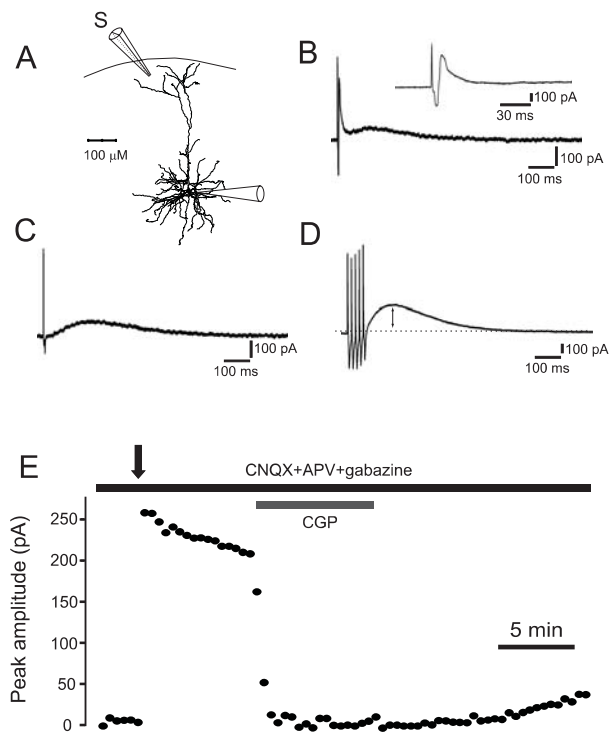


Figure 3
Wang et al.

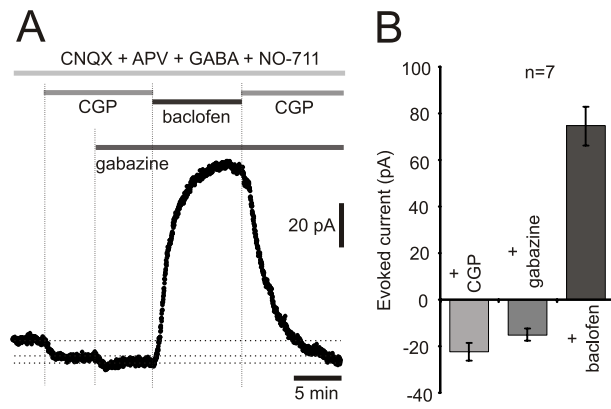


Figure 4
Wang et al.

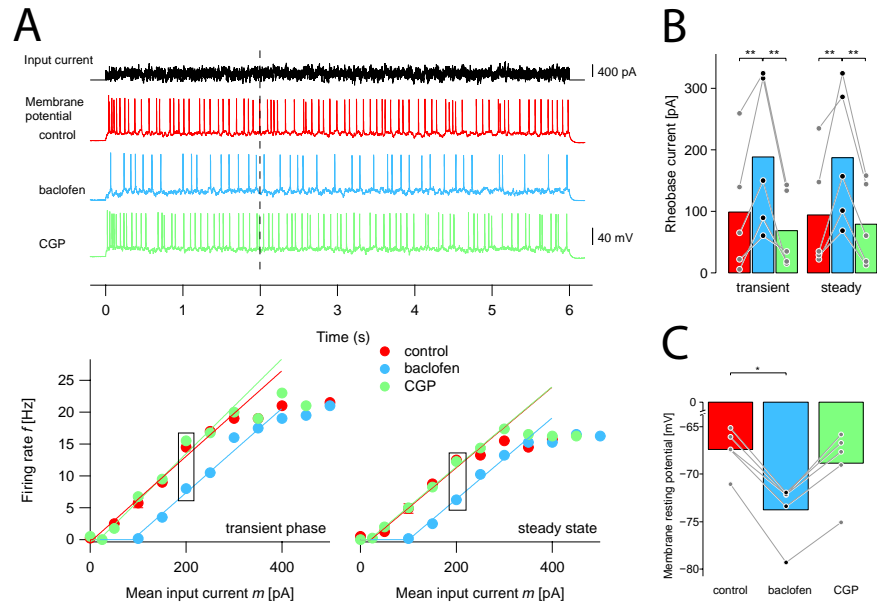


Figure 5
 Wang et al.

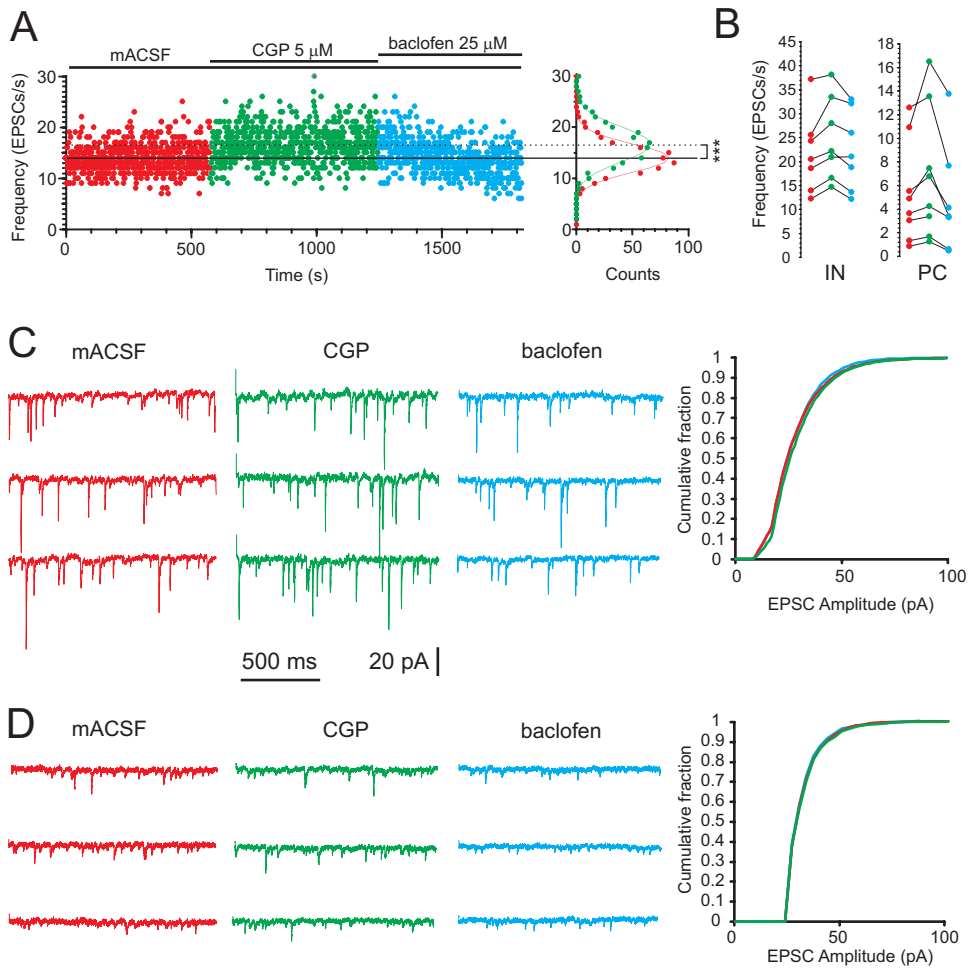


Figure 6
Wang et al.

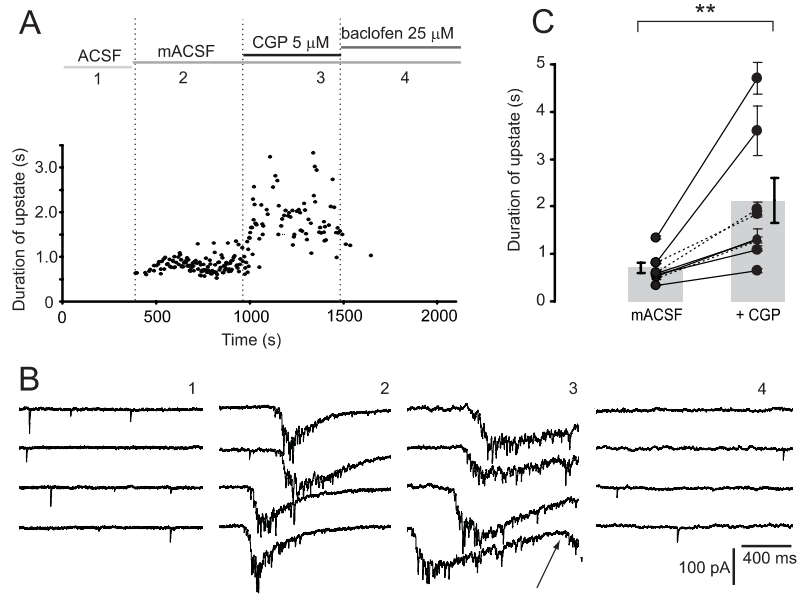


Figure 7
Wang et al.

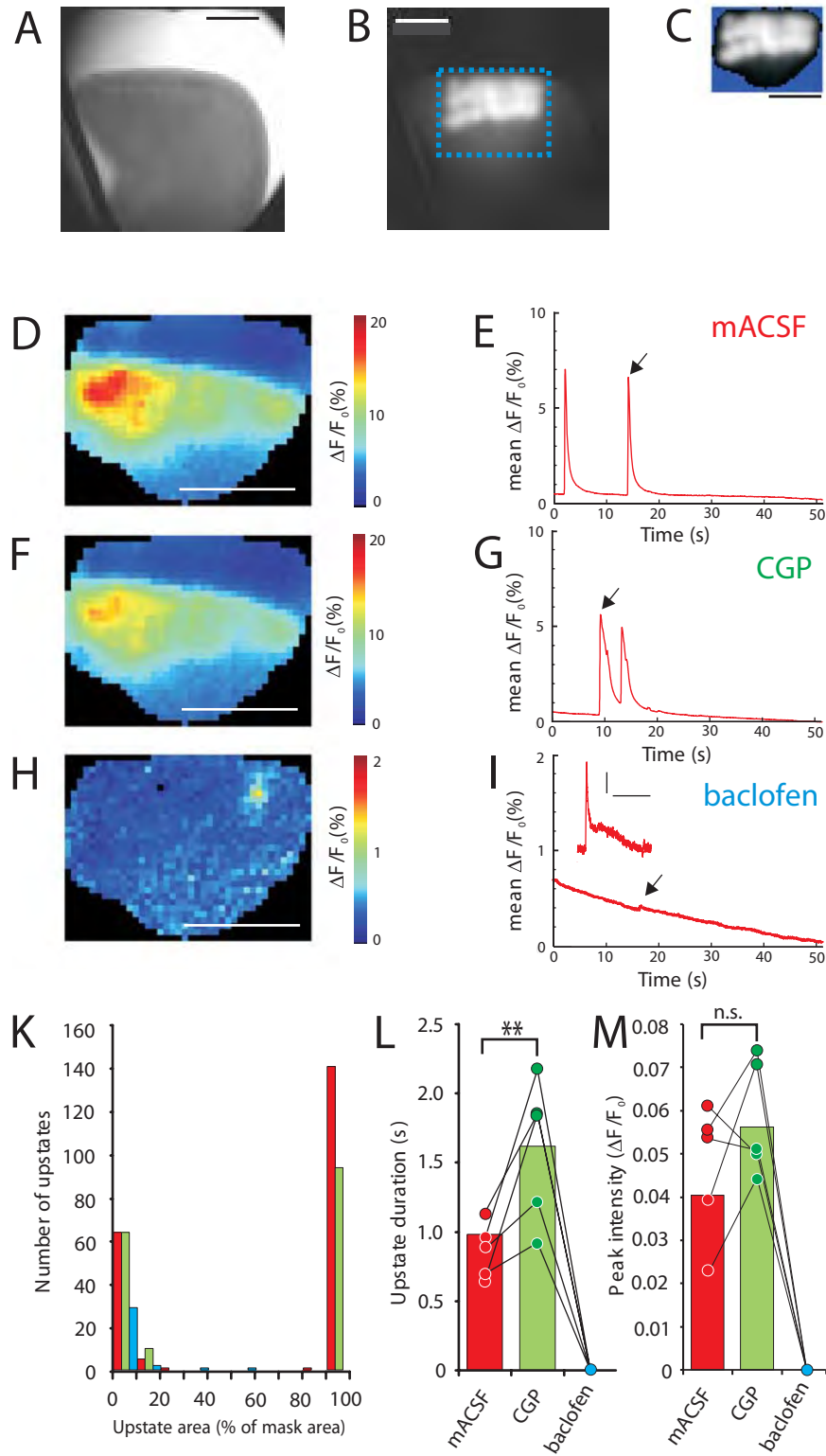


Figure 8

Wang et al.

Bibliography

- Anderson PW (1972) More Is Different. *Science* 177:393-396.
- Araque A, Perea G (2004) Glial modulation of synaptic transmission in culture. *Glia* 47:241-248.
- Azevedo FA, Carvalho LR, Grinberg LT, Farfel JM, Ferretti RE, Leite RE, Jacob Filho W, Lent R, Herculano-Houzel S (2009) Equal numbers of neuronal and nonneuronal cells make the human brain an isometrically scaled-up primate brain. *J Comp Neurol* 513:532-541.
- Baars B (1988) *A Cognitive Theory of Consciousness*. Cambridge, Mass.: Cambridge University Press.
- Bedau MA (2003) Downward causation and autonomy in weak emergence. *Principia* 6:5-50.
- Berger T (2007) Dendritic Activity in Layer 5 Pyramidal Cells During Upstates (abstract 402.5). In: Society for Neuroscience: Neuroscience meeting 2007. San Diego, California.
- Berger T, Borgdorff A, Crochet S, Neubauer FB, Lefort S, Fauvet B, Ferezou I, Carleton A, Lüscher HR, Petersen CC (2007) Combined voltage and calcium epifluorescence imaging in vitro and in vivo reveals subthreshold and suprathreshold dynamics of mouse barrel cortex. *J Neurophysiol* 97:3751-3762.
- Besley NA (2007) Computing protein infrared spectroscopy with quantum chemistry. *Philosophical Transactions of the Royal Society A* 365:2799–2812.
- Blanke O, Metzinger T (2009) Full-body illusions and minimal phenomenal selfhood. *Trends Cogn Sci* 13:7-13.
- Blanke O, Ortigue S, Landis T, Seeck M (2002) Stimulating illusory own-body perceptions. *Nature* 419:269-270.
- Briggman KL, Denk W (2006) Towards neural circuit reconstruction with volume electron microscopy techniques. *Curr Opin Neurobiol* 16:562-570.
- Brodmann K (1909) *Vergleichende Lokalisationslehre der Grosshirnrinde in ihren Prinzipien dargestellt auf Grund des Zellenbaues*. Leipzig: Johann Ambrosius Barth Verlag.
- Carruthers P (2008) Higher-Order Theories of Consciousness. In: *The Stanford Encyclopedia of Philosophy*, Fall 2008 Edition (Zalta EN, ed). <http://plato.stanford.edu/archives/win2008/entries/consciousness-higher>

- Chalmers DJ (1995) Facing Up to the Problem of Consciousness. *Journal of Consciousness Studies* 2:200-219.
- Chomsky N (1966) *Cartesian Linguistics: A Chapter in the History of Rationalist Thought*. New York: Harper & Row.
- Cossart R, Ikegaya Y, Yuste R (2005) Calcium imaging of cortical networks dynamics. *Cell Calcium* 37:451-457.
- Crane T (2000) Dualism, Monism, Physicalism. *Mind & Society* 1:73-85.
- Crick F, Koch C (1990) Towards a neurobiological theory of consciousness. *Seminars in the Neurosciences* 2:263-275.
- Crick F, Koch C (2003) A framework for consciousness. *Nat Neurosci* 6:119-126.
- Crochet S, Petersen CC (2006) Correlating whisker behavior with membrane potential in barrel cortex of awake mice. *Nat Neurosci* 9:608-610.
- Dawkins R (1986) *The Blind Watchmaker*. New York: W. W. Norton & Co Ltd.
- Dayan P, Abbott LF (2001) *Theoretical Neuroscience: Computational and Mathematical Modeling of Neural Systems*. Cambridge, Mass.: MIT Press.
- Dennett CD (1996) *Darwin's Dangerous Idea: Evolution and the Meanings of Life*. London: Penguin Books.
- Fellin T, Pascual O, Gobbo S, Pozzan T, Haydon PG, Carmignoto G (2004) Neuronal synchrony mediated by astrocytic glutamate through activation of extrasynaptic NMDA receptors. *Neuron* 43:729-743.
- Fodor JA (1974) Special Sciences, or the Disunity of Science as a Working Hypothesis. *SYNTHESE* 28:97-115.
- Fodor JA (1975) *The Language of Thought*. New York: Thomas Y. Crowell Co.
- Fodor JA (1994) *The Elm and the Expert: Mentalese and Its Semantics*. Cambridge, Mass.: MIT Press.
- Fodor JA, Pylyshyn ZW (1988) Connectionism and cognitive architecture: a critical analysis. *Cognition* 28:3-71.
- Garson J (2008) Connectionism. In: *The Stanford Encyclopedia of Philosophy*, Fall 2008 Edition (Zalta EN, ed). <http://plato.stanford.edu/archives/fall2008/entries/connectionism>

- Grush R (2004) The emulation theory of representation: motor control, imagery, and perception. *Behav Brain Sci* 27:377-442.
- Hameroff SR, Penrose R (1996) Conscious events as orchestrated spacetime selections. *Journal of Consciousness Studies* 3:36-53.
- Hanson NR (1958) *Patterns of Discovery: An Inquiry into the Conceptual Foundations of Science*. Cambridge: Cambridge University Press.
- Hesslow G (2002) Conscious thought as simulation of behaviour and perception. *Trends Cogn Sci* 6:242-247.
- Hodgkin AL, Huxley AF (1952) A quantitative description of membrane current and its application to conduction and excitation in nerve. *J Physiol* 117:500-544.
- Horst S (2008) The Computational Theory of Mind. In: *The Stanford Encyclopedia of Philosophy*, Fall 2008 Edition (Zalta EN, ed).
<http://plato.stanford.edu/archives/fall2008/entries/computational-mind>
- Kim Y, Vladimirskiy BB, Senn W (2008) Modulating the granularity of category formation by global cortical states. *Frontiers in Computational Neuroscience* 2.
- Koch C (2004) *The Quest for Consciousness. A Neurobiological Approach*. Englewood, Colorado: Roberts & Company Publishers.
- Koch C, Hepp K (2006) Quantum mechanics in the brain. *Nature* 440:611.
- Kuhn TS (1962) *The Structure of Scientific Revolutions*. Chicago: University of Chicago Press.
- Lefort S, Tomm C, Floyd Sarria JC, Petersen CC (2009) The excitatory neuronal network of the C2 barrel column in mouse primary somatosensory cortex. *Neuron* 61:301-316.
- Levine J (1983) Materialism and Qualia: The Explanatory Gap. *Pacific Philosophical Quarterly* 64:354 - 361.
- Levine J (1999) Conceivability, Identity, and the Explanatory Gap. In: *Toward a Science of Consciousness III: The Third Tucson Discussions and Debates* (Hameroff SR, Kaszniak AW, Chalmers DJ, eds), pp 3-12. Cambridge, Mass.: MIT Press.
- Maclean JN, Watson BO, Aaron GB, Yuste R (2005) Internal Dynamics Determine the Cortical Response to Thalamic Stimulation. *Neuron* 48:811-823.
- Markopoulos F, Neubauer FB, Berger T, Scotti AL (2008) Reassembling a system from the sensor to cerebral representation: the olfactory system in vitro. *Neuroscience* 156:1048-1063.

- Markram H (2005) Dendritic object theory: a theory of the neural code where 3D electrical objects are formed across dendrites by neural microcircuits (abstract 196). In: Swiss Society for Neuroscience Annual Meeting 2005. Zürich, Switzerland.
- Markram H (2006) The blue brain project. *Nat Rev Neurosci* 7:153-160.
- McCulloch WS, Pitts W (1943) A logical calculus of the ideas immanent in nervous activity. *Bulletin of Mathematical Biophysics* 5:115-133.
- McFadden J (2002) Synchronous Firing and Its Influence on the Brain's Electromagnetic Field - Evidence for an Electromagnetic Field Theory of Consciousness. *Journal of Consciousness Studies* 9:23-50.
- McNaughton BL, Battaglia FP, Jensen O, Moser EI, Moser MB (2006) Path integration and the neural basis of the 'cognitive map'. *Nat Rev Neurosci* 7:663-678.
- Minsky M (1982) Why People Think Computers Can't. *AI Magazine* 3:3-15.
- Molnar G, Olah S, Komlosi G, Fule M, Szabadics J, Varga C, Barzo P, Tamas G (2008) Complex events initiated by individual spikes in the human cerebral cortex. *PLoS Biol* 6.
- Nagel E (1961) *The Structure of Science: Problems in the Logic of Scientific Explanation*. New York: Harcourt, Brace & World.
- Nagel T (1974) What is it Like to Be a Bat? *The Philosophical Review* 83:435-450.
- Nakazawa K, McHugh TJ, Wilson MA, Tonegawa S (2004) NMDA receptors, place cells and hippocampal spatial memory. *Nat Rev Neurosci* 5:361-372.
- Neubauer FB, Berger T (2008) Somatodendritic integration under increased network activity in layer 5 pyramidal cells of the somatosensory cortex. *Pflugers Arch* 455:1063-1079.
- Niiniluoto I (2008) Scientific Progress. In: *The Stanford Encyclopedia of Philosophy*, Fall 2008 Edition (Zalta EN, ed). <http://plato.stanford.edu/archives/fall2008/entries/scientific-progress>
- Nimmerjahn A, Kirchhoff F, Kerr JN, Helmchen F (2004) Sulforhodamine 101 as a specific marker of astroglia in the neocortex in vivo. *Nat Methods* 1:31-37.
- Papineau D (1998) Mind the Gap. *Noûs* 32:373-388.
- Papineau D (2003) Could There Be A Science of Consciousness? *Philosophical Issues* 13:205-220.
- Popper KR, Eccles JC (1977) *The Self and Its Brain*. New York: Springer-Verlag.

- Poulet JF, Petersen CC (2008) Internal brain state regulates membrane potential synchrony in barrel cortex of behaving mice. *Nature* 454:881-885.
- Putnam H (1967) Psychological Predicates. In: *Art, Mind, Religion: Proceedings* (Capitan WH, Merrill DD, eds), pp 37-48. Pittsburgh: University of Pittsburgh Press.
- Putnam H (1980) Brains and Behavior. In: *Readings in Philosophy of Psychology* (Block N, ed). London: Routledge.
- Rosen R (1985) *Anticipatory Systems: Philosophical, Mathematical and Methodological Foundations*. Oxford: Pergamon Press.
- Searle J (1980) Minds, Brains, and Programs. *Behavioral and Brain Sciences* 3:417-424.
- Searle J (1992) *The Rediscovery of the Mind*. Cambridge, Mass.: MIT Press.
- Sejnowski TJ, Koch C, Churchland PS (1988) Computational Neuroscience. *Science* 241:1299-1306.
- Shannon CE (1948) A Mathematical Theory of Communication. *The Bell System Technical Journal* 27:379-423.
- Siegelmann HT, Sontag ED (1995) On the Computational Power of Neural Nets. *Journal of Computer and System Sciences* 50:132-150.
- Simon HA (1962) The architecture of complexity. *Proceedings of the American Philosophical Society* 106:467-482.
- Sperling JM, Prvulovic D, Linden DE, Singer W, Stirn A (2006) Neuronal correlates of colour-graphemic synaesthesia: a fMRI study. *Cortex* 42:295-303.
- Stein RB, Gossen ER, Jones KE (2005) Neuronal variability: noise or part of the signal? *Nat Rev Neurosci* 6:389-397.
- Szabadics J, Tamas G, Soltesz I (2007) Different transmitter transients underlie presynaptic cell type specificity of GABA_A, slow and GABA_A, fast. *Proc Natl Acad Sci U S A* 104:14831-14836.
- Thagard P (2008) Cognitive Science. In: *The Stanford Encyclopedia of Philosophy*, Fall 2008 Edition (Zalta EN, ed). <http://plato.stanford.edu/archives/fall2008/entries/cognitive-science>
- Thompson E, Varela FJ (2001) Radical embodiment: neural dynamics and consciousness. *Trends Cogn Sci* 5:418-425.

- Turing AM (1937) Computability and λ -Definability. *The Journal of Symbolic Logic* 2:153-163.
- Van Gulick R (2004) Consciousness. In: *The Stanford Encyclopedia of Philosophy*, Winter 2008 Edition (Zalta EN, ed). <http://plato.stanford.edu/archives/win2008/entries/consciousness>
- Volterra A, Meldolesi J (2005) Astrocytes, from brain glue to communication elements: the revolution continues. *Nat Rev Neurosci* 6:626-640.
- Wang Y, Thurley K, Neubauer FB, Lüscher HR (submitted 02/2009) Modulation of network activity through GABA-B receptor-mediated tonic inhibition in the rat medial prefrontal cortex *in vitro*.
- Weiss PH, Fink GR (2009) Grapheme-colour synaesthetes show increased grey matter volumes of parietal and fusiform cortex. *Brain* 132:65-70.
- Woodward J (2008) Scientific Explanation. In: *The Stanford Encyclopedia of Philosophy*, Fall 2008 Edition (Zalta EN, ed). <http://plato.stanford.edu/archives/fall2008/entries/scientific-explanation>

Abbreviations

CASD	calcium-sensitive dye
EEG	electroencephalography
GABA	γ -aminobutyric acid
MEG	magnetoencephalography
fMRI	functional magnetic resonance imaging
NCC	neuronal correlate(s) of consciousness
PET	positron emission tomography
VSD	voltage-sensitive dye

Curriculum Vitae

Florian Neubauer
6019 South Ingleside Avenue
Chicago, IL 60637
USA

PERSONAL DATA

Date of birth February 7, 1975
Place of birth Würzburg, Germany
Citizenship German

Married with 2 children

EDUCATION

2005 – 2009 PhD student at the Department of Physiology, University of Bern

2004 Doctor of Medicine, "Magna cum laude",
thesis in molecular biology on TGF- β signal transduction.
Department of Physiological Chemistry, University Würzburg

1995 – 2003 Medical degree at the Julius-Maximilians-University Würzburg,
Germany. *Staatsexamen*, final grade "A-"

1985 – 1994 Secondary school (*Gymnasium*), Würzburg, Germany.
High school degree (*Abitur*), final grade: "A+"

AWARDS

2009 – 2011 Fellowship from the Swiss National Science Foundation for
prospective researchers (for 18 month)

1999 – 2003 Scholarship from the German National Academic Foundation
(*Studienstiftung des deutschen Volkes*)

Acknowledgements

Mein herzlicher Dank gilt am Ende dieser Arbeit

PD Dr. Thomas Berger, der fast drei Jahre lang mein Doktorvater war und nur wegen seines Wechsels an die Universität Mainz 2008 nicht als solcher auf dieser Arbeit erscheint. Er ist ein exzellenter Lehrer. Den überwiegenden Teil dessen, was ich über neurophysiologische Forschungsmethoden weiss, habe ich von ihm.

Professor Hans-Rudolf Lüscher für meine Aufnahme am Institut für Physiologie der Universität Bern, das er bis März 2009 mit Weitblick und einzigartiger Fürsorge für die Freiheit der Forschenden geleitet hat. Ich danke ihm für wegweisende Diskussionen bezüglich meiner Arbeit und darüber hinaus. Er hat mich im letzten Jahr meiner PhD-Zeit als zweiter Doktorvater begleitet und ist Erstgutachter dieser Dissertation.

Professor Hans Imboden vom Institut für Zellbiologie, der als externer Tutor immer für mich da war und freundlicherweise das Koreferat für diese Arbeit übernommen hat.

Meinen Mitautoren des Projekts über spontane Upstates im somatosensorischen Cortex, dessen Publikation noch in Vorbereitung ist. Ganz besonders Debora Ledergerber, die mir die Methode der 2-Photonen-Mikroskopie beigebracht und alle entsprechenden Experimente mit mir durchgeführt hat. Dr. Hartwig Spors, der mich animiert hat, für dieses Projekt MATLAB zu lernen, und Dr. Frederic von Wegner, der den Algorithmus zur räumlichen Detektion von Zellen in Imaging-Rohdaten entwickelt hat.

Den geduldigen Korrektoren früherer Versionen dieser Arbeit, Professor Hans Peter Clamann, Debora Ledergerber, Dr. Kay Thurley, Daniel Dietrich und Professor Matthew Larkum.

Den technischen Assistentinnen, Elektronikern und Feinmechanikern im Hause für ihre perfekte Arbeit.

Allen Mitarbeiterinnen und Mitarbeitern an unserem und an den benachbarten Instituten, ob wir nun täglichen oder nur gelegentlichen Kontakt hatten, für die immer herzliche Freundlichkeit und für alle Hilfe, die ich für meine Experimente von ihnen bekommen habe.

Ganz prominent meiner geliebten Frau Barbara, die mir während meiner Zeit in Bern zwei wundervolle Kinder geschenkt und unter enormem persönlichen Einsatz gleichzeitig weiter in ihrem Beruf als Physikerin gearbeitet hat.